Title	BIOINSPIRED COMPOSITE GYROID AND BIOMIMETIC VORONOI LATTICES FOR BIOMECHANICAL APPLICATIONS
Author(s)	Alemayehu, Dawit Bogale
Degree Grantor	北海道大学
Degree Name	博士(工学)
Dissertation Number	甲第16536号
Issue Date	2025-06-30
DOI	https://doi.org/10.14943/doctoral.k16536
Doc URL	https://hdl.handle.net/2115/95701
Type	doctoral thesis
File Information	Dawit_Bogale_Alemayehu.pdf

BIOINSPIRED COMPOSITE GYROID AND BIOMIMETIC VORONOI LATTICES FOR BIOMECHANICAL APPLICATIONS

Dawit Bogale Alemayehu

Laboratory of Biomechanical Design
Graduate School of Engineering
Hokkaido University

A thesis submitted in partial fulfillment of the requirements of Hokkaido University
for the degree of **Doctor of Philosophy**

Division of Human Mechanical Systems and Design (HMSD)

May 2025

Acknowledgments

Starting a PhD journey is like setting sail on unknown waters, with both storms and calm seas. The search for knowledge in the field of biomechanical engineering has been both demanding and gratifying. There were times of uncertainty and frustration, but also several possibilities for learning and growth. This adventure has improved my writing abilities, taught me new software, and allowed me to delve deeply into mechanical engineering literature. It has taught me to be resilient, persevere, and enjoy the process of discovery. As I think about this transforming experience, I am overwhelmed with gratitude to everyone who has helped me along the journey. Throughout my PhD path, I wanted to give up. In my darkest moments, the Lord Jesus Christ was the only one who stood by my side. His unconditional devotion and persistent presence provided me with the courage to persevere. He gave me comfort and hope when I needed them most. Praise the Lord! First and foremost, I would like to thank my respected Prof.Masahiro Todoh. Todoh-Sensei consistent support, intelligent instruction, and encouragement have served as the foundation for my study. Your insight and experience have had a significant impact on my academic career, and I am forever thankful. I express my heartfelt gratitude to my former teacher and co-supervisor, Prof. Song-Jeng Huang. His mentorship has been priceless—providing vital insights and constructive feedback that have greatly enriched my research. His unwavering patience and passion continue to inspire me to push the limits of my abilities. Moreover, under his guidance, I have learned the profound importance of family values and the priority of loving the Lord, the King of the world. Thankful to Dr.Eng. Satoshi Yamada, invaluable assistance and guidance in mechanical compression testing requirements for porous plastic materials and structures have significantly aided my research. My heartfelt thanks go to my former teacher, Prof. Yeau-Ren Jeng, a renowned Taiwanese scientist in tribology, for teaching me the essential lesson of how vital time is with only three words: ”Life is short,” prompting me to prioritize my family. I'm quite thankful to Dr. Shu-Kai Yeh. During my tenure as a part-time research assistant in his laboratory, he taught me crucial skills such as discovering relevant literature, organizing it using software, extracting and understanding significant material, and writing papers. I want to express my special gratitude to my family, who have been pillars of support during this challenging road. To my grandmother, Yeshiye Wudeneh, whose unwavering love and support from my childhood have been the cornerstone of my journey to this PhD. My beloved mother, Martha Mulatu Weldemedhen—my first home for nine months, my lifelong hero, and my greatest blessing. Your unwavering love, sacrifices, and prayers have shaped who I am. I am forever grateful for you. And to my dear father, Bogale Alemayehu Weldemichael—thank you for your quiet strength, steady support, and unconditional love. Your guidance has been a constant light on my path. I cherish and honor you deeply. To my hero aunt, Tsedeku Alemayehu Weldemichael—thank you for your encouraging advice and steadfast support. I will never forget the role model you have been, showing me what it means to be a truly resilient and compassionate human being. My lovely wife, Azeb Kebere Gizaw, your steadfast support, love, and understanding have been my sanctuary in times of apprehension. My daughter, Zetseat Dawit Bogale, your innocence and delight have served as a continual reminder of life's beauty and the value of endurance. I extend my heartfelt gratitude to the Kim family—Abba Kim Ki-Moon, Sister Kim (Omma), and Sister Yamamoto—and all the brothers and sisters in Sapporo for their unwavering kindness and family-like support. Your warmth made us feel truly at home, and we are forever grateful. God bless you all. Mr. Shun Maki and Keigo-San, my lab mates, deserve appreciation for teaching me how to use the FDM 3D printer. Your assistance in using the slicer software RAISE 3D PRO 2 and the integrated software Idea Maker, as well as determining the best printing settings, has been critical to my trials. Shun-San, thank you for sharing your experience traveling to a new country at the age of five and linking it to my circumstances in Japan. I truly valued your guidance regarding my family. Finally, this PhD journey has been a transforming experience, made possible by the continuous support and encouragement of many extraordinary people. I am deeply grateful to each of you for your contributions to my academic and personal development. This study is as much yours as mine, and I will be eternally thankful for your presence in my life. Many thanks.

Abstract

This study investigates the design, fabrication, and optimization of bioinspired lattice structures to address challenges in automotive safety and dental implant performance. The research is organized into three interrelated studies that leverage advanced additive manufacturing and finite element analysis to mimic natural bone properties and enhance mechanical functionality. In the first study, composite triply periodic minimal surface (TPMS) gyroid lattices are developed and fabricated as shock absorbers for automotive applications. By combining two different TPMS gyroid structures, the study demonstrates that these structures can significantly improve energy absorption and mechanical resilience under impact conditions. Finite element analysis and experimental tests validate the influence of lattice varied relative density on energy dissipation, demonstrating the potential of these designs to enhance crashworthiness. The second study focuses on dental implant design, where fully and hybrid configurations integrate both solid and gyroid TPMS lattice structures to optimize stress distribution and reduce stress shielding. By varying lattice cell sizes and incorporating features such as anti-rotational connectors and square threads for initial stability, the fully and hybrid implants achieve improved stability and enhanced osseointegration. Dynamic loading simulations confirm that these implants maintain a balanced stiffness-to-compliance ratio, minimizing strains at the bone-implant interface and paving the way for personalized implant solutions. In the third study, a novel approach is presented to advance three-dimensional finite element analysis of dental implants by incorporating biomimetic Voronoi lattice models. These models accurately replicate the complex porosity of cancellous bone by varying pore sizes, which leads to a more realistic depiction of stress and strain distributions during functional loading. This biomimetic strategy deepens our understanding of implant-bone interactions and supports the development of implants that better accommodate the anisotropic nature of natural bone. Generally, the findings demonstrate the ground-breaking potential of tailored lattice structures across different biomechanical engineering applications. By integrating bioinspired design principles, additive manufacturing techniques, and robust computational analysis, this study offers promising approaches for enhancing both vehicle safety and dental implant systems, ultimately contributing to improved performance and clinical outcomes.

- Chapter 1 establishes the background by investigating the impact of bioinspired lattice structures on a variety of applications, including automobile crashworthiness and dental implant stability. It describes the study's scope, methodology, and the potential influence these structures might have on biomechanical engineering.

- Chapter 2 investigates the significance of bioinspired lattice structures, especially composite TPMS-Gyroid lattices made using fused filament fabrication (FFF), in improving energy absorption in automotive and medicinal settings. It discusses the design, manufacturing procedures, mechanical testing, and finite element analysis used to optimize these structures for use in automotive safety equipment.

- Chapter 3 introduces a hybrid biomechanical approach to dental implant design that combines solid and gyroid TPMS lattice structures. It describes the use of sophisticated CAD modeling and finite element techniques to modify stress distribution and increase implant stability. The chapter compares fully and hybrid latticed implants, highlighting their significance in lowering stress concentrations, increasing implant lifespan, and enhancing outcomes in clinical trials.

- Chapter 4 explores the use of biomimetic Voronoi lattice models in finite element analysis (FEA) to replicate human mandibular cancellous bone porosity and mechanical properties in dental implants. The study reveals that a 2.0 mm pore size enhances implant life and performance, emphasizing the importance of biomimetic designs in dental implant design.

- Chapter 5 of the thesis summarizes major results and outlines future research topics. It summarizes

the study's contributions to biomechanical engineering, notably improving lattice structures for automotive and dentistry applications, and makes recommendations for furthering the field of study.

List of Acronyms and Abbreviations

2D Two-Dimensional

3D Three-Dimensional

ABAQUS/CAE Complete Abaqus Environment

ABS Acrylonitrile Butadiene Styrene

AM Additive Manufacturing

ASTM American Society for Testing Materials

BCCO Body Center Cubic-Octahedron

BCs Boundary Conditions

BSTL Boolean Subtracted Composite TPMS Lattice

CAD Computer-Aided Design

CAE Computer-Aided Engineering

CF Carbon Fiber

CLIP Continuous Liquid Interface Production

CTG Composite Gyroid Lattice

CTL Conventional TPMS Gyroid Lattice

DfAM Design for Additive Manufacturing

DLP Digital Light Processing

DMD Direct Metal Deposition

DMLS Direct Metal Laser Sintering

EBAM Electron Beam Additive Manufacturing

EBM Electron Beam Melting

FEA Finite Element Analysis

FE-SEM Field Emission Scanning Electron Microscope

FEM Finite Element Method

FDM Fused Deposition Modeling

FFF Filament Fused Fabrication

FGS Functionally Graded Scaffold

FI Fully Latticed Dental Implant

GTLS Gyroid TPMS Lattice Structure

GWTL Gyroid Walled-TPMS Lattice

HI Hybrid Latticed Dental Implant

I-WP I-Graph-Wrapped Package Curved Surface

LENS Laser Engineered Net Shaping

LOM Laminated Object Manufacturing

LWSM Light Weight Structures Modeling

MJP Multi-Jet Printing

nTop nTopology

PBF Powder Bed Fusion

PEEK Polyether Ether Ketone

PEO Plasma Electrolytic Oxidation

PETG Polyethylene Terephthalate Glycol

PLA Polylactic Acid

PTC Parametric Technology Corporation

SEM Scanning Electron Microscope

SLA Stereolithography

SLM Selective Laser Melting

SLS Selective Laser Sintering

TPMS Triply Periodic Minimal Surface

UAM Ultrasonic Additive Manufacturing

UV Ultraviolet

PUBLICATIONS

- Alemayehu, Dawit Bogale, Masahiro Todoh, and Song-Jeng Huang. 2024. *"Nonlinear Finite Element Analysis of Bone–Implant Contact in Three Short Dental Implant Models with Varying Osseointegration Percentages" Oral* 4, no. 4: 505-524. https://doi.org/10.3390/oral4040040.
- Alemayehu, Dawit Bogale, Masahiro Todoh, and Song-Jeng Huang. 2024. *"Hybrid Biomechanical Design of Dental Implants: Integrating Solid and Gyroid TPMS Lattice Architectures for Optimized Stress Distribution" Journal of Functional Biomaterials* 15, no. 4: 94. https://doi.org/10.3390/jfb16020054. .
- Alemayehu, Dawit Bogale, and Masahiro Todoh. 2024. *"Enhanced Energy Absorption with Bioinspired Composite Triply Periodic Minimal Surface Gyroid Lattices Fabricated via Fused Filament Fabrication (FFF)" Journal of Manufacturing and Materials Processing* 8, no. 3: 86. https://doi.org/10.3390/jmmp8030086.
- Alemayehu, Dawit Bogale, Masahiro Todoh, and Song-Jeng Huang. 2024. *"Advancing 3D Dental Implant Finite Element Analysis: Incorporating Biomimetic Trabecular Bone with Varied Pore Sizes in Voronoi Lattices" Journal of Functional Biomaterials* 15, no. 4: 94. https://doi.org/10.3390/jfb15040094.

Contents

List of Figures

List of Tables

List of Equations

Chapter 1

Introduction

This chapter introduces the research's background, motivations, and objectives, providing an overview of the emerging field of lattice structures.

1.1 Background

Modern engineering, notably in automotive, aerospace, and biomedical research, is continuously looking for new methods to produce robust but lightweight structures. Although lattice structures are lightweight and excel at energy absorption, their stress-strain curves contain three distinct regions—elastic, plastic plateau, and densification [**1, 2**]. Consequently, simulating the entire deformation region, including the post-softening processes that occur upon crushing, remains exceedingly difficult in finite element analysis[**3, 4**]. In addition, despite their widespread usage, typical solid-threaded dental implant CAD models often fail to precisely reproduce real-world clinical settings, limiting their ability to mimic accurate stress distribution and osseointegration. Therefore, several alternative approaches have been proposed to overcome these limitations by creating porous biomaterials as substitutes for classical solid structures, as lattice structures can provide a suitable biological environment for host tissue to grow into the pores [**5–7**]. Such simplistic assumptions limit the capacity of computer simulations to predict biomechanical performance with clinical significance. Emerging lattice architectures such as TPMS gyroids and biomimetic Voronoi lattices are reshaping design strategies by offering structurally efficient models that balance mechanical strength, deformation capacity, and biological integration[**8, 9**]. Gyroid lattices stand out for their remarkable energy absorption capabilities and ability to improve stress distribution, making them excellent choices for shock-absorbing applications in automobile engineering [**10, 11**]. Similarly, Voronoi lattices simulate the uneven porous structure of cancellous bone, improving the realism of FEA in dental biomechanics and paving the way for more successful osseointegration under dynamic loading scenarios [**12, 13**]. These bioinspired technologies bridge the gap between conventional design constraints and the complicated mechanical and biological demands of advanced applications. The need for novel materials in biomechanical engineering is greater than ever. Vehicle crash components extensively employ traditional materials like foams, which offer excellent lightweight energy absorption, but they have significant limitations. Their complicated stress-strain diagram, such as elastic, plastic plateau, and densification areas, make finite element analysis (FEA) modeling and optimization problematic. Similarly, standard solid-threaded designs in dental implants do not reproduce the complex, anisotropic structure of human cancellous bone, resulting in poor stress distribution, insufficient osseointegration, and shorter implant lifespans. Bioinspired lattice techniques, such as triply periodic minimum surface (TPMS) gyroid lattices and Voronoi lattices, provide distinct solutions to a number of these challenges. These lattices are meant to closely resemble natural ideal designs, providing a balance of strength, flexibility, and biological compatibility that ordinary materials frequently lack. For example, TPMS gyroid lattices excel at stress distribution and energy absorption, making them ideal for usage in vehicles such as crash parts. Furthermore, Voronoi lattices, inspired by human bone structure, improve mechanical compatibility and osseointegration, both of which are important to the success of dental implant systems. This study aims to investigate the prospect of bioinspired lattice structures to bridge significant gaps in biomechanical engineering. This project attempts to build solutions that not only satisfy the problems provided by conventional designs but also push the frontiers of what is feasible in both domains, using computational modeling, additive manufacturing, and experimental validation. Traditional energy-absorbing components for vehicle crashworthiness confront substantial design issues, including trade-offs between material strength, deformation modes, and peak force requirements [**14, 15**]. While foam-filled and multi-cell constructions have demonstrated improved energy absorption and stability, their complexity and flexibility emphasize continued constraints. Previous research has employed thin-walled tubular constructions extensively, but their performance frequently falls short of current needs for lighter, safer, and more efficient systems. Recent advances, such as multi-stage structures, provide viable solutions by enhancing energy dissipation and deformation control; therefore, they fill significant gaps in traditional designs [**16, 17**]. Traditional solid-threaded dental implant designs have long struggled with issues such as effective bone-implant contact, osseointegration, and avoiding stress shielding effects that cause bone resorption. These designs frequently fail to transfer stress uniformly, resulting in zones of excessive stress or shielding that accelerate peri-implant bone loss and lower the implant's lifetime [**18, 19**]. According to previous studies, excessive stiffness in solid implants concentrates stresses around the implant collar, increasing marginal bone resorption and limiting biomechanical performance [**20, 21**]. Similarly, FEA models that use solid CAD rectangular cross-sections to depict cancellous bone have major drawbacks. These models fail to capture the porous, anisotropic property of human cancellous bone, resulting in stiffness mismatches that impede uniform stress distribution and raise the likelihood of stress shielding. This mismatch affects simulation accuracy and relevance to clinical circumstances[**22, 23**]. Innovative techniques, such as porous or lattice structures, have been proposed to fill these gaps and promote improved biomechanical compatibility by replicating the structural property of real bone[**9**]. These problems highlight the need for new implant designs and modeling methodologies that are more closely aligned with biological and mechanical reality to improve clinical outcomes and implant durability.

This chapter presents novel, bioinspired solutions addressing major challenges in energy absorption systems, crashworthiness component design, and dental biomechanics. By combining sophisticated computational modeling, additive printing, and experimental validation, the goal is to develop transformational designs that address current gaps and advance the frontiers of engineering and biomechanical applications. Triply Periodic Minimal Surface (TPMS) gyroid lattice structures are my preferred choice for energy absorption and crashworthiness owing to their remarkable ability to distribute stress and absorb energy effectively. Five different types of gyroid lattices with relative densities of 14%, 25%, 33%, 38%, and 54% were developed and fabricated to evaluate their crash and impact energy absorption capacities. These changes enable me to determine the best lattice for crash box design that needs a delicate balance of lightweight construction and high-energy absorption. According to my hypothesis, the optimum lattice that is chosen will exhibit improved stability and efficiency under dynamic loading circumstances, providing a notable advancement above conventional design. In dental implant biomechanics, TPMS gyroid lattices are used to create new implants with both fully latticed and hybrid designs. These designs use three different cell sizes to identify the best structure for providing uniform stress distribution while reducing strains. These innovative implants, which replicate the structural property of natural bone, hope to improve osseointegration and minimize marginal bone resorption. The optimized hybrid lattice implant is expected to outperform traditional solid-threaded designs by enhancing biomechanical compatibility and extending implant lifetime. To mimic the complicated behavior of human cancellous bone in finite element simulations, biomimetic Voronoi latticed structures with four different pore diameters were created. These lattices are particularly intended to replicate the porous structure and mechanical behavior of cancellous bone, allowing for precise simulations of stress distribution and load-bearing capability. My research aims to determine the ideal pore size that strikes a compromise between mechanical performance and stiffness, guaranteeing accurate simulation of bone behavior in physiological settings. The optimized lattice is expected to significantly improve FEA model accuracy, enabling more effective scaffold designs for tissue engineering applications. Through these bioinspired and multidisciplinary approaches, my thesis aims to provide practical and innovative solutions to longstanding challenges in energy absorption, crashworthiness, and biomedical engineering. These contributions are expected to significantly advance the field and open new possibilities for real-world applications.

1.2 Literature on Lattice Structures

Lattice structures, also known as lattice structures, are manufactured materials defined by a regular arrangement of linked parts or cells [**11, 24**]. These structures have distinct mechanical qualities that make them suited for a variety of applications in the biomechanical engineering fields [**7**]. Lattice structures aim to be lightweight yet sturdy, exhibiting great energy absorption and efficient load distribution. They are especially useful in applications requiring material economy and performance, such as automobile crash components and biomedical implants [**7**]. Modern processes such as additive manufacturing can produce lattice structures, distinguished by their repeating unit cells [25]. This allows for precise control over the structure's geometry and mechanical properties, allowing for the fabrication of intricate designs that would be impossible to produce using standard manufacturing processes. Lattice structures in the automobile sector enhance vehicle safety during crashes by improving component energy absorption [26]. The biomedical industry uses lattice structures to create porous implants and scaffolds that mimic human bone, thereby promoting improved osseointegration and tissue regeneration [27]. Triply Periodic Minimal Surface (TPMS) gyroid lattices are a type of cell structure that can be recognized by its smooth, continuous surface that repeats itself regularly in three dimensions [28]. The minimum surface attribute, properyized by zero mean curvature at all points, distinguishes these structures. Because of this special quality, TPMS gyroid lattices can transmit loads uniformly and have excellent mechanical efficiency. The gyroid TPMS structure is well-known for its superior mechanical qualities, such as a high strength-to-weight ratio and isotropic behavior, making it suitable for applications that need consistent performance in all directions [29]. Gyroid, Schwarz D, Schwarz P, and Diamond structures are examples of TPMS lattice structures, each specified by a distinct mathematical equation [30]. The following formula provides the governing equation for the gyroid lattice is:

$$\sin(x)\cos(y) + \sin(y)\cos(z) + \sin(z)\cos(x) = 0 \tag{1.1}$$

For the Schwarz D surface:

$$\cos(x) + \cos(y) + \cos(z) = 0 \tag{1.2}$$

And for the Schwarz P surface:

$$\cos(x)\cos(y)\cos(z) - \sin(x)\sin(y)\sin(z) = 0 \tag{1.3}$$

The Diamond TPMS is defined by:

$$\sin(x)\sin(y)\sin(z) + \sin(x)\cos(y)\cos(z) + \cos(x)\sin(y)\cos(z) + \cos(x)\cos(y)\sin(z) = 0 \tag{1.4}$$

This study holds significant promise for both the biomechanical applications. In automotive engineering, the development of composite TPMS gyroid lattices for crash components could lead to safer vehicles by improving energy absorption and reducing the impact forces transferred to passengers during collisions. These advancements could make cars lighter and safer, ultimately reducing injuries and fatalities in high-speed crashes.

In the biomedical field, Voronoi lattice implants could revolutionize dental implant design. By more closely replicating the mechanical properties of human bone, these implants could offer better osseointegration, more uniform stress distribution, and a longer lifespan. These improvements would lead to more reliable dental implants and better patient outcomes. Beyond dental applications, bioinspired lattice structures could also extend to orthopedic implants, tissue scaffolds, and prosthetics, where biomechanical compatibility is crucial.

Furthermore, the bioinspired design principles explored in this research have the potential to influence other industries, such as aerospace, where lightweight, high-performance materials are vital. The development of efficient lattice structures for aerospace applications, such as aircraft fuselages or wings, could offer significant improvements in material strength and weight. In orthopedics, these structures might help reduce implant failure and improve recovery times by better mimicking the mechanical properties of bone.

On the other hand, we form Voronoi lattice structures by dividing space into sections based on the distance from a predetermined set of seed points. A Voronoi structure's cells include all points that are closer to their own seed point than to any other seed point. This approach produces irregular but highly controlled porous structures that may be customized to resemble the complicatedstructureof actual bones. Voronoi lattices are especially beneficial in biological applications that demand a high level of porosity for tissue integration and nutrition transport [31]. This specification assures that each cell is uniquely associated with a seed point and provides a foundation for creating complicated lattice structures with specified mechanical and biological features. Finally, the fact that lattice structures like TPMS gyroid lattices and Voronoi lattices are used in both mechanical and biological settings show how powerful advanced manufacturing methods and materials engineering can be. These structures have substantial benefits in terms of weight reduction, mechanical performance, and biocompatibility, making them important for the development of next-generation biomechanical solutions [32].

1.3 Bioinspired Lattice Structures

Bioinspired lattice structures have revolutionized material science and engineering by imitating nature's complex geometries and efficient mechanical qualities. Nature provides various examples of structures that attain great strength and low weight via sophisticated design, such as honeycomb patterns in beehives, tiny structures in butterfly wings, and the porous structureof cancellous bone. Natural structures have evolved to maximize material consumption and mechanical performance, inspiring contemporary engineering solutions [**33**]. Figure 1.1 shows the inspiration and structural comparison between gyroid TPMS lattices and butterfly wings, as well as between Voronoi lattices and human cancellous bone. The gyroid TPMS lattices in Figure 1.1a, inspired by the natural structure of butterfly wings, underwent investigation under a high-resolution scanning electron microscope. The picture shows the gyroid structure's precise and periodic organization, with a unit cell size of 360 nm, demonstrating the detailed and highly structured morphology. In contrast, Figure 1.1b depicts a schematic of human cancellous bone, emphasizing the intricate and linked porosity network that defines this biological structure. Figure 1.1c shows a Voronoi-like pattern on the cancellous bone as seen using a high-resolution scanning electron microscope. This comprehensive study demonstrates the resemblance in porousstructurebetween real bone and Voronoi lattice systems[**31**]. Comparing gyroid TPMS lattices to human cancellous bone shows that biomimetic design can be used to make materials with better mechanical properties and structural efficiency by taking ideas from nature's best solutions.

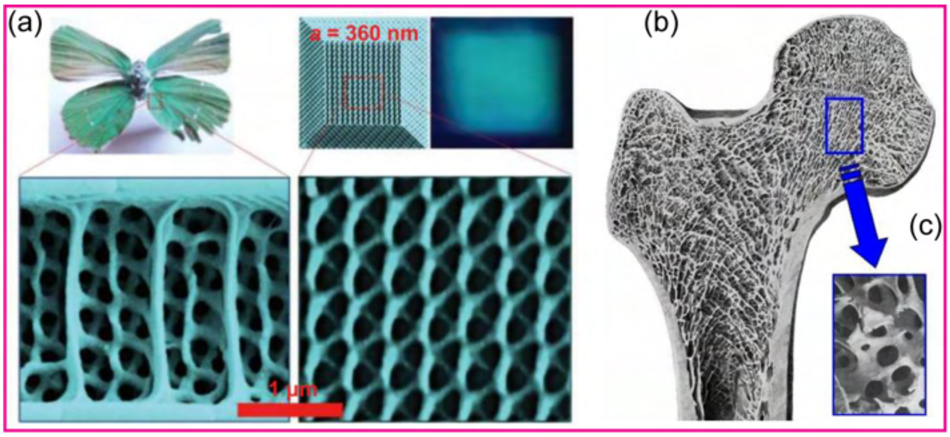

Figure 1.1: Natural TPMS-like porous structures. (a) Wings of a butterfly [**33**]. Copyright 2022, the Authors, CC BY 3.0., and Voronoi-like human cancellous bone. (b) Cancellous bone structure and Voronoi-like human cancellous bone observed by scanning electron microscope (SEM) [**31**]. Copyright 2010, the Author, CC BY 3.0.

The advent of Triply Periodic Minimal Surfaces (TPMS) and Voronoi lattices was a huge step forward in this subject. Complex, continuous geometries distinguish these structures, reducing surface area for a given volume and resulting in superior mechanical qualities. Researchers have widely explored TPMS, which includes geometries like the Gyroid, Schwartz Diamond, and Neovius surfaces, for its capacity to distribute stress and absorb energy efficiently [**18**–**20**]. The Gyroid TPMS lattice's high strength and low weight make it ideal for industrial applications [**21**–**23**]. Similarly, Voronoi lattices are inspired by the natural partition of space seen in plant and animal lattice systems. The lattices are generated by dividing space into sections depending on the distance to a set of seed points, generating a network of irregular, open-cell structures that closely imitate the porous propery of cancellous bone [**31**–**33**]. Voronoi lattices have superior mechanical qualities and biological compatibility, making them suitable for biomedical applications such tissue engineering scaffolds and load-bearing implants [**34**–**36**]. Bioinspired lattice structures combine biology and engineering, using natural design principles to tackle complicated mechanical challenges. Engineers may build materials that not only fulfill but surpass the performance criteria of standard materials by understanding and duplicating nature's efficient structural techniques. Bioinspired design has greatly influenced current technology, resulting in important advances in fields such as biomechanical engineering [**32**].

1.4 Classification of Lattice Structures and Their Families

Lattice structures are broadly divided into three types: random, periodic, and pseudo-periodic. Random lattices, akin to Voronoi and Delaunay structures, consist of beams or struts arranged irregularly. Types of periodic lattices are further classified as conformal and non-conformal (refer to Figure 1. 2) [**37**].

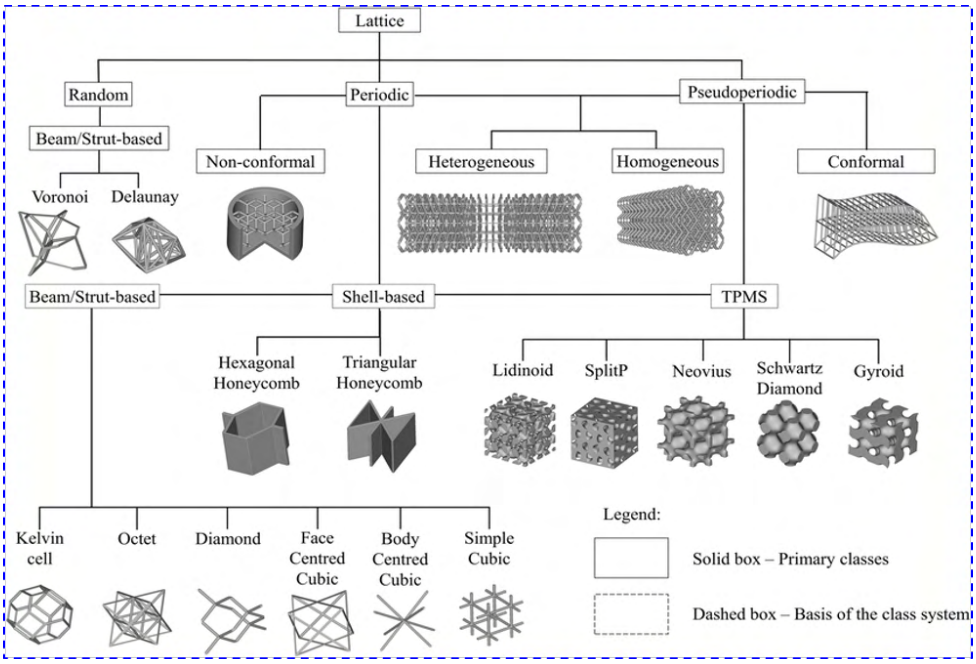

Figure 1.2: Classification of Lattice Structures [**37**].

Conformal periodic lattices, such as homogeneous TPMS, have configurations like Lidinoid, SplitP, Neovius, Schwartz Diamond, and Gyroid. In non-conformal periodic lattices, there are beam/strut-based and shell-based structures, like honeycombs with hexagons and triangles, Kelvin cells, octets, and diamonds. There are also cubic versions, such as face-centered cubic and body-centered cubic lattices. Pseudo-periodic lattices combine random and periodic lattices, providing distinct mechanical properties for engineering applications (see Figure 1.3) [**34**]. A useful group of materials is called Triply Periodic Minimal Surface (TPMS) gyroid lattices. They have complex, periodic structures that give them great mechanical properties and a high strength-to-weight ratio. There are numerous criteria for classifying these lattices. Geometrically, they consist of single gyroid lattices with a continuous surface and double gyroid lattices with two interpenetrating networks [**35**]. Different types of lattices are based on the materials they are made of Metallic lattices are strong and are used in aerospace and biomedical applications [**36**] (See Figure 1.3a); polymeric lattices are lightweight and flexible [**38**] (See Figure 1.3b); ceramic lattices are used for high thermal resistance [**39**] (See Figure 1.3c); and composite lattices combine different materials to make them stronger and lighter [**40**] (See Figure 1.3d).Structurally, they are either homogenous with constant property or graded with changing parameters to achieve certain mechanical properties.

1.5 Applications of Lattice Structures

Functional applications of TPMS gyroid lattices include energy absorption in mechanical and structural components [**41**], thermal management in heat exchangers due to their large surface area [**42**], biomedical implants for biocompatibility and tissue integration [**43**], and acoustic applications for soundproofing [**44**] (refer to Figure 1.4). Finally, their relative density divides them into two types: low-density lattices, which are lighter with better energy absorption [**45**] but lower strength, and high-density lattices, which are heavier with greater strength but lower energy absorption [19]. This thorough classification highlights TPMS gyroid lattices' flexibility over a wide range of technical difficulties. Because of their unique features and adaptability, lattice structures have found widespread use in both the biomechanical engineering fields. These structures stand out for their lightweight yet robust configurations, which can

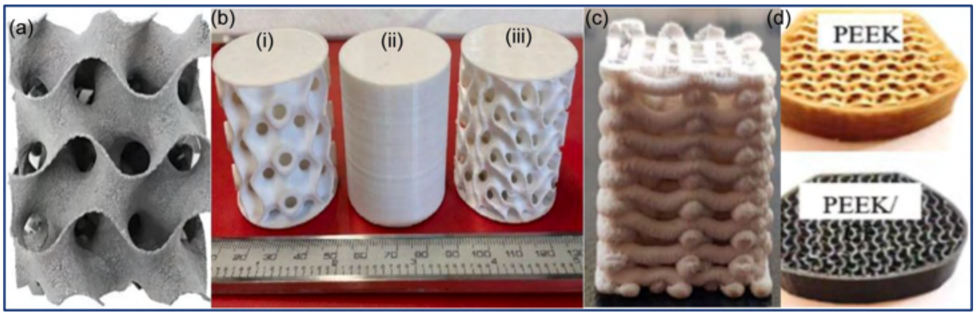

Figure 1.3: a) Ti-6Al-4V Gyroid specimen fabricated via SLM [**36**], b) FDM-3D printed specimens of i) Schwarz Primitive structure, ii) solid control cylinder, and iii) Schoen Gyroid structure with 1.75 mm white PLA filament [**38**], c) ZrO2-lattice ceramic structure manufactured via extrusion-free forming AM technologies [**39**], and d) FFF-printed PEEK and PEEK/CF cages [**40**].

be customized to meet specific functional requirements. Biomedical applications use lattice structures to improve implant efficacy and integration. For example, they may replicate bone's natural structure , facilitating improved osseointegration and minimizing stress shielding effects, which are crucial for implant durability and stability. Furthermore, we can use lattice structures to create porous scaffolds that support tissue engineering and regenerative medicine by encouraging cell adhesion, proliferation, and differentiation [**46–50**].

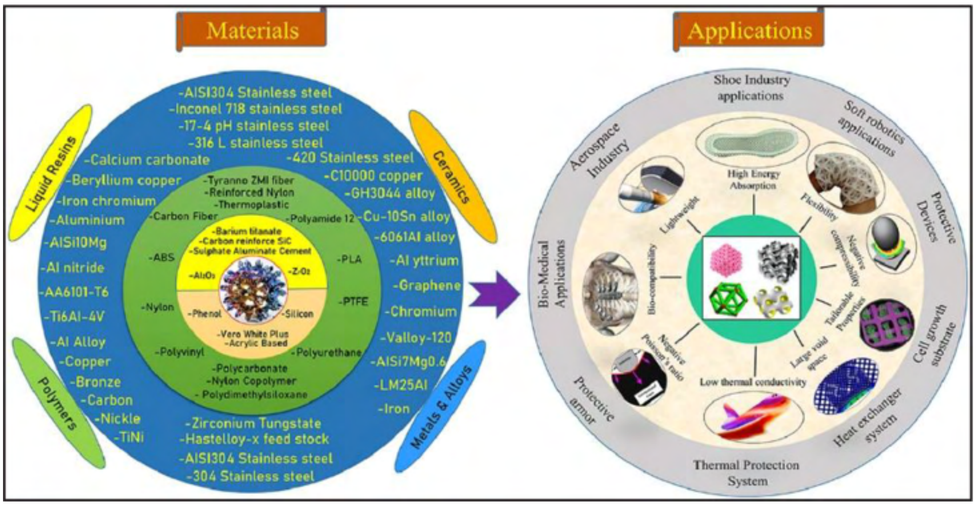

Figure 1.4: Various lattice structure materials and their uses in different industries [**51**].

In the automobile sector, lattice structures increase vehicle safety and performance. Their outstanding energy absorption capacity makes them excellent for components like crash boxes and energy absorbers, which are critical in reducing the impacts of crashes. We can construct these structures to bend predictably after impact, dispersing energy and protecting passengers. The use of sophisticated manufacturing techniques, such as additive manufacturing (AM), enables the creation of complicated lattice structures that are not possible with older methods. This allows for the optimization of mechanical attributes like stiffness and strength while decreasing weight, resulting in more efficient and safer cars [**52**].

Traditional FEA models of dental implants assume isotropic bone and use solid CAD models, which can lead to inaccuracies in stress distribution and performance predictions. While these models provide a simplified solution, they fail to capture the complex, anisotropic properties of cancellous bone, leading to suboptimal implant design. Bioinspired lattice structures, such as those mimicking cancellous bone, offer superior performance by accurately replicating bone behavior, improving stress distribution, and enhancing osseointegration. The traditional FEA approach, shown in Figure 1.5, helps in basic design but lacks the precision and efficiency provided by bioinspired lattice models [**53**].

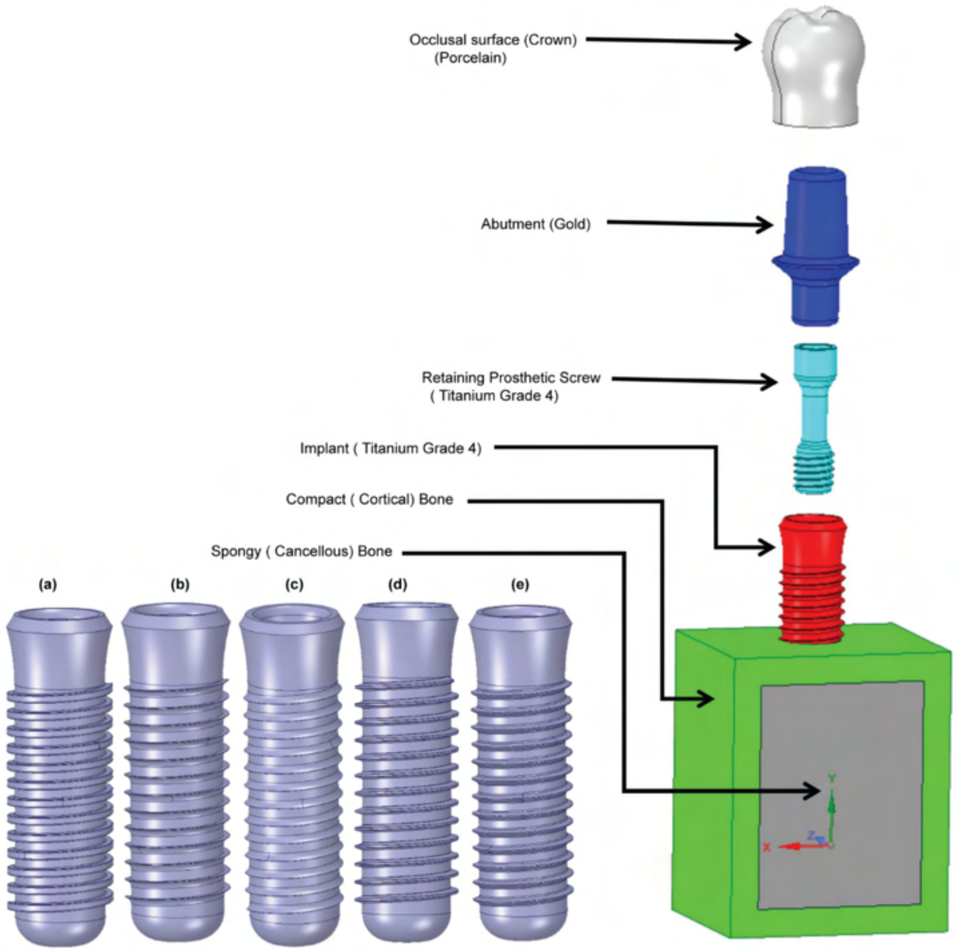

Figure 1.5: The 3D models of implants and bone: (a) square, (b) buttress (CF), (c) reverse buttress(CF), (d) trapezoidal, and (e) triangular [**53**].

Lattice structures have transformed the design and function of dental implants (as shown in Figure 1.6). By mimicking the cancellous structure of natural bone, biomimetic lattice designs like Voronoi and gyroid lattices improve mechanical compatibility and osseointegration. These features help to distribute pressure more uniformly throughout the implant, lowering the chance of failure and encouraging long-term stability. These lattices' porous structure promotes bone ingrowth and vascularization, both of which are critical to the success of dental implants. We often use CAD tools like nTopology and ANSYS to design and model these complex structures, ensuring they meet mechanical and biological performance requirements.

Orthopedics uses lattice structures to create implants that mimic the mechanical properties of bone. This is critical for load-bearing applications that need accurate stress distribution and bone-implant interface stability. We can design gyroids and other lattice structures to match the stiffness and strength of cortical bone, which will reduce stress shielding and promote bone remodeling. Additive manufacturing enables the modification of these implants to meet specific patient anatomy, improving their fit and function. According to studies, lattice structures may greatly increase the mechanical strength and lifespan of orthopedic implants, making them a potential option for a wide range of orthopedic applications [**47**].

The automobile sector is increasingly employing lattice structures due to their superior energy absorption and lightweight qualities. Components like crash boxes, bumpers, and protective panels incorporate them to enhance vehicle safety [**54**]. Lattice structures' ability to bend after impact and absorb energy effectively reduces the force transferred to passengers during crashes. CAD programs like ANSYS and Creo, along with advanced simulations using finite element analysis (FEA), optimize these structures for optimal performance. The use of materials like PLA and titanium in lattice construction guarantees that they offer enough strength while keeping the total vehicle weight low [**52**]. Traditional crashworthiness designs, such as stainless-steel bumper beams or crash boxes, struggle with energy absorption efficiency

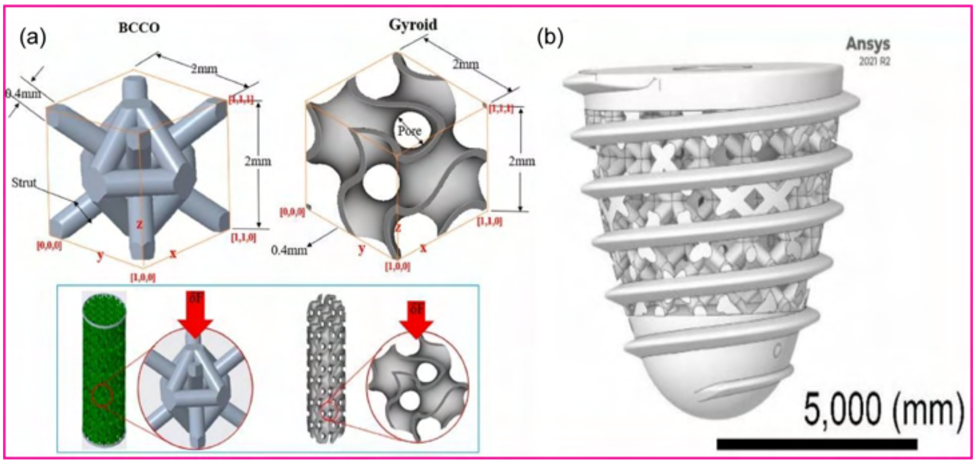

Figure 1.6: a) BCCO and Gyroid lattice CAD models for dental scaffold structures [**46**] and, b) ultra-short implant with added diamond lattice [**48**].

and car weight reduction. Crash boxes in this study, made from thin-walled aluminum tubes, are designed to absorb impact energy during frontal collisions. The design focuses on protecting the vehicle's rear components by controlling deformation, with various filling methods improving energy absorption. However, foam-filled crash boxes are heavier and more costly due to the materials used [**55**]. Bioinspired latticed crash boxes, such as TPMS gyroids, provide superior energy absorption and strength-to-weight ratios, making them more efficient and cost-effective. The foam-filled design, shown in Figure 1.7, enhances energy absorption but is limited in weight and structural efficiency compared to bioinspired lattices [**55**].

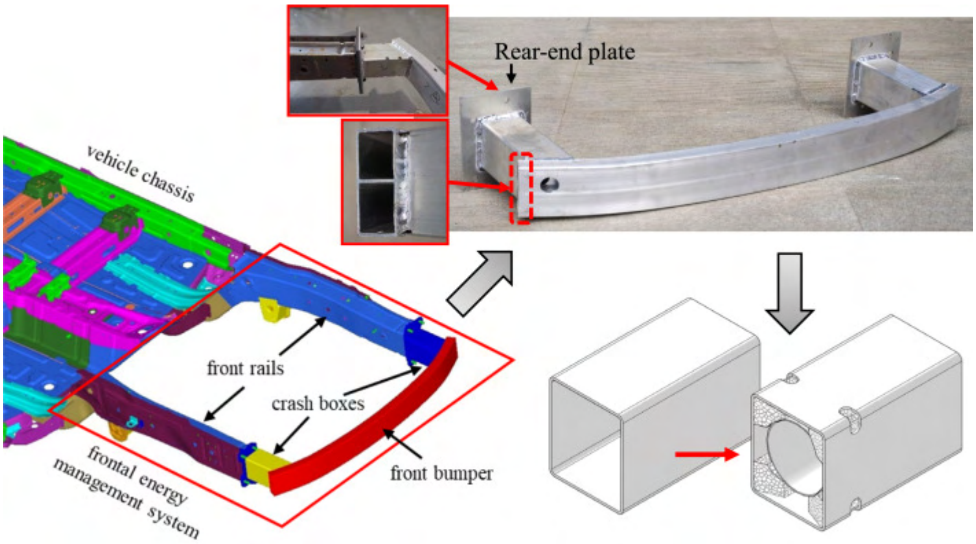

Figure 1.7: Schematic of the frontal crash management system in a vehicle [**55**].

Foam-filled crash boxes enhance energy absorption by using aluminum foam within thin-walled tubes to manage impact forces effectively. However, they contribute to increased structural mass and manufacturing cost, limiting their efficiency for lightweight applications [**56**]. Bioinspired latticed crash boxes, such as TPMS gyroid lattices, offer better energy absorption and superior strength-to-weight ratios, making them more efficient and cost-effective. The foam-filled design, shown in Figure 1.8, helps prevent premature collapse during collisions but is limited in its energy absorption capacity and structural efficiency compared to latticed structures [**57**].

Energy-absorbing rods with impressions, made from thermo-hardened aluminum alloy, effectively manage impact forces by initiating deformation at specific zones. However, they are limited by their heavier weight and the complexities in manufacturing the impressions, which can lead to increased costs [**58**]. In contrast, bioinspired latticed structures, such as TPMS gyroids, offer superior energy absorption and strength-to-weight ratios, making them more efficient and lightweight. The impression-based energy

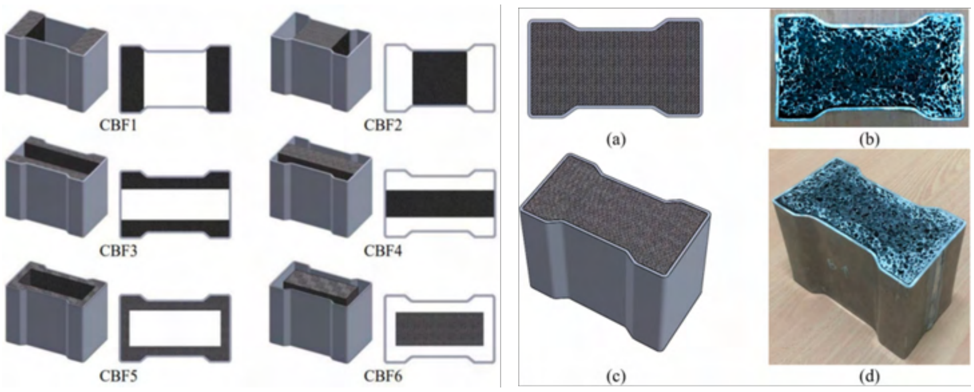

Figure 1.8: Six different foam filled crash boxes cross section and Top view of specimens (a) simulation and (b) experiment. Isometric view of the specimen (c) simulation and (d) experiment [**57**].

absorber design, shown in Figure 1.9, provides controlled deformation but lacks the energy efficiency and structural optimization seen in lattice designs [**58**].

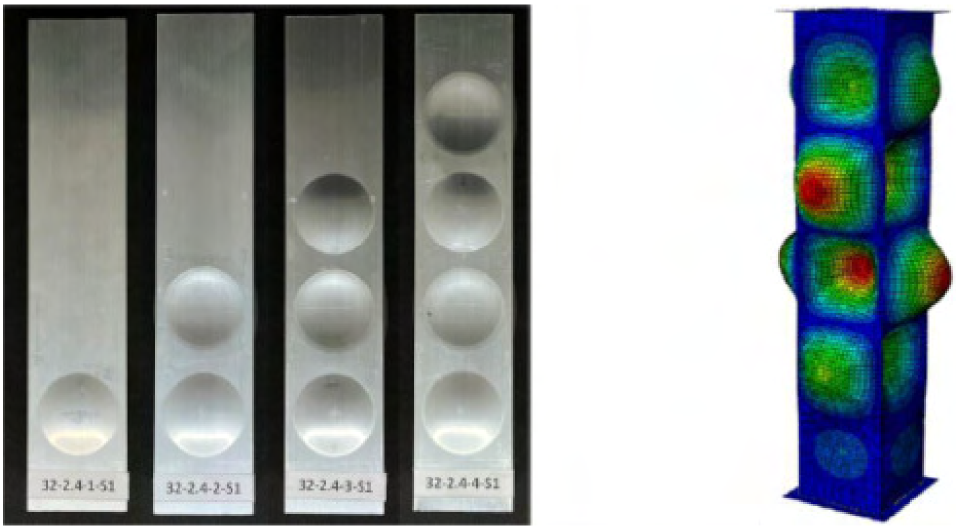

Figure 1.9: Visualized forms of studied energy-absorbers, real mechanical appearance (left), FEM environment (right) [**58**].

Lattice structures are essential in the creation of scaffolds for tissue engineering (see Figure 1.10). Their porous structure promotes cell adhesion and proliferation, which are required for tissue regeneration. You can modify the designs of these scaffolds to control their mechanical qualities and degradation rates, making them suitable for a variety of biomedical applications. CAD tools and additive manufacturing processes can precisely fabricate these structures with specific pore sizes and geometries. This tailoring ensures that the scaffolds provide the necessary support and environment for the formation of new tissue, boosting the efficacy of regenerative medicine therapies [**50**].

Lattice structures are a lightweight but effective option for reducing the effects of explosions and impacts on armor protection. Their capacity to absorb and disperse energy makes them excellent for use in protective equipment and vehicle armor. We can use the various geometries of lattice structures to equally disperse impact force, thereby lowering the chance of penetration and damage. According to research, metallic lattices, such as those composed of titanium or steel, offer excellent protection while remaining lightweight. This makes them appropriate for use in personal protection equipment and armored vehicles, thereby improving user safety and mobility [**52, 59**].

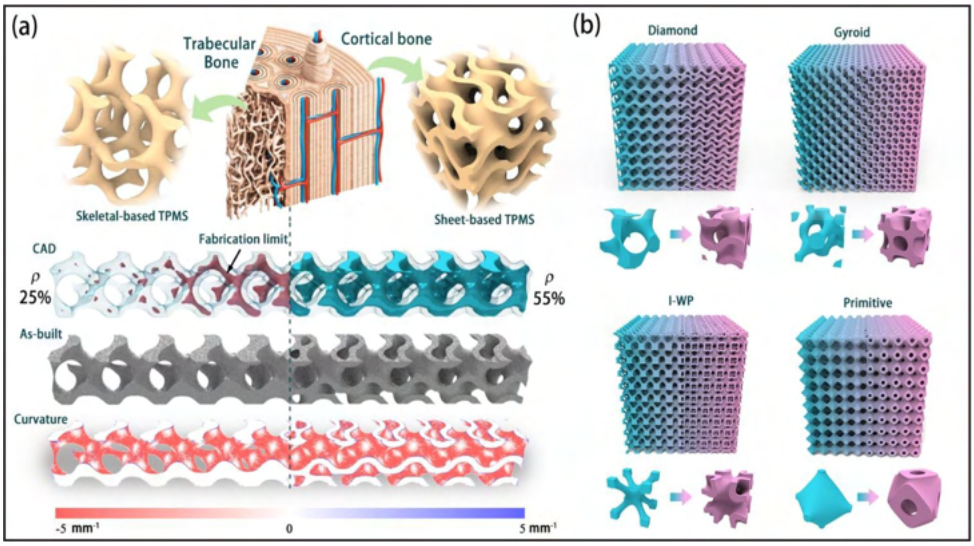

Figure 1.10: Biomimetic Strategy and Graded Structures of TPMS-FGS:(a) Biomimetic strategy showing the design process, CAD model, constructed sample, and Gaussian curvature distribution for Gyroid TPMS, and (b) Graded structures featuring skeletal and sheet TPMS designs based on diamond, Gyroid, I-WP, and primitive TPMS [**50**].

1.5.1 Why Use TPMS Gyroid Lattices in Dental Implant Design?

In dental implant design, one of the critical biomechanical challenges is the mismatch between the stiffness of commercially pure titanium (110 GPa) and that of natural cortical bone (15 GPa). This mismatch can lead to stress shielding, bone resorption, and eventual implant failure. To address this, porous structures—particularly those based on triply periodic minimal surfaces (TPMS)—have emerged as a promising solution. Among TPMS topologies, the gyroid lattice offers a unique balance of high porosity, continuous curvature, and interconnected pathways, enabling mechanical compliance, improved cell adhesion, and enhanced nutrient and oxygen diffusion. Recent findings by Araya et al. (2024) demonstrate that TPMS-gyroid and stochastic Ti6Al4V lattices manufactured via laser powder bed fusion exhibit excellent mechanical strength and deformation capacity, making them highly suitable for biomedical applications. As illustrated in Figure 1.11, the gyroid's ability to tailor mechanical stiffness while promoting osseointegration underpins its selection for the development of advanced dental implant systems [**60**].

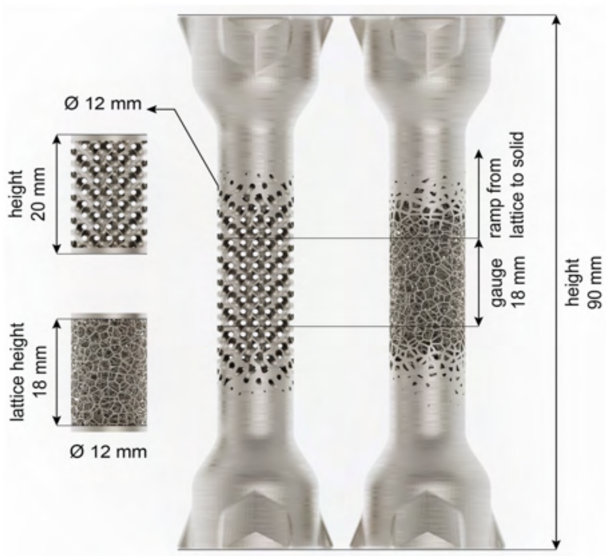

Figure 1.11: Porous titanium gyroid (left) and stochastic (Voronoi) (right) lattice structures used to reduce stiffness mismatch in dental implants. Adapted from Araya et al. (2024) [**60**].

1.5.2 Why Voronoi Lattices for Cancellous Bone in FEA?

Voronoi lattices have gained increasing attention in implant design due to their unique ability to replicate the complex, irregular architecture of human cancellous bone. Unlike periodic lattice structures, Voronoi-based designs exhibit non-repetitive geometries that closely mimic natural trabecular networks, enabling more accurate biomechanical simulation and stress distribution under physiological loading. Their tunable porosity—typically ranging from 50% to 90%—allows precise control of mechanical stiffness and biological integration. This bioinspired configuration facilitates efficient stress transfer through pore-guided load paths, much like native cancellous bone. Such characteristics significantly enhance implant osseointegration and structural compatibility (refer to Figure 1.12). Fantini et al. (2016) demonstrated the morphological similarity between stochastic Voronoi structures and actual cancellous bone, reinforcing their relevance in finite element modeling for biomedical applications[**8**] .

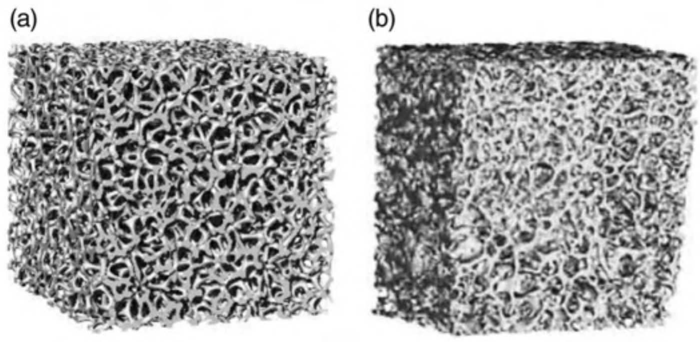

Figure 1.12: Comparison of (a) Voronoi lattice structure and (b) natural cancellous bone [**8**].

1.6 Lattice Structure Modeling and Production

1.6.1 CAD Design for Lattice Structures

Computer-aided design (CAD) is essential for designing lattice structures such as gyroid and Voronoi lattices for additive manufacturing (AM). CAD provides exact control over the complicated geometry of these lattice systems, ensuring that they fulfill specified mechanical and functional criteria. This accuracy is critical for the success of AM technologies, which construct components layer-by-layer using CAD models [**61**]. Design for Additive Manufacturing (DfAM) highlights additive manufacturing's (AM) transformational influence on the product development cycle. DfAM encourages designers to take advantage of AM technology's unique capabilities, which allow the fabrication of complicated geometries and optimized structures that are not possible with conventional manufacturing processes. The Lightweight Structures Modeling (LWSM) tool is a significant example in this discipline; it was created using the Python programming language and is included in the open-source Free CAD software. This tool aims to help designers use AM-oriented tasks daily, cultivating an "additive mindset" that fully realizes the promise of AM technologies. The LWSM tool makes it simple to create lattice structures that are both lightweight and efficient. This leads to significant advancements in the design and manufacture of complicated components, improving the overall performance and efficiency of the designed products. Figure 4 shows the application of the LWSM tool in the construction and optimization of intricate lattice structures, highlighting the significant impact of DfAM concepts on contemporary engineering processes. Several modern CAD software packages make it easier to create lattice structures, each with distinct features and add-ins tailored specifically to lattice design. These tools include ANSYS SpaceClaim, Creo Parametric, Free CAD, and nTopology. ANSYS SpaceClaim is well-known for its direct modeling capabilities, which enable users to design complicated lattice structures with ease. Space Claim contains specialized tools for creating and optimizing lattice structures. The program interfaces with ANSYS' advanced simulation capabilities, allowing engineers to do structural assessments and iterative design optimization. Space Claim's lattice design module enables the creation of periodic and random lattice structures, making it ideal for use in biomedical implants and lightweight aircraft components. Research has shown that utilizing ANSYS Space Claim to create complicated lattice patterns improves mechanical properties while using less material [**62, 63**]. Another reliable CAD program for lattice structure design is PTC's Creo Parametric. Creo provides a specific add-in for lattice design, which allows you to create stochastic and periodic lattice structures. The software's parametric design features make it possible to easily and precisely change lattice properties, including cell size, shape, and orientation. Creo's interface with PTC's simulation tools enables the assessment of lattice structures' mechanical performance under various loading conditions. Studies have demonstrated Creo's efficiency in creating complex lattice structures for additive manufacturing, particularly in optimizing weight and mechanical qualities for industrial applications [**64, 65**].

1.6.2 Additive Manufacturing

Additive manufacturing (AM) is a method of producing complicated structures by gradually stacking materials based on 3D model data. CAD software creates the design, which different AM processes then generate, enabling the creation of components not possible with traditional manufacturing methods. AM has several benefits, including the capacity to make sophisticated patterns at lower prices, faster manufacturing times, and decreased material waste. Quick prototyping and data analysis were the initial uses of AM, which emerged in the 1980s. Over the years, its applications have grown, and by the early 2010's, it had made significant strides in industrial production, particularly in the metalworking industry. The market for AM devices has grown dramatically, and their prices have dropped significantly. While 3D printing is the most well-known kind of additive manufacturing, other approaches help to create efficient and adaptable production processes[**66, 67**]. The common materials for such manufacturing technology are showed in Table 1.1.

Table 1.1: Materials and their applications in additive manufacturing [**66**].

Material	**Properties**	**Applications**
Plastics	Affordable, easy to process, wide range of properties	Prototypes, toys, household items, medical devices
Metals	Strong, durable, heat-resistant	Aerospace parts, medical implants, automotive components
Resins	High accuracy, smooth finish	Jewelry, dental models, figurines
Ceramics	Biocompatible, heat-resistant, wear-resistant	Dental implants, surgical guides, cutting tools

Advantages and Challenges of Additive Manufacturing

Additive manufacturing (AM) processes have various advantages, including the capacity to build complicated geometries and highly customizable components with unparalleled precision and accuracy [**62, 65–67**]. This approach lowers material waste, shortens production times, and enables on-demand manufacturing. Despite these benefits, each AM method has its own set of restrictions and obstacles, such as a limited range of suitable materials, the need for post-processing, and the possibility of faults or mistakes in the final result [**68, 69**]. The research community is becoming interested in AM technologies for manufacturing physical goods from 3D models because they can generate complex objects of varied sizes with high resolution, decreased failure rates, and improved mechanical qualities. However, given the advantages and disadvantages of each approach, certain firms offer a range of materials, including powders and polymers, tailored to the specific requirements of the product.

1.6.3 Classification of Additive Manufacturing

Beyond 3D printing, additive manufacturing includes a wide range of techniques, each with its own set of capabilities and design criteria (refer to Figure 1.11). Manufacturing speed, surface quality, resolution, efficiency, dimensional accuracy, build size, cost, and component strength are important aspects of additive manufacturing.

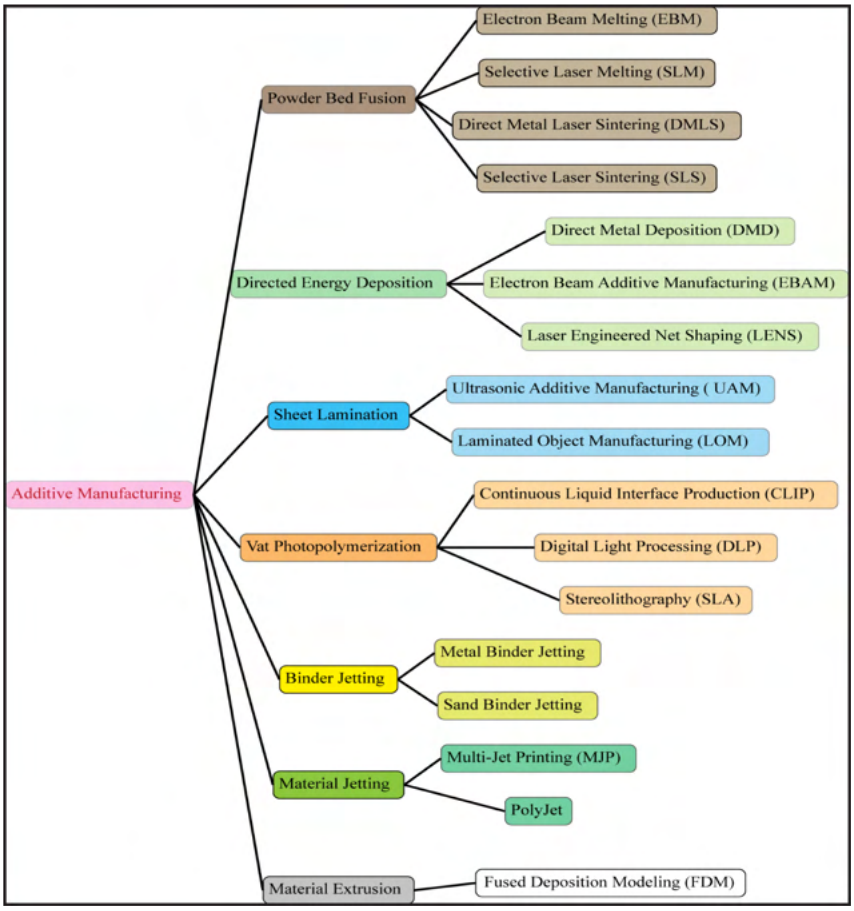

Figure 1.13: Classification of additive manufacturing methods.

The production of lightweight materials, increasingly used in a variety of industrial applications, depends on these critical criteria. Alternative additive manufacturing processes have the potential to satisfy these requirements. Fabrication methods further divide TPMS gyroid lattices into two groups: those made with additive manufacturing methods, like selective laser sintering (SLS), fused deposition modeling (FDM), and stereolithography (SLA); and those made with traditional manufacturing methods, like casting and milling, which are harder to work with because of the complicated shapes [**32, 34, 70, 71**].

Material Extrusion

Material extrusion is one of the most popular additive manufacturing (AM) techniques, notably in desktop 3D printing. This method includes driving a thermoplastic filament through a heated nozzle, which melts the material and deposits it layer by layer on a build platform.The nozzle travels in a preset pattern based on the CAD model, resulting in a three-dimensional object.

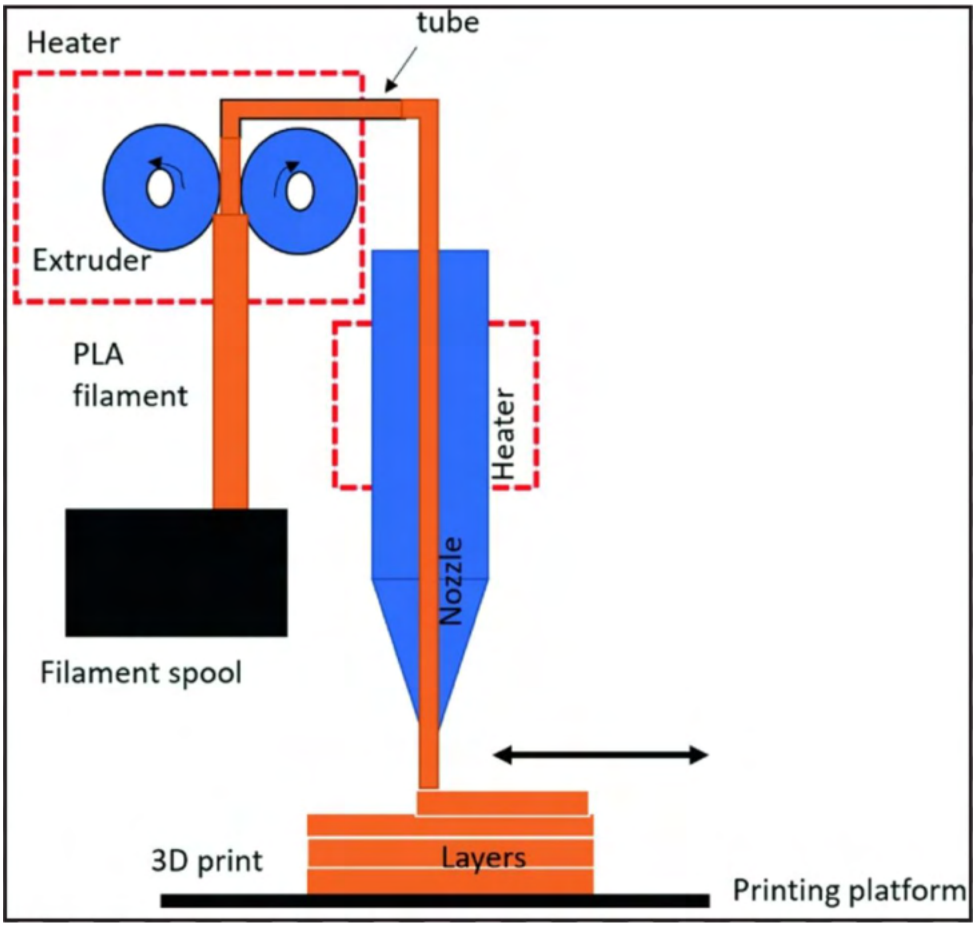

Figure 1.14: A schematic diagram of the material extrusion process [**72**].

Fused deposition modeling (FDM) and fused filament fabrication (FFF) systems widely utilize this approach. The key benefits of material extrusion are its simplicity, cost-effectiveness, and variety in using thermoplastic materials such as PLA, ABS, and PETG. Material extrusion enables the production of complicated shapes and functioning prototypes. However, the technique has drawbacks, such as slower build rates and layer adhesion concerns, which may impair the mechanical qualities of the finished product. A schematic diagram of the material extrusion process generally depicts the filament spool, heated nozzle, and build platform, as well as the step-by-step material deposition that results in the finished product (refer to Figure 1.12).

Material Jetting

Material jetting is an advanced additive manufacturing technology that involves dropping droplets onto a build platform, where they solidify to produce a three-dimensional item (refer to Figure 1.13). This technique is comparable to inkjet printing but works in three dimensions. Material jetting is well-known for its ability to generate items with a smooth surface finish and precise dimensions. UV light cures photopolymers, enabling the fabrication of delicate and detailed components. Material jetting technologies, such as Polyjet and multi-jet printing (MJP), may jet numerous materials at the same time, allowing for the creation of objects with different mechanical properties and colors inside a single build. Despite its advantages, certain applications often limit material jetting to photopolymer materials, which may not possess the necessary mechanical strength. The schematic design for material jetting depicts the print head, UV light source, and build platform, emphasizing the exact droplet positioning and curing processes (refer to Figure 1.13).

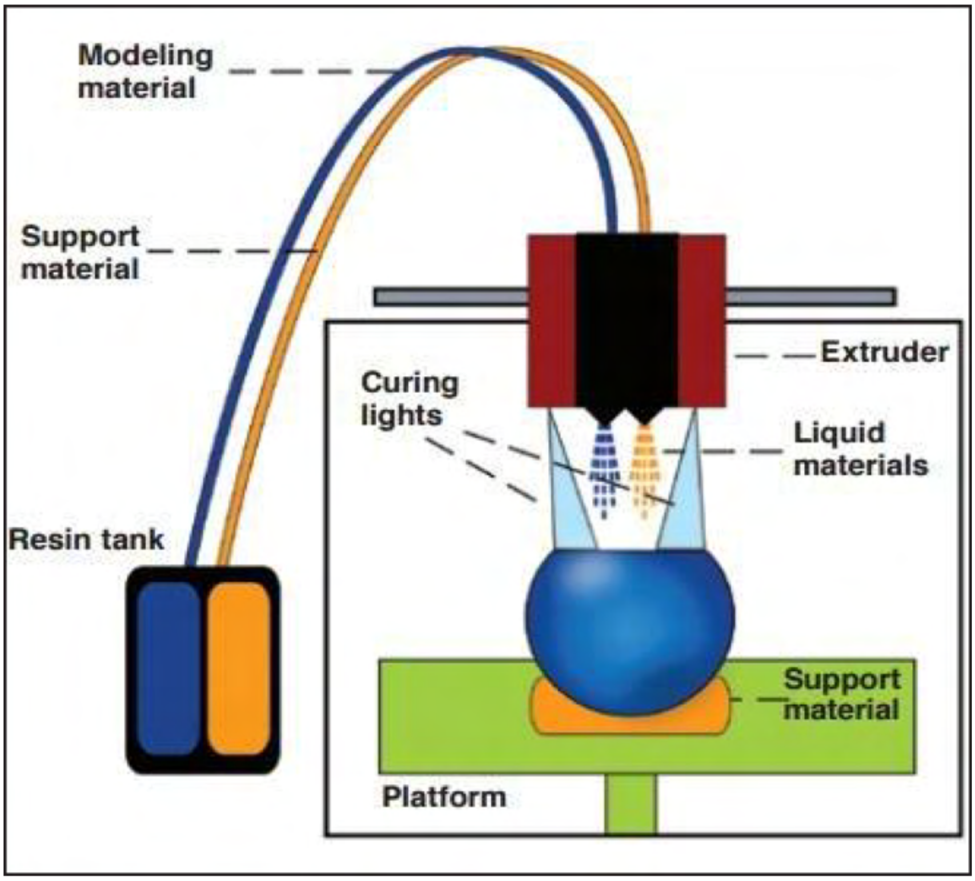

Figure 1.15: The schematic diagram for material jetting depicts emphasizing the exact droplet positioning and curing processes [**73**].

Poly-Jet

Polyjet is a kind of material jetting that provides exceptional detail and flawless surface finishes, making it excellent for prototyping and manufacturing complicated geometries. The Polyjet method blasts liquid photopolymer droplets onto the build platform, curing them layer by layer under UV light. This technique can print with different materials at the same time, enabling you to combine stiff and flexible elements in one construction. Areas such as dentistry, medicine, and consumer products especially prize Polyjet for its ability to create extremely precise and detailed models. However, the materials used in Polyjet are primarily photopolymers, which may be less durable than thermoplastics used in other AM processes. The Polyjet schematic would show the jetting heads, UV curing system, and build platform, showing the layer-by-layer build process and multi-material possibilities (refer to Figure 1.14).

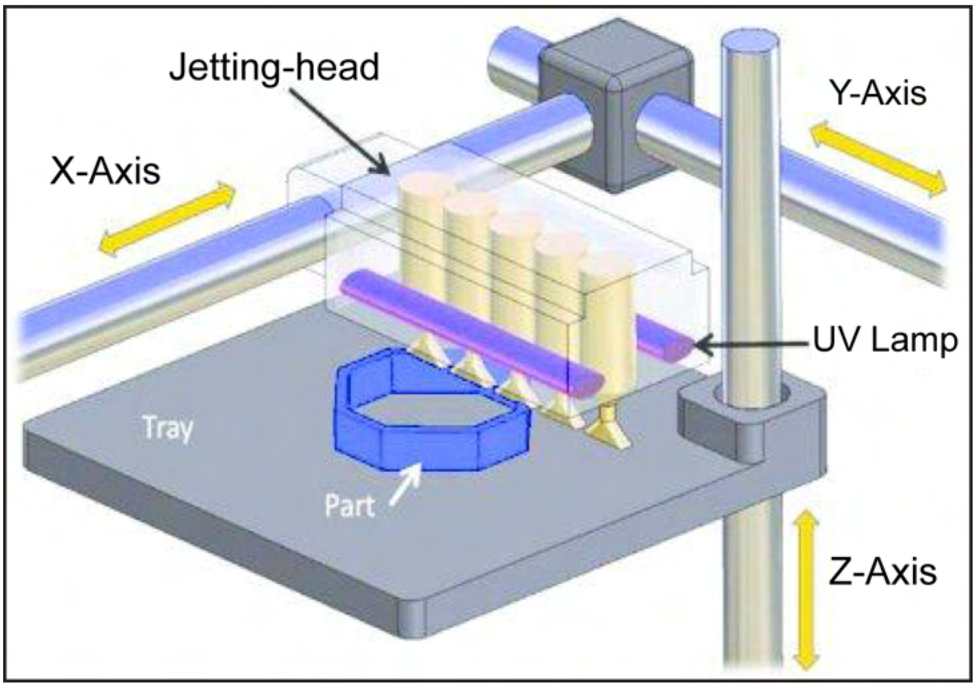

Figure 1.16: PolyJet schematic showing the layer-by-layer build process [**74**].

Vat Photo-Polymerization

Vat photopolymerization, also known as stereolithography (SLA), involves curing liquid photopolymer resin using a UV laser or light source. The method begins by filling a vat with photopolymer resin, then selectively curing it layer by layer using a laser, guided by the CAD model. This process is known for generating items with outstanding resolution and a smooth surface finish. This technique has many variants, including digital light processing (DLP) and continuous liquid interface production. Industries that require precise and complex components, like medical devices and jewelry, frequently utilize SLA. However, the mechanical qualities of SLA products often face limitations due to the use of photopolymer resins. A diagram of the vat photopolymerization process would represent the resin vat, UV laser or light source, and the build platform, demonstrating selective curing and layer-by-layer item construction (as shown in Figure 1.15).

Sheet Lamination

Sheet lamination is an additive manufacturing technique that involves layer-by-layer adhesion of material sheets to create a three-dimensional structure.

Adhesive, ultrasonic welding, or brazing can accomplish this bonding. Metal, plastic, and paper are common materials used in sheet lamination. This technique includes laminated object manufacturing (LOM) and ultrasonic additive manufacturing. Sheet lamination is very useful for quickly and affordably producing large components with minimal waste. However, the procedure may need post-processing to attain the appropriate surface polish and dimensional precision. The sheet lamination schematic shows the feed of the sheet material, the cutting or bonding mechanism, and the construction platform, showing the precise cutting and bonding of each layer to create the final product (refer to Figure 1.16).

Directed Energy Deposition

The AM method known as Directed Energy Deposition (DED) uses concentrated thermal energy, like a laser, electron beam, or plasma arc, to fuse materials by melting them as they deposit.

The material, usually in the form of powder or wire, is supplied via a nozzle and aimed to the desired deposition region. The industrial fields particularly use DED to repair or add features to existing components. The process is compatible with a broad variety of materials, including metals, ceramics, and composites. To eliminate residual strains and distortion, the procedure needs careful temperature input control. A DED graphic depicts the energy source, material feed, and build platform, emphasizing the precise deposition and fusing of materials to create or repair components (refer to Figure 1.17).

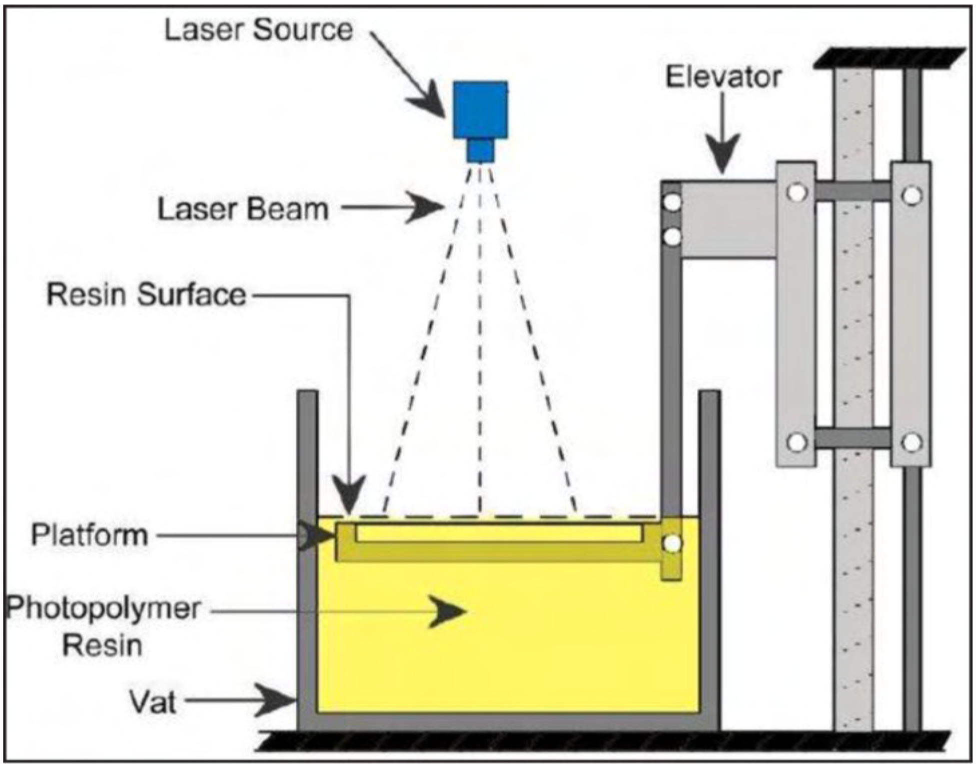

Figure 1.17: Schematic for Vat photo-polymerization process [**73**].

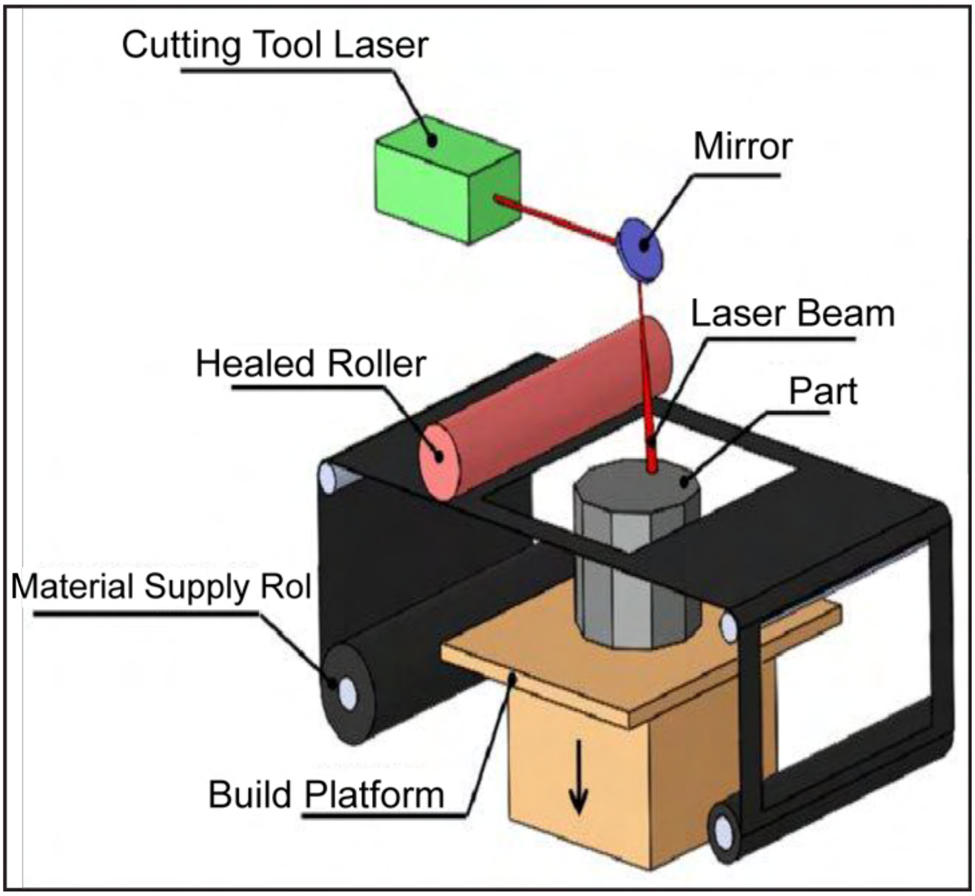

Figure 1.18: Schematic for sheet lamination [**73**].

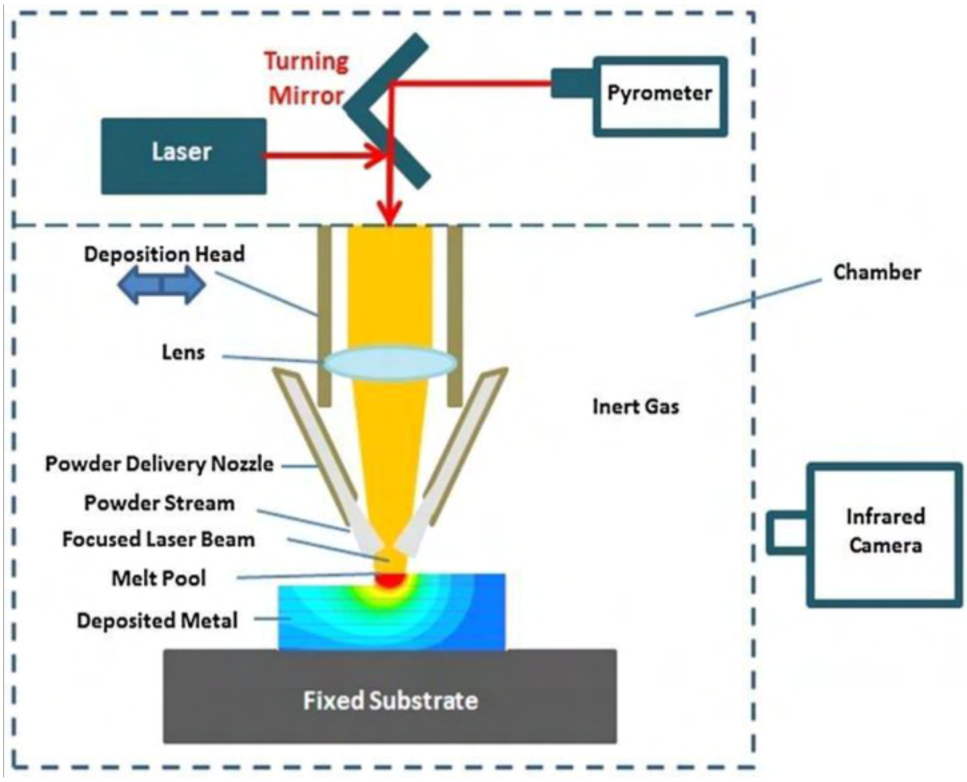

Figure 1.19: Schematics of directed energy deposition (DED) [**75**].

Powder Bed Fusion

Powder Bed Fusion (PBF) refers to a class of AM methods that selectively fuse powder bed areas using a thermal energy source. PBF technologies include selective laser sintering (SLS), direct metal laser sintering (DMLS), selective laser melting (SLM), and electron beam melting. These procedures include spreading a thin layer of powder material before selectively fusing it with a laser or electron beam. PBF is well-known for creating parts with high accuracy and superior mechanical qualities, making it ideal for functional prototypes and end-of-life components in sectors such as aerospace and healthcare. However, build size and the need for significant post-processing constrain PBF procedures. The PBF diagram depicts the powder bed, recoating process, and energy supply, as well as the layer-by-layer fusion of powder to produce the finished item (as shown in Figure 1.18 below).

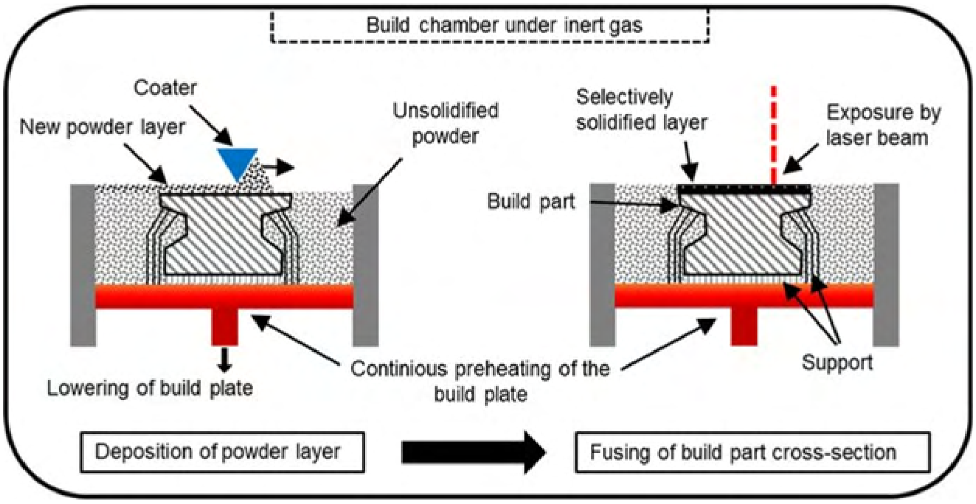

Figure 1.20: Schematics of powder bed fusion of metals using laser based system [**76**].

1.7 Mechanical Compression Testing of Lattice Structures

Mechanical compression testing of lattice systems is essential for determining their performance, especially in applications demanding significant energy absorption. The stress-strain curve derived from such testing generally has three separate regions: elastic, plateau, and densification (refer to Figure 1.19). The material deforms linearly in the elastic area with applied tension, returning to its original shape upon removal of the load. The plateau zone follows, where the material deforms plastically with a relatively constant tension, absorbing a significant amount of energy. The densification zone starts when the material's pores collapse and the structure compacts, resulting in a significant rise in stress. A longer plateau zone is favorable since it shows more energy absorption prior to densification, making the structure suitable for applications such as crash absorbers in the engineering fields. Following ASTM standards, notably ASTM D1621-16, is critical to obtaining accurate and dependable outcomes. These standards define the dimensions of the lattice structure as well as the maximum allowable deformation during compression testing. ASTM D1621-16, for example, recommends that the specimen's height-to-diameter ratio be between 2:1 and 3:1, with a maximum deformation of 10% of the original height to avoid end effects distorting the findings [**77**].

The research combines computational modeling, additive manufacturing, and experimental validation. Lattice structures will be designed using advanced CAD tools, such as nTopology and Creo Parametric, which provide precise control over lattice geometry. TPMS gyroid lattices will be fabricated using fused deposition modeling (FDM) with PLA bioplastics, chosen for their balance of strength, flexibility, and suitability for additive manufacturing. For the dental implants, biocompatible materials such as titanium alloys will be used to ensure compatibility with human bone tissue.

Additive manufacturing enables the creation of complex lattice structures that are difficult, if not impossible, to produce with traditional manufacturing methods. However, challenges such as ensuring material properties, addressing layer adhesion issues, and minimizing defects remain. These challenges will be addressed through iterative design modifications and rigorous testing to ensure that the printed structures meet the required mechanical and biological properties.

1.7.1 Lattice Structures and Gibson-Ashby Model

Gibson and Ashby et al. [**78**] investigate into how the mechanical properties of lattice structures affect their relative density. They focus on Young's modulus, plateau stress, and densification strain, which can be seen in Figure 1-19. The Gibson-Ashby model, which captures these connections, is well known. This model offers a complete foundation for comprehending how the mechanical behavior of lattice materials, such as foams and lattice structures, varies with density. For instance, the stiffness of a material, as measured by Young's modulus, directly correlates with the square of its relative density, suggesting that even minor changes in density can significantly enhance stiffness. Similarly, plateau stress, which is the stress level during significant plastic deformation, is proportional to relative density, determining the structure's ability to absorb energy. Densification strain, or the strain at which the material switches from the plateau area to densification, is critical. Understanding these interactions enables accurate design and optimization of lattice materials for specific purposes, such as cushioning and impact prevention. Engineers and material scientists may use the Gibson-Ashby model's insights to modify the mechanical properties of lattice structures to fit the needs of varied industrial applications, ultimately improving performance and efficiency [**78**].

The equation for stiffness ratio and relative density:

$$\frac{E_L}{E_S} = C_1 \left(\frac{\rho_L}{\rho_S} \right)^n \tag{1.5}$$

The equation for mechanical strength ratio and relative density:

$$\frac{\sigma_L}{\sigma_S} = C_2 \left(\frac{\rho_L}{\rho_S} \right)^m \tag{1.6}$$

The equation for evaluating densification strain and relative density:

$$\epsilon_D = 1 - \alpha \left(\frac{\rho_L}{\rho_S} \right) \tag{1.7}$$

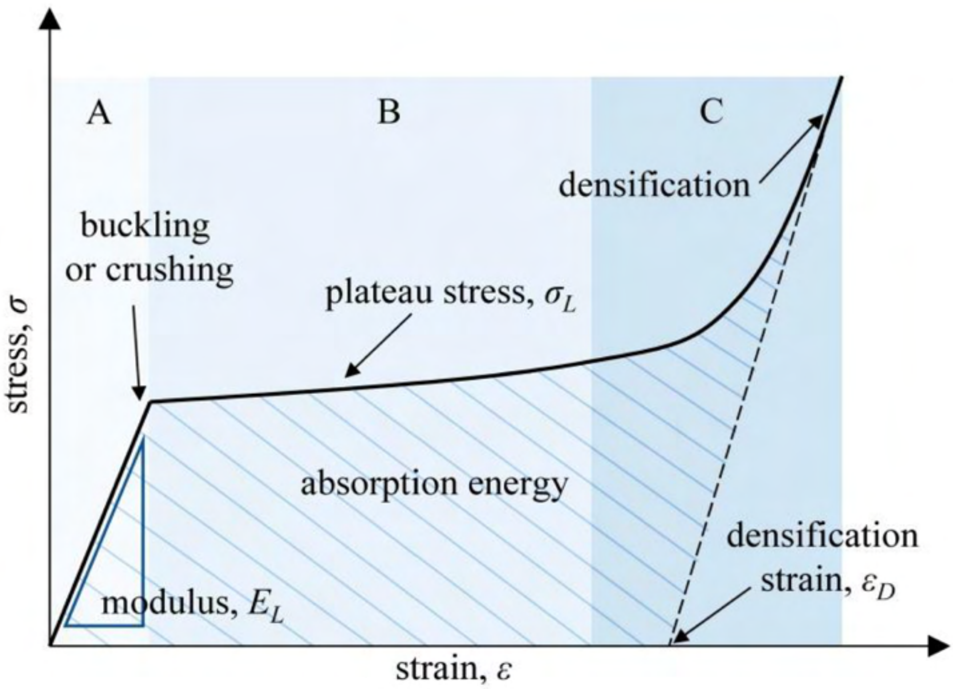

Figure 1.21: The regions of stress strain from mechanical compression of lattice cells [**79**].

where ϵ_D, ρ_L, and σ_L represent the elastic modulus, density, and yield strength of the lattice structures, respectively; E_S, ρ_S, and σ_S signify the properties of the underlying solid material. The onset densification strain, ϵ_D, indicates the start of the densification phase in the lattice stress-strain curve. This strain is an important metric in energy absorption applications because it specifies a realistic limit for how well the lattice structure can absorb energy without causing significant stress transmission. Beyond this limit, the structure continues to absorb energy, but at the expense of greater stress transfer, which may cause damage to adjacent items or harm to people.

Fitting the experimental data from compression tests determines the parameters C_1, C_2, n, m, and α. This fitting procedure aids in precisely defining lattice structures' mechanical behavior and ensuring the model's dependability for practical applications. These factors create correlations that are very important for better designing lattice materials so that they have the right mechanical properties and work better in load-bearing and energy-absorbing situations. Engineers may customize material qualities to particular use situations by knowing and using these constants, ensuring optimal efficiency and safety.

1.7.2 Energy Absorption and Lattice Structures

The mathematical formulations and implementations guarantee that lattice structures are not only functional but also efficient in real-world applications, resulting in safer and more lasting engineering solutions. Mechanical compression test data, such as stress-strain curves, give critical parameters for assessing lattice structure performance. The stress-strain curve provides information on the material's response to load, showing crucial spots including the elastic, plateau, and densification regions. One of the most important factors generated from these curves is the energy absorption per unit volume (W) [**78**]. We compute this by integrating the area under the stress-strain curve up to the strain at the start of densification. This integral shows the overall energy received by the material prior to significant densification, indicating its ability to absorb energy effectively without causing undue stress. We use the following computations to integrate these metrics into the design process:

The energy absorption per unit volume (W):

$$\int_0^{\epsilon_D} \sigma \, d\epsilon \tag{1.8}$$

Another important metric is energy absorption efficiency (η), which is defined as the ratio of energy absorbed in the plateau zone to the total energy absorbed up to the densification strain. This efficiency represents how efficiently the material achieves its intended function of absorbing energy. The ideal energy absorption efficiency (η_i) compares the energy absorbed by the lattice structure to that of an ideal absorber, serving as a performance standard.

The energy absorption efficiency (η):

$$\eta = \frac{\int_0^{\epsilon_m} \sigma \, d\epsilon}{\sigma_m} \tag{1.9}$$

The ideal energy absorption efficiency (η_i):

$$\eta_i = \frac{\int_0^{\epsilon_m} \sigma \, d\epsilon}{\sigma_m \epsilon_m} \tag{1.10}$$

The stress in the plateau zone (σ_p) is derived by averaging the stress values inside this region when the material endures large deformation without commensurate stress rise. This plateau stress is critical for applications that require materials to withstand impact or compression pressures without failure. The strain at the commencement of densification (ϵ_d) is determined when the stress-strain curve suddenly increases after the plateau area, signifying the material's shift to a denser state **[80]**. These values are critical for developing lattice structures with the best energy-absorption qualities. By understanding and using these mathematical principles, engineers can ensure that lattice structures are not only effective but also efficient in real-world applications. This helps to produce safer and more lasting technical solutions, especially in industries that need high energy absorption materials, such as automobile crash components and protective gear.

1.8 Finite Element Methods for Lattice Structures

1.8.1 Finite Element Analysis (FEA)

Finite element analysis (FEA) has become an indispensable tool for evaluating and optimizing lattice structures, particularly in engineering applications. Its capability to simulate complex mechanical behavior under various loading conditions allows researchers to study stress-strain responses with a high degree of accuracy. However, significant challenges remain in fully capturing the nuanced behavior of stress-strain curves, especially for lattice and foam structures where distinct regions of elasticity, plastic plateau, and densification play critical roles.

One persistent issue is the difficulty in validating FEA predictions against experimental results, particularly in compression tests of lattice structures. Accurately replicating the transition between elastic deformation, the plastic plateau region, and the densification phase has proven elusive. Discrepancies often arise due to limitations in the material models used in FEA, as well as oversimplifications in geometry and boundary condition assumptions. These gaps hinder the reliability of simulations and emphasize the need for improved methodologies.

In automotive applications, traditional crash box designs typically rely on thick-walled square or cylindrical cross-sections. While these designs offer simplicity, their energy absorption efficiency and strength-to-weight ratio remain suboptimal. Consequently, researchers continue to seek novel approaches to improve energy absorption while maintaining structural integrity. Similarly, in biomechanical engineering, the conventional design of dental implants—featuring a solid stem with screw threads—fails to consider the porous nature of cancellous bone. Modeling bone as a solid CAD structure in FEA introduces significant errors, with percentage deviations often exceeding acceptable thresholds. These inaccuracies call into question the reliability of such simulations in predicting real-world performance.

To address these limitations, our approach employs bioinspired lattice structures, such as Triply Periodic Minimal Surface (TPMS) gyroids and Voronoi lattices. These designs mimic natural lattice structures, providing superior mechanical properties, including enhanced energy absorption and improved strength-to-weight ratios. By integrating these advanced geometries into FEA workflows, we aim to overcome the traditional challenges of modeling stress-strain behavior and validate our results against experimental data with higher fidelity. This innovative methodology represents a significant departure from conventional design and modeling practices, offering a more reliable and efficient solution for engineering applications.

1.8.2 Lattice Simulation Challenges

Previous research on TPMS structures, such as Gyroid, Schwarz Diamond, and Schwarz Primitive, shows discrepancies between experimental and FEA results, especially in the stress-strain curve. The lattices, as shown in Figure 1.20, exhibit minimal deformation, failing to fully capture the three regions (Elastic, Plastic Plateau, and Densification) essential for accurate energy absorption analysis. While these traditional models provide some insight into the deformation behavior, they fall short in accurately representing the full range of stress-strain responses. Bioinspired lattice structures, like more refined TPMS models, offer improved deformation properties and more accurate stress-strain curves, addressing these gaps by providing a better representation of the energy absorption process and material performance [**3**].

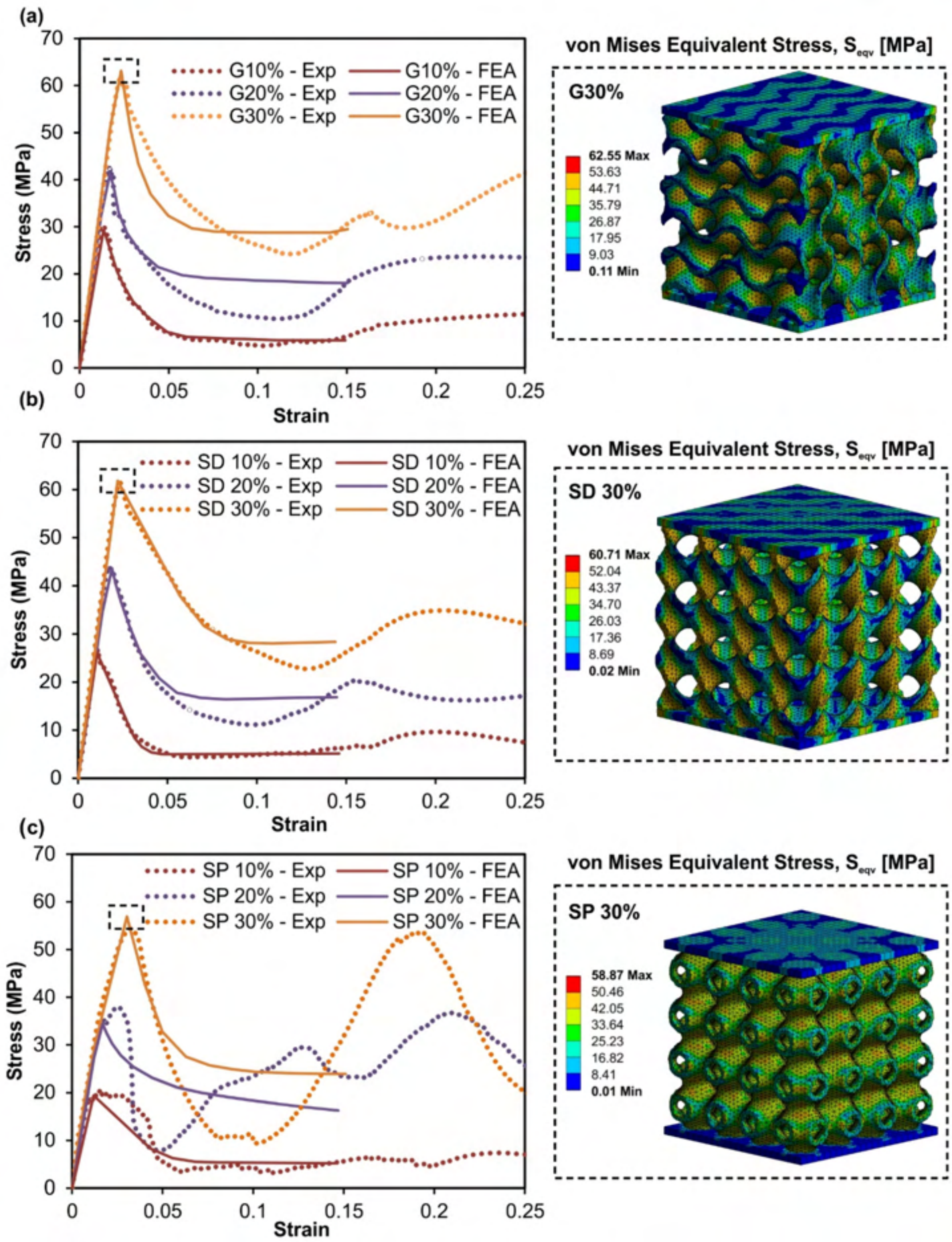

Figure 1.22: Comparison between experimental and FEA-determined stress-strain curves for (a) Gyroid, (b) Schwarz Diamond and (c) Schwarz Primitive TPMS structures at different relative densities [**3**].

1.8.3 Mesh Techniques

The quality of the finite element mesh is critical to achieving accurate and computationally efficient simulations. Mesh generation for lattice structures presents unique challenges due to their intricate geometries. Depending on the complexity and precision requirements, two primary meshing techniques are commonly used: voxel-based meshing and tetrahedral meshing.

Voxel-based meshing divides the lattice geometry into a grid of hexahedral elements. This technique is particularly effective for regular and periodic geometries, as it balances computational efficiency with sufficient accuracy. For instance, voxel meshes have been employed to model gyroid lattice structures, successfully capturing their mechanical behavior during compression tests.

In contrast, tetrahedral meshing offers greater flexibility for modeling irregular or complex geometries, such as Voronoi-based lattices or TPMS structures. A mesh convergence study is essential to determine the optimal element size that balances computational cost with accuracy. For example, simulations of sheet-based gyroid lattices in Abaqus showed that a mesh with approximately 40,000 elements achieved results within 1% of finer meshes, demonstrating the effectiveness of this approach. Refining the mesh and conducting convergence studies are essential steps to ensure the reliability of simulation results.

1.8.4 Boundary Conditions

To correctly simulate real-world situations, FEM requires the use of suitable boundary conditions and loading scenarios. Common boundary conditions for lattice structures include permanent support and frictionless contacts, which imitate limitations and interactions with surrounding materials. For instance, studies that looked at how gyroid lattices behave mechanically used fixed limits on the lower surface and a downward movement on the upper surface to represent compressive loads.

1.8.5 Loading Conditions

The accuracy of finite element analysis (FEA) heavily depends on the loading conditions considered during simulations. However, a common limitation in prior research is the assumption of static loading or unidirectional (axial) forces applied to dental implants during mastication. Such simplifications fail to represent the true clinical environment, where masticatory forces are dynamic, cyclic, and multidirectional. These assumptions introduce significant errors in FEA results, often leading to discrepancies between simulated predictions and experimental or clinical observations. Consequently, the reliability of such FEA outcomes remains questionable.

In this study, we addressed these gaps by incorporating clinically relevant dynamic cyclic loading conditions. Specifically, the loading was applied for durations of 0.5 sec, and 1.5 sec, at a frequency of 2 Hz, accurately replicating the cyclic nature of masticatory forces. Furthermore, we accounted for the multidirectional nature of these forces by implementing dynamic oblique loading. Equivalent forces, as experienced during mastication, were decomposed into three components—axial, mesiodistal, and buccolingual directions—and applied using a smooth step time function. This approach allowed us to simulate a realistic loading scenario that aligns more closely with clinical settings.

By adopting these advanced loading conditions, we significantly enhanced the reliability of the FEA results, reducing the margin of error and increasing their correlation with experimental data. This methodology sets our research apart from previous studies that relied on static or simplified loading assumptions. Moreover, our findings underscore the importance of considering dynamic and multidirectional forces in FEA studies of dental implants to ensure accurate predictions of mechanical behavior and clinical performance.

1.8.6 Parameters obtained from Finite Element Analysis (FEA)

FEM modeling variables, such as stress distributions, strain patterns, and energy absorption properties, are critical for optimizing lattice design. For example, stress in the plateau area and strain at the start of densification are important metrics for determining the energy absorption efficiency of lattice systems. These measurements allow for the creation of structures that optimize energy absorption while maintaining structural integrity. We can use mathematical parameters such as energy absorption per unit volume and stress-strain correlations to compare lattice designs and select the most efficient arrangement. FEM offers a complete framework for creating and optimizing lattice structures for a variety of engineering applications by combining CAD design, sophisticated meshing methods, and suitable boundary and load conditions. Our methodology advances the state of the art by integrating bioinspired lattice geometries, robust meshing techniques, and carefully calibrated boundary and loading conditions. By addressing the limitations of traditional designs and validation methods, we aim to achieve a more accurate and reliable framework for engineering applications, ranging from automotive crash boxes to biomechanical implants.

1.9 Motivation for the Study

The biomechanical field have significant problems in improving the mechanical performance and safety of their respective products. In the automotive industry, energy absorption during high-speed collisions remains a key concern. Traditional materials and designs frequently fail to provide adequate crashworthiness, resulting in fatal effects for automotive occupants. While traditional materials may absorb energy to some degree, they generally fall short of the standards for impact resistance and structural integrity during collisions. Current solutions sometimes include compromises between strength, weight, and energy dissipation, which limits their usefulness.Similarly, dental implants require proper stress distribution and interaction with the underlying bone tissue. Conventional designs, such as solid-threaded implants, do not reproduce the complex, anisotropic structure of human cancellous bone, resulting in poor osseointegration and mechanical stability. These constraints underscore the need for novel, more efficient materials that can more closely imitate the mechanical and biological features of real bone, thereby increasing both performance and patient outcomes. Traditional solid-threaded dental implant designs have long struggled with challenges such as effective bone-implant contact, osseointegration, and preventing stress-induced bone resorption. These designs frequently fail to transfer stress uniformly, resulting in areas of high stress or shielding that accelerate peri-implant bone loss and shorten the implant's life.Bioinspired lattice designs, such as composite TPMS gyroid lattices and Voronoi lattice structures, show potential for addressing such difficulties. Hybrid gyroid TPMS latticed implants, which feature both a solid neck and lattice structures, have demonstrated enhanced stress distribution under dynamic loading, making them particularly beneficial in clinical applications. These lattices, modeled after the efficiency of natural structures, provide a superior blend of strength, flexibility, and biological compatibility than standard materials. For example, TPMS gyroid lattices are excellent at spreading stress and absorbing energy, making them perfect for automobile applications like crash components. Voronoi lattices, inspired by bone's porous design, enhance mechanical compatibility and osseointegration in dental implants. These bioinspired designs fill the gap between traditional materials and the intricate mechanical and biological requirements of real-world applications.The primary objective of this research is to close current gaps in the mechanical performance of materials used for energy absorption in automotive applications, as well as to improve stress distribution in dental implants by taking advantage of the unique features of bioinspired lattice patterns. The research will specifically focus on TPMS gyroid lattices for crash components and Voronoi lattices for dental implants, with the goal of generating optimum designs that overcome the constraints provided by existing materials in both sectors. This study develops and evaluates novel lattice structures, such as composite and hybrid gyroid TPMS designs, to improve the safety and efficacy of automotive and biomedical applications using extensive experimental testing, finite element analysis (FEA), and sophisticated modeling techniques.

This study highlights the crucial need for innovation in biomechanical engineering to enhance safety and performance. In the automobile industry, the goal is to create materials that can efficiently absorb energy during high-speed accidents. Composite TPMS gyroid lattice structures (CTG) offer a viable alternative. These designs exhibit higher energy absorption capabilities by combining walled and regular TPMS gyroid lattices utilizing nTop's Boolean subtraction approach and producing them using fused deposition modeling (FDM) using PLA bioplastics. Experimental testing and finite element analysis (FEA) demonstrate its efficiency, with the Gibson-Ashby model finding bending as the dominant deformation mechanism, especially at relative densities below 15In parallel, the biomedical industry, notably dental implant engineering, is challenged with reproducing the intricate structure of human cancellous bone. Full and hybrid gyroid TPMS latticed dental implants with three different cell sizes provide improved stress distribution and biomechanical stability under dynamic loading. These designs promote mechanical compatibility with bone tissue and osseointegration. Furthermore, biomimetic Voronoi lattice structures with porosity like real bone (60–90%) overcome the constraints of previous designs by reducing deformation under biting forces and boosting tissue ingrowth. Advanced modeling tools and FEA optimize these designs to enhance implant stability and mechanical performance. This study shows how bioinspired lattice structures may improve energy absorption in biomechanical applications and advance dental implant design. This study intends to improve lattice structures for safer and more effective solutions in biomechanical engineering by integrating experimental validation with FEA. This study covers the design, construction, and analysis of bioinspired lattice structures aimed at addressing significant challenges in crash box energy absorption and dental implant optimization. The research integrates findings from three main areas: the development of composite TPMS gyroid lattice structures for automotive applications, the design of fully and hybrid gyroid TPMS latticed dental implants with varying cell sizes, and the creation of biomimetic Voronoi lattice structures to replicate the porosity of human cancellous bone.

The automotive component of this study focuses on optimizing composite TPMS gyroid lattice structures with different relative densities, created using fused deposition modeling (FDM) and PLA bioplastics. Mechanical testing is conducted using Shimadzu 100 kN equipment to validate the findings, while finite element analysis (FEA) is employed to determine the optimal configurations for energy absorption and mechanical performance in high-speed collisions. The aim is to identify the best lattice designs that improve crashworthiness, occupant safety, and energy dissipation in automotive crash components.

In the biomedical domain, the study explores fully and hybrid TPMS gyroid latticed dental implants. These designs incorporate three different cell sizes to improve stress distribution and mechanical stability, offering potential solutions to issues such as poor osseointegration and stress shielding that affect traditional implants. The research also investigates biomimetic Voronoi lattice structures, designed with pore sizes ranging from 1.0 to 2.5 mm and porosities of 70% to 95%. These lattices are optimized for improved osseointegration, mechanical stability, and load transfer, with FEA simulations conducted to investigate their biomechanical behavior under simulated biting stresses. The goal is to enhance the longevity and performance of dental implants while mimicking the mechanical properties of human bone.

Furthermore, this study incorporates a thorough review of existing literature on bioinspired lattice structures. This literature analysis provides the foundational knowledge required for the experimental and computational work undertaken in this research. By addressing both automotive and biomedical applications, this work highlights the adaptability of bioinspired lattice structures and their potential to overcome a range of technical challenges across diverse industries.

In addition to the specific areas covered, this study aims to push the boundaries of current engineering practices by demonstrating how bioinspired design principles can be applied to improve safety, efficiency, and biocompatibility in automotive and biomedical fields. The research aims to provide innovative solutions to long-standing problems and pave the way for the future integration of lattice structures into real-world applications.

1.10 Research Objectives

This PhD thesis explores the potential of bioinspired lattice structures to address major difficulties in biomechanical engineering. The first research investigates the creation of composite gyroid TPMS lattices by combining walled and conventional gyroid lattices using a Boolean subtraction method, resulting in five configurations with varying relative densities. The second fully explores hybrid gyroid TPMS latticed dental implants with three different cell sizes to improve stress distribution and mechanical stability. The third study examines biomimetic Voronoi lattice structures with four different hole diameters to simulate the porous property of human cancellous bone.

The main study topics include how these lattice structures may increase energy absorption for vehicle crash box design and optimize stress distribution, osseointegration, and mechanical stability in dental implants. The study's goal is to answer these concerns by constructing and testing composite TPMS gyroid lattices with relative densities ranging from 14% to 54% to improve crashworthiness, utilizing sophisticated manufacturing processes and finite element analysis (FEA). Furthermore, it aims to create and test fully versus hybrid gyroid TPMS latticed implants with three different cell sizes, as well as biomimetic Voronoi lattice structures with pore diameters ranging from 1.0 to 2.5 mm and porosities ranging from 70% to 95%. This study attempts to determine ideal designs for energy absorption and implant stability by studying their biomechanical behavior under dynamic loads and biting stresses. This study presents unique answers to issues in biomechanical engineering by thoroughly evaluating these revolutionary ideas.

The main objectives of this research are as follows:

- **For Energy Absoprtion Componenet Design:** To optimize TPMS gyroid lattice structures for energy absorption in crash components. The study will focus on developing five different lattice configurations, varying relative densities between 14% and 54%, and testing their performance under dynamic loading conditions. FEA will be used to simulate their behavior, while experimental testing will validate these simulations.

- **For Biomedical Applications:** To explore the use of Voronoi lattice structures in dental implants, focusing on improving stress distribution, osseointegration, and implant stability. The research will compare fully latticed designs to hybrid implants using three different cell sizes to identify the most effective configuration. FEA will simulate their mechanical behavior under dynamic biting forces, and experimental validation will be conducted to confirm these results.

The research will align these objectives with the methods and tools employed later in the thesis- ensuring that the lattice structures' performance in real-world conditions is thoroughly tested.

The study will explore the following research questions:

- **For Energy Absoprtion Componenet Design:** How can TPMS gyroid lattice structures be optimized to improve energy absorption in automotive crash components, and what lattice configurations offer the best balance of strength and lightweight construction?
- **For Biomedical Applications:** How can Voronoi lattice structures improve the biomechanical performance of dental implants, specifically in terms of stress distribution, osseointegration, and long-term stability?

These questions will be addressed through a combination of FEA simulations and experimental validation, with the aim of identifying optimal lattice configurations that can be applied to engineering applications.

1.11 Summary

In conclusion, Chapter 1 established the framework for this study by explaining the study's major issues and establishing its main components. The issue statement emphasized the shortcomings of existing designs in terms of vehicle crashworthiness and dental implant stability, highlighting the need for creative solutions inspired by nature. We developed research goals and objectives to propel the study of bioinspired lattice structures, focusing on enhancing mechanical performance in biomechanical applications. We defined the study's parameters, which included the creation, manufacturing, and examination of Voronoi lattice structures for dental implants and composite TPMS gyroid lattices for automobile use. We emphasized the study's relevance, especially its potential impact on automobile safety, dental implant integration, and the broader field of biomechanical engineering. This chapter lays the groundwork for the ensuing extensive investigation of bioinspired lattice structures, offering a complete foundation for the research reported in this study. The next chapters will go further into the literature review, methodology, experimental data, and analysis, expanding on the groundwork laid here to show bioinspired designs' revolutionary potential in tackling difficult engineering issues.

Chapter 2

ENHANCED ENERGY ABSORPTION WITH BIOINSPIRED COMPOSITE TPMS-GYROID LATTICES MANUFACTURED VIA FUSED FILAMENT FABRICATION

This chapter addresses the design and optimization of bio-inspired composite TPMS-gyroid lattices for improved energy absorption in engineering applications.

2.1 Introduction

Lattice structures are classified into three types: random, periodic, and pseudo-periodic. Voronoi and Delaunay structures, which are formed using beams or struts, are examples of random lattices. Periodic lattices are further classified into conformal, homogeneous Triply Periodic Minimal Surfaces (TPMS) and non-conformal, heterogeneous structures such as beam/strut-based and shell-based. The TPMS family includes popular configurations such as Lidinoid, SplitP, Neovius, Schwartz Diamond, and Gyroid. Meanwhile, beam/strut-based periodic lattices are made up of basic geometric shapes like hexagonal honeycomb and triangular honeycomb, while more sophisticated forms include Kelvin cell, octet, and diamond, as well as cubic versions like face-centered cubic and body-centered cubic[**37, 81, 82**]. Lattice structures—especially the Gyroid TPMS lattice, which is based on the triply periodic minimal surface (TPMS)—are becoming more and more popular in fields like biomedical, aerospace, and automotive engineering. This is due to their remarkable mechanical properties and adaptability [**83**–**88**] enhancing both shape and function, the bio-inspired Gyroid TPMS lattice draws its design ideas from nature, such as insect wings [**89**–**93**]. These lattices are perfect for distributing stress and absorbing energy, which are essential for creating robust yet lightweight solutions. The main advantages associated with TPMS lattices are their complex, continuous surfaces, which have better mechanical properties than typical lattice types. They have distinct deformation properties, such as bending rather than buckling, which contribute to improved energy absorption during impacts. However, innovative lattice structures require precise production, modeling, finite element analysis, and precise parameter management for impact absorption, while advanced fused filament fabrication challenges material constraints like polylactic acid (PLA) [**94, 95**]. Due to its biodegradability, PLA is a desirable material for a variety of applications, including orthopedic bone fixation, surgical sutures, drug delivery systems, and eco-friendly food packaging. PLA also breaks down into non-toxic compounds [**96**]. Moreover, PLA's application has been extended by recent studies, which take into account its ability to enhance vehicle crashworthiness [**97, 98**]. The butterfly wings are a magnificent example of structure matching function. The gyroid TPMS lattice structure (GTLS) was derived from the gyroid-type triply periodic minimum surface (TPMS) structure in this study. This pattern was inspired by the scales on a butterfly's wing (Figure 2.1a) [**92**], showing how inventive engineering solutions frequently draw inspiration from natural designs. Because they have high stiffness-to-weight ratios and can absorb energy, lattice structures are great for load-bearing and biocompatible uses. Their patterns are repeated and connected [**89, 99–101**]. Lattice structures' adaptability in design contributes to their versatility by allowing modification for certain applications [**99, 100**]. In numerous disciplines, the efficacy of lattice structures, which are characterized by repetitive patterns of interconnected elements, has been demonstrated. High stiffness-to-weight ratios and energy absorption capacities are just two of the extraordinary mechanical properties provided by the lattice's inherent porosity and shape [**101**]. Applications requiring load-bearing capacity and biocompatibility, such as structural engineering, aircraft, and medical implants, significantly benefit from these properties. Changing configurational features such as cell size, shape, and arrangement enables lattice structures to be tailored to specific applications [**89**]. Similar to this research, recent studies have attempted to increase the energy-absorbing capacity of lattice structures by combining two distinct lattice topologies [**101**]. Using this method, it is possible to construct a composite lattice with superior mechanical properties by combining the advantages of multiple lattices. Previous research has demonstrated the effectiveness of this method in enhancing energy absorption within lattice structures for impact reduction [**102**]. Such efforts demonstrate the necessity of developing new techniques to enhance the inherent lattice benefits in numerous engineering disciplines. Studies aimed at enhancing the mechanical strength of lattice structures have led to advancements in manufacturing and design [**99**]. Studying bio-inspired lattice structures with TPMS diamond shapes displays their promise for aerospace applications owing to their increased lightweight and strength [**103**]. This research examines the flexural properties of ABS TPMS diamond sandwich panels at different densities (25%, 35%, 45%, and graded). And it uses digital image correlation for deflection experiments and theoretical analysis for mechanical efficiency findings. Based on the shape of the human tibia, one study showed hybrid structures that combine elliptical and circular connections between IWP and Gyroid TPMS types, showing better energy absorption abilities [**104**]. This achievement highlights the possibility of developing lightweight porous structures with improved energy absorption and impact resistance, providing valuable insights for future engineering applications. There has been little research on hybrid Triply Periodic Minimal Surface (TPMS) designs that either gradient modify their parameters or integrate numerous patterns into a single design influenced by natural shapes [**105**]. Another study explored this terrain by creating hybrid structures that included linear and radial aspects of diamond and gyroid shapes and then evaluating their mechanical properties using both experimental and theoretical methods. Their results revealed a significant rise in plateau stresses of 19% and 11% in hybrid models compared to uniform equivalents, with hybrid designs also demonstrating 10% and 7% improved specific energy absorption. Furthermore, a strong correlation was found between the actual data and the simulation results [**106**]. Extending their study, they found that hybrid structures outperform solitary solutions in terms of mechanical performance, notably compressive strength and energy absorption [**107**]. Researchers have used the Gibson-Ashby model to evaluate 3D-printed lattice structures made from materials like PLA [**88, 108, 109**]. The interplay between lattice geometry, material properties, and mechanical response controls engineered lattice behaviors.

These advancements enable the production of lattice structures with properties that surpass those of conventional engineering materials, paving the way for new ways of exploring lattices [**87, 110, 111**]. The combinations of two TPMS-gyroid lattice structures and advancements in additive manufacturing techniques has revolutionized lattice fabrication [**88, 112–114**]. Their controlled deformation and energy dissipation upon impact has shown that they could be used for shock absorption applications, especially in crash boxes and bumper beams for cars [106–110]. Previous research has verified the effectiveness of lattice-based bumper beams in absorbing impact energy and mitigating vehicle damage [**48–50**]. These applications demonstrate the suitability of lattice structures in regulating the absorption of energy in a variety of scenarios. This work aims to explore the mechanical properties of a newly designed composite Gyroid TPMS lattice that is advanced and bioinspired. This unique lattice combines walled TPMS with normal TPMS gyroid lattices using a Boolean subtraction method. The finite element method (FEM) is a powerful computer methodology for structural analysis that provides insights into complicated behaviors under different situations [**53, 115, 116**]. We extensively use finite element analysis software to simulate and numerically assess various lattice structures. In biomimetic engineering, FEM simulates stress distribution in dental implant systems using variable-pore size Voronoi lattices, replicating trabecular bone structures [**117**]. This method is necessary to evaluate how much energy quasi-statically loaded hybrid lattice structures can absorb, which leads to better mechanical performance [**118, 119**]. This study examines how well the lattice works at five different relative densities to further research if it has

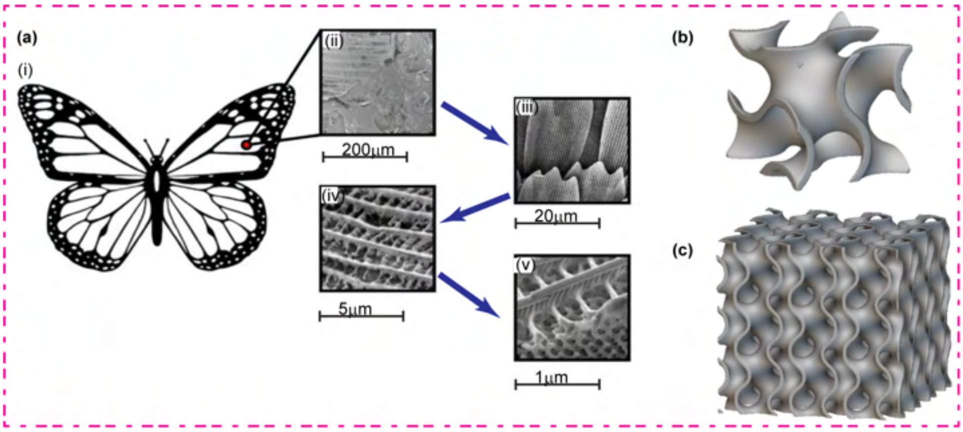

Figure 2.1: Natural TPMS-like structures: (a) Gyroid patterns in butterfly wings: (i) Diagram of the butterfly sourced from **[91]** ; (ii-v) Scanning electron micrographs depicting the cross-sectional view of a butterfly wing scale, with (v) being adapted from **[92]**; (b) unit cell of walled gyroid TPMS lattice, and (c) walled TPMS gyroid lattice structure.

better mechanical properties than the single TPMS-gyroid and walled TPMS-gyroid lattices. We investigate the nuances of the Gibson-Ashby model, in particular its energy-absorbing ability and deformation behavior. Our new approach provides a comprehensive analysis of the PLA material family by comparing normalized energy absorption efficiency with normalized stress. Using the finite element method, we demonstrate that the stress-strain curve from mechanical compression tests accurately reshows the linear elastic, plastic plateau, and densification phases. Our results are used in a real-world scenario utilizing a crash box case study that is built from a composite TPMS gyroid lattice with various relative densities. Our goal is to further advance the study of bio-inspired lattice structures, specifically enhancing vehicle structural dynamics to increase crashworthiness.The of symbols and their corresponding explanationsused in this study specifically for Chapter 2, are listed below in Table 2.1.

Table 2.1: List of symbols and their corresponding descriptions utilized in this study.

Symbols	**Descriptions**
ρ	Density of the gyroid lattice structure, Kg/m^3.
ρ_{PLA}	Density of the bulk materials from which the gyroid lattice is made, Kg/m^3.
ρ^*	Volume fraction, or relative density, of the gyroid lattice; ρ/ρ_S.
E	Young's modulus of gyroid lattice.
E_S	Young's modulus of the bulk materials from which the gyroid lattice is made.
E^*	Relative Young's modulus of the Composite TPMS gyroid lattice, E/E_S.
σ_{pl}	Plateau stress of composite TPMS gyroid lattice structure.
σ_y	The yield stress of the bulk materials from which the gyroid lattice is made.
σ^*	Relative plateau stress of the gyroid lattice.
ε	Effective strain of the gyroid lattice structure.
σ_{latt}	Stress of composite TPMS gyroid lattice structure.
p	The porosity of the composite lattice.
ε_D	Densification strain of composite TPMS gyroid lattice.
MCG	Mass of composite TPMS gyroid lattice, kg.
WV	Energy absorption per volume of composite TPMS gyroid lattice, MJ/m^3.
η	Ideal energy absorption efficiency of composite lattice.
γ	Efficiency of energy absorption by composite TPMS gyroid lattice.
C	Gibson–Ashby constant.
n	Gibson–Ashby exponent.

2.2 Materials and Methods

2.2.1 Lattice 3D CAD Design

The lattice structure's design began with the creation of a comprehensive 3D CAD model using nTopology's software (Figure 2.2).

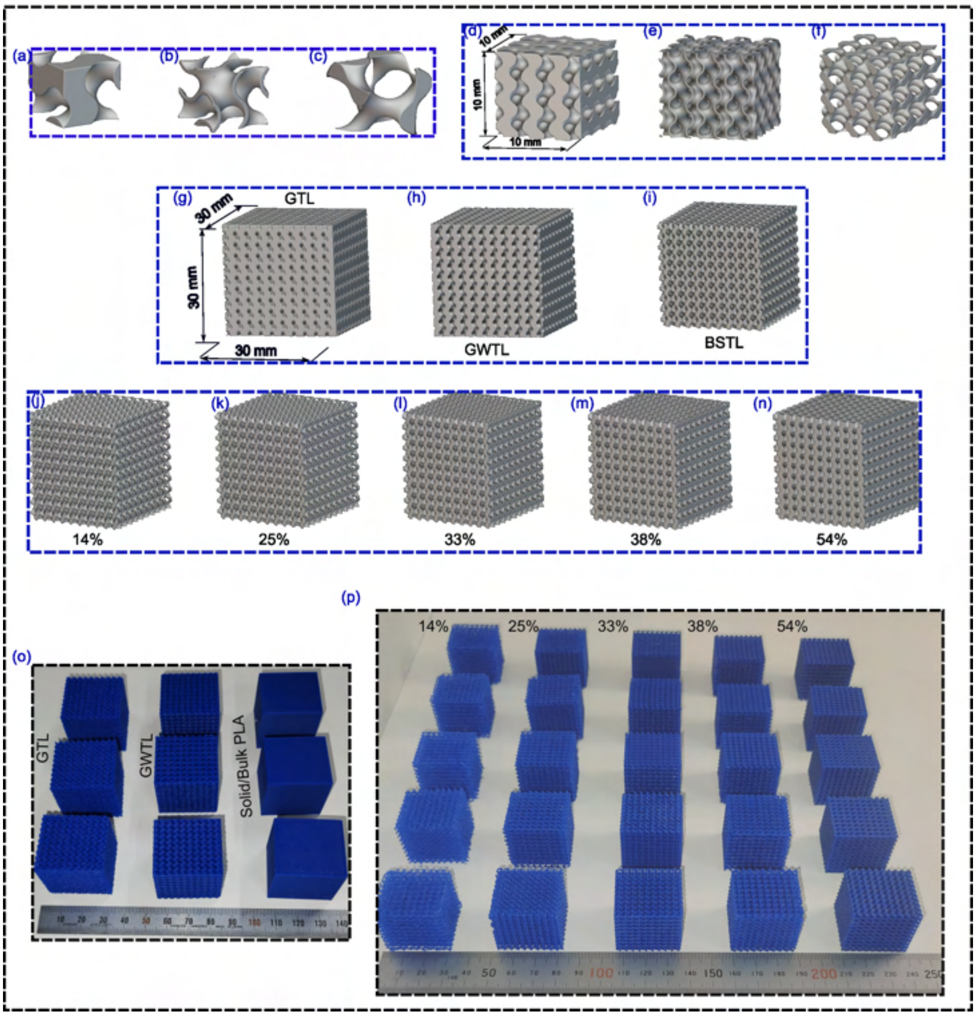

Figure 2.2: The TPMS-gyroid, walled TPMS-gyroid, and composite TPMS-gyroid structures with a uniform cell size of 10×10×10 cubic millimeters and an overall dimension of 30×30×30 cubic millimeters (d, e, f, g, h, and i), alongside the unit cell (a, b, and c). And Computer-Aided Design (CAD) model of the composite TPMS-gyroid with five distinct relative densities is showed (j, k, l, m, and n).3D-printed blue PLA lattice structures are depicted (o and p) for visual reference. GTL: gyroid TPMS lattice; GWTL: gyroid walled-TPMS lattice; and BSTL: Boolean subtracted composite TPMS lattice.

The intricate geometry of the TPMS-gyroid composite TPMS lattice was accurately constructed, incorporating the specific parameters necessary for evaluating mechanical performance as outlined in Table 2.1. The relative densities of the composite lattice were systematically varied to encompass a broad spectrum of potential applications. The lattice design accounted for loading conditions, ensuring that the targeted mechanical parameters were reshowative of real-world scenarios. A new TPMS gyroid lattice unit cell (see Figure 2.2c) is made by putting together a regular TPMS gyroid lattice unit cell (see Figure 2.2a) and a walled TPMS gyroid unit cell (see Figure 2.2a). As seen in Figure 2.2, the normal unit cell has a closed-cell design with thick walls, while the walled unit cell has a closed-cell, sheet-type TPMS gyroid lattice. In contrast, the newly developed composite unit cell has an open-cell structure with beam-type walls, which are especially visible at lower relative densities.

2.2.2 Lattice Additive Manufacturing

To transform the conceptual lattice structures into physical objects, we employed fused deposition modeling (FDM) using a 3D printer. For this procedure, we picked a 1.75-mm-diameter blue PLA filament because of its excellent mechanical properties and adaptability for the manufacturing process. Table 2.3 outlines the specific settings for the RAISE3D PRO 2 printer, which we used to create all lattice samples, while Table 2.4 lists the properties of the PLA material. The slicing software 3DRaise was utilized to convert the intricate 3D CAD model into precise print paths, accounting for layer-by-layer deposition to accurately reproduce the lattice design (refer to Figure 2.2). The orientation of the lattice samples during 3D printing was in the flat (X-Y) plane. This orientation is chosen because lattice structures are self-supporting, eliminating the need for additional support during manufacturing.

Table 2.2: Unit cell thickness of constituent gyroid lattice and relative density of corresponding novel lattice.

Thickness of Sheet TPMS-gyroid (mm)	**Thickness of Walled TPMS-gyroid (mm)**	**Composite TPMS-gyroid (ρ/ρ_s)**
0.4	1.2	14%
0.3	1.0	25%
0.25	0.75	33%
0.2	0.6	38%
0.1	0.1	54%

Table 2.3: Parameters for fused deposition modeling (FDM) 3D printing of lattice specimens.

Printing Parameters	**Values**
Printing speed	50 mm/s
Printing temperature	205 °C
Bed temperature	65 °C
Infill	100%
Extrusion width	0.48 mm
Filament diameter	1.75 mm
Raster angle	45°/-45°

Table 2.4: Physical and mechanical properties of blue PLA filament.

Property	**Value**	**Testing Conditions**
Density	1.2 g/cm^3 @ 21.5 °C	ASTM D792 - ISO
Young's modulus	2636 ± 330 MPa	ASTM D638-ISO 527, Flat (X-Y)
Tensile strength	46.6 ± 0.9 MPa	ASTM D638-ISO 527, Flat (X-Y)
Elongation at break	1.90 ± 0.2 %	ASTM D638-ISO 527, Flat (X-Y)

2.2.3 Measurement of Density and Relative Density

The Shimadzu Electronic Balance TW223N Series (Shimadzu Corporation, Kyoto, Japan) was used to accurately measure the density of the 3D-printed PLA-based TPMS gyroid lattice structures. PLA's inherent theoretical density was determined to be 1.24 g/cm$^{\mathbf{3}}$. For increased precision, a set of six measurements were carefully recorded. Both the relative density and the porosity percentage were calculated precisely in accordance with ASTM D792-98 [**120**]. To do this, the equations (Eq. 2.1), (Eq. 2.2), and (Eq. 2.3) in the referenced standard were used.

The actual density of the composite TPMS gyroid lattice cube is calculated by:

$$\rho_{\text{actual}} = \frac{M_{\text{CG}}}{V_{\text{CG}}} \tag{2.1}$$

The relative density of each composite TPMS gyroid lattice cube is calculated as follows:

$$\rho^* = \frac{\rho}{\rho_{\text{PLA}}} \tag{2.2}$$

The porosity of the composite lattice can be calculated as:

$$P = \frac{\rho_{\text{PLA}} - \rho}{\rho_{\text{PLA}}} = 1 - \rho^* \tag{2.3}$$

2.2.4 Mechanical Compression of Lattice

The quasi-static compression load test was conducted on all sample TPMS samples with universal testing machine SHIMADZU AG-100kNXplus equipped with 100kN load cell and with 0.005 -1000mm/min crosshead speed. All the TPMS Samples were compressed between hardened steel plates with flatten surface top and bottom to avoid any small misalignment during compression loading according to ASTM D638-14 [**96**]. The sample specimens were placed between the moving top plate and fixed bottom plate of the test machine where the compressive strain in this reached up to 60% of the original specimen heights in the building direction, which is the point where the densification dominates. The strain rate utilized for this study was 0.03 mm/s. To assess the mechanical properties of composite TPMS gyroid lattice (CTL) structures, we designed an experiment with five different relative densities. For a more comprehensive analysis, we tested a solid PLA cube, a standard TPMS gyroid lattice, and walled TPMS gyroid lattices. We performed at least three repeated mechanical compression tests on each sample type to confirm the findings' reliability and accuracy. The setup for testing the mechanical compression of TPMS gyroid lattices and solid PLA cubes is shown in Table 2.5. This enabled the determination of peak stress, plateau stress, densification strain, and other vital parameters. The specimens underwent gradual compression until densification, allowing a comprehensive understanding of their deformation behavior and energy absorption capacities. We used (Eq. 2.4) for experimental design.

The total number of tests can be calculated as:

$$\text{Total no. tests} = \text{no. levels} \times \text{no. replicas} \tag{2.4}$$

Gibson-Ashby Model

The parameter 'n' is of considerable importance in characterizing the various forms of deformation that occur within cellular structures [**85, 121–123**]. The Gibson-Ashby model, a cornerstone in the analysis of cellular materials [**123, 124**], establishes critical relationships among a multitude of parameters inherent to cellular structures. These fundamental parameters encompass relative density (E/E_S), plateau strength (σ_{pl}), elastic modulus (E), and the strain at the densification point (ϵ_D). These intricate relationships, elegantly described by power law equations (2.5) and (2.6), offer profound insights into the mechanical properties of composite TPMS gyroid lattice structures. Theoretically, power indices n and m are anticipated to be 1.5 and 2 for structures dominated by bending and emphasizing strength, and 1 for those governed by stretching. A value of "n" equal to or greater than 2 indicates a prioritization of rigidity. 'n' values that fall within the range serve as an alternative definition of a mixed mode of deformation.

Table 2.5: Experimental design for mechanical compression testing of composite TPMS gyroid lattices and solid PLA cubes.

Levels	**Relative Density (%)**	**Replica**
Solid PLA Cube	-	3
GTL	-	3
WGTL	-	3
CTL14	14%	3
CTL25	25%	3
CTL33	33%	3
CTL38	38%	3
CTL54	54%	3

GTL: Conventional gyroid TPMS lattice; WGTL: Walled gyroid TPMS lattice; CTL: Composite TPMS lattice with relative density range.

The relationship between mechanical stiffness and relative density is given by:

$$\left(\frac{E}{E_S}\right) = C_1 \left(\frac{\rho}{\rho_S}\right)^{n_1} \tag{2.5}$$

The relationship between mechanical strength and relative density is given by:

$$\left(\frac{\sigma_{\text{pl}}}{\sigma_{\text{ys}}}\right) = C_2 \left(\frac{\rho}{\rho_S}\right)^{n_2} \tag{2.6}$$

The modified Gibson-Ashby model is crucial for applications requiring higher stiffness, like orthopedic surgical scaffolds and vehicle shock absorption systems. It is obtained from combination of equations (2.5) and (2.6). It aligns with previous lattice design studies and allows comparison of strength-to-stiffness ratios among different relative density composite TPMS gyroid lattice structures **[125][126][127]**.

The modified Gibson-Ashby model for the relationship between relative stiffness and relative strength is given by:

$$\left(\frac{\sigma_{\text{pl}}}{\sigma_{\text{ys}}}\right) = C_3 \left(\frac{E}{E_S}\right)^{n_3} \tag{2.7}$$

The densification strain can be evaluated using:

$$\epsilon_D = 1 - \alpha \left(\frac{\rho}{\rho_S}\right) \tag{2.8}$$

2.2.5 SEM of Deformed and Undeformed Lattice

The SEM image of newly constructed TPMS lattice with 38% relative density were captured from two different planes XZ and YZ for both before and after compression testing. For such purposes the JSM-7400F field emission scanning electron microscope (FE-SEM) was utilized. The morphology and deformation behavior of 3D printed TPMS-gyroid lattice structure was observed using FE-SEM. Scanning electron microscopy (SEM) analysis was conducted on both deformed and undeformed lattice specimens. This microscopic examination provided insights into the microstructural changes induced by mechanical deformation. SEM imaging aided in visualizing lattice distortions, fracture patterns, and any material irregularities arising from the compression testing process. And there are defects from the FDM printing due to printing filament melting rate variations which reduce the mechanical strength.

2.2.6 finite element analysis (FEA) of Lattice

To accurately capture the stress-strain characteristic of the 3D printed TPMS lattice structure a Finite element model (FEM) was developed. In the numerical simulation, the commercial software package ANSYS 2022 was utilized. Following the experimental setting, similar boundary conditions are applied to all FE models. The FE mesh entirely consists of tetrahedrons. Since FEM is an approximate solution for the purpose of reducing numerical errors, Ramesh surface, robust tetrahedral mesh, followed by FE volume mesh were applied during FE discretization. Further, to accurately capture the experimental compression scenario from ANSYS Workbench 2022 the LS-DYNA analysis system was used. The TPMS lattice structure has an overall seed size of 0.2mm and different mesh elements for all structures. To better simulate the post-softening (plasticity) behaviors after the lattice yield, multi-linear isotropic hardening model was utilized by supplying the plastic strain and stress in the plastic region. However, the elastic region just needs the young's modulus and poison's ratio calculated from experimental results.To support the experimental findings and gain further insights into the mechanical behavior of the bio-inspired gyroid composite TPMS lattice, finite element analysis (FEA) was conducted. Computational simulations were performed to predict mechanical responses under varying loading conditions. The FEA models were designed to replicate the experimental setup, allowing the extraction of stress-strain relationships and energy absorption properties. The FEA outcomes served as a validation tool for the experimental data

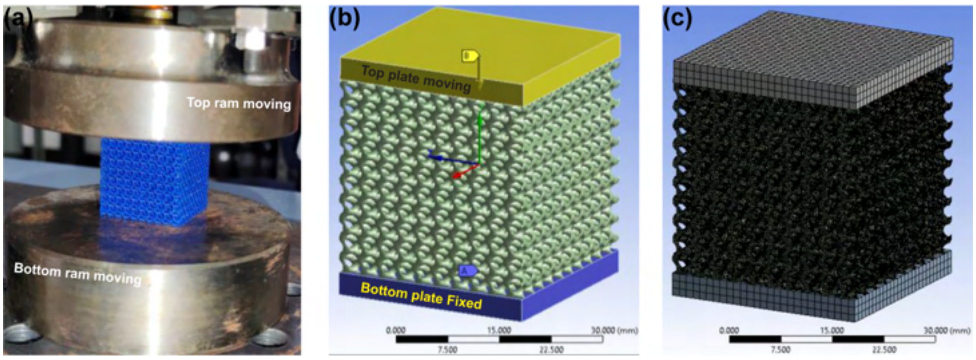

Figure 2.3: a) The physical lattice specimen fabricated for mechanical compression testing, b) The three-dimensional (CAD) model of the lattice structure with boundary conditions (BCs) configured for finite flement analysis (FEA), and c) The finite element (FE) mesh representation of the lattice model.

and provided a deeper understanding of the composite lattice's intricate mechanical behavior. The FE boundary conditions, and the corresponding FE meshing of the sample is shown in Figure 2.3b and 2.3c, respectively. Figure 2.4 shows the assembly of top and bottom plates with five varied relative density composite TPMS gyroid lattice utilizing ANSYS space Claim and effortlessly linked into ANSYS LS-DYNA for further dynamic explicit compression analysis.

2.2.7 Energy Absorptions

Extensive research has been conducted on the complex energy absorption properties of a PLA-based composite TPMS gyroid lattice, leveraging key parameters including energy absorption value (W_V), energy absorption efficiency (γ), and ideal energy absorption efficiency (η). In this particular framework, the symbol (W_V) reshows "energy absorption," and Equation (2.9) provides a dependable approach to calculating it in relation to volume **[128]**.

$$W_V = \int_0^{\epsilon} \sigma(\epsilon)\, d\epsilon \tag{2.9}$$

In this particular case, ϵ denotes a stochastic strain, σ_{latt} reshows stress, and ϵ_{latt} is the corresponding strain; σ is a function that depends on ϵ **[129]**. The determination of the optimal energy absorption state in this composite lattice involves consideration of the energy absorption efficiency parameter, which can be mathematically expressed as **[128]** using Equation (2.10):

$$\gamma = \frac{\int_0^{\epsilon_{\text{latt}}} \sigma_{\text{latt}}(\epsilon_{\text{latt}})\, d\epsilon_{\text{latt}}}{\sigma_{\text{latt}}(\epsilon_{\text{latt}})} \tag{2.10}$$

In this case, γ reshows the efficiency of energy absorption by the PLA-based composite gyroid lattice during compression deformation, thereby decreasing the flow stress.

In addition, we include the following concept: ideal energy absorption efficiency (η) **[128]**, defined using Equation (2.11):

$$\eta = \frac{\int_0^{\epsilon_{\text{latt}}} \sigma_{\text{latt}}(\epsilon_{\text{latt}})\, d\epsilon_{\text{latt}}}{\sigma_{\text{latt}}(\epsilon_{\text{latt}})\, \epsilon_{\text{latt}}} \tag{2.11}$$

The ratio of the area enclosed by the stress-strain curve of the composite lattice to the rectangular area it encompasses shows the ideal energy absorption efficiency at any given strain. Furthermore, an energy envelope concerning lattice structures composed of PLA materials can be obtained by normalizing the cumulative energy absorption per unit volume of this composite TPMS gyroid lattice by the Young's modulus of its base material and plotting a curve against the normalized stress (which is also divided by the Young's modulus) **[35]**. It is important to remember that both the normalized stress axis and the normalized energy absorption efficiency axis are logarithmic. This makes it possible to accurately show the complex mechanical properties that these lattice structures exhibit.

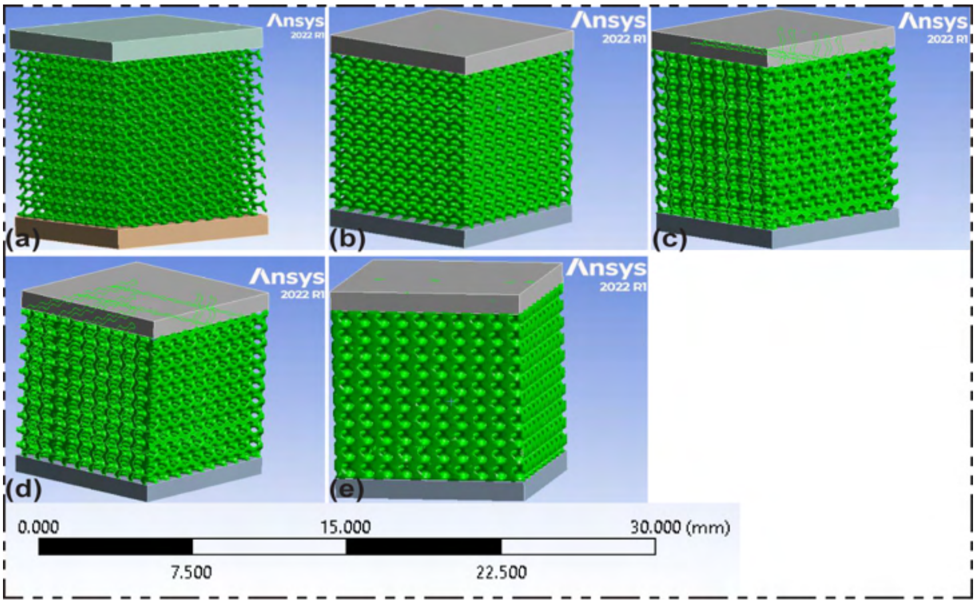

Figure 2.4: Assembly combination using ANSYS SpaceClaim: top and bottom gripper with composite TPMS gyroid lattices at varied relative densities - a) 14%, b) 25%, c) 33%, d) 38%, e) 54%.

2.2.8 Case Study on Vehicle Crush Box Energy Absorption

The aim of this case study is to evaluate the composite TPMS-gyroid lattice structure's high-energy absorption capabilities under 15.6 m/s impact scenarios **[130]**. We classify this as a high-velocity impact because it is significantly faster than the norm of 3-5 m / s. Thus, test results are expected to provide a more reliable indicator of the composite lattice or compression box's resistance in real-world conditions. The implications of the results of mechanical compression experiments on TPMS-gyroid lattice structures with relative densities of 14%, 25%, 33%, 38%, and 54% for enhancing the crashworthiness and safety of automobiles are optimistic. For the purpose of the investigation, a 50 mm × 50 mm × 200 mm square shell-type box with a 1.5 mm thickness was used **[131, 132]**, as shown in Figure 2.5. We properly designed and constructed five TPMS gyroid latticed square crash boxes using nTop software, each of which corresponded to one of the five relative densities examined in this work. this as a high-velocity impact because it is significantly faster than the norm of 5–6 m/s. Thus, test results are expected to provide a more reliable indicator of the composite lattice or compression box's resistance in real-world conditions. The implications of the results of mechanical compression experiments on TPMS-gyroid lattice structures with relative densities of 14%, 25%, 33%, 38%, and 54% for enhancing the crashworthiness and safety of automobiles are optimistic. For the purpose of the investigation, a 50 mm × 50 mm × 200 mm square shell-type box with a 1.5 mm thickness was used **[131, 132]**, as shown in Figure 2.5. We properly designed and constructed five TPMS gyroid latticed square crash boxes using nTop software, each of which corresponded to one of the five relative densities examined in this work.

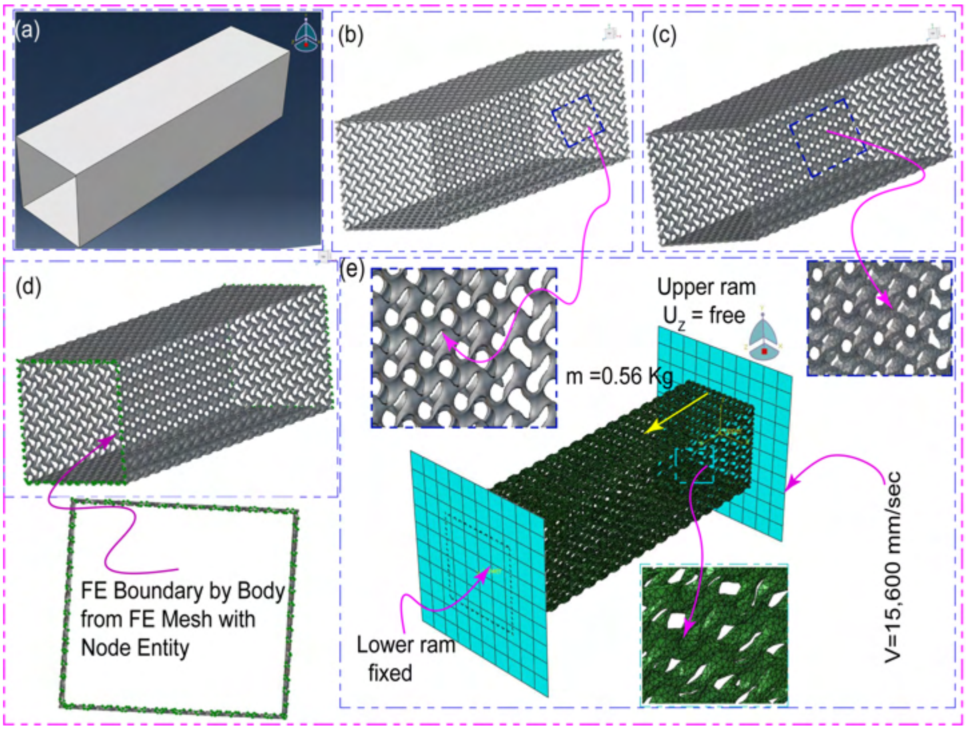

Figure 2.5: Illustration of a) Conventional square crush box, b) composite TPMS-gyroid lattices crush box, c) fine meshed latticed crush box using nTop, d) Node extraction from FE volume mesh for applying BCs and Crash box-lower ram and crash box-upper ram interactions, and e) parameters for simulation of latticed crush box impact.

2.3 Results

2.3.1 Lattice Samples Density and Porosity Measurement

The density and porosity of FFF-printed PLA TPMS gyroid lattice samples are shown in Table 2.6. The table displays the average weight, measured actual densities, relative densities, and porosities for various lattice samples. The findings show that these properties vary significantly across various kinds of lattice samples. The printed samples' densities differ from the theoretical density of PLA (1.24 g/cm^3). The sample identified as CTL14 had the lowest relative density at 14% and the greatest porosity level at 86%. Other samples, such as GTL and WGTL, exhibited greater densities and lower porosities, with GTL having a relative density of 61% and a porosity of 39%. The differences in measured weights of the samples show a similar correlation with the changes in density and porosity, suggesting that the manufacturing process significantly influences these attributes.

2.3.2 The Mechanical Properties and Compressive Response

The stress-strain curves for fused deposition modeling (FDM) 3D printed PLA samples with different relative densities can be seen in Figures 2.6a through 2.6d. Our results closely support Ashby's theories, showing that an ideal energy absorber has a longer plateau phase in the stress-strain curve, with the plateau stress falling below the protected object's stress threshold [**78**]. Figure 2.6a and Figure 2.6b show the compressive stress-strain curve of Solid printed PLA TPMS lattice with five different relative density and TPMS lattice type, respectively All three graphs show the elastic, plastic plateau, and densification areas, with the slowest strain rate exhibiting a longer plastic plateau, indicating improved energy absorption capacities. The sample with a relative density of 38% is shown in Figure 2.6c. The walled and conventional TPMS gyroid lattice samples are also shown. All these samples show elastic, protracted plastic plateau, and densification phases. Finally, Figure 2.6d shows the relative densities of five samples ranging from 14% to 54%. The mechanical stress-strain response of the composite TPMS-gyroid lattice with 33% and 38% relative density are approximately overlapped, indicating repeatability.

Table 2.6: Measured weight, calculated actual densities, relative densities, and porosities of the 3D printed PLA gyroid lattice samples.

Lattice Type	**Measured Average Weight (g)**	**Actual Density (g/cm^3)**	**Relative Density (%)**	**Porosity (%)**
GTL	$20.38 \pm 2.50 \times 10^{-2}$	$0.75 \pm 1.93 \times 10^{-3}$	61	39
WGTL	$13.08 \pm 2.40 \times 10^{-3}$	$0.48 \pm 4.10 \times 10^{-4}$	39	61
CTL14	$4.69 \pm 2.38 \times 10^{-3}$	$0.17 \pm 9.00 \times 10^{-5}$	14	86
CTL 25	$8.37 \pm 1.87 \times 10^{-2}$	$0.31 \pm 6.90 \times 10^{-4}$	25	75
CTL 33	$11.05 \pm 2.06 \times 10^{-2}$	$0.41 \pm 7.60 \times 10^{-4}$	33	67
CTL 38	$12.70 \pm 2.10 \times 10^{-2}$	$0.47 \pm 7.60 \times 10^{-4}$	38	62
CTL 54	$18.08 \pm 2.51 \times 10^{-2}$	$0.67 \pm 9.30 \times 10^{-4}$	54	46

There were no significant mechanical properties lost during the collapse scenario, except for composite TPMS-gyroid lattice with relative density lower than 15% (Figure 2-6c and Figure 2-6d). This was expected since stiffness is expressed as the ratio of force to displacement and is directly affected by size effect [**53**]. Figure 7 depicts the results of mechanical compression testing at five different relative densities and five strain stages, with a maximum displacement of 17 mm and a corresponding strain of roughly 60%. Beyond this point, the lattice stops deforming and enters the densification stage. The studied deformation patterns clearly show the elastic, plastic plateau, and final densification properties.

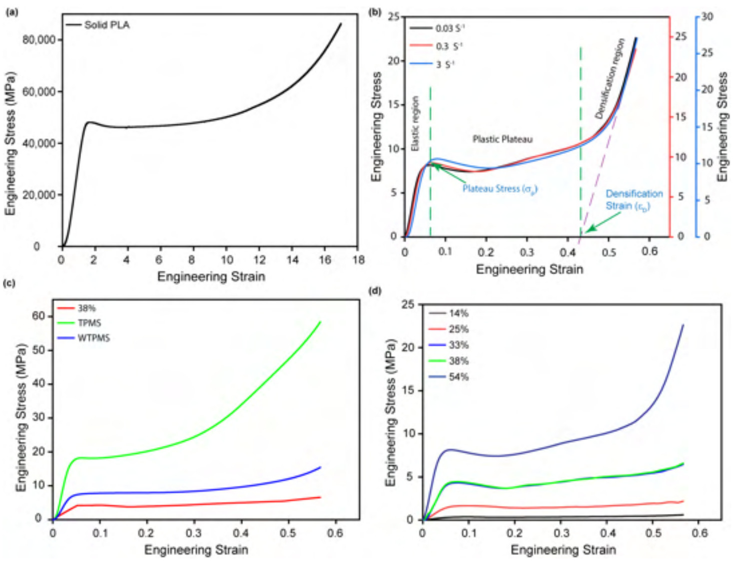

Figure 2.6: The stress versus strain of a) solid cube PLA printed, b) 54% composite lattice for three varied strain rates, c) TPMS-gyroid, walled TPMS-gyroid, and composite TPMS-gyroid (38% ρ/ρ_s), and d) composite TPMS-gyroid for five varied ρ/ρ_s.

The combined results of mechanical compression tests and finite element method (FEM) compression deformation studies are shown in Figure 2.7. These show that the composite TPMS gyroid lattice structure fails in two different planes, each with a different cause. The vertical walls collapsing down by buckling and the horizontal walls collapsing down by bending are the two types of failure modes that our technique predicted. This duality in failure behavior endows the innovative lattice structure with unique properties under external compressive pressures, as demonstrated in Figure 2.7.

Figure 2.8 displays the outcomes of tests that put 3D-printed PLA lattices under mechanical compression. The relative densities of the lattices were 14%, 25%, 33%, 38%, and 54%. The experiments monitored the deformation phases over several strain levels: initially undeformed, then 25%, 40%, 50%,

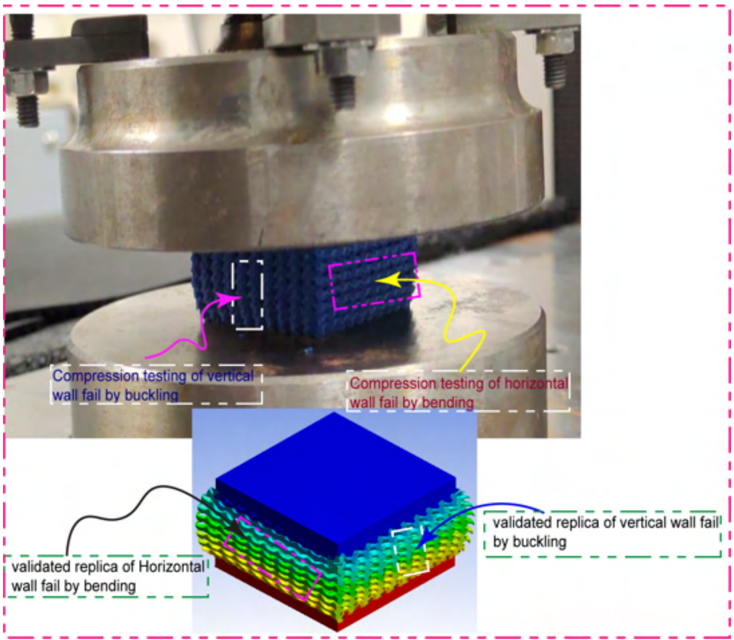

Figure 2.7: Vertical buckling and horizontal bending collapse in composite TPMS gyroid lattice under mechanical compression testing and FEA deformation analysis.

and eventually 60% strain, resulting in a 17.74 mm displacement from the total height of 30 mm. At the lowest relative density of 14%, both vertical and horizontal lattice walls experienced considerable mechanical deterioration and fractures. In contrast, the rest of the composite TPMS gyroid lattice structures resisted mechanical compression. During the tests, the lattices behaved in three different ways: at 25% strain, they failed elastically; at 40% to 50% strain, they entered a plastic plateau zone that showed permanent deformation; and at 60% strain, densification took over as the walls touched, mimicking the behavior of solid bulk PLA and preventing any further deformation.

2.3.3 Plastic Plateau Stress and Young's Modulus

Young's modulus (the primary axis) and plateau stress (the secondary axis) are shown on a graph in Figure 2-9a. It shows how these two parameters change for five different relative densities of the composite TPMS gyroid lattice in both mechanical compression and finite element (FE) simulations. The stress vs. strain curves of the composite lattice structures is the source of these mechanical properties. The findings indicate a clear relationship: as the relative density of the composite lattice increases, consequently, the elastic modulus and plateau stress rise. Both simulated and experimental data exhibit this property.

Table 2.7: Percentage error between experimental and simulation results for Young's Modulus and plateau stress with corresponding standard deviation across.

Relative Density	**Experiment (Elastic Modulus, MPa)**	**Simulation (Elastic Modulus, MPa)**	**Error (%)**	**Experiment (Plastic Plateau, MPa)**	**Simulation (Plastic Plateau, MPa)**	**Error (%)**
14%	6.34 ± 0.10	5.96 ± 0.10	6.05	0.36 ± 0.10	0.36 ± 0.10	0.21
25%	32.24 ± 0.35	30.10 ± 0.35	6.64	1.48 ± 0.35	1.48 ± 0.35	0.02
33%	90.47 ± 1.08	83.62 ± 1.12	7.57	4.43 ± 1.08	4.44 ± 1.12	0.35
38%	93.66 ± 1.08	87.27 ± 1.10	6.82	4.44 ± 1.08	4.45 ± 1.10	0.09
54%	176.93 ± 3.75	163.98 ± 3.55	7.32	8.83 ± 3.75	8.83 ± 3.55	0.03

The highest and lowest percentage errors, when comparing the Young's modulus between the findings of the simulation and the experiment, are 9.21% and 10.02%, respectively. In contrast, the highest and

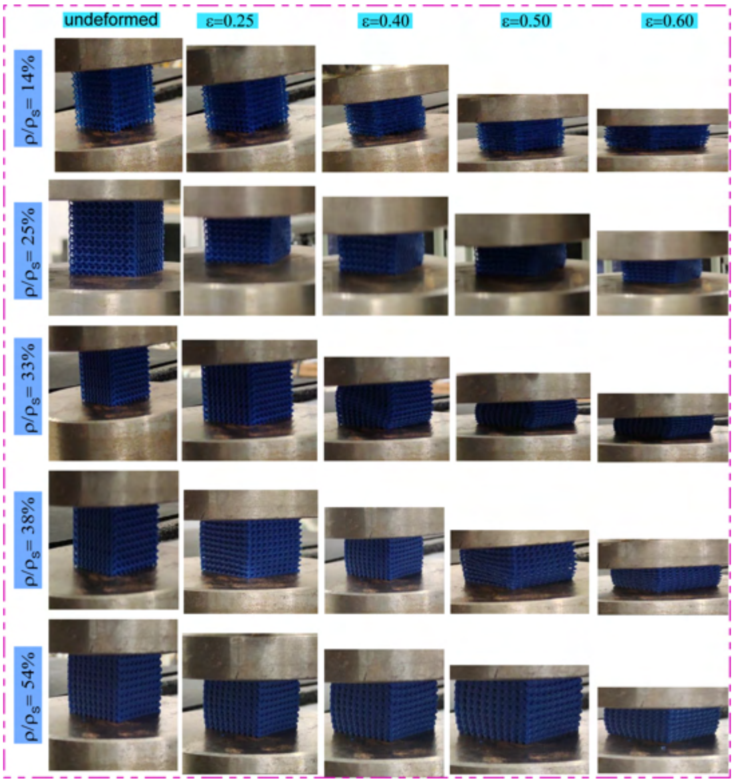

Figure 2.8: Mechanical compression across strain stages in 3D-printed PLA lattices with variable relative densities.

lowest percentage errors between the simulation and experiment data for the plateau stress are 0.017% and 0.22%, respectively. For the mechanically compressed composite lattice structure, the percentage error in Young's modulus is greater than the percentage error in plateau stress. This indicates that the finite element analysis accurately captured the plastic plateau zones. The current study stands out from previous studies due to successfully capturing all three regions of the stress versus strain curve from mechanical compression testing using the multilinear plasticity hardening model [**3, 133**], as shown in Figures 2.9a and 2.9b. Table 2-6 displays the percentage errors between the simulation and experimental results for Young's modulus and plateau stress. This demonstrates how accurate the models were, as well as how they varied for different relative densities of TPMS gyroid lattices. This is important for making sure that the models used in the study are accurate.

2.3.4 Gibson-Ashby Power Fitting Analysis

Figures 2.9b and 2.9c show the results of mechanical compression tests and finite element method (FEM) simulations, which give a detailed investigation of the mechanical properties associated with varying relative densities in composite TPMS gyroid lattice structures. Experimental findings show that increasing the relative density of the structures significantly increases both the relative modulus and the plateau stress. Specifically, for the TPMS Gyroid composite structure, the experimental values for n1 and C1 are 0.45 and 2.52, respectively. The FEM simulations confirm these results, showing slightly altered values of 2.49 for n1 and 0.43 for C1. Figure 3-9b clearly shows the steady rise across multiple relative densities (14%, 25%, 33%, 38%, and 54%), as well as the fact that the relative modulus of the 54% composite TPMS Gyroid structure is approximately five times that of the 14% relative density composite lattice. This wide range of mechanical properties highlights the material's structural integrity's reactivity to variations in relative density. The research highlights the disparities in mechanical performance, notably the mismatches between experimental and simulated data, which become more prominent at increasing densities. Figures 2-9b and 2-6b show variations in relative modulus and plateau stress as relative density rises in composite TPMS gyroid lattice structures. These modifications are based on both mechanical compression testing and finite element analysis (FEA) simulations. As relative density rises, the experimental and simulation results diverge, notably in terms of relative modulus and plateau stress. Simulation findings of 1.04 and 2.47 closely match the experimental values of 1.05 and 2.44 for C2

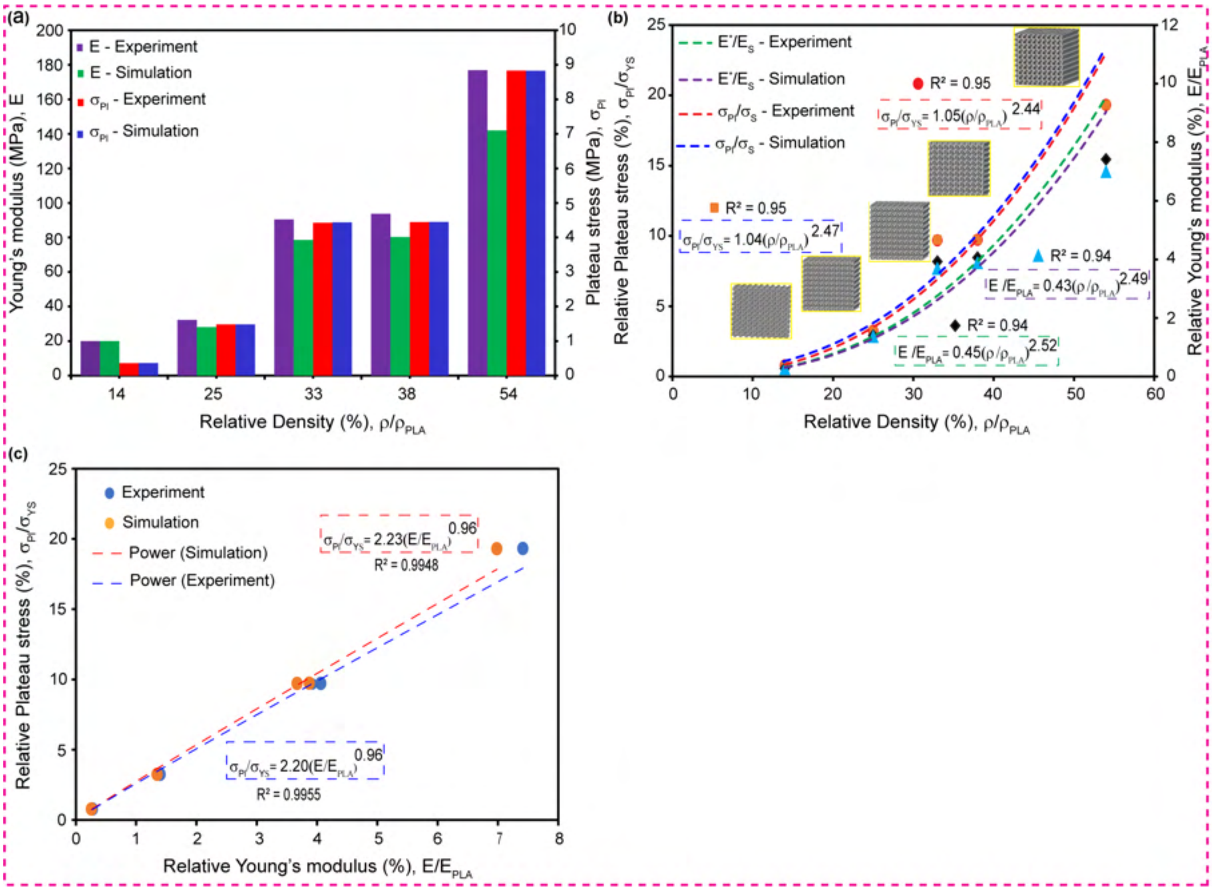

Figure 2.9: Visualization of composite TPMS gyroid lattice structures, detailing mechanical properties and modeling: (a) Correlation among Young's modulus, lattice plateau stress, and relative density; (b) Gibson-Ashby power fitting analysis showing the relationship between relative plateau stress and Young's modulus as a function of relative density; (c) Modified Gibson-Ashby power fitting showing the dependency of relative plateau stress on relative Young's modulus.

and n2, respectively, showing a tight correlation but noticeable variances as density varies. This pattern is obvious in the data from the different relative densities evaluated, with significant differences becoming more prominent as densities increase. Specifically, under experimental conditions at 54% density, the relative plateau stress is roughly 0.2, which is over 20% higher than the simulated value of 0.18. The findings shown in Figures 2.9b and 2.9c, as well as further investigations, demonstrate that relative density is critical in defining the mechanical properties of composite TPMS gyroid lattice structures. Notably, both modeling studies and mechanical compression measurements show that changes in relative density have a considerable influence on relative plateau stress in five distinct kinds of these structures. The modified Gibson-Ashby model shows that there is a complex relationship between relative Young's modulus and relative plateau stress, as shown in Figure 2.9c. Data fitting from this research yields values for n3 and C3 of 0.96 and 2.32, respectively, in experimental settings, whereas simulation results deviate slightly at 0.96 and 2.20, demonstrating minor differences but general consistency in trends across various relative densities. The findings clearly show that the relative stiffness of these lattice structures has an integrated impact on their strength ratio, which is critical for their design and function.

2.3.5 Microstructure of Undeformed and Deformed Lattice Structure

Figure 2.10 shows side-by-side scanning electron microscopy (SEM) pictures of TPMS-gyroid structures made by fused deposition modeling (FDM) that are not deformed and are deformed. The photos show the microstructural features before and after mechanical compression, highlighting the tiny morphological changes caused by applied stresses. The first SEM pictures, taken at a magnification of 25X, show the microstructure of the lattices that haven't been deformed. They show clear layers of different sizes and non-melted filament-bonded particles in a sample that has a relative density of 14%. Post-deformation, improved 100X magnification photos indicate considerable changes: the 14% density sample has severe mechanical deterioration, with broken layers and clearly distorted holes, while the 54% density sample has bending-dominated behavior, with layers bending evenly.

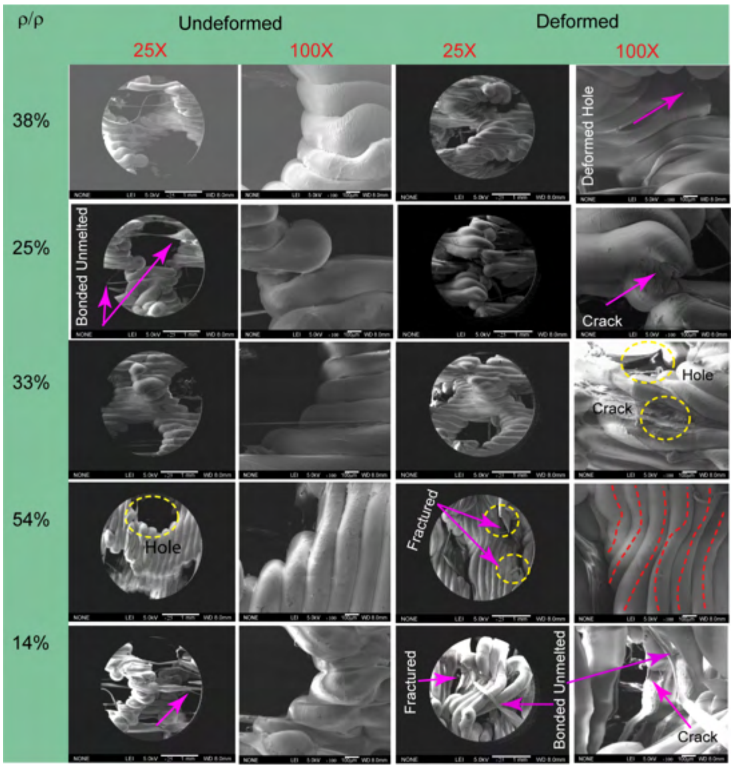

Figure 2.10: SEM images of five relative density FDM-printed composite TPMS-gyroid structures in their original (undeformed) and mechanically compressed (deformed) states, captured at magnifications of 25X and 100X, respectively.

2.3.6 FEM Simulation of Mechanical Compression and Validation of Stress-Strain Curve

Mesh Convergence Study

A mesh sensitivity study is critical for improving finite element analysis's accuracy, stability, and computing efficiency. As a result, we conducted a mesh convergence investigation, concentrating specifically on the CTL with a relative density of 54%. We examined the following seven finite element mesh sizes: 0.8 mm, 0.6 mm, 0.4 mm, 0.35 mm, 0.3 mm, 0.25 mm, and 0.2 mm. These sizes correspond to element counts of 588,453, 735,566, 919,458, 1,379,187, 1,746,970 and 1,838,917, respectively. The simulation set the dynamic compression displacement to 58.89% of the real lattice height, which corresponds to the FDM printing orientation. Figure 11 shows the stress-strain curves obtained from simulations with varied mesh sizes. The differences between curves for mesh sizes 0.25 mm and 0.2 mm are negligible. To balance computational performance, cost, and accuracy, we chose a 0.25-mm mesh size for all lattice designs.

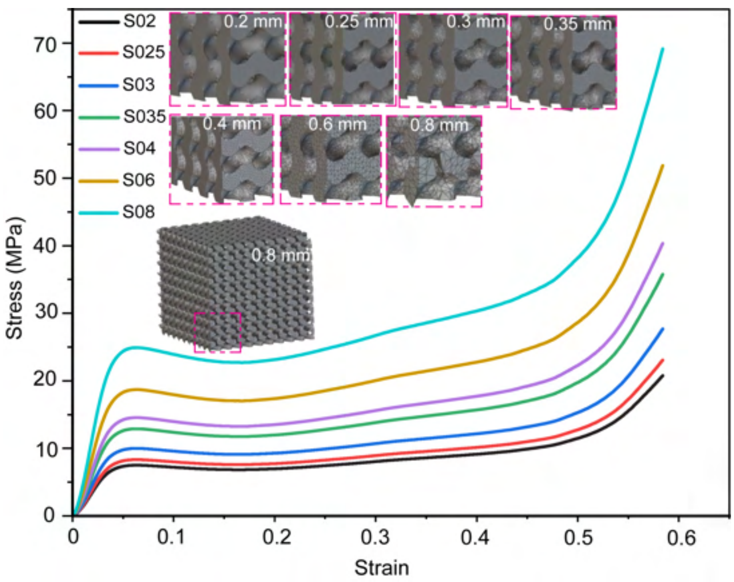

Figure 2.11: The mesh sensitivity study for CTL with 54% relative density effect on stress-strain response.

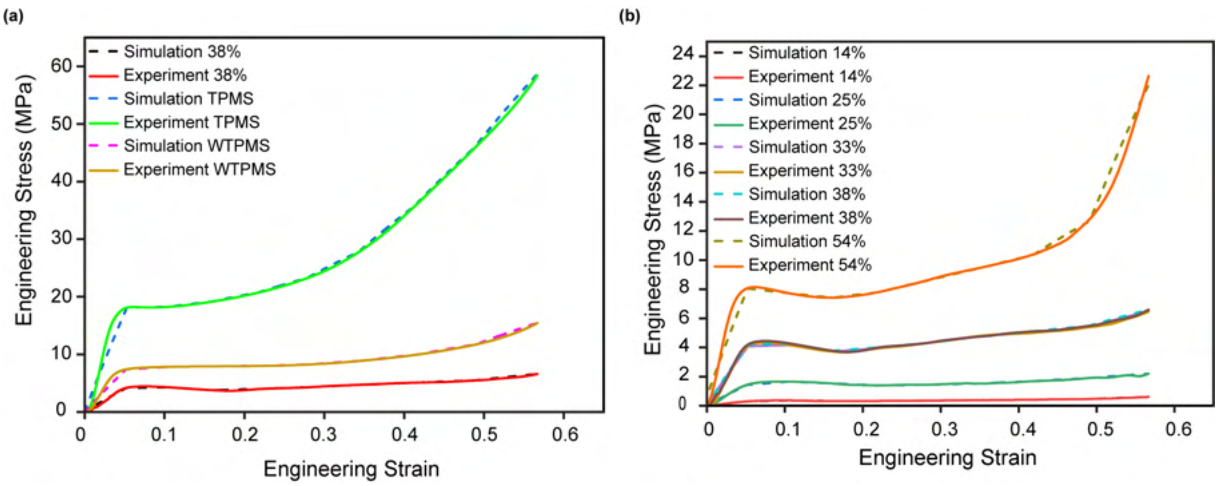

Figure 2.12: The stress-strain curves alongside their corresponding finite element analysis (FEA) validations for: (a) the standard TPMS gyroid lattice, the walled-TPMS gyroid lattice, and the composite TPMS gyroid lattice with a 38% relative density, and (b) the five unique composite TPMS gyroid lattice structures with varying relative densities.

Figures 2.12 and Figure 2.13 show how different relative densities affect the mechanical behavior of composite TPMS-gyroid structures.Figure 2.14 shows how these structures perform under various situations. The figure displays the deformation and failure mechanisms of these structures. Notably, when these lattice structures move from the linear elastic area, local buckling events become visible, mainly at the structures' bottom portions. After the first yielding point, the stress-strain curve significantly reduces due to local buckling. Figure 2.12 shows that fractures appear in the bottom parts of the composite TPMS-gyroid structures at a strain level of 60%, particularly when the relative density is 14%. Finite element (FE) simulations further support these findings by demonstrating how, between strain levels of 50% and 60%, a homogeneous deformation pattern is seen throughout all composite lattice structures, often accompanied by self-contacting.

These results are important because they provide a further understanding of the reasons for structural failure in composite TPMS-gyroid structures and might lead to improvements in their use in a variety of applications. mechanical compression testing at five different relative densities and five strain stages, with a maximum displacement of 17 mm and a corresponding strain of roughly 60%. Beyond this point, the lattice stops deforming and enters the densification stage. The deformation patterns studied clearly show the elastic, plastic plateau, and final densification properties.

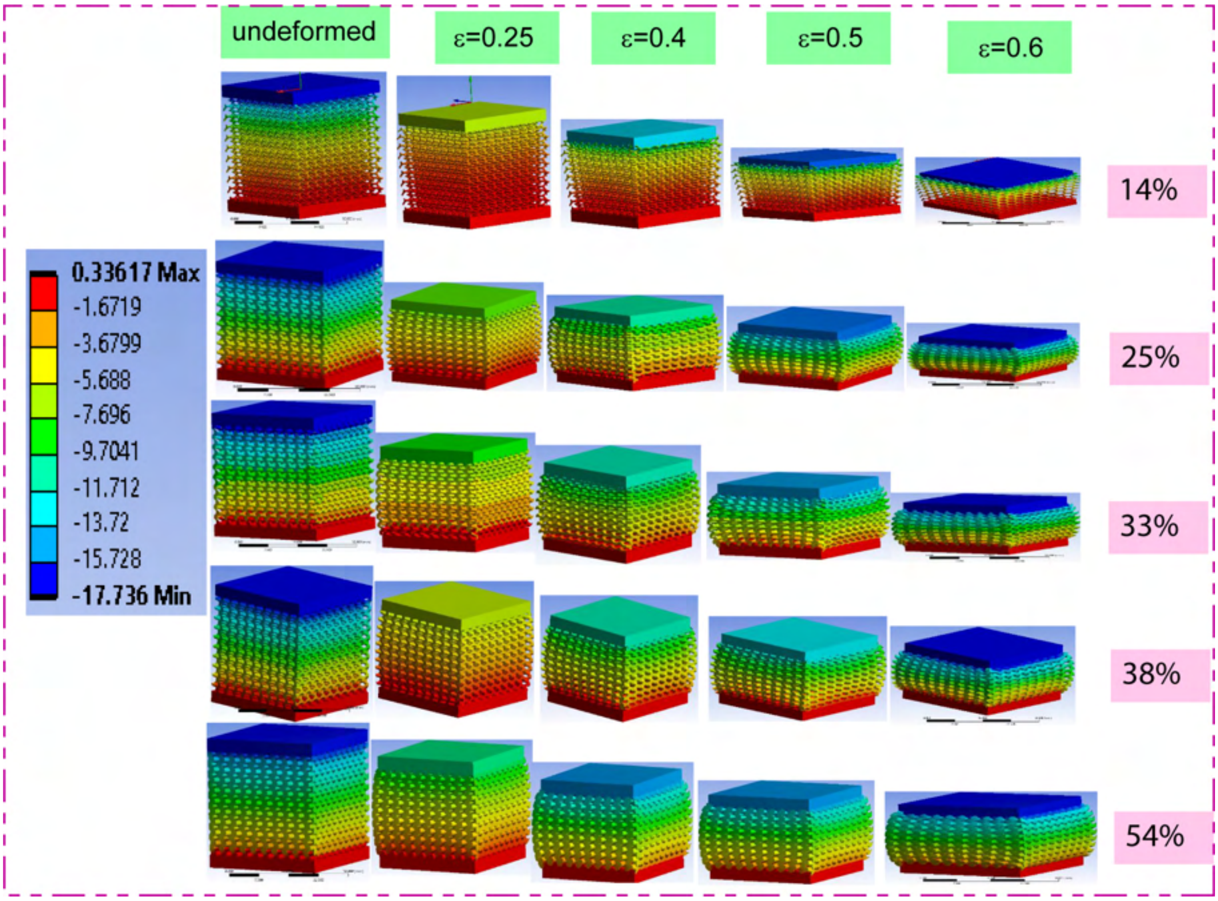

Figure 2.13: FEA simulation of composite TPMS gyroid lattices with variable relative densities across five different strain Stages under 3D-Printed PLA lattices with variable relative densities.

2.3.7 Energy Absorption

The significance of energy absorption in the testing of materials is crucial. The parameter in question is energy absorption per unit volume of the specimen. To effectively represent the degree to which a material can absorb energy during deformation, this measure can often be expressed geometrically by the area confined under the stress-strain curve. It is important to describe the PLA Composite TPMS Gyroid Lattice so that we can figure out how much energy it can hold when it is compressed mechanically. The pictures 2.15a through 2.15d show how the energy absorption of composite TPMS gyroid lattices changes when they are compressed mechanically at different relative densities. These graphs show the measurable energy absorption per unit volume, expressed as the area under the stress-strain curves. Figure 2.15a shows a linear rise in energy absorption with strain, showing that as strain grows, so does the material's capacity to absorb energy, especially in the elastic-plastic phase. This pattern is shown graphically in Figure 2.15b, which plots normalized cumulative energy absorption per unit volume against normalized Stress.

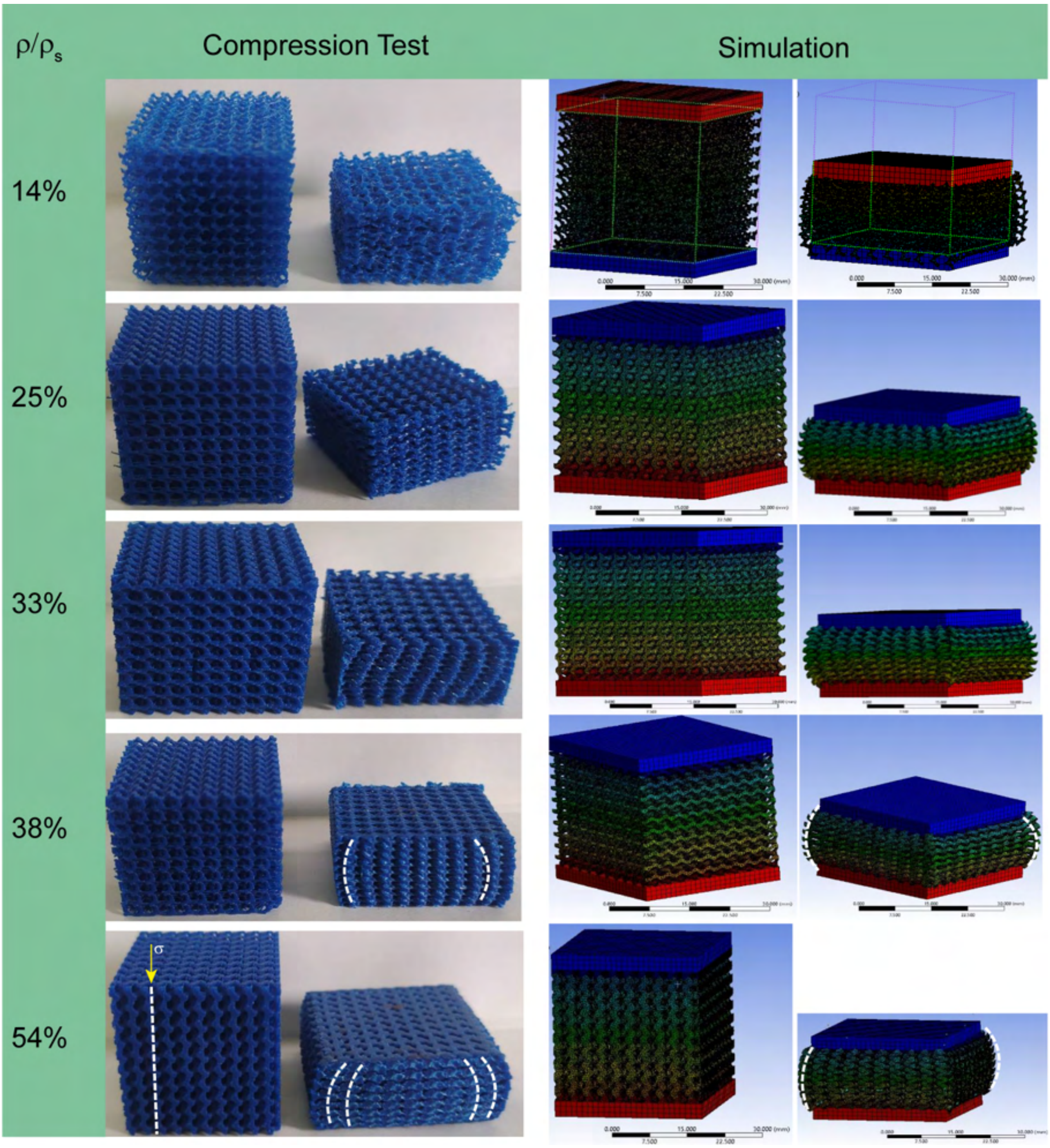

Figure 2.14: The (undeformed) and (deformed) mechanical compression testing along with their corresponding simulations for five relative density FDM printed and FE meshed CAD models of the composite TPMS-gyroid.

This shows that the efficiency of energy absorption is related to strain. In addition to these results, Figures 2-15c and 2-15d show different stages of energy absorption with relative densities ranging from 14% to 54%. They do this by plotting energy absorption efficiency and the ideality of energy absorption efficiency over different strains. We can see on the graphs how composite TPMS gyroid structures respond to compressive loads. It is important to note that the structures become more efficient at absorbing energy as they are stretched, and they work best at certain strain levels that correspond to different densities. Figure 2-15a shows the correlation between strain and energy absorption at various relative densities. The bioinspired composite TPMS gyroid foam absorbs less energy during the elastic-plastic phase, based on results. This decline is primarily due to the energy absorption mechanism being dependent on pore structure collapse, which is predominantly observed in the plateau region. As strain increases, energy absorption exhibits a linear correlation with strain, which is remarkable. It is possible to see a power function relationship between energy absorption and strain at lower relative densities because this type of

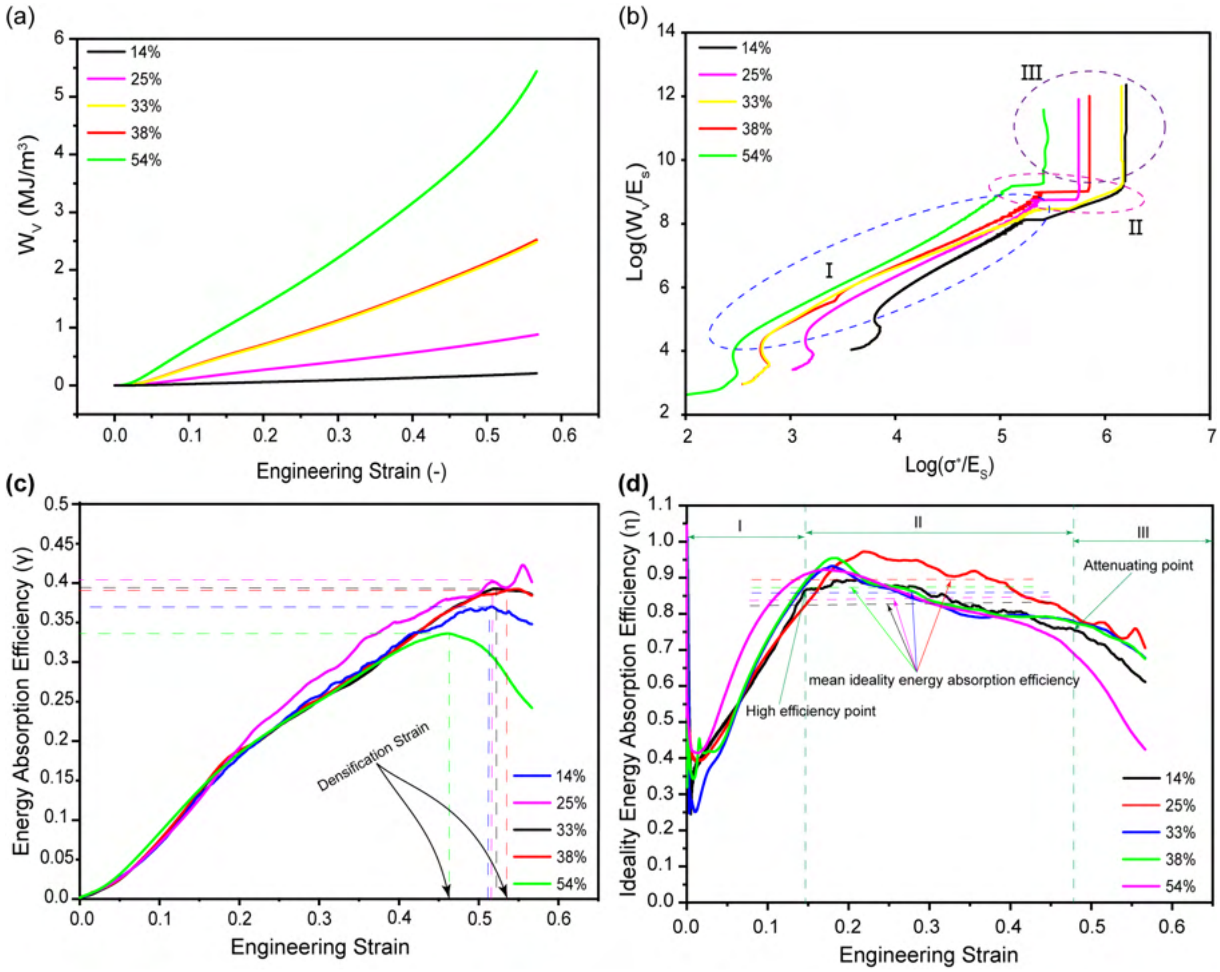

Figure 2.15: The performance of five composite TPMS gyroid lattice structures, detailing: a) the cumulative energy absorption per unit volume in MJ/m^3 as a function of strain, b) normalized energy absorption per unit volume versus normalized Stress, utilizing the bulk PLA elastic modulus, c) energy absorption efficiency in relation to strain, and d) the ideality of energy absorption efficiency versus strains.

biopolymer foam has strain hardening and a high plastic modulus. As densification strain approaches, the energy absorption of the composite lattice foam increases dramatically in response to stress. Densification phases are observable even in low-relative-density composite lattices, which were not discernible in the stress-strain curves produced in this investigation. Because of the results, the composite TPMS gyroid lattice, which has normalized energy absorption and stress, seems to be a great model for creating foam structures out of a group of PLA materials that are designed to absorb energy. The complex relationship between strain and energy absorption efficiency across five different relative densities are shown in Figure 2.15c. This figure makes an evident of the peak energy absorption efficiency, which is characterized by values ranging from 0.34, 0.37, 0.38, 0.39, and 0.43, corresponding to relative densities of 54%, 14%, 33%, 38%, and 25%, respectively. Energy absorption efficiency in PLA composite TPMS gyroid foam, which has these five relative densities, peaks with increasing deformation during mechanical compression and then gradually declines as strain continues to rise. It peaks during the compression deformation phase when strain is increasing and then progressively decreases as strain keeps rising. Nevertheless, when it reaches its maximum within the range of relative densities from 33% to 38%, energy absorption efficiency stays constant, showing remarkable resistance to increasing deformation extents. It's interesting that when the relative density is higher and the strain-hardening effect is amplified at the plateau stage, the presence of larger pore walls leads to a higher plastic modulus. The maximum energy absorption efficiencies correspond to strains of 0.46, 0.51, 0.51, 0.53, and 0.55, respectively. It's interesting that these strain values are a lot like the densification strain on the stress-strain curve. This means that the PLA composite TPMS gyroid foam works best as an energy absorber when all its pores are compressed. By expanding our focus to Figure 2.15d, we investigate the interesting range of ideal energy absorption efficiency with respect to strain across a range of relative densities. Figure 2.10d shows that peak ideal energy absorption efficiencies of 0.90, 0.93, 0.94, 0.955, and 0.97 can be seen across a range of relative densities from 14% to 54%. When these efficiencies are at their peak, the corresponding strain values are 0.21, 0.16, 0.19, 0.18, and 0.23, respectively. A pattern becomes apparent: with decreasing relative densities, the optimum energy absorption efficiency becomes convincingly close to 1. The complex interaction between the plastic modulus and relative density during the plateau phase is what causes this effect. Composite TPMS gyroid PLA foam hardens in amazing ways as relative densities rise, acting a lot like the best materials for absorbing energy when they are compressed.

Maximum energy absorption and Densification strain

Figure 2.16 show the peak energy absorbed by the five composite TPMS Gyroid Lattice structure during Mechanical compression and its corresponding densification strain. The composite TPMS Gyroid TPMS with 14% relative density absorbed the lowest energy per volume at 56.05% deformation.

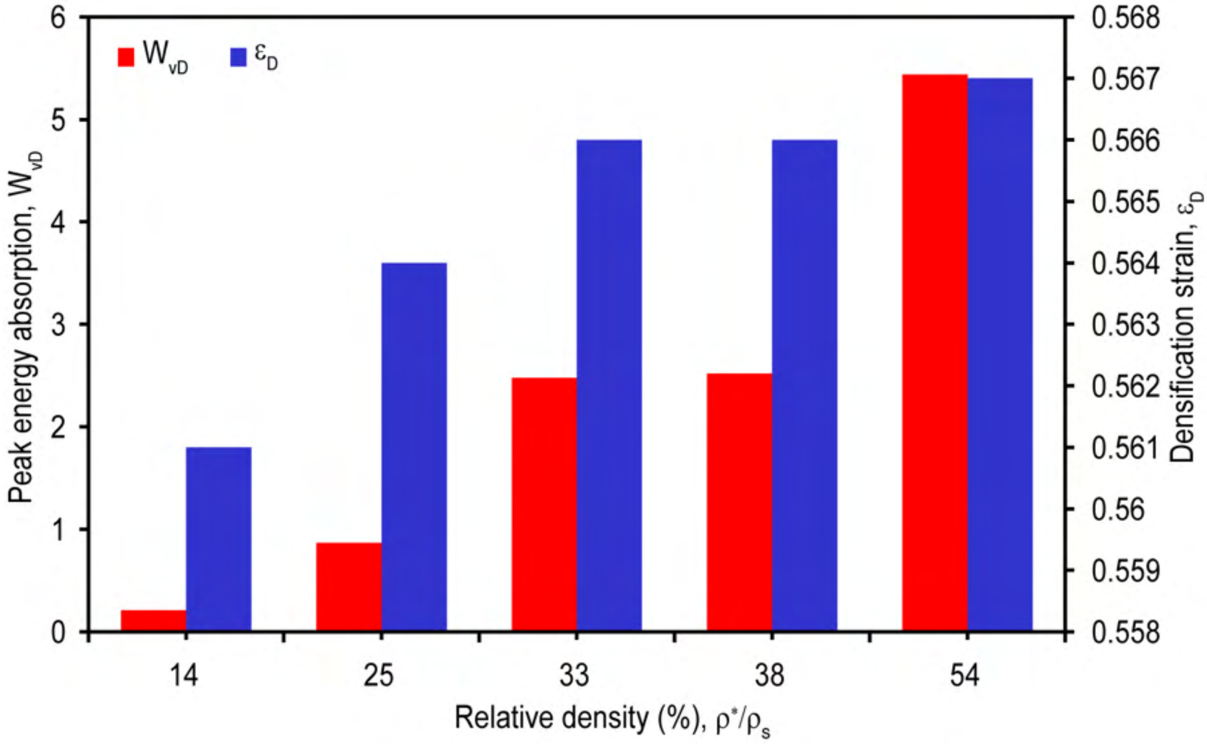

Figure 2.16: The maximum energy absorption and corresponding densification strain in five composite TPMS Gyroid lattice structures subjected to mechanical compression.

This is due to its lowest strength to overcome buckling and bending dominated deformation during mechanical compression. And this result coincides with both SEM and mechanical property result in this study which reinforce clearly that size effect leads to the mechanical property deterioration of lattice structure below 15% relative density. And 5.54 MJ/ m3, absorbed at 56.70% strain by the composite lattice with 54% relative density.

2.3.8 Case Study on Composite TPMS Gyroid Latticed Crash Box

Figure 2.17 shows the displacement contours of composite TPMS gyroid lattices exposed to a high-speed impact of 15600 mm/s for 12.5 msec at five different relative densities—54%, 38%, 33%, 25%, and 14%. The findings reveal a clear trend: the lowest relative density of 14% causes the most displacement, indicating considerable deformation under impact, while the highest density of 54% causes the least displacement, implying higher structural resistance.

Figure 2.18 depicts the Von Mises stress contours for the same latticed crash boxes under similar impact circumstances as seen in Figure 2.17. It demonstrates that the lattice with a 54% relative density withstands the largest stresses before yielding, in stark contrast to the 14% density lattice, which has the lowest stress resistance and is vulnerable to early material failure under comparable impact loads. Figure 2.19a depicts the force-versus-displacement behavior of composite TPMS gyroid lattices under

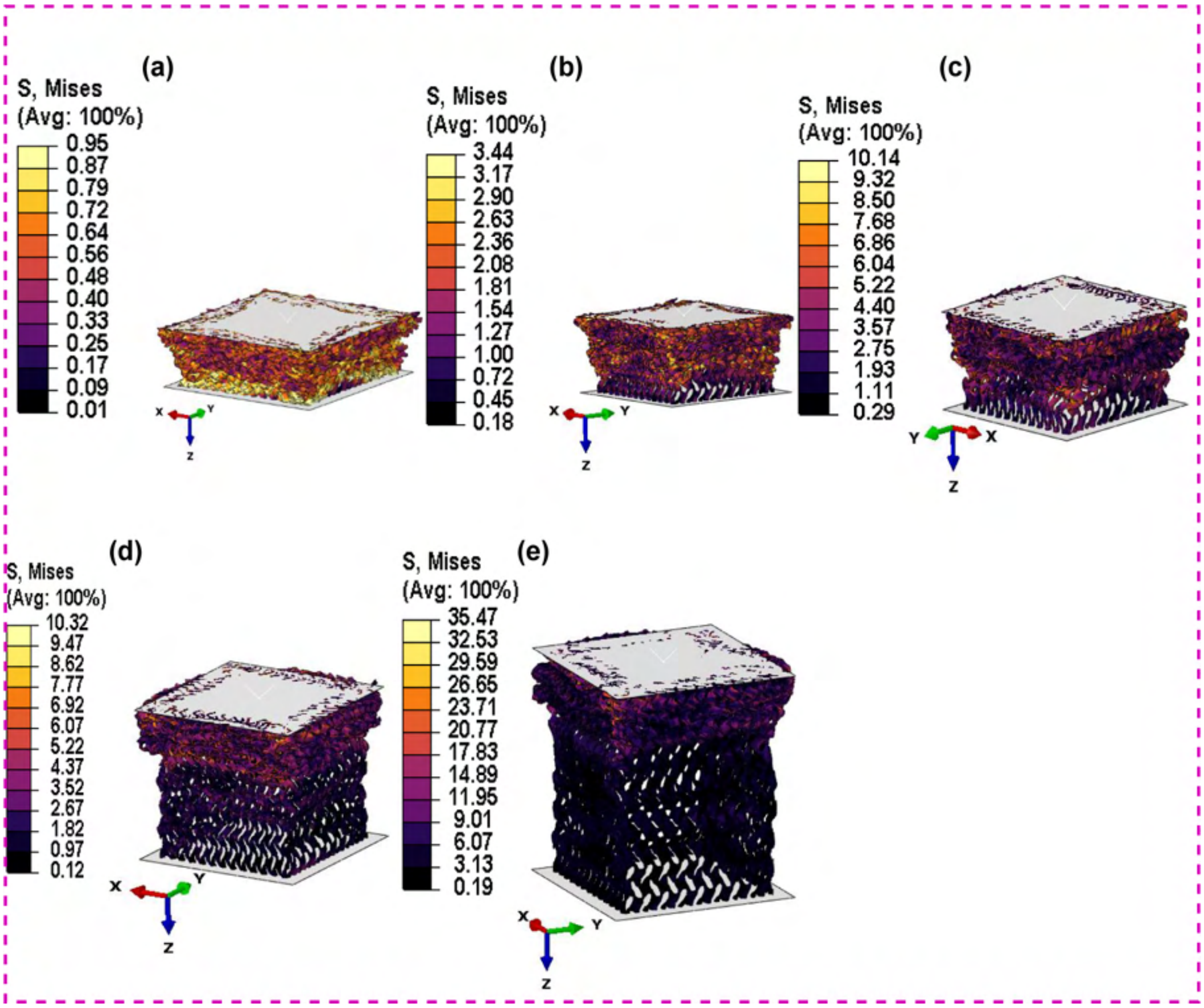

Figure 2.17: Maximum von Mises stress contour result from simulation of Lattice Crash Box at Impact Speed of 15600 mm/s for 12.5 msec with Relative Densities of; a) 14%, b) 25%, c) 33%, d)38%, and e) 54%.

high-speed impacts at the same densities. This figure demonstrates a significant range in mechanical response; the highest density of 54% has the greatest resistance to force, while the lowest density of 14% has considerable compliance, suggesting a lower threshold for force absorption. Figure 2.19b shows the strain energy absorption over time for composite TPMS gyroid lattices exposed to high-speed impacts. It demonstrates that larger relative densities greatly reduce the densification phase while increasing strain energy storage capacity, implying more effective energy management under dynamic impacts.

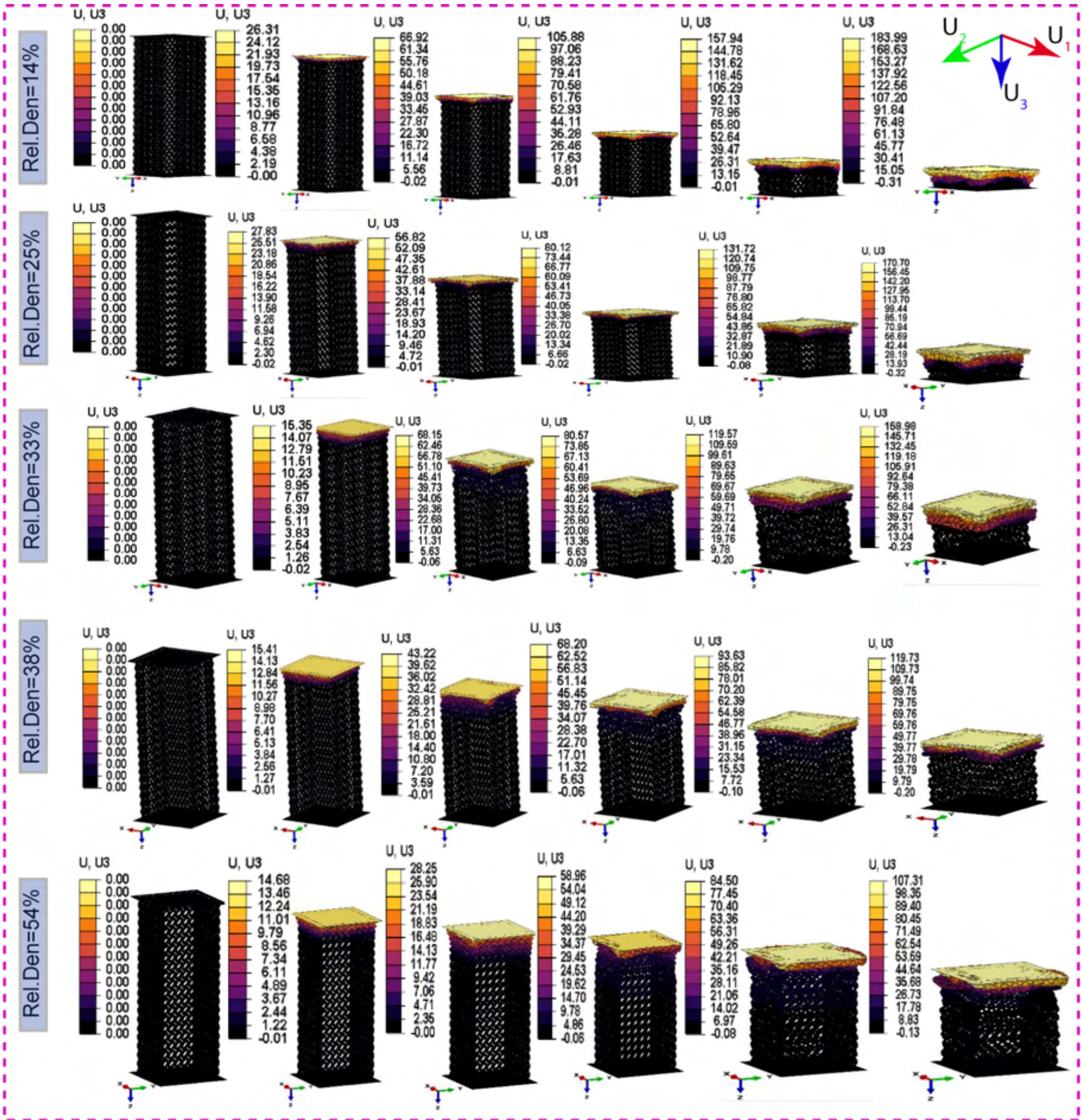

Figure 2.18: Maximum displacement contour result from simulation of Lattice Crash Box at Impact Speed of 15600 mm/s for 12.5 msec with Relative Densities of; a) 14%, b) 25%, c) 33%, d)38%, and e) 54%.

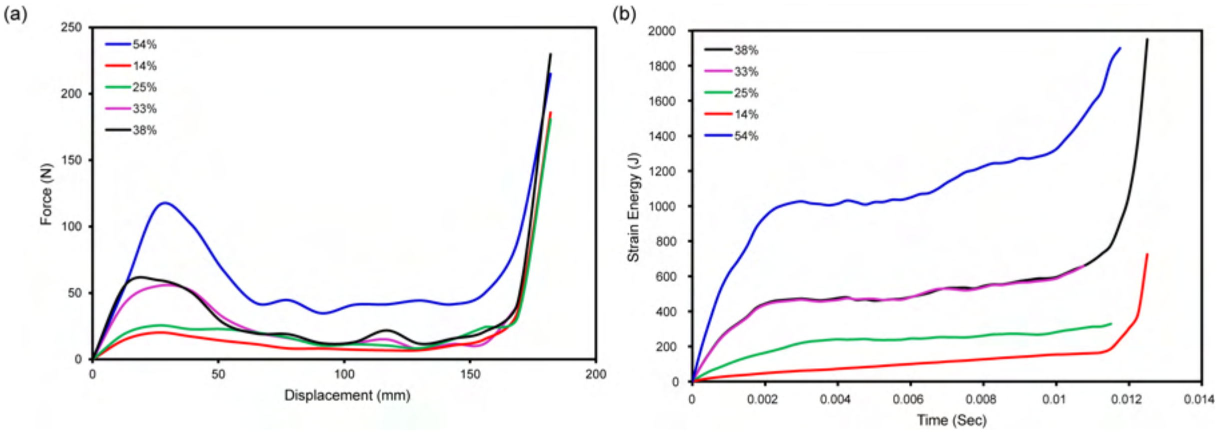

Figure 2.19: The analysis of five crash boxes, each constructed from a corresponding composite TPMS gyroid lattice structure, depicting a) the relationship between force and displacement, and b) the variation of strain energy with respect to the time duration leading to the densification phase.

2.4 Discussion

Table 2.5 shows the complicated connection between manufacturing factors and the material properties of 3D-printed TPMS gyroid lattices. The different densities and porosities show how the FFF printing process affects the consistency and compaction of the material. Notably, the CTL14 sample has an extraordinarily high porosity of 86% with a relative density of just 14%, suggesting considerable material reduction during printing. This degree of porosity is beneficial for lightweight constructions, but it raises worries about mechanical degradation, especially in situations where structural integrity is critical. Such a high porosity is required for biomedical applications because it promotes bone ingrowth and osseointegration, resulting in improved implant biomechanical compatibility. However, the trade-off is the possibility of diminished mechanical strength, particularly in constructions with relative densities less than 15%, where the size effect may result in an unfavorable weight-to-strength ratio. Lower porosity and higher density, as shown in GTL and WGTL, may be better suited to structural applications requiring greater strength. These results show that FFF printing can make lattice structures with different densities and porosities to meet many different functional needs. This will help with improving lattice design and the manufacturing process, so it works better in both industrial and biomedical settings.
A detailed stress-strain analysis is shown in Figures 2.6a to 2.6d. It shows how different strain rates and cell densities change the mechanical behavior of 3D printed lattice structures. It also shows how design parameters affect how well they absorb energy and how safe they are in crashes. Notably, the longer plastic plateau seen in the 54% relative density sample at slow strain rates (Figure 2.6b) shows the best way to lose energy. This is in line with Ashby's theory that the best energy absorber has a longer plateau phase to make it safer in crashes by absorbing energy over time. This conclusion is critical for applications in automotive and aircraft safety systems because bending-dominant foam-like materials outperform stretch-dominant structures in terms of energy management. Furthermore, the mechanical failure in the 14% relative density sample (Figure 2.6d) due to high porosity and size effects highlights the difficulties in developing lattice structures that balance porosity and mechanical integrity. The repeatability of mechanical responses in composite TPMS-gyroid lattices with 33% and 38% relative densities shows that these configurations can be relied on to perform consistently in demanding applications. This shows that custom 3D printed materials are a good choice for fields that need advanced material solutions.
The mechanical behaviors shown in Figure 2.7 show how the lattice structure performs under compressive loads, especially in terms of its mechanical properties, effects of size, and ability to absorb energy. Early failure and deterioration at 14% relative density show the size effect, where materials with lower densities have weaker mechanical integrity and break down before they should underload. This is critical in crashworthiness applications where controlled deformation is essential to energy absorption. The change from elastic failure to a plastic plateau and then to densification at higher stresses shows that the lattices can slowly take in and spread-out energy, which makes the aerospace and automotive industries safer. The clear plastic plateau phase in higher density samples shows better energy absorption, which is better in crashworthiness situations because it lets the structure absorb impact energy for a longer time before it densifies, keeping sudden forces from reaching protected objects. This long and smooth plateau phase

is common in bending-dominant foam structures rather than stretch-dominant ones. It makes it easier for forces to spread out evenly throughout the structure, which improves safety and efficiency in energy absorption applications by making the material better suited to certain mechanical thresholds.

Figure 2.8 shows the results of the mechanical compression tests and finite element method (FEM) investigations. It shows that the vertical walls of the composite TPMS gyroid lattice structures fail by buckling, while the horizontal walls fail by bending. This duality in failure behavior reshows how the orientation and structural alignment of the lattice affect its reaction to external compressive stress. When the compressive load is higher than the critical buckling load, vertical walls usually buckle, causing rapid lateral deflection. When the flexural stress is higher than the material's yield strength, horizontal walls bend, causing progressive deformation. This discrepancy in failure modes shows not only the lattice structure's anisotropic mechanical capabilities but also the need for careful design and optimization of such systems to properly exploit their unique features. In automotive crashworthiness, the ability to manage and anticipate how components deform upon impact is critical. Automotive components such as bumpers and crash zones, crucial for absorbing and dispersing energy after a collision, can strategically utilize the outlined buckling and bending behaviors. Designing these components with a lattice structure that buckles and bends under predefined weights allows for maximum absorption of kinetic energy from a collision, reducing the force imparted to the vehicle's passengers. Specifically, the buckling of vertical walls in the lattice may be used to generate crumple zones that collapse in a controlled way, gradually absorbing energy during an impact. This controlled deformation serves to lower the peak forces encountered by the vehicle and its passengers, which is an important part of an excellent crashworthiness design. Similarly, bending horizontal walls provides a layer of flexibility and durability, enabling the structure to deform without breaking, preserving integrity under stress, and increasing energy absorption capacity.

Figure 2.9a and Table 2.6 show that relative density has a significant impact on the mechanical properties of TPMS gyroid lattices, particularly Young's modulus and plateau stress, which are critical for applications requiring robust mechanical performance, such as automotive crashworthiness. As relative density rises, the lattices become stiffer and stronger, which are important properties for resisting deformation and retaining structural integrity upon impact. Higher plateau stress suggests a greater capacity to absorb and release energy before achieving densification, which is an important feature of successful energy management in crash situations. The accurate capture of these features by FE simulations, as well as their tight agreement with actual data, validates the models' dependability, emphasizing their usefulness in designing novel materials customized to performance needs. This precision is critical, especially when designing automotive components such as bumpers and crash zones that must fulfill strict safety regulations. The ability to reliably adjust lattice structures to achieve the desired mechanical reactions aids in the optimization of these components, increasing their energy absorption capacity. Additionally, the focus on longer, smooth plateau stress in these structures suggests that they work better with bending-dominant foam structures than stretch-dominant ones. This is in line with crashworthiness standards, which say that bending deformation is better for absorbing impact energy while keeping the vehicle's protective shell integrity.

The increased Young's modulus and plateau stress, combined with increasing relative density, have far-reaching implications for material design and use in crashworthiness situations. Figures 2-9b and 2-9c show that denser TPMS gyroid lattices may make materials used in car safety systems much more stable and better at absorbing energy. Although the difference between experimental and simulated data is minor, it gives important insights into mechanical behavior under stress and the effectiveness of existing simulation models in predicting real-world material reactions. This thorough knowledge of how lattice structures deform under compression, particularly the various responses at different densities, enables optimum design solutions that maximize energy absorption while minimizing danger to vehicle passengers during crashes. Bending-dominated deformation modes, as opposed to stretch-dominated ones, observed in these lattice structures are well suited for crashworthiness applications, where materials must absorb substantial impact energy while maintaining structural integrity. The results are in line with the Gibson–Ashby model, which suggests that structures exhibiting a deformation exponent $n \geq 2$ predominantly deform via bending **[134, 135]**. This observation confirms that the designed lattice topologies are promising candidates for advanced energy-absorbing systems in engineering applications. To further support this, the deformation behavior observed in our study agrees well with prior literature on bending-dominated architectures. As illustrated in Figure 2.20, bending-dominated lattices display a characteristic mechanical response: an initial linear elastic regime, followed by a pronounced yield point and a nearly flat stress plateau, culminating in densification. Unlike stretch-dominated structures, which exhibit localized and sequential collapse with stress fluctuations, bending-dominated lattices deform in a more uniform and progressive manner under compressive loads. This uniform collapse mechanism minimizes localized stress concentrations and enhances the predictability of energy absorption—an essential feature in impact-critical applications such as automotive crash components, protective gear, and bio-inspired implants. The post-yield response, marked by a stable plateau and smooth densification transition, further validates the effective energy dissipation capabilities of bending-dominated architectures, as consistently observed in our compressive testing results [**136**].

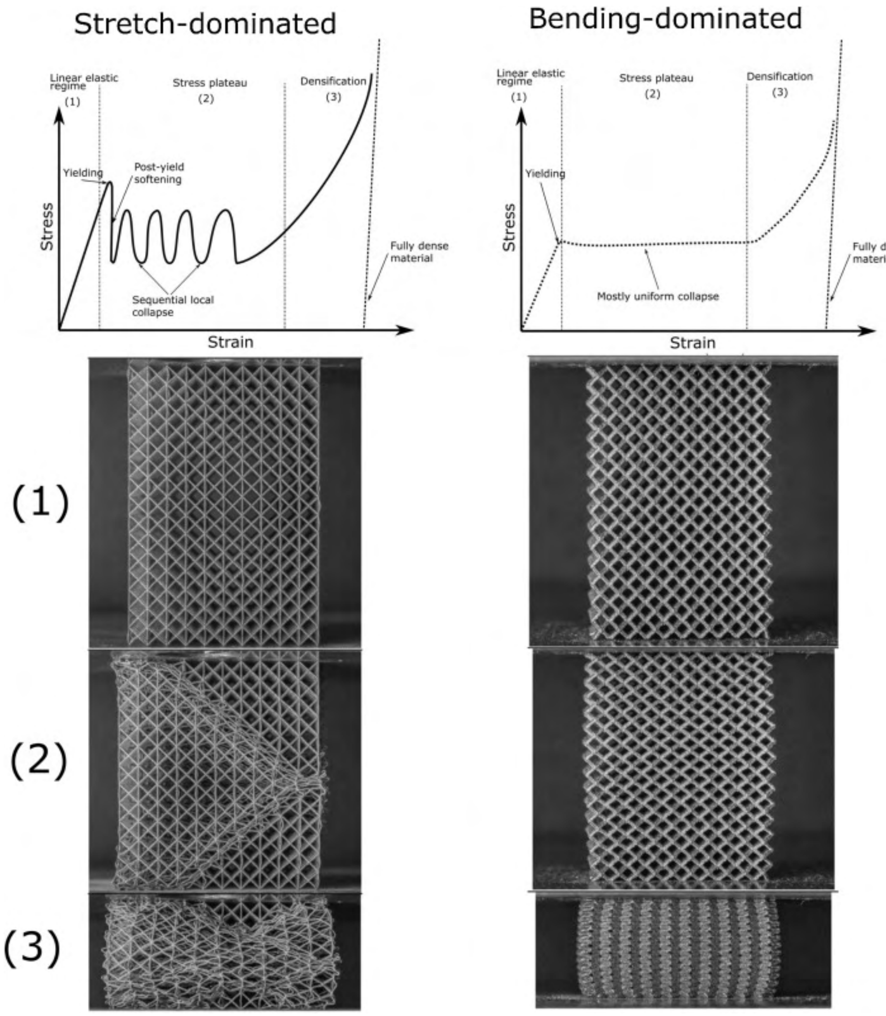

Figure 2.20: Comparison of deformation mechanisms between stretch-dominated and bending-dominated lattices. The stress–strain curves depict three stages: (1) linear elastic regime, (2) stress plateau, and (3) densification. The corresponding images show progressive deformation under compression. Adapted from [**136**].

This shows that the materials can be used in advanced engineering tasks. Engineers can use these findings to design vehicle components that not only meet stringent safety standards, but also contribute to the overall resilience and performance of safety systems in crash scenarios, resulting in vehicles that provide greater protection and durability in accidents.

Figures 2.9b and 2.6b demonstrate that relative density has a significant impact on the mechanical properties of composite TPMS gyroid lattices, particularly relative modulus and plateau stress. The divergence between experimental and simulated data as relative density increases highlights the difficulties in accurately predicting material behavior under varying conditions. In crashworthiness applications, the precision of mechanical property assessment plays a crucial role, directly influencing the design and efficacy of vehicle safety systems. The increased relative modulus and plateau stress with density improve the lattice's capacity to absorb and disperse energy more effectively, which is an important property for materials used in car safety components like crumple zones and bumpers. These results align well with the Gibson-Ashby model, which elucidates the impact of structural topology and density on mechanical behavior. These supports using these new materials in safety-critical situations. It says that denser lattice structures will be stiffer and stronger, better able to handle impact forces, and safer for people inside vehicles during crashes. Furthermore, the close yet varying results from experimental and FEA studies highlight the need for ongoing refinement in simulation techniques to better match real-world outcomes. This is critical for evolving the crashworthiness sector, where understanding the nuanced behaviors of engineered materials under impact can lead to vehicles that are not only safer, but also optimally designed to use new materials that offer superior performance in crash scenarios.

The experimental and simulation investigations' findings have significant implications for the use of composite TPMS gyroid structures in crashworthiness. The bending-dominated deformation mode observed in these structures, especially as relative density increases, suggests that they can effectively absorb and dissipate energy under crash conditions, akin to the behaviors predicted by the Gibson-Ashby model [**125, 126**], which indicates a value of $n \geq 2$. This model is consistent with the observed data, indicating that these lattices are well suited to situations where efficient impact energy management is crucial. The exact link between relative Young's modulus and plateau stress, especially in structures with higher relative densities, supports the idea that changing stiffness through design could lead to the best energy absorption. This personalized method maximizes protective features in automobile safety systems, thereby improving vehicle crashworthiness. Incorporating these systematic design alterations based on Boolean subtract operations modifies the architectural shape of the PLA lattice family, enhancing structural integrity and functional performance under dynamic load situations. This strategic innovation not only enhances safety results but also makes use of new material science to fulfill the automobile industry's strict safety criteria. Figure 2.10 SEM study highlights the significant impact of relative density on the mechanical behavior and structural integrity of 3D-printed TPMS-gyroid lattices. The size impact is most noticeable in lattices with relative densities as low as 14%, resulting in severe mechanical quality loss under compressive stresses. The shattered layers and distorted holes seen in the SEM images after deformation demonstrate this degradation. These results underscore the susceptibility of lower-density lattice systems to mechanical failures, potentially due to insufficient material continuity and structural support within the lattice. Higher density lattices, on the other hand, show a more durable bending-dominated deformation mode (54%). This means that more material makes it easier to distribute and handle stress without breaking completely. These findings emphasize the importance of precise control over printing parameters in additive manufacturing, as these settings have a significant impact on the microstructure and, consequently, the mechanical performance of the final product. Understanding these relationships is critical for optimizing the design and manufacture of lattice structures intended for applications where mechanical reliability is essential, such as in automotive crashworthiness scenarios, where the ability to absorb and dissipate energy effectively can save lives. Figures 2.12, 2.13, and 2.14 show important details about how composite TPMS-gyroid structures behave mechanically at different levels of relative density and strain. Local buckling occurrences, particularly in the structures' lower sections as they transition from the linear elastic area to the first yielding point, highlight a major weakness in structural integrity at lower densities. The formation of fractures in these places at a 60% strain level, especially at a 14% relative density, as shown in Figure 2.12, demonstrates the mechanical limits of less dense lattice systems under high strain situations. Finite element (FE) simulations confirm these experimental findings, exhibiting a homogenous deformation pattern of 50% to 60% strain levels across all densities, often resulting in self-contacting events inside the structures. Mechanical compression testing further investigates this consistent deformation behavior up to densification, revealing the three mechanical phases these materials undergo under compressive stress: elastic, plastic plateau, and densification. These results are very important for understanding how TPMS-gyroid lattices fail and how their structure changes over time. This is especially true in situations where the material needs to be very durable and flexible. By identifying the conditions that lead to local buckling and fractures, we can enhance the design and material composition of these structures to enhance their performance in practical applications in engineering fields, where reliable energy absorption and mechanical resilience are crucial.

The full set of data in Figures 2.15a to 2.15d shows how relative density affects the ability of composite TPMS gyroid structures to absorb energy, which is very important for crashworthiness. The increase in energy absorption with strain, as shown in the linear correlation in Figure 2.15a, suggests that higher-density materials are better at managing and dissipating energy under stress, which is an important characteristic for materials used in automotive safety components such as bumpers and crumple zones. The change from elastic to plastic deformation phases often results in less effective energy absorption, as shown by the fact that peak absorption efficiencies start to rise earlier. This is especially true for materials with lower relative densities (14% to 25%). On the other hand, materials with larger densities exhibit longer energy absorption capabilities, which is consistent with crashworthiness requirements where sustained energy dissipation is critical.

Figures 2.15c and 2.15d show that as relative densities go down, the best energy absorption efficiency gets closer to 1. This shows that the best energy management happens during the plateau phase of deformation. These findings on composite TPMS gyroid structures' deformation properties and energy absorption efficiency not only advance our understanding of material behavior under compressive loads but also inform the design and optimization of materials for enhanced safety in automotive applications, leveraging the unique properties of additively manufactured lattices to improve crashworthiness. Energy absorption efficiency and ideal energy absorption efficiency were suggested by previous studies [**137**], as methods to measure the energy absorption properties of foam materials for use in their study of various forms of energy absorption capacity. The normalized energy absorption properties of the composite TPMS gyroid structures are shown in Figure 2.15b. This graphical representation assigns logarithmic values to two significant ratios: The lattice stress to Young's modulus of solid PLA material (σ^*/E_S) and the total energy absorption to the elastic modulus of bulk PLA materials (W_v/E_S). The graph contained in this representation shows the relationship between strains and the cumulative energy per unit volume. One can gain a more comprehensive understanding of the different compression phases by implementing these logarithmic modifications. To elucidate the intricate mechanisms underlying energy absorption in diverse architectural configurations, Gibson and Ashby initially introduced the concept that serves as the foundation for the aforementioned mathematical expression [**84, 88, 101, 138**]. This normalized graphical curve is one of the most effective methods to show how foam structures maximize energy absorption while minimizing stress. Figure 2.15b depicts three unique zones that give varied information on compression-phase energy absorption properties based on altering slopes of the curves. The elastic deformation phase of composite TPMS gyroid structures correspond to Region I. The pictures above show that TPMS Gyroid structures with relative densities of 14% and 25% fail, even though they only absorb a small amount of energy when they are compressed. The reason for this limitation is due to the size effect of the Gibson and Ashby composite gyroid lattices with relative densities of 25%, 38%, and 54%. Based on such findings, this lattice structure seems to be an excellent match for use in impact-resistant applications since it mimics foam structures. models. The entire structural collapse of the composite TPMS gyroid lattice provides a large increase in energy absorption with minimal stress increases as we investigate Region II. This behavior is most noticeable in Composite TPMS Gyroid designs, on the other hand, have steeper curve slopes, indicating a quick rise in energy absorption even for minor variations in stress. Prominent inflection points demonstrate that composite lattices enter the densification phase in Region III at all five relative densities.

Figure 2.16 shows the results, which are very important for the use of composite TPMS Gyroid lattices in crashworthiness applications where absorbing energy is a key function requirement. The demonstrated decrease in energy absorption capabilities at lower relative densities (14%), underscores the limitations of implementing less dense lattice structures in vehicle safety-critical areas. This constraint is due to the size effect, in which smaller, less dense structures are more prone to mechanical property deterioration under stress, resulting in buckling and bending deformations. This is especially problematic in accident conditions, when the capacity to absorb large amounts of energy might influence the degree of occupant injuries. On the other hand, the denser (54% relative density) lattice structures absorb energy much better, which suggests they could be useful in areas that need more strength and energy absorption. Car designs might deliberately incorporate denser lattices like these to enhance crumple zones and other safety measures, which disperse energy to reduce the impact forces experienced by car passengers. By combining the requirements of contemporary crashworthiness standards with the mechanical benefits of high-density lattice designs, this strategic integration might maximize the overall safety profile of the vehicle.

2.5 Conclusions

This study includes an intensive investigation of the mechanical behavior of five different kinds of composite TPMS latticed structures. These structures were designed by combining walled-TPMS and normal TPMS gyroid lattices using the Boolean subtraction technique. After that, they were 3D printed from PLA using fused deposition modeling (FDM). The study explores the mechanical properties and energy absorption capabilities under dynamic mechanical compression loading. And examine the stress-strain response and deformation modes at various relative densities. Experimental and numerical simulations are both included in the broad scope of this study. The impacts of five different relative densities (14%, 25%, 33%, 38%, and 54%) on the mechanical properties and energy absorption efficiency of the TPMS structures are the most significant findings. The following results reflect the conclusions that have been drawn from the current study.

- A newly created composite TPMS gyroid lattice, created by Boolean subtraction, exhibits a deformation mode that is primarily bending, which is consistent with idealized gyroid and ligament-based TPMS behaviors.
- The 54% relative density crash box has a significantly shorter densification phase while having a larger strain energy storage capacity than the 33% and 38% relative density crash boxes, which show ideal energy absorption prior to densification.
- The findings suggest that the composite TPMS gyroid lattice, with its normalized stress and energy absorption, is an excellent model for fabricating foam structures from a class of PLA materials engineered for energy absorption.
- Our findings support the Gibson-Ashby model by confirming the significant influence of relative density on the mechanical properties of composite TPMS gyroid lattices. They also emphasize the importance of tailoring lattice structure to optimize energy absorption capabilities.
- A comprehensive force-displacement and strain energy-time analysis elucidates the mechanical behavior of latticed crash boxes when subjected to impact. This analysis has significance for the advancement of design and implementation in high-impact scenarios.
- According to the study, composite TPMS gyroid-latticed crash boxes with lower relative densities outperform in energy absorption and deformability, particularly at 25% density, which provides an optimal balance of displacement capacity and mechanical rigidity, promising improved crashworthiness for automotive safety applications.
- This study gives a comprehensive examination of composite TPMS gyroid lattices intended for optimum energy absorption, which is critical for improving automobile safety. This study not only investigates the mechanical reactions under compression but also demonstrates the lattices' applicability in dynamic automobile settings by combining walled-TPMS and regular TPMS gyroid lattices using Boolean subtraction and FDM for manufacture.
- The use of these structures in car crash boxes demonstrates their capacity to increase impact resistance and safety. Specifically, the 33% and 38% relative density crash boxes have superior energy absorption properties that outperform lesser density arrangements, making them appropriate for high-impact applications in vehicle design.This verifies the design's effectiveness in real-world automotive applications, particularly for boosting vehicle crashworthiness, thereby leading to safer and more robust automotive structures.
- In conclusion, this study successfully delineates the boundaries of optimal energy absorption and accurately models plastic plateau regions by combining mechanical compression testing with finite element analysis to improve our understanding of the behavior of composite lattice structures built using FDM 3D printing from blue PLA material under stress.

Chapter 3

HYBRID BIOMECHANICAL DESIGN OF DENTAL IMPLANTS: INTEGRATING SOLID AND GYROID TPMS LATTICE STRUCTURES FOR OPTIMIZED STRESS DISTRIBUTION

This chapter describes a fully and hybrid latticed design strategy for dental implants that uses sophisticated CAD software and finite element analysis (FEA) to optimize stress distribution and improve biomechanical stability.

3.1 Introduction

The lattice structure, a subset of the triply periodic minimum surfaces (TPMS) family, has a highly interwoven and sophisticated structure, with the gyroid TPMS lattice standing out as a particularly notable subtype [**139, 140**]. In recent years, a unique type of sophisticated biomimetic lattice structure known as triply periodic minimum surfaces (TPMS) has received a lot of interest in the field of bone tissue engineering. These structures are distinguished by their distinct periodic geometric variations in three coordinate directions and their zero-mean curvature, making them ideal for the tissue engineering sector [**141**]. Many industries, particularly dental applications and the broader field of tissue engineering, praise this structure for its immense potential [**142**]. Its intricate and precision-driven design is ideal for incorporation into dental implants, where rigorous standards are required [**143**]. The gyroid lattice enables the precise adjustment of sophisticated geometric arrangements to meet specific medical requirements. This potential is the result of taking advantage of cutting-edge 3-D printing technology [**144, 145**]. The porous structure of the gyroid lattice makes it ideal for tissue engineering applications [**60, 146, 147**]. These structures' particular porosity promotes vascularization and cell proliferation, both of which are required for implants to successfully integrate with surrounding biological tissues [**148–150**]. Porous implant shapes, such as gyroid and Voronoi designs, promote osteointegration by optimizing stress distribution and opening channels for improved blood flow and nutrient transfer, as shown in bone scaffolds and hip implants. These properties make porous designs biomechanically and physiologically superior to solid implants in clinical applications [**151, 152**]. Throughout the 3-D printing process, precise regulation of this porosity enables excellent bone ingrowth and osseointegration, crucial for the long-term success of dental implants [**141, 153, 154**]. Furthermore, the intrinsic complexity of lattice geometry, rather than being a disadvantage, is a tremendous benefit in the age of additive manufacturing [**60, 155**]. The higher porosity of the gyroid TPMS lattice improves both structural integrity and osseointegration where the implant meets the bone [**156–158**]. This feature is crucial for the long-term success of dental implants by promoting better bone in growth and stability [**159, 160**]. These structures' versatility in responding to many forms of advanced manufacturing, particularly additive manufacturing, emphasizes their usefulness even more. Since the introduction of additive manufacturing technology, the capacity to produce intricate and complicated structures such as gyroid TPMS lattices has transformed dental implant design [**60**]. Among the many current manufacturing processes, laser powder bed fusion (L-PBF) and other metal 3D printing techniques stand out. L-PBF, in particular, offers a highly effective solution for creating implants with detailed internal structures [**161**]. Its capacity to deposit material precisely layer by layer makes it appropriate for both tissue engineering scaffolds and complicated dental implants [**162–164**]. Smaller lattice cell sizes increase stress distribution and mechanical dependability, addressing limits in manufacturability and load-bearing capability encountered with larger cell sizes, making them ideal for hybrid dental implant designs [**87**][**165**]. Commercially, pure titanium and its alloys are the preferred materials for these applications because they are known for their superior mechanical qualities and biocompatibility, making them perfect for medical use [**166**]. Usually, exact equations regulate the design and propertiesof lattice structures, which are complex mathematical creations [**154, 167, 168**]. These elaborate designs are not just theoretical but also have practical applications in a variety of sectors, owing to the employment of advanced computational tools. CAD software, such as PTC Creo Parametric, provides robust tools for detailed design and engineering, which is critical for integrating specific mechanical requirements of lattice structures into functional products [**169, 170**], whereas nTopology optimization software stands out for its ability to fine-tune designs for performance criteria, making it invaluable in optimizing structural efficiency [**171**]. The gyroid lattice implant demonstrates how these various software applications may work together to create a very practical and unique design [**60, 147, 172**]. We used these sophisticated techniques to create the basic CAD model for this implant, showcasing the flexibility and adaptability of lattice design across diverse applications [**173**][**117, 174, 175**]. Engineers and designers can use sophisticated software solutions to push the boundaries of what is possible in lattice fabrication, resulting in breakthroughs in fields ranging from aerospace to biomedical engineering, emphasizing the collaborative role of various advanced software in refining and realizing these designs [**106, 175–177**]. In research, the finite element method (FEM) is a well-known numerical technique that not only reduces material waste but also saves money and time, improving overall efficiency in engineering projects [**178–181**]. Most FEM research has primarily focused on using quasi-static loading analysis to effectively simulate the compression behavior of lattice structures, which is critical for evaluating their structural integrity under varying load situations [**180**]. However, despite its widespread use, only a few studies have investigated the possibilities of dynamic explicit analysis [**182**]. This approach has demonstrated high dependability in confirming experimental results by precisely mimicking real-world dynamic impacts and stress conditions that lattice structures may experience [**183–186**]. The effectiveness of dynamic explicit analysis in generating informative data and exposing unique response properties under dynamic loading situations offers a potential field of study that is mostly unexplored [**53**]. Given this context, the current work aims to delve deeper into this understudied topic. The main goal of this study is to use explicit dynamic finite element analysis to fully understand how initially fully latticed dental implants behave mechanically when they are under dynamic load. Based on these analytical findings, the project intends to systematically create an optimum dental implant with a novel hybrid design. This design combines a solid neck with a lattice construction for the rest of the implant, with a focus on improving biomechanical compatibility and structural stability. The hybrid structure aims to minimize stress accumulation in crucial areas of the implant, particularly the neck and first thread, which have the highest risk of failure. Using the finite element method (FEM), this study thoroughly assesses stresses and strains inside the implant structure, providing a solid basis for improving the suggested design. This extensive evaluation not only improves the ability to comprehend stress distribution patterns, but it also allows for implant optimization to better resist physiological loading conditions. We believe that the inclusion of a square-threaded region would improve the hybrid lattice structure's capability to optimize mechanical properties and lower stress intensities more effectively than the fully latticed design, especially in regulating deformations under cyclic masticatory loading. Finally, the goal of this research is to apply these enhanced analytical insights to actual implant design advances, therefore creating new standards in dental implantology and providing considerable advantages to patient care.

3.2 Materials and Methods

3.2.1 Assembly CAD Model and 2D Drawing

Creo Parametric version 8.0 software precisely designed the dental implant system's primary components: including cancellous and cortical bone structures.Each model used an implant length of 13 mm, diameter of 4.1 mm, and pitch of 0.8 mm, based on the clinically validated Straumann® Standard Plus (SP) dental implant (Straumann, Basel, Switzerland) for biomechanical relevance [**53**]. As seen in Figure 3.1; the software assisted in the creation of both two-dimensional drawings and three-dimensional models, ensuring that all dimensions were appropriately displayed. The primary focus of this design effort is the implant itself, which will incorporate a Gyroid lattice structure in various configurations, including both fully and hybrid latticed dental implant designs. This method not only enhances the implant's visibility in its functional environment but also enables precise design modifications specifically tailored to integrate the Gyroid lattice structure efficiently. Both fully and hybrid lattice implants now have a square-threaded section on the bottom to improve initial stability and clinical survivability (refer to Figure 3.1 and Figure 3.2). This property enhances primary stability during implant placement, especially in softer bone types. Furthermore, we added an anti-rotational connection to the prosthetic screw-retaining mechanism to limit rotational movement and maintain a stable, long-term fit between the implant and prosthetic components.

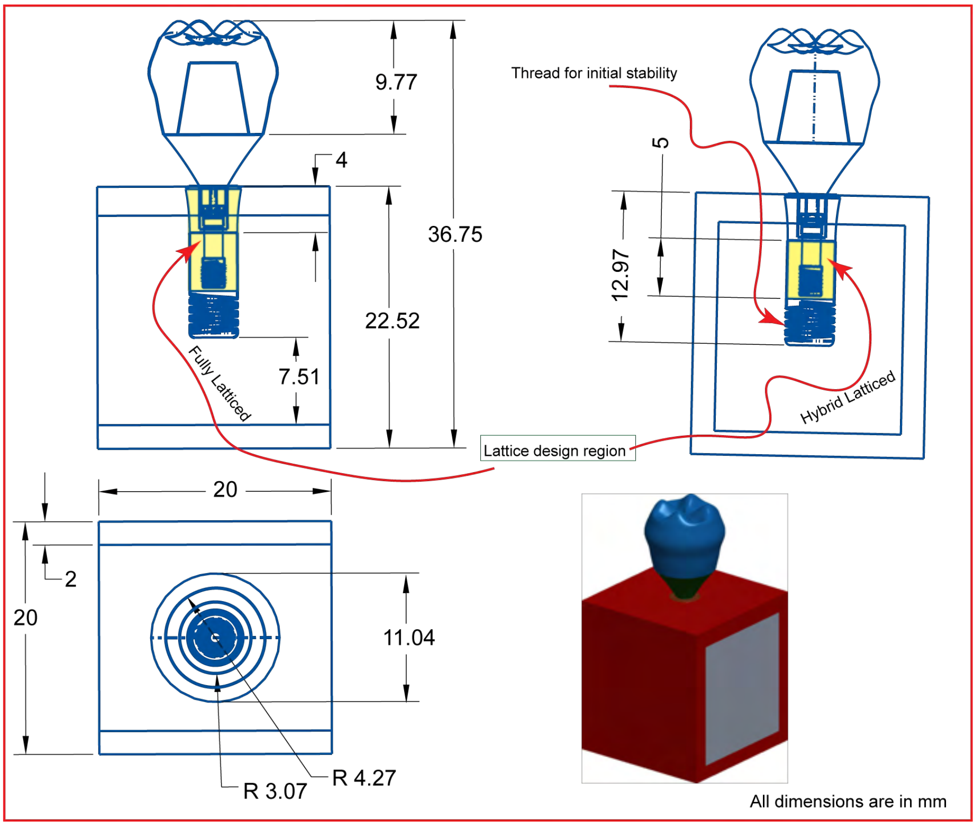

Figure 3.1: Assembled implant system 3D and 2D drawings.

3.2.2 Dental Implant Lattice Design

Figure 3.2 shows a dental implant filled with a Gyroid lattice structure in two different layouts. These layouts include fully, and hybrid latticed dental implant designs that use three different cell sizes, which are 111, 222, and 333.

The three-dimensional (3D) model employed in this work was based on a rectangular slice of cortical and cancellous bone extracted from a human jaw. We methodically created the original implant design using PTC Creo Parametric, a powerful Computer-Aided Design (CAD) application. We accurately established the specific dimensions of each model, which included a length of 14.32 mm, a diameter of 4.1

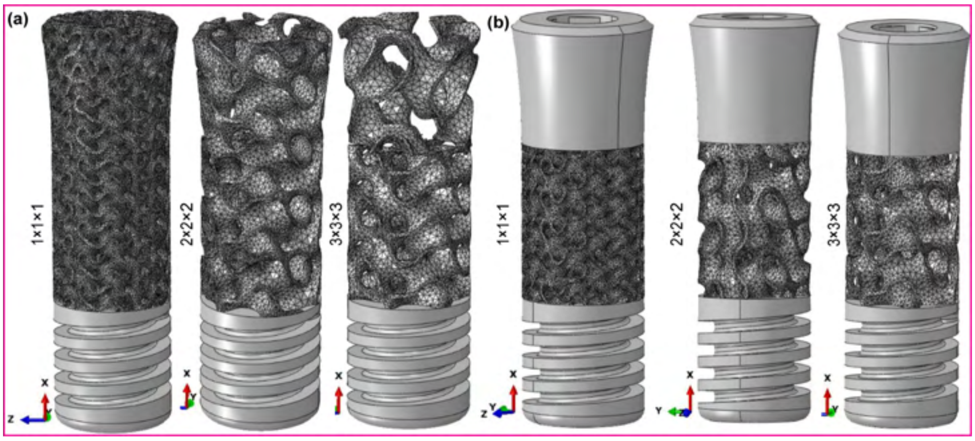

Figure 3.2: a) Fully gyroid TPMS latticed, and b) Hybrid dental implant.

mm, and a wall thickness of 0.8 mm. This accuracy in design parameters guarantees that the implants are ideally structured to fulfill biomechanical criteria and allows for the examination of structural variations dependent on cell size within lattice designs.

3.2.3 Dental Implant FE-Meshing and Mechanical Properties

Figure 3.3 shows the process of saving the dental implant configurations within the system components as SAT file extensions. We then export these files to nTopology for the creation of finite element meshes. Both the fully latticed and hybrid latticed dental implants use three distinct cell sizes: 111, 222, and 333. We mesh each model using 0.1 mm finite element (FE) sizes and 1.0 mm edge length. 0.1 mm elements mesh the retaining screw and solid neck in the hybrid lattice. The compact bone and spongy porous bone, which are crucial for implant stability, are finer meshed around the implant hole, improving the reliability of stress evaluation in these key locations. On the other hand, we mesh the remaining areas with a coarser element size of 0.3 mm to effectively manage computational resources while maintaining model fidelity. This method of precise meshing ensures the appropriate design of every dental implant system component for structural study, enabling a deeper exploration of the biomechanical propertiespresent in both fully and hybrid latticed systems. The mesh statistics for the dental implant, its components, and assembly models are presented in Table 3.2. This method intends to create a biomimetic scaffold that not only closely resembles the structure of natural bone, but also maximizes the implant's biomechanical performance by incorporating strategic design changes. And the physical properties of the materials for the dental implant, its components, and bones are listed in Table 3.1.

3.2.4 Dynamic Mastication Loading and Boundary Conditions.

Figure 3.4a and Figure 3.4b shows the constructed implant system under dynamic load, using one of the two latticed implant designs investigated in this work. Dynamic explicit analysis was used to mimic real-world events that might occur during the implant's clinical usage. This picture (Figure 3. 4a) shows the implant when it is loaded at an angle of 78.58 degrees, with forces acting in the mesiodistal, axial, and buccolingual directions. We subjected the occlusal crown surface to stresses from three different directions—mesiodistal, buccal-lingual, and apical—to evaluate the biomechanical response of the dental implant under multi-axial dynamic oblique loading. We strategically delivered force magnitudes of 23.4 N, 17.1 N, and 114.6 N, converging at an ill-defined reference point 3 mm from the occlusal surface using a multi-point constraint (MPC) technique. We created this arrangement to simulate the complex pressures experienced during clinical mastication, resulting in an equivalent force of 118.2 N, inclined at 75.8 degrees relative to the occlusal plane **[180, 187]**. We reduced the explicit dynamic loading to a slower rate to replicate the cyclic stress of mastication, typically detected at 2 Hz over a 0.5-second interval. Furthermore, carefully created boundary conditions mimicked real-world restrictions at the implant-mandible interface. A six-degree-of-freedom (DoF) Encastre boundary condition held the implant securely in all three spatial dimensions (X, Y, and Z). This made it possible to replicate the stress distribution exactly in many directions. With this thorough setup, exact measurements of compressive and tensile stresses inside the implant system could be made using finite element analysis with ABAQUS 2021. This made the study more reliable.

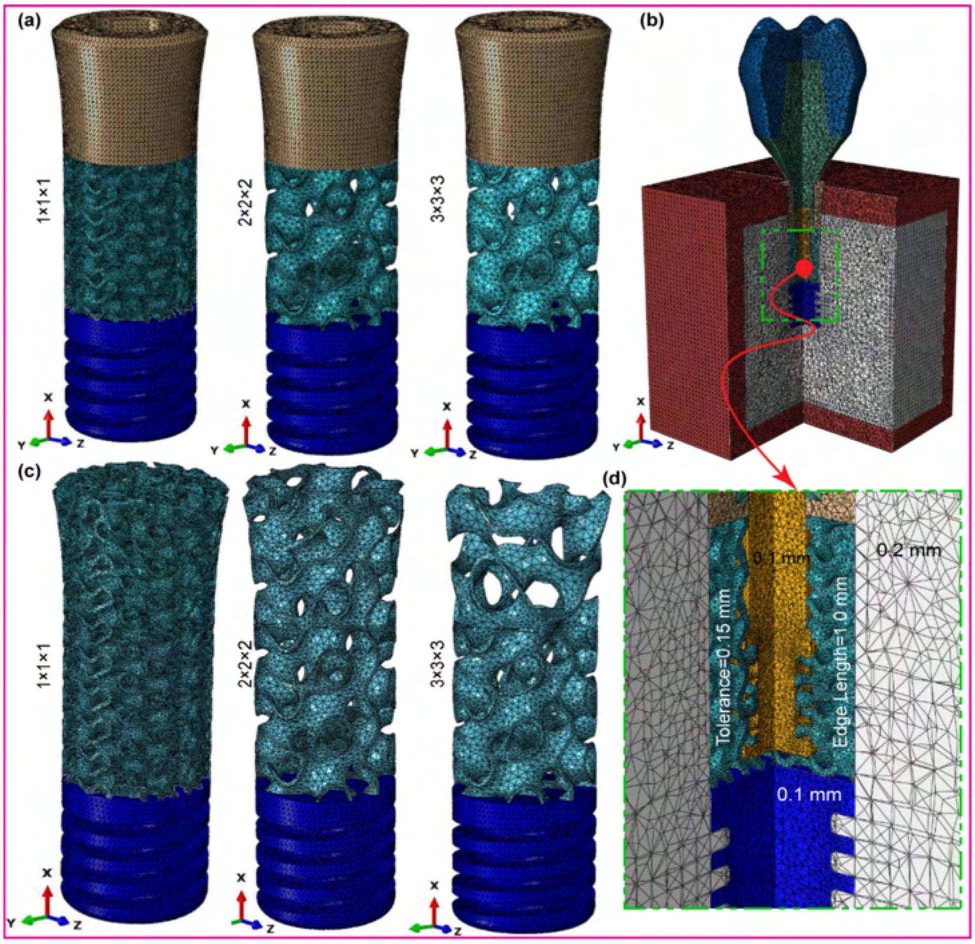

Figure 3.3: FE mesh for (a), Fully latticed implant, (b) assembled dental implant, (c) Hybrid latticed implant, and (d) zoomed FE mesh details indicated by rectangle.

3.2.5 Contact Definition

This approach adequately predicts stress and strain distributions at the bone-implant interface, which is critical for assessing implant mechanical performance under a variety of loading circumstances. Nonlinear contact zones were established at one of crucial interfaces: the implant-bone interactions but for bone-bone contact a Tie contact constraint, as there should be no relative motion between the cortical and cancellous bone surfaces. The contact analysis demonstrated how load and deformation are transmitted between various components. The cortical bone-implant contact was given a friction coefficient (µ) of 0.65 [**188**], while the cancellous bone-implant interface was assigned a value of 0.77 [**189**]. Furthermore, the connections between the crown and abutment, the abutment and screw-retaining mechanism, and the implant and screw-retaining system were designated as bonded connections to provide secure and stable interaction between these components for maximum load transfer and structural integrity.

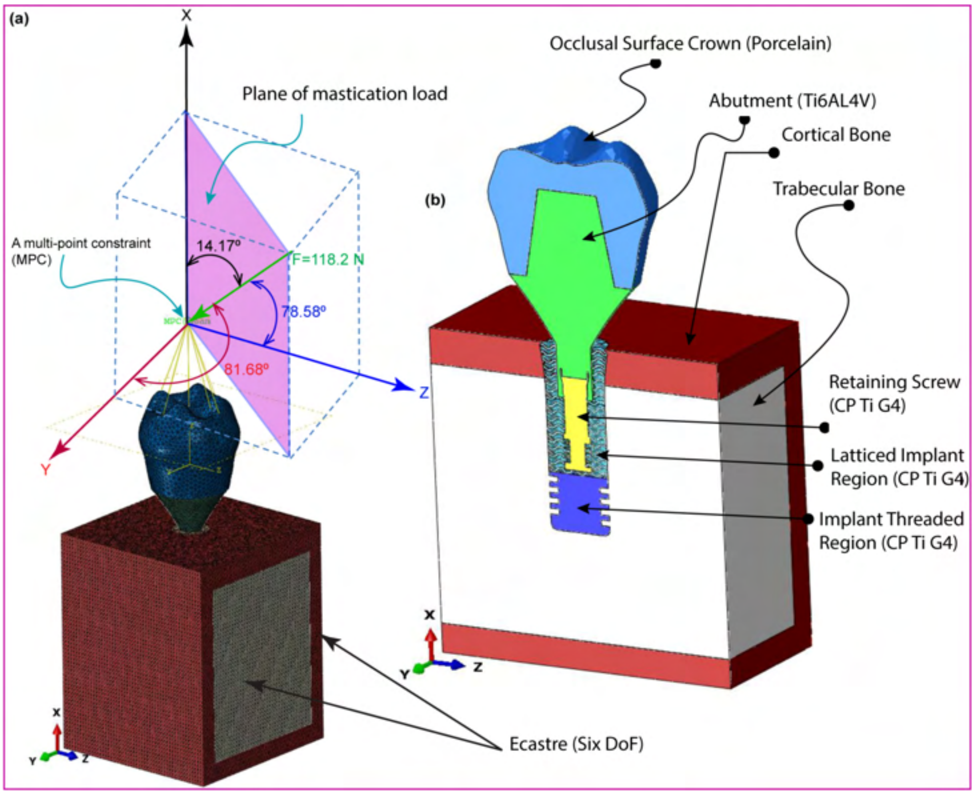

Figure 3.4: Dental implant system, (a) Dynamic mastication loading for 0.5 sec with 2 Hz in a single cycle, and (b) its components.

3.2.6 Design and Manufacturing Process

We used several integrated stages to develop and manufacture the dental implants suggested .Two novel designs were created: a totally TPMS (triply periodic minimal surface) gyroid lattice structure with a square-threaded bottom area and a hybrid design with a solid neck, TPMS lattice middle portion, and square-threaded lower region. CAD models were made in Creo Parametric version 8.0, and lattice structures were made in nTop 4.17.3 so that the size of the pores and the thickness of the struts could be controlled by parameters. Validation was carried out using the 3D finite element analysis (FEA), which replicated physiological loading conditions to assess stress distribution, durability, and structural integrity. The Materialise Magics slicing technique improved layer thickness (30-50 μm) and incorporated support strategies for difficult shapes. Selective Laser Melting (SLM) using Titanium Grade 23 (Ti-6Al-4V ELI) was used in additive production, with validated parameters ensuring structural accuracy. Heat treatment at 650°C for stress relief was followed by surface treatments such as sandblasting, acid etching, and micro-arc oxidation (MAO) to improve osseointegration and CNC machining for dimensional precision. Non-destructive testing (e.g., X-ray CT scanning) and mechanical testing (compression, fatigue) were used for quality control, in accordance with ISO 14801 standards, as well as biocompatibility assessments according to ISO 10993 criteria. The final sterilization process included gamma irradiation or ethylene oxide gas, with sterile packing guaranteeing compliance with medical equipment laws. This approach, underpinned by thorough testing and validation, shows the viability and preparedness of the implants for clinical use.

Table 3.1: Mechanical properties of materials for finite element analysis [**53, 179, 180**].

Material	**Young's Modulus** E **(MPa)**	**Poisson's Ratio** ν	**Density (g/cm^3)**	**Strength (MPa)**
Cortical bone	$E_x = 12,600$	$\nu_{xy} = 0.3$	1.79	190
	$E_y = 12,600$	$\nu_{yz} = 0.253$		
	$E_z = 19,400$	$\nu_{xz} = 0.253$		
		$\nu_{yx} = 0.3$		
		$\nu_{zy} = 0.39$		
		$\nu_{zx} = 0.39$		
Cancellous bone	$E_x = 1148$	$\nu_{xy} = 0.055$	0.45	10
	$E_y = 210$	$\nu_{yz} = 0.01$		
	$E_z = 1148$	$\nu_{xz} = 0.322$		
		$\nu_{yx} = 0.01$		
		$\nu_{zy} = 0.055$		
		$\nu_{zx} = 0.322$		
Gold abutment *	136,000	0.37	17.5	765
Porcelain	68,900	0.28	2.44	145
Titanium grade 4 *	110,000	0.34	4.5	550

3.3 Results

3.3.1 Cyclic Mastication Loading

Figure 3.6 shows how an oblique dynamic load of 118.2 N is applied to the occlusal surface of a dental crown in the buccal-lingual, axial, and mesiodistal directions.Human mastication frequencies generally vary from 0.94 Hz to 2.17 Hz [**195**], which cor-responds to the physiological chewing patterns investigated in this work. This loading replicates a 2 Hz mastication cycle, which accurately reproduces the dynamic stress patterns over a 1.5-second period. The figure depicts increasing load variation throughout the mesiodistal, buccal-lingual, and apical orientations, revealing a smooth shift in load amplitude. The use of multi-point constraints (MPC) with a reference point as the master control considerably improved the accuracy of masticatory force replication, reflecting the complex dynamics found in clinical situations. The cell sizes of the fully latticed designs were FI-111, FI-222, and FI-333, while the hybrid latticed designs were HI-111, HI-222, and HI-333. The results of this explicit dynamic loading and the related boundary conditions closely matched previous findings, demonstrating the simulation's resilience in representing real-world biomechanical phenomena.

Table 3.2: FE mesh statistics of fully and hybrid latticed dental implants, implant components, and their assembly models.

Component	FI-111	FI-222	FI-333	HI-111	HI-222	HI-333
Crown: No. Elements	107,954	107,954	107,954	32,352	32,352	32,352
Crown: No. Nodes	20,670	20,670	20,670	6,658	6,658	6,658
Abutment: No. Elements	85,243	85,243	85,243	23,665	23,665	23,665
Abutment: No. Nodes	17,463	17,463	17,463	5,331	5,331	5,331
Screw: No. Elements	627,098	536,738	536,738	627,098	47,087	47,087
Screw: No. Nodes	121,624	104,716	104,716	121,624	10,674	10,674
Implant: No. Elements	407,478	72,654	37,294	408,753	64,362	25,634
Implant: No. Nodes	134,806	25,465	12,640	126,828	21,636	9,193
Cortical Bone: No. Elements	75,894	75,894	75,894	75,775	75,775	75,775
Cortical Bone: No. Nodes	16,979	16,979	16,979	16,948	16,948	16,948
cancellous Bone: No. Elements	76,821	76,821	76,821	755,638	755,638	755,638
cancellous Bone: No. Nodes	14,782	14,782	14,782	136,485	136,485	136,485
Total: No. Elements	1,290,128	955,304	919,944	1,372,798	1,028,407	989,679
Total: No. Nodes	309,416	200,075	187,250	309,700	204,508	192,065

FI-111 = Fully latticed implant with 111 cell size, HI-111 = Hybrid latticed implant with 111 cell size.

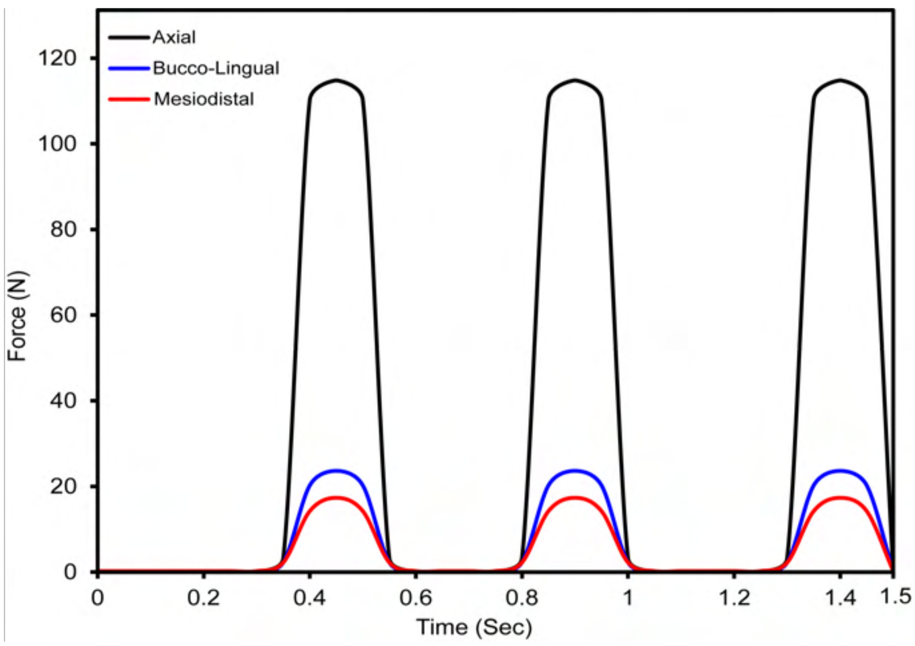

Figure 3.5: Oblique dynamic loading distribution at 118.2 N in buccal-lingual, axial, and mesiodistal directions over a 1.5-second mastication cycle.

3.3.2 Mesh Sensitivity Study

We performed a mesh sensitivity analysis on a completely latticed dental implant with 333 cells. This cell size was chosen because it is computationally efficient and requires less simulation time (Refer to Figure 3.7) . The walls of the TPMS (Triply Periodic Minimal Surface) lattice with a cell size of 333 require less travel distance to reach the next layer than lattices with cell sizes of 111 and 222, which require more travel distance. We investigated element sizes ranging from 0.1 mm to 0.5 mm to see how maximum stress varies with mesh size. The stress vs. time graphs shows minimal difference in maximum stress

Table 3.3: Comparison table for current latticed and previous implant design.

Implant Length	**Thread Type**	**Lattice Structure Type**	**Reference**
Long	Square	Gyroid Triply Periodic Minimal Surface (TPMS)	Current paper
Ultra-Short	Buttress	Diamond lattice	[**Binobaid2024**]]
Long	V-screw	Gyroid and body center cubic octahedron (BCCO)	[**46**]
Long	Fully latticed	Body center cubic octahedron (BCC)	[**190**]
Long	Fully latticed	Diagonal lattice	[**191**]
Long	V-thread	Body-centered cubic (BCC)	[**192**]
Long	V-thread	Diamond lattice	[**193**]
Long	V-thread	Gyroid Triply Periodic Minimal Surface (TPMS)	[**194**]

between 0.1 mm and 0.15 mm element sizes (refer to Figure 3.7). The ideal mesh size for a fully latticed dental implant with a cell size of 333 is 0.1 mm, based on the precision required for finite element analysis and the measured peak stress of 396 MPa.

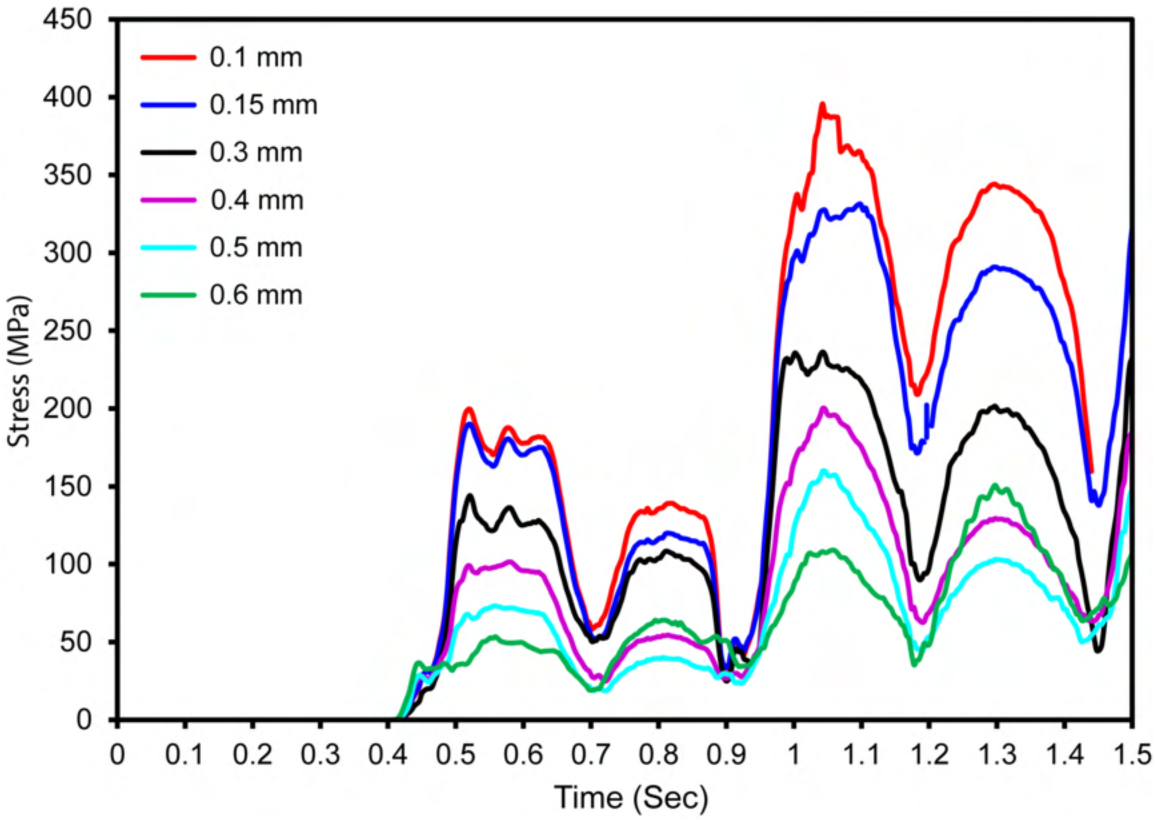

Figure 3.6: Fully latticed implant with cell size of 333 mesh sensitivity analysis, showing maximum stress against time with different element sizes.

3.3.3 Maximum Von Mises Stress in Dental Implant Assembly

Fully Latticed Dental Implant

Figure 3.8 presents the highest von Mises stresses that were found in three totally gyroid latticed dental implants with different-sized cells. The smallest cell-size implant, FLI-111 (1x1x1), has the greatest stress, measured at 533.48 MPa. This degree of stress indicates a more concentrated load-bearing capability, perhaps because of the narrower lattice structure, which may give less distribution room for stress. In comparison, the FLI-222 implant, with a cell size of 2x2x2, showed a decrease in von Mises stress of 420.11 MPa. This suggests increased stress distribution capabilities, most likely due to the larger cell size, which allows for more efficient mechanical force distribution over the implant structure. The biggest cell size studied, FLI-333 (3x3x3), had the lowest von Mises stress of 394.24 MPa. This further decline implies that the implant's capacity to disperse mechanical stress increases with cell growth, leading to reduced total stress levels. Stress concentrations were highest around the implant-bone contact areas, especially near the holes in the cortical and cancellous bone, as well as the implant neck. Furthermore, the highest stress was focused at important interfaces such as the crown-abutment, abutment-implant, screw-retaining, and abutment-implant contact areas.

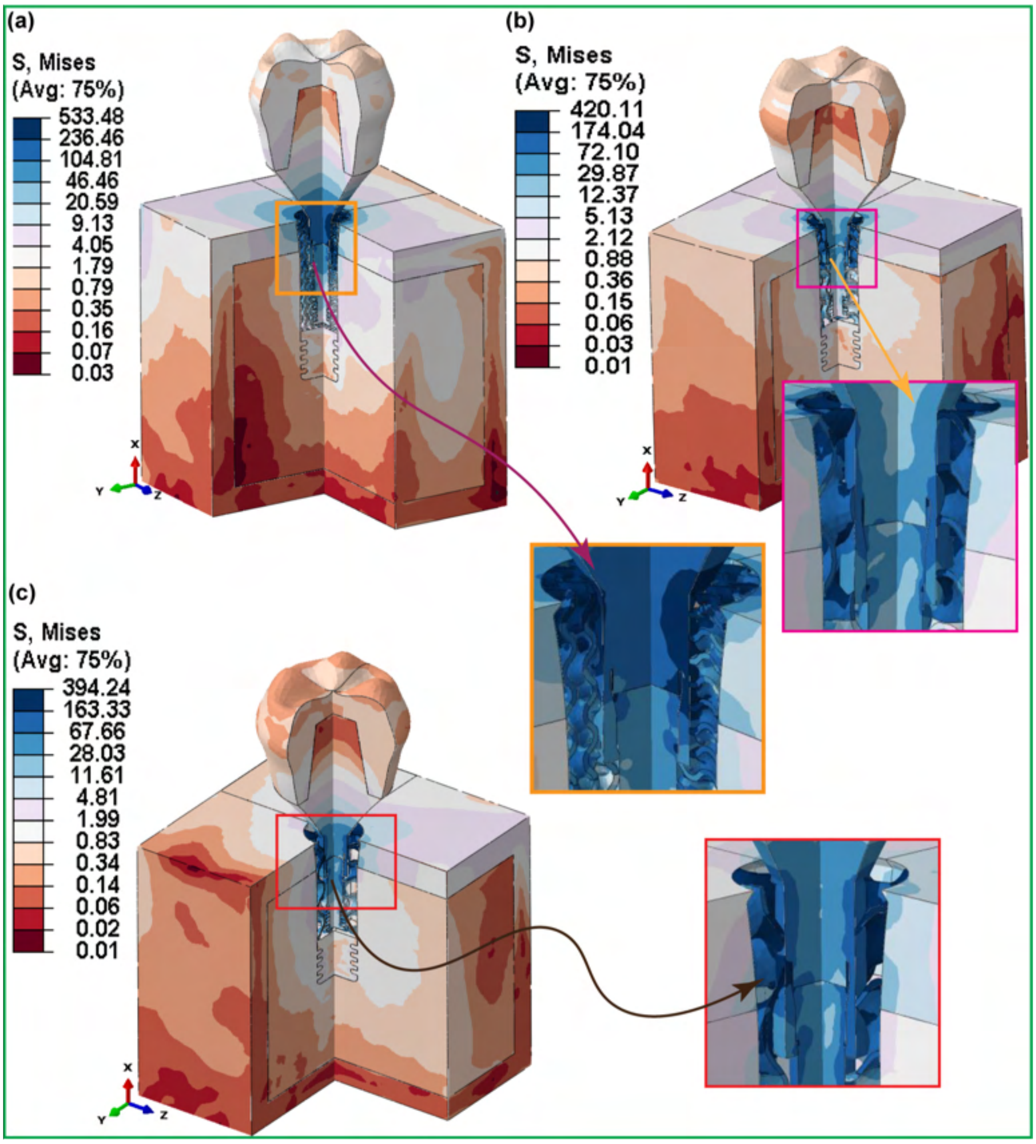

Figure 3.7: FEA Stress Contour Plots for von Mises stress distributions in assembled and cross-sectioned views of three fully gyroid latticed dental implants with varying cell sizes: a) FI-111, b) FI-222, and c) FI-333.

Hybrid Latticed Dental Implant

Figure 3.9 displays how the stresses behave under simulated biting forces for the highest von Mises stresses in three hybrid gyroid latticed dental implants, whose cell sizes were varied. The HI-111 implant, with a 1x1x1 cell size design, has a maximum stress of 512.58 MPa. However, HI-222 has a reduced stress level (407.93 MPa) due to its larger cell size of 2x2x2. Likewise, the largest cell-size implant, HI-333 (3x3x3), had a lower stress value of 366.52 MPa. These findings indicate that among hybrid latticed designs, the implant with a smaller cell size suffered the most stress, while both smaller and larger cell topologies resulted in lower stress levels. In contrast, in the case of completely latticed implants, as cell size rose from FLI-111 to FLI-333, von Mises stress decreased consistently, demonstrating that larger cell sizes result in better stress distribution. The hybrid latticed implants, on the other hand, showed a non-linear pattern, with the largest stress recorded in the medium cell size (HI-222). This was different from the trend seen in the fully latticed implants. This variation emphasizes the complicated relationship between lattice structure and stress distribution in dental implants. Stress concentrations were highest around the implant-bone contact areas, especially near the holes in the cortical and cancellous bone, as well as the implant neck. Furthermore, the highest stress was focused at important interfaces such as the crown-abutment, abutment-implant, screw-retaining, and abutment-implant contact areas.

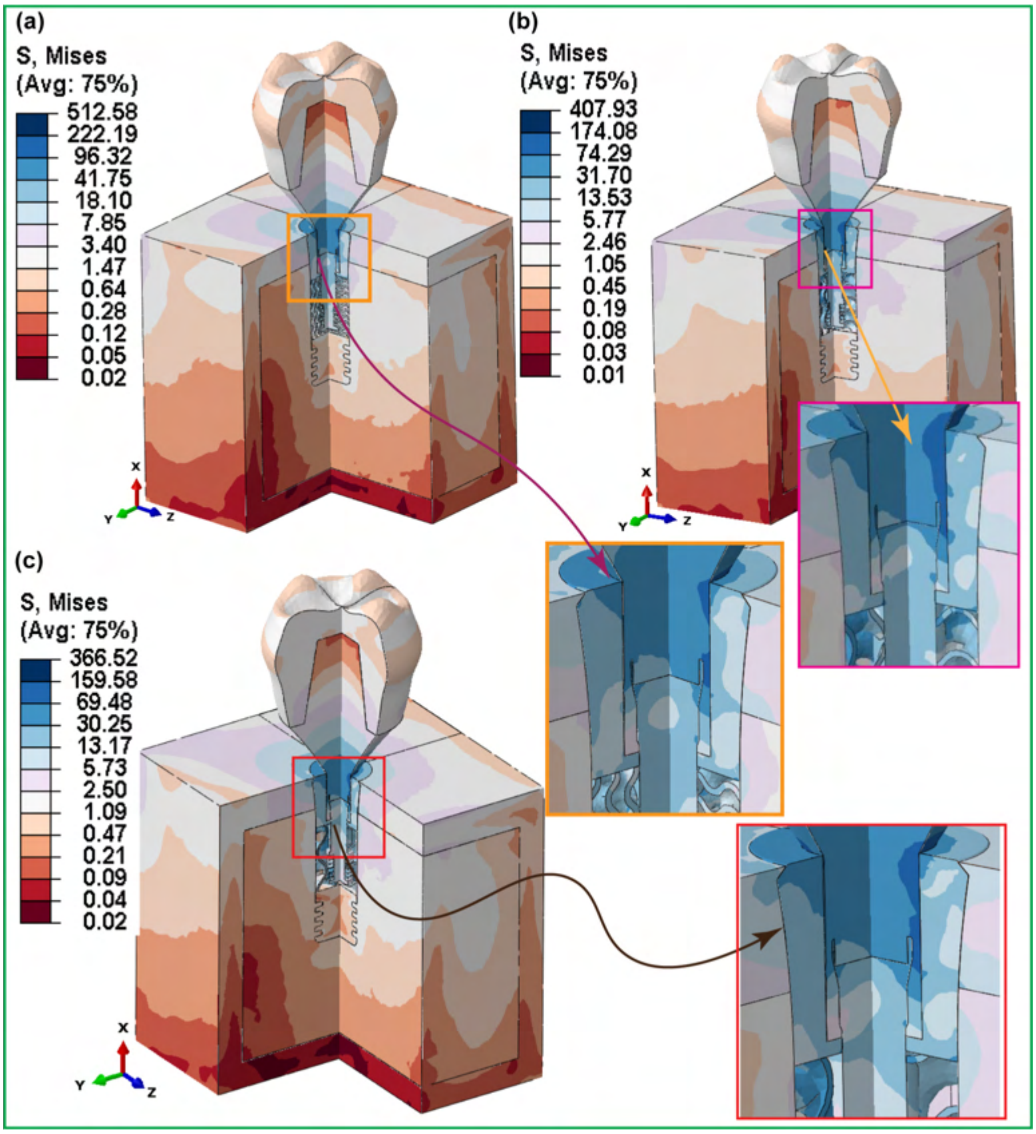

Figure 3.8: FEA Stress Contour Plots for the von Mises stress distributions in assembled and cross-sectioned views of three hybrid gyroid latticed dental implants, each with different cell sizes: a) HI-111, b) HI-222, and c) HI-333.

3.3.4 Fully and Hybrid Latticed Dental Implant and Retaining Screw

Figure 3.10 and Figure 3.11 shows a comparison of the maximum von Mises stresses for completely gyroid latticed and hybrid gyroid latticed dental implants, as well as their corresponding retention screws, across various cell sizes. Fully latticed implants show a clear pattern in which von Mises stress reduces with increasing cell size. The FLI_111 implant, with the smallest cell size of $1 \times 1 \times 1$, exhibited the highest stress at 460.25 MPa. This high stress level suggests that smaller lattice cells may concentrate stress more than larger ones. The FLI_222 and FLI_333 implants, with cell sizes of $2 \times 2 \times 2$ and $3 \times 3 \times 3$, respectively, demonstrated reduced stress values of 410.86 MPa and 395.67 MPa. As the cell size increases, the stress distribution over the implant structure improves, potentially enhancing implant endurance and performance.

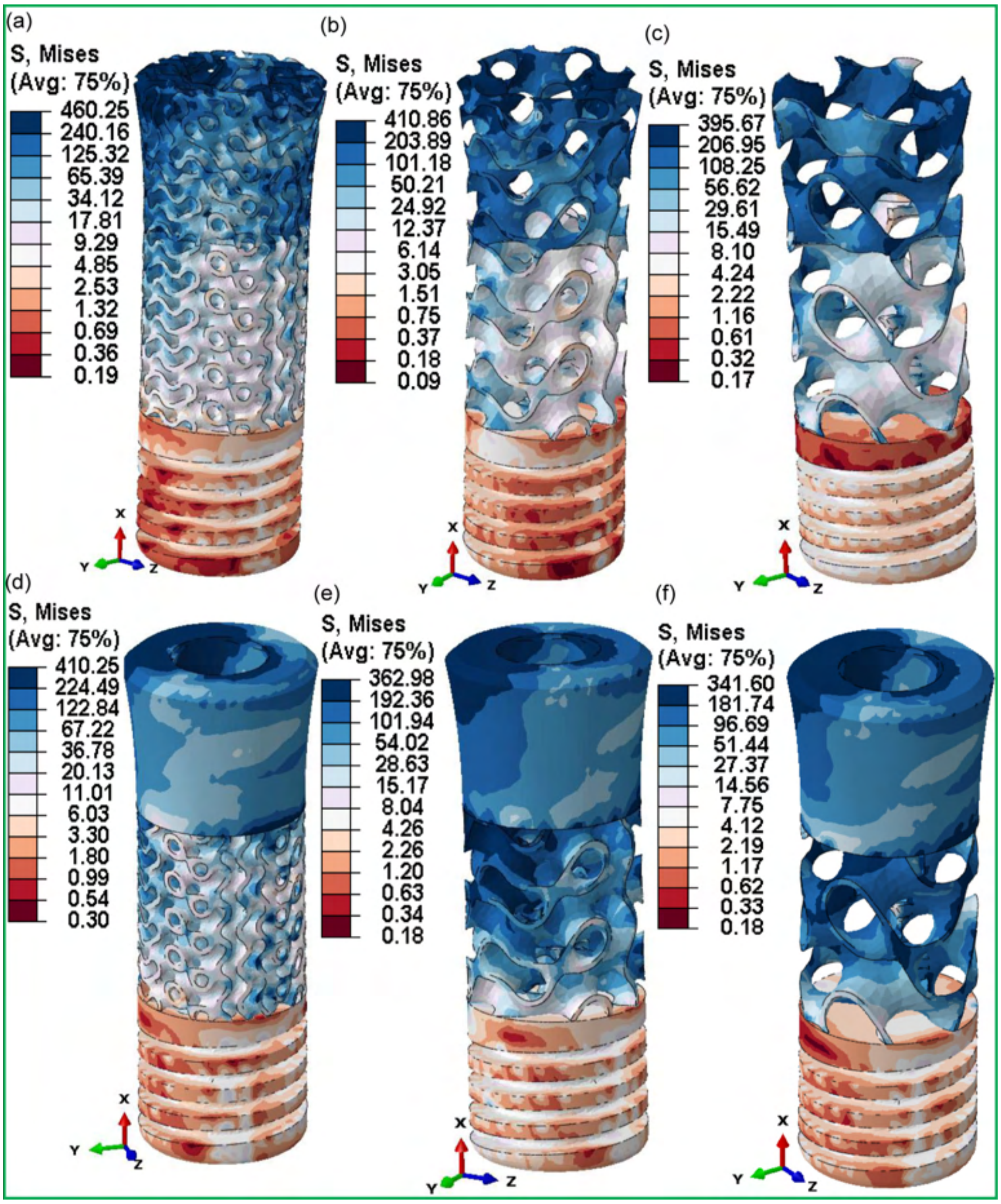

Figure 3.9: Maximum von Mises stress distribution for fully latticed implants: (a) FLI_111, (b) FLI_222, (c) FLI_333; and for hybrid latticed implants: (d) HI_111, (e) HI_222, (f) HI_333.

The retention screws associated with these implants followed a similar stress pattern (refer to Figure 3.11), with the FLI_111 screw experiencing the maximum stress at 425.11 MPa, followed by 420.11 MPa and 390.30 MPa for the FLI_222 and FLI_333 screws, respectively. This trend highlights the influence of cell size not only on the implant body but also on critical components like screws, which play a vital role in the overall mechanical stability of the implant system. In contrast, the hybrid latticed implants exhibited a more variable stress distribution pattern. The HI_111, with a cell size of $1 \times 1 \times 1$, had a stress of 410.25 MPa, lower than its fully latticed counterpart but still significant. The HI_222 and HI_333 implants recorded stress values of 362.98 MPa and 341.60 MPa, respectively, showing a less consistent decrease in stress with increasing cell size compared to the fully latticed designs. The stresses in the retaining screws of these hybrid models also varied. The HI_111 screw exhibited significantly lower stress at 312.58 MPa compared to its fully latticed counterpart, indicating that the hybrid design may influence stress distribution differently. This difference could be attributed to structural integrity variations or load-bearing pathways within the implant.

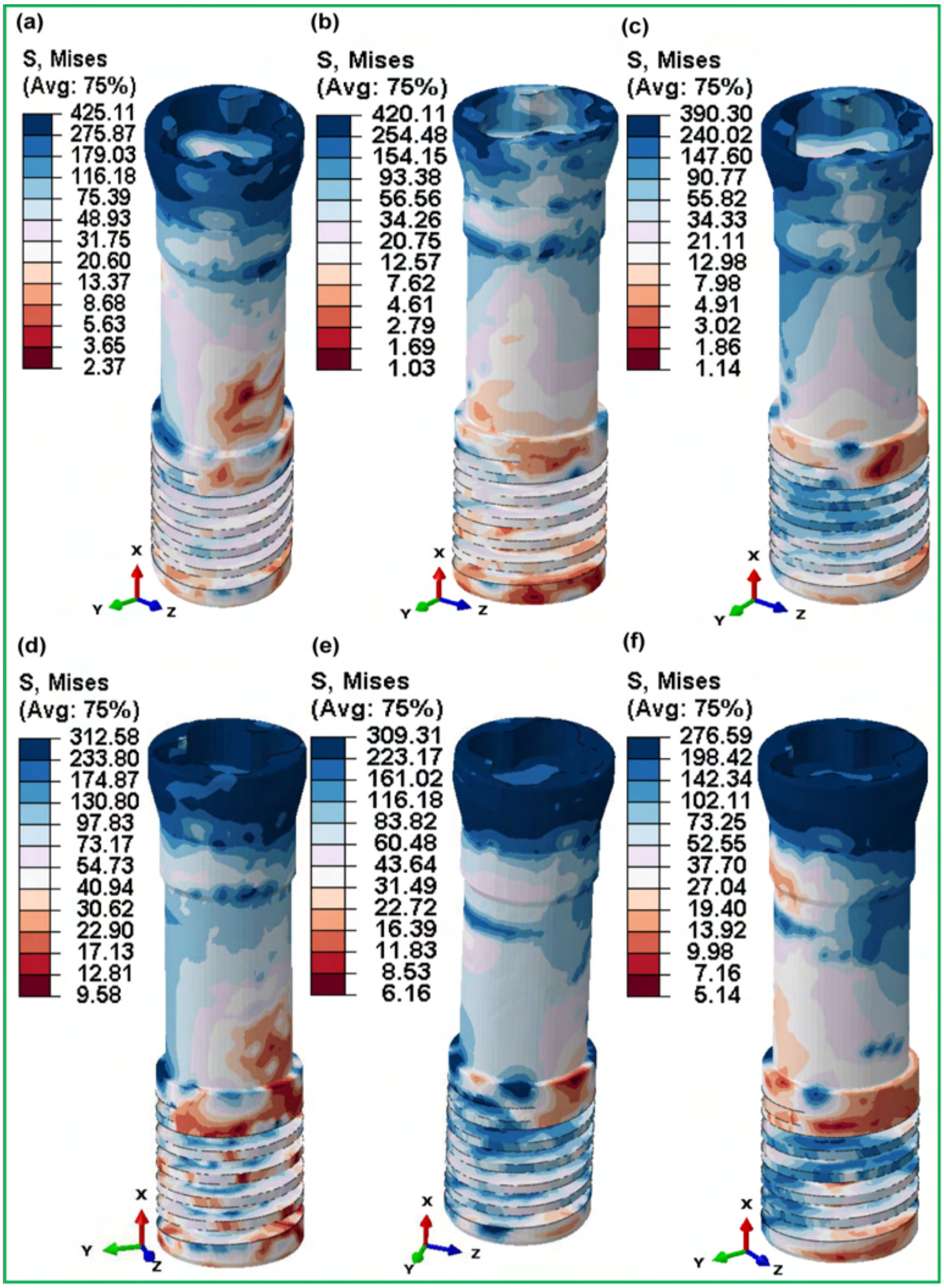

Figure 3.10: Maximum von Mises stress distribution in retaining screws for various cell sizes: (a) FLI_111, FLI_222, FLI_333 for fully latticed implants, and (b) HI_111, HI_222, HI_333 for hybrid latticed implants.

3.3.5 Fully and Hybrid Lattices Dental Implant in Cortical and Cancellous Region

Figure 3.12 and Figure 3.13 show in detail the highest von Mises stresses in the cortical and cancellous region that are connected to fully hybrid latticed dental implants at various cell sizes.

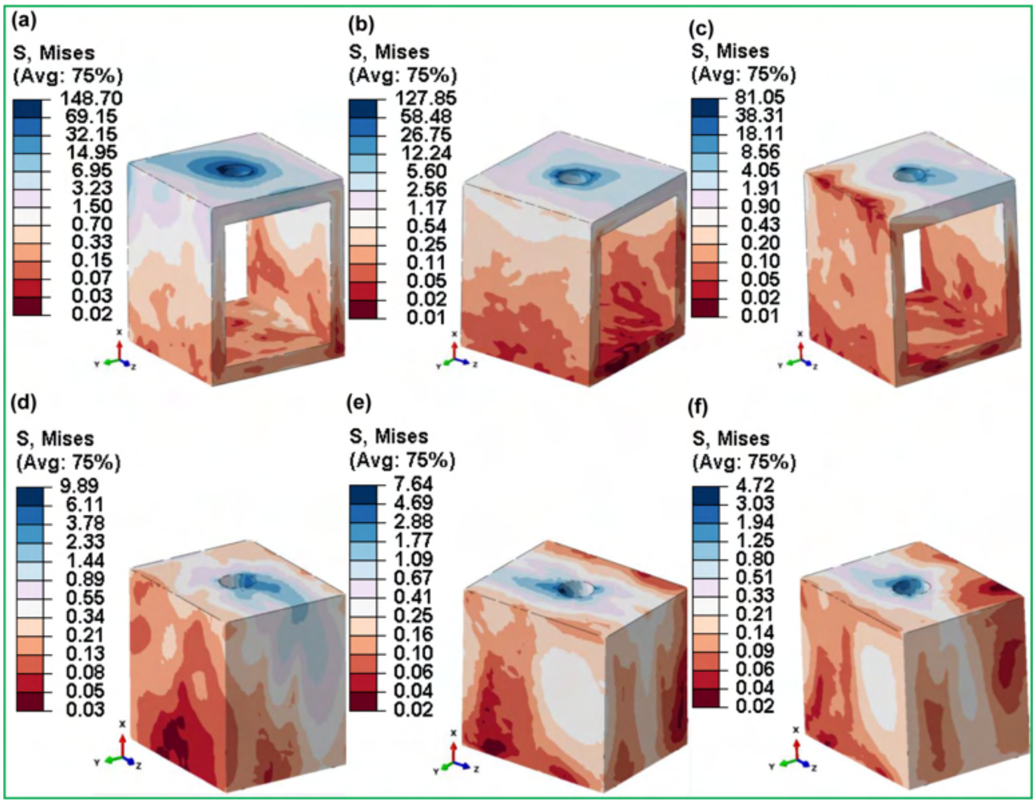

Figure 3.11: Maximum von Mises stress distributions for fully gyroid latticed dental implants across various cell sizes in the cortical region: (a) FLI_111, (b) FLI_222, (c) FLI_333; and in the cancellous region: (d) FLI_111, (e) FLI_222, (f) FLI_333.

The von Mises stress results for the fully latticed implants (FLI-111, FLI-222, and FLI-333) show considerable differences depending on cell size and bone type. FLI-111 had the maximum stress in the cortical bone at 148.70 MPa, indicating a significant concentration of stress, especially in the implant-bone interface around the neck, where the implant and bone are in close contact. This region is crucial because it absorbs the majority of mechanical stresses during mastication. In contrast, FLI-333 exhibits the lowest stress in cortical bone at 81.05 MPa, suggesting a more advantageous stress distribution that may improve implant lifetime and lower the risk of bone resorption. In Figure 3.12d, the FLI-111 again records increased stress at 9.89 MPa for the cancellous region. This is consistent with studies in cortical bone and highlights a pattern in which smaller cell sizes could aggravate stress concentrations, particularly around the implant neck and hole. Meanwhile, FLI-222 and FLI-333 exhibit lower stresses (7.64 MPa and 4.72 MPa, respectively), suggesting that smaller cell sizes may reduce stress peaks in less dense bone formations. The stress levels in the cortical and cancellous bones for hybrid gyroid latticed dental implants with a solid neck (HI-111, HI-222, and HI-333) are shown in Figure 3.13. The HI-111 model has the maximum stress level inside the cortical bone (118.64 MPa). The implant hole, a crucial area where the implant closely contacts the bone, concentrates this peak stress. Such high stress concentration is important because it shows places where the implant's structure and overall therapeutic performance could be damaged. This suggests that the HI-111 cell size and lattice design may not be as good at distributing stress. In contrast, the HI-222 implant exhibits substantially lower stress levels, with 97.27 MPa in cortical bone and a remarkably low 6.12 MPa in cancellous bone. These results indicate that the HI-222's lattice structure and cell size are very efficient in distributing stress throughout the implant structure. This optimum stress mitigation not only increases the implant's longevity but also reduces the likelihood of bone resorption and implant failure, suggesting better biomechanical performance compared to its contenders.

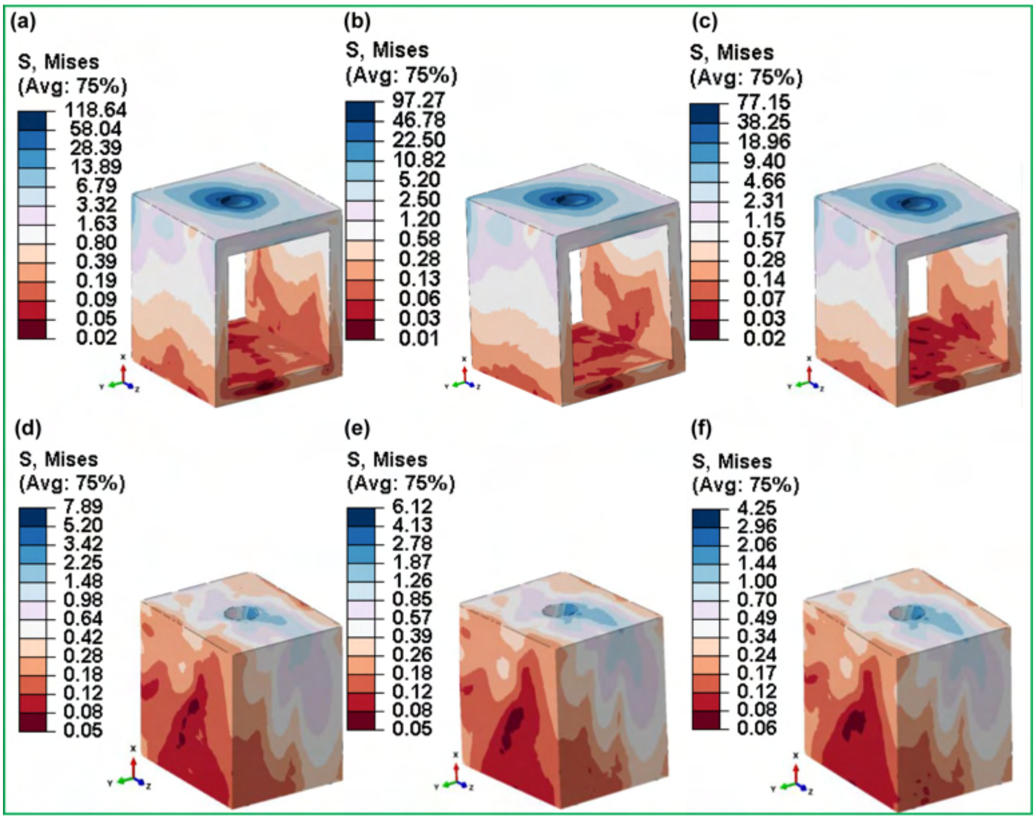

Figure 3.12: Maximum von Mises stress distributions for hybrid gyroid latticed dental implants across various cell sizes in the cortical region: (a) HI_111, (b) HI_222, (c) HI_333; and in the cancellous region: (d) HI_111, (e) HI_222, (f) HI_333.

3.3.6 Fully and Hybrid Latticed in Crown and Abutment

The highest von Mises stresses can be seen in Figures 3.14 and 3.15, which show the crown and abutment parts of fully and hybrid latticed dental implants with three different cell sizes.

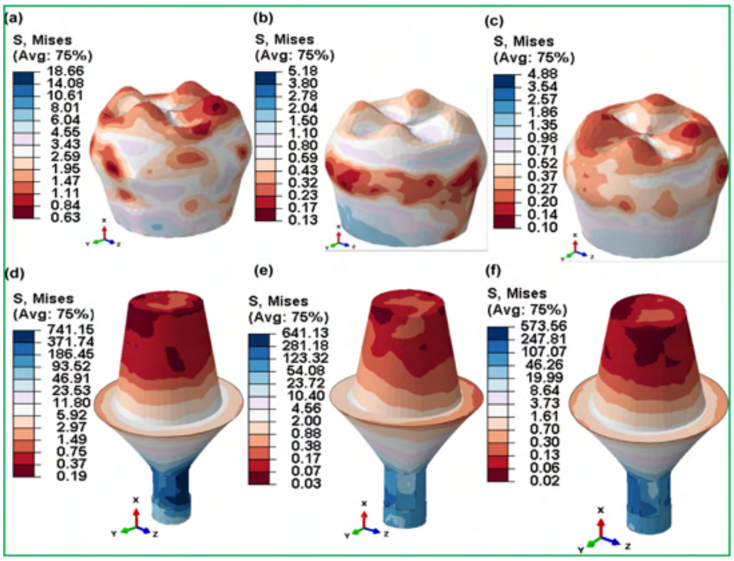

Figure 3.13: Maximum von Mises stress distributions for fully gyroid latticed dental implants across various cell sizes in the crown: (a) FLI_111, (b) FLI_222, (c) FLI_333; and in the abutment: (d) FLI_111, (e) FLI_222, (f) FLI_333.

The crown components of fully latticed implants (refer to Figure 3.14) had relatively higher in FLI-111, with 18.66 MPa, and lower stress values, with, FLI-222 at 5.18 MPa, and FLI-333 at 4.88 MPa. On the contrary, the abutment components in the same group experience notably higher stresses: FLI-111 at 741.15 MPa, FLI-222 at 641.13 MPa, and FLI-333 at 573.56 MPa. Conversely, the hybrid latticed implants (refer to Figure 3.14) demonstrate comparatively lower stress levels in the crown compared to their fully latticed counterparts, with HI-111 at 15.03 MPa, HI-222 at 4.88 MPa, and HI-333 at the lowest at 4.04 MPa.The abutment stresses in these hybrid models are much higher, resulting in a stiffer dental implant for stress distribution: HI-111 672.38 MPa, HI-222 581.92 MPa, and HI-333 492.72 MPa. Compared to

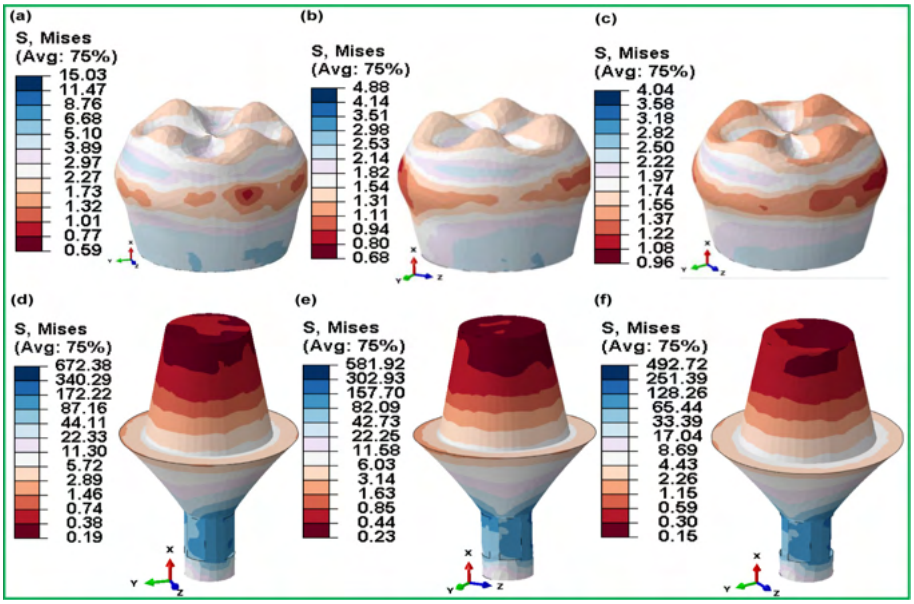

Figure 3.14: Maximum von Mises stress distributions for hybrid gyroid latticed dental implants across various cell sizes in the crown: (a) HI_111, (b) HI_222, (c) HI_333; and in the abutment: (d) HI_111, (e) HI_222, (f) HI_333.

fully latticed designs, hybrid lattice implants show a more uniform distribution of stresses between the crown and the abutment, as well as lower stress levels in the abutment. The hybrid arrangements provide much lower stress in the abutment portion compared to their completely latticed counterparts, suggesting possibly greater mechanical performance in clinical situations. Furthermore, within each configuration, the crown consistently exhibits lower stresses than the abutment, indicating a significant difference in stress management between these two key components of dental implants.

3.3.7 Strain in Assembled Dental Implant for Fully and Hybrid Latticed

Figure 3.16 shows the strain ($\mu\varepsilon$) of fully latticed dental implant setups with different cell sizes (FLI-111, FLI-222 and FLI-333) during a 1.5 sec oblique load cycle over three cycles. At first, strain in all three designs was zero, indicating strong initial stability under load. However, after roughly 0.4 sec., the strain shifts positively, reaching 450 $\mu\varepsilon$ for FLI-222 and 415 $\mu\varepsilon$ for FLI-333. The figure shows the behavior of fully latticed implants (FLI-111, FLI-222, and FLI-333) under oblique dynamic stress during a three-mastication cycle (1.5 sec. or 2 Hz). The strains steadily rise for all three lattice configurations over the first 0.4 sec. of loading. Beyond this time, the curves exhibit substantial slope fluctuations, with more stable behavior nearing 1.5 sec. The FLI-333 has the most strain, followed by the FLI-222 and the FLI-111, which have the least movement, showing that mechanical responses vary across lattice configurations under the same dynamic situation. These variances indicate that the implants have varying stiffness and flexibility, which influences their mechanical performance under dynamic mastication stresses.

As the cycle progresses, the strain exhibits dynamic, cyclic behavior that is consistent with the loading patterns observed during clinical mastication. Specifically, FLI-333 and FLI-222 show a large strain, peaking at 1100 $\mu\varepsilon$ and 1095 $\mu\varepsilon$, respectively. This implies that it is more flexible under stress, which could affect the deformation at the bone-implant interface. In comparison, FLI-111 has more controlled strain of 24 μm and 17 μm, respectively. These changes show the effect of cell size on implant biomechanical performance, with smaller cell sizes (FLI-111) allowing for higher displacement and maybe more deformation, which may compromise osseointegration and stability. The bigger cell sizes (FLI-333 and FLI-222) exhibit reduced displacement, suggesting a more stable interface under similar loading conditions.

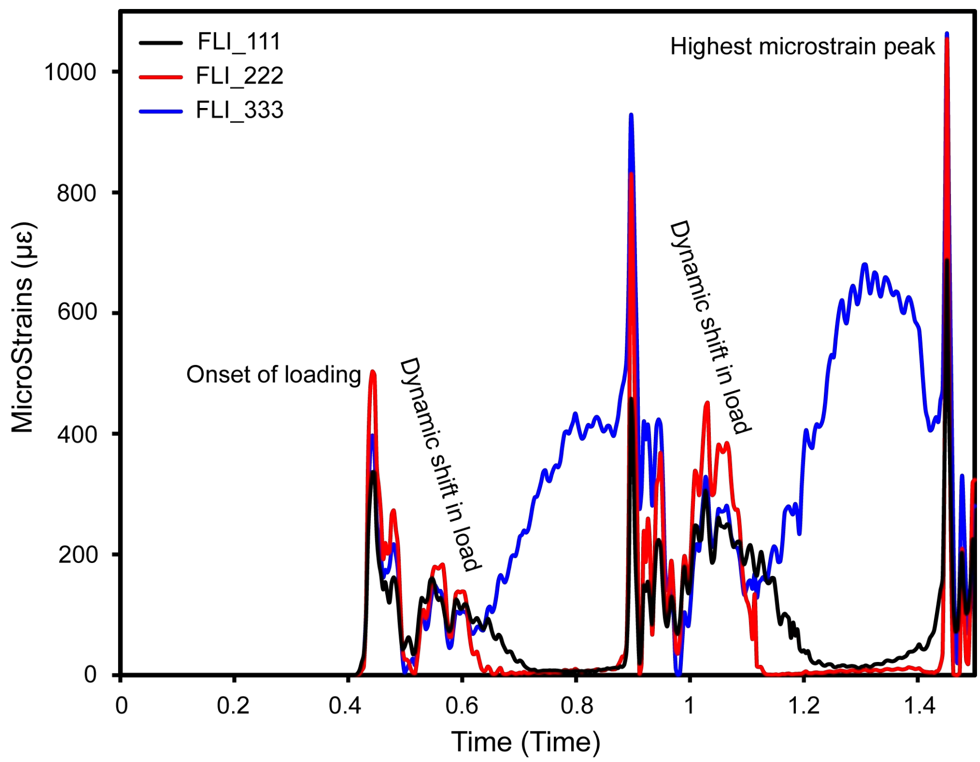

Figure 3.15: Strains within three cycles of mastication for fully latticed configurations at various cell sizes (FI-111, FI-222, and FI-333).

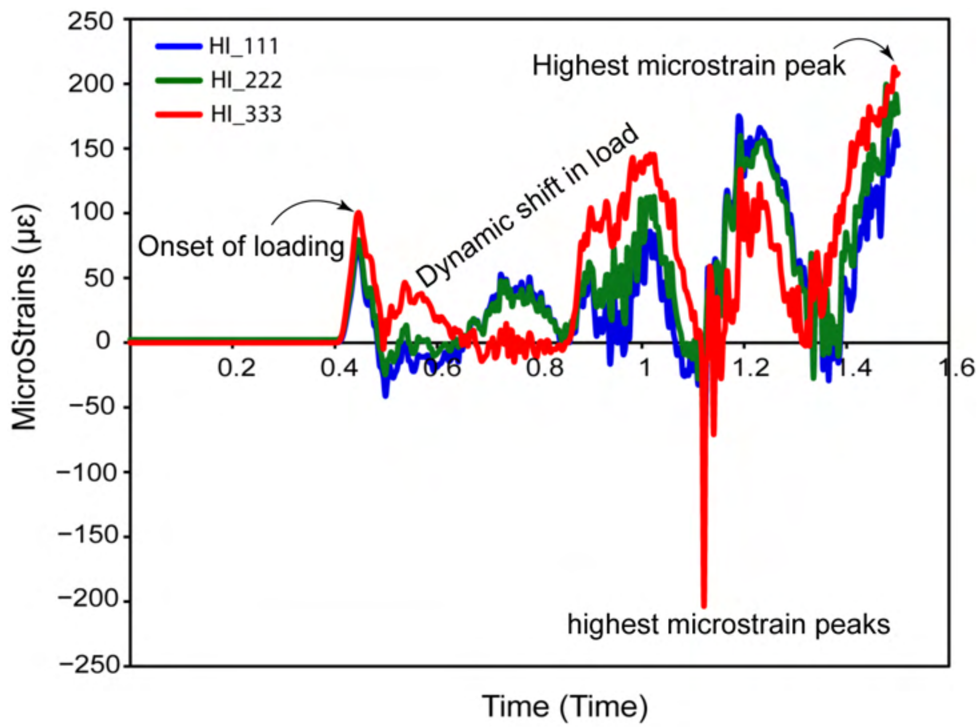

Figure 3.16: Strains within three cycles of mastication for hybrid latticed configurations at various cell sizes (HI-111, HI-222, and HI-333).

These findings emphasize the importance of lattice structure and cell size in regulating dental implant deformations and subsequent deformation. Such deformations are critical for determining the mechanical integration of the implant into the surrounding bone structure, which influences both immediate post-operative stability and long-term osseointegration success. In Figure 3.17, you can see in detail how the deformation responses change in the cortical bone for hybrid latticed dental implants with different cell sizes during the three cycles of 1.5 sec of mastication oblique loading. Initially, all configurations exhibit zero strains at around 0.4 sec., indicating early stability. However, immediately after 0.4 sec., it peaks at 100 $\mu\varepsilon$ for HI-333, then further rises to 150 $\mu\varepsilon$ at 1.0 sec.. Strains shift negative, significantly rising to 200 $\mu\varepsilon$ for HI-333 at 1.17 sec and then to 225 $\mu\varepsilon$ for HI-333, 190 $\mu\varepsilon$ for HI-222, and 160 $\mu\varepsilon$ for HI-111 at around 1.5 sec. This implies an initial inward movement under strain, similar to the compressive action seen in masticatory activity.

The strain then enters a dynamic phase with cyclic fluctuations, including peaks and troughs. At around 1.10 sec., HI-333 has the most significant minimal strain at 220 $\mu\varepsilon$. The strain follows a cyclic pattern with variable increments of amplitude, demonstrating the implant structure's durability under cyclic stresses. This cyclic action resembles the normal masticatory process, which is important for determining the implants' biomechanical compatibility and functional stability.

Comparing these findings to those from Figure 3.14 for fully latticed implants, it is noticeable that hybrid latticed implants have lower peak displacements, demonstrating that hybrid arrangements may better limit strains at the bone-implant interface. Smaller strains promote osseointegration by lowering possible micromechanical instabilities that might jeopardize implant life and success. These nuanced deformations in behavior in hybrid implants, characterized by lower peak values and more regulated cyclic changes, highlight their potential for improved clinical performance, especially under dynamic loading circumstances like normal masticatory activities.

3.4 Discussion

The results of our dynamic explicit finite element analyses provide compelling evidence supporting the hypothesis outlined in the introduction: This study presents an innovative dental implant design that incorporates gyroid TPMS lattice components precisely placed utilizing additive manufacturing. The gyroid lattice is positioned in the very middle region of the hybrid lattice design, whereas the fully latticed design extends it to both the neck and middle sections. To assure initial stability, both designs have a square-threaded section at the base. Our dynamic explicit finite element analysis demonstrates that these improvements enhance stress distribution as osseointegration advances. The square-threaded region increases implant stiffness, and the gyroid lattice decreases stress concentrations in key locations like the implant neck and surrounding bone. Furthermore, it improves deformations under cyclic masticatory stress. These improvements are critical for long-term implant success because they ensure mechanical stability and optimal load distribution. Fully solid implants are frequently associated with increased marginal bone loss and less bone-to-implant contact, which reduces their long-term stability. Hybrid dental implants with lattice structures and screw threads optimize stress distribution, implant stability, and bone integration [**87, 192, 196**].

Figure 3.6 shows the modeling of an oblique dynamic load of 118.2 N applied throughout three cycles of masticatory loading at a frequency of 2 Hz for 1.5 sec. This technique is consistent with earlier studies using comparable loading settings, verifying the accuracy of the results. Multi-point constraints (MPC) properly mimic mesiodistal, buccal-lingual, and apical load orientations, resulting in a realistic replication of masticatory scenarios. This innovative simulation accurately captures stress and strain distributions under dynamic loading, giving reputable data on implant performance. The findings emphasize the importance of dynamic loading models in connecting theoretical pre-dictions to clinical reality, providing a reliable tool for preclinical evaluation and optimization of dental implant designs This demonstrates the simulation tools' ability to reliably predict clinical performance and validates their effectiveness. This alignment emphasizes the importance of dynamic loading models in the preclinical evaluation of dental implants, providing the groundwork for future breakthroughs in implant design and testing [**53, 179, 180**].The mesh sensitivity study reveals that element size has little to no impact on final outcomes between 0.1 mm and 0.15 mm. The highest stress values were essentially equal, demonstrating that finer mesh sizes greater than 0.1 mm do not considerably enhance accuracy. As a result, a mesh size of 0.1 mm is adequate for accurate stress predictions, with a peak stress of 396 MPa. This option achieves the perfect interaction between computational economy and accuracy, making it excellent for finite element analysis of latticed dental implants with a 333-cell size.

Figure 3.8 and Figure 3.9 demonstrate the significance of medium cell sizes in maintaining biomechanical stability in dental implants. The FLI-222 fully latticed implant has an ideal stress distribution (422.34 MPa), but the HI-222 hybrid balances stress at 504.43 MPa. Non-linear designs, with HI-111 exhibiting greater stress than HI-222 and HI-333, emphasize the intricate link between lattice structure and stress. Medium cell sizes optimize deformations, increase osseointegration and stress distribution, and and lowering potential risks associated with early healing. These designs increase the lifespan of the implant while decreasing the danger of bone resorption and mechanical failure. The findings are consistent with past studies, highlighting the significance of improved lattice geometries in enhancing stability and outcomes, especially in situations of low bone quality or severe loading. Previous studies found that optimized lattice structures increase stress distribution and implant lifetime [**46, 48, 191, 193, 194**]. These new results support the idea that medium lattice topologies may improve mechanical stability. Furthermore, another research reported that hybrid designs in dental implants had an advantage in terms of biomechanical performance due to cell size optimization [**46, 191**]. The current research expands on this information by revealing that the HI-222 is a clinically ideal option, notably for minimizing implant failure and improving patient outcomes.

Figure 3.10 and Figure 3 11 shows a striking comparison of maximum von Mises stresses in fully and hybrid gyroid latticed dental implants and their accompanying retention screws at various cell sizes. In fully latticed implants, stress reduces consistently with increasing cell size: the smallest FLI-111 implant has the maximum stress at 460.25 MPa, which reduces to 410.86 MPa for FLI-222 and 395.67 MPa for FLI-333 (refer to Figure 3.10a). This pattern indicates that medium cell sizes improve stress distribution, possibly increasing the implant's mechanical stability and function. In the case of the hybrid gyroid TPMS lattice design, there is a clear trend of decreasing maximum von Mises stress as the cell size increases. Specifically, the HI-111 model has a maximum stress of 410.25 MPa, which reduces to 362.98 MPa for HI-222 and 341.60 MPa for HI-333 (refer to Figure 3.10d, 3.10e, and 3.10f). This pattern shows a continuous decrease in stress with increasing cell size. Similarly, the accompanying retention screws follow a similar pattern, with stress decreasing from 452.68 MPa in the FLI-111 to 387.22 MPa in the FLI-333, demonstrating how cell size optimization may improve overall implant system integrity (refer to Figure 3.11a, 3.11b, and 3.11c).This arrangement not only enhances the implant's functional lifetime by preventing mechanical failures, but it also protects accompanying components such as retaining screws and surrounding bones. Hybrid latticed implants find the best balance between porosity and strength by increasing cell size and adding solid structural elements. This leads to new implant designs that meet both biomechanical and clinical standards. In contrast to prior studies that suggested lower stress at the implant neck for porous designs [**197**], our data show that tension is highly concentrated in the lattice and neck hole areas in both completely and hybrid latticed implants. This approach emphasizes the need for improved design considerations in these crucial areas.

Figure 3.12 and Figure 3.13 show stress distribution at the bone-implant contact, which has significant clinical outcomes. Among fully latticed designs, the FLI-333 model has the highest stress concentration in cortical bone, increasing the possibility of mechanical failure in load-bearing locations. In contrast, the FLI-222 design increases stress distribution, lowering biomechanical challenges like bone resorption and implant instability. Hybrid designs improve performance even further, with HI-222 exhibiting the greatest stiffness-to-flexibility ratio. By combining lattice structures with solid components, this arrangement significantly reduces stress and enhances implant lifespan. Clinically, these findings highlight the effectiveness of hybrid implants like HI-222 in minimizing localized bone loss and increasing outcomes under difficult settings such as poor bone quality or heavy loading. These findings are consistent with previous research highlighting the importance of optimal lattice and hybrid designs in ensuring long-term biomechanical stability and implant success. This property effectively reduces peak stress concentrations commonly found around the holes of cortical and cancellous bones, aligning with prior research that pinpoints potential sites for bone resorption [**46, 189, 197**].

Figure 3.14 and Figure 3.15 depict stress distribution in the crowns and abutments of fully and hybrid lattice implants, which have substantial medical outcomes. Fully latticed implants, such as the FLI-111, have significant abutment stresses (504.43 MPa), which might cause mechanical fatigue under clinical loads. In contrast, hybrid designs, notably HI-222, lower abutment stress to 251.17 MPa, increasing implant longevity. Clinically, this stress decrease reduces the chance of abutment failure and boosts implant life. Previous research has shown that integrating lattice systems with solid parts improves biomechanical performance and reduces problems such as abutment loosening or fracture.

Figure 3.16 and Figure 3.17 show the strain responses of completely and hybrid Gyroid TPMS lattice implants to cyclical masticatory stress for 1.5 sec. Fully latticed implants, especially FLI-333 and FLI-222, have larger strains (1100 μm and 1095 μm, respectively), suggesting more flexibility but increased deformation, which could inhibit osseointegration. Hybrid designs lower strains substantially, with HI-333,

HI-222, and HI-111 peaking at 225 $\mu\varepsilon$, 190 $\mu\varepsilon$, and 160 $\mu\varepsilon$, respectively, exhibiting greater biomechanical stability. With hybrid designs providing greater displacement control and enhanced potential for osseointegration during dynamic mastication, our findings emphasize the impact of lattice structure and cell size on implant function, making them more appropriate for long-term clinical success.
We compared our results to prior research on lattice-based implants made using additive manufacturing (AM). Barba et al. [**198**] emphasized the need of matching lattice mechanical propertiesto bone in order to improve osseointegration and minimize stress shielding. Burton et al. [**199**] confirmed that optimized lattice geometries make structures more mechanically stable. This fits with our results that gyroid lattice implants make stress distribution better and reduce deformation. Similarly, Wang et al. [**200**] found that 60%–70% porous lattices increase bone ingrowth, which supports our design's pore connection for better integration. These results support the biomechanical viability of gyroid lattice-based dental implants.
Additive fabrication of lattice-structured orthopedic implants reduces weight and improves mechanical performance. However, the longevity of these implants under biological conditions such as corrosion and fatigue, as well as the intricacy of their manufacture, present hurdles. Kladovasilakis et al. [**91**] state that addressing these challenges will be critical to their effective clinical utilization. While additively made implants, especially those with unique designs, have shown encouraging clinical results, questions remain about their long-term biological function. Studies by Anitua et al. [**201**] reveal good implant survival rates in the short term but emphasize the danger of problems such as soft tissue exposure and infection, which might possibly be connected to the implant's complicated design. According to Roy et al. [**202**], the greater complexity of these designs may result in higher production costs, which may impact the broad acceptance of these implants in clinical settings. Nonetheless, as progress is made and more data is acquired, these issues may be addressed by new materials and production methods. As a result, more long-term studies are required to establish the overall practicality of these implants in clinical settings.

The current work applies dynamic explicit finite element analysis to fully and hybrid-latticed dental implants with a square-threaded design in the implant's bottom area. While the findings are impressive and provide important insights into clinical and customized dental implant design, further study is required before use in clinical trials. Future research should focus on creating the implants utilizing metal additive manufacturing techniques, such as powder bed fusion with titanium, to assess their fatigue resistance. In vivo testing is also advised to confirm their performance under physiological settings. In summary, the results underscore the critical role of lattice cell size and hybrid design in optimizing mechanical stability and stress distribution. Hybrid latticed implants, particularly the HI-222 model, outperform other designs by reducing mechanical stresses, minimizing deformations, and enhancing osseointegration. These findings offer valuable insights for advancing implant designs to meet both biomechanical and clinical requirements, paving the way for improved patient outcomes and long-term implant success.

3.5 Conclusions

This research investigates the biomechanical performance of dental implants, with an emphasis on the effects of lattice structure and cell size on stress distribution, mechanical stiffness, and deformation stability. The study's goal is to improve clinical outcomes by comparing fully gyroid-latticed and hybrid gyroid-latticed implants with a solid neck across various cell sizes. The investigation came to the following key conclusions:

- Hybrid latticed implants, especially those with medium cell sizes (HI-222), exhibit excellent stress distribution. These designs efficiently lower stress concentrations in crucial locations, possibly improving implant lifetime and success.
- In comparison to fully latticed implants, hybrid designs provide higher mechanical rigidity. This improvement is critical for preserving structural integrity under typical masticatory stresses, which is necessary for the implants' long-term durability.
- The researchers discovered that hybrid latticed implants with solid necks had significantly reduced deformations at the bone-implant contact. This decrease is critical for improving osseointegration and lowering the possibility of implant failure due to biomechanical instabilities.
- Tailored hybrid latticed designs with optimal cell sizes show promise in clinical applications, outperforming standard fully latticed implants. The HI-222 arrangement is especially advantageous, offering a mix of flexibility and load-bearing capability appropriate for a wide range of clinical conditions.

- Adding a solid neck to hybrid latticed implants makes stress distribution much better, managing stress in a way that a fully latticed configuration can't. Medium-sized cells, particularly in hybrid topologies like HI-222, function optimally, establishing new standards in dental implant design by combining light weight with high mechanical propertys.
- This research demonstrates the efficacy of additive manufacturing for producing biomechanically optimized dental implants. These improved manufacturing procedures substantially enhance patient outcomes by precisely matching bone's inherent biomechanical propertys, indicating an optimistic future for dental implant technology. These findings emphasize the need for rigorous design and material selection in the creation of dental implants to fulfill the stringent demands of clinical application.
- The study's results provide a basis for future research and development in dental implant technologies, with the goal of achieving optimum biomechanical compatibility and performance.

Chapter 4

ADVANCING 3D DENTAL IMPLANT FEA: INCORPORATING BIOMIMETIC VORONOI LATTICES WITH VARIED PORE SIZES FOR CANCELLOUS BONE

This chapter explores the use of biomimetic Voronoi lattice models in finite element analysis of dental implants to accurately depict the porosity and mechanical properties of human mandibular cancellous bone.

4.1 Introduction

The complex structure of human bone, particularly the cancellous or spongy bone in the jaw, is a significant challenge to dental implant design and biomimetic engineering. As a result, the field of study has implemented advanced modeling techniques, with Voronoi lattice structures being widely preferred [**203, 204**]. Notorious for their distinct open-cell structure that sets them apart from other lattice families like TPMS gyroid and sheet-type lattices, Voronoi lattices are recognized for their remarkable ability to precisely resemble the intricate and porous properties of human bone [**104, 145, 156, 205–208**]. Voronoi lattices are made up of a network of irregular, mathematically determined cell shapes that are very different in how they change shape and how well they can handle mechanical forces. Thus, making them extremely advantageous for scaffolding applications in the field of biomedical engineering. These scaffolds improve osseointegration and tissue ingrowth in addition to mimicking the natural porosity of bone, which usually varies from 60% to 90% [**86, 209–212**]. Because of this, Voronoi lattices are necessary for making biomimetic implants because they offer a customized method that is better at copying the complex anatomical and functional details of human bone than other types of lattices [**152, 213–216**]. Similar to composite materials, bone has directional dependency under external loads [**83, 217–221**], which is crucial yet challenging to accurately simulate using traditional computer-aided design (CAD) models [**222–224**]. These conventional models, which frequently assume isotropic or orthotropic features, considerably simplify the complex behavior of human cancellous bone. When compared to actual clinical dental scenarios, this simplification significantly reduces the accuracy of computational simulations [**222**]. The majority of earlier research has resorted to replacing human cancellous bone in finite element analysis with solid cross-section block CAD models, a technique that severely reduces the precision of numerical approximations [**53, 224–228**]. Voronoi lattice structures provide a remedy to this problem due to their capacity for customized design. They make it possible to adjust Young's modulus such that it more nearly resembles the modulus of common implant materials, including titanium and its alloys. This tailoring facilitates the mechanical synergy that is necessary for dental implants to integrate effortlessly and remain stable over time inside the human mandible. By strategically using Voronoi lattices, researchers can potentially guarantee a better level of accuracy and clinical relevance in implant design by bridging the gap between simplified assumptions and the complicated nature of biomechanical behavior. The focus of this work is to study biomimetic Voronoi lattice structures, which are unique in that they can mimic the porous properties of cancellous bone, which is an important part of human cancellous bone. The porosity of human cancellous bone, which usually ranges from 30% to 90%, is noteworthy and significant for its biomechanical function [**156, 170, 212, 229**]. The Gibson-Ashby theory demonstrates the significance of porosity and relative density in defining the mechanical strength and stiffness of cancellous bone by relating the mechanical properties and physical structure of porous materials [**165, 205, 230, 231**]. This theory demonstrates how the relative density of cancellous bone, which is a measure of its structural solidity against porosity, directly affects its biomechanical properties. This is how Voronoi lattice structures are different from other types of lattices, like sheet-type lattices, because they can perfectly replicate the unevenly distributed, networked porosity of cancellous bone. This feature improves the biomechanical reliability of finite element analysis (FEA) simulations in addition to promoting osseointegration. The finite element method (FEM) is used in this study to improve the mechanobiology analysis of dental implants [**232–235**]. FEM is a well-known computer method for modeling and analyzing complex physical events by breaking a continuum into a few discrete parts. The use of FEM in biomechanics and biomimetics has transformed the study of cancellous bone structures by providing a comprehensive understanding of how they behave under different stress scenarios [**236–239**]. This work uses finite element modeling (FEM) to simulate dynamic, slow loading conditions that are precisely designed to mimic the cyclic biting forces applied to dental implants during mastication. This robust approach differs from earlier research that mostly relied on static loading assumptions, ignoring the dynamic and cyclical nature of mandibular stress during chewing [**20, 200, 223, 238, 240–243**]. By using smooth step-time convergence, this study is more like the explicit dynamic loading that happens in clinical settings. It gives a more accurate and complete look at the stress, strain, and displacement that happen in dental implants. This improved modeling method provides insight into the mechanical behavior of the implants over time, which is a major advancement over previous static loading assumptions. Previous studies that have highlighted the shortcomings of static models in representing the complex biomechanical environment of the jaw [**53, 227**]. These studies have advocated for the incorporation of dynamic loading parameters to more accurately simulate the physiological conditions of mastication. This study carefully assesses how differences in pore size in biomimetic Voronoi lattice structures affect their capacity to bear external stresses, with particular emphasis on improving dental implant biomechanics. An adequate pore size not only increases the load-bearing capacity of the implant but also promotes an ideal biomechanical environment by reducing stress shielding effects and enabling uniform stress distribution [**185**]. In order to acquire mechanical properties that match those of natural bone, pore size modifications are strategically used to control porosity and relative density [**244–246**]. This promotes osseointegration and improves the long-term durability of the implant. The mechanical integrity and biological performance of implants are greatly influenced by pore sizes within a certain range [**60, 200, 247**]. These studies show that increased porosity often results in decreased mechanical strength, even if it is advantageous for biological integration. Nonetheless, a tailored approach that maximizes the strength-to-weight ratio while maintaining biological functioning is made possible using Voronoi lattice structures, which are in line with cancellous bone's inherent properties [**248**]. By using finite element analysis (FEA), the main goal of this study is to improve the comprehension of the biomechanical properties of dental implants. It focuses on using biomimetic Voronoi lattice structures with different pore diameters to effectively mimic human cancellous bone properties. To precisely replicate masticatory conditions seen in real life, every component of the dental implant is thoroughly examined in the present study. It also explores the effects on the implant parts and the cancellous bone mimic when the pore size changes in the Voronoi lattice. Thus, this work anticipates that the biomimetic Voronoi lattice pore size changes will have a significant impact on the lattice's relative density and porosity, which are required to replicate the integrity and strength of real cancellous bone. This work clarifies the crucial role that structural changes play in varying the overall biomechanical effectiveness of dental implant systems through a thorough investigation of biomechanical parameters—displacements, stresses, and strains—derived from FEA.

4.2 Materials and Methods

4.2.1 2D CAD Drawing and Dimensions

The dental implant system's main parts—cancellous and cortical bone structures—were designed using Creo Parametric software.As seen in Figure 4.1, this method constructed both two-dimensional sketches and three-dimensional designed models with precise dimensions.

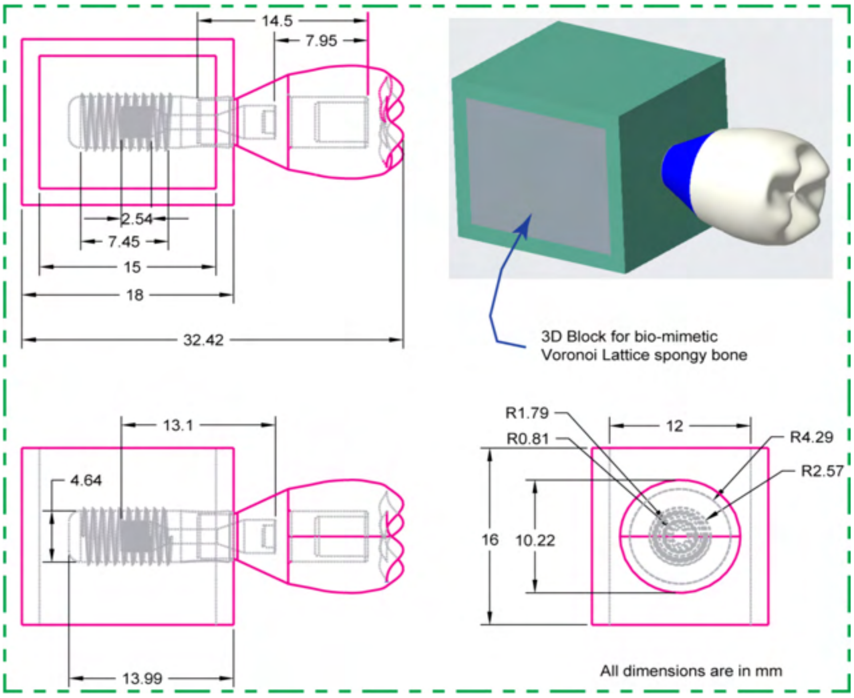

Figure 4.1: 2D drawing of dental implant assembly in Creo parametric: front, side, and top views with detailed dimensions (mm).

4.2.2 Pore Sizes and Voronoi Latticed Bone

Compact bone is defined by a relatively low porosity, usually less than 15%, while certain instances show a porosity range of around 5–30% [**248**]. On the other hand, cancellous bone, has much greater porosity; it often exceeds 70%; however, there are variances ranging from around 30% to over 90% [**249**]. This cancellous structure has a relative density that varies between 0.05 and 0.3, indicating that it is very cellular [**250**]. Building on the earlier reported information about the natural porosity of human cancellous bone, this study utilizes the nTopology software to design four biomimetic Voronoi lattice models with 1.0 mm, 1.5 mm, 2.0 mm, and 2.5 mm distinct pore diameters. The four biomimetic Voronoi lattice structures with pore sizes are designated as VTB10, VTB15, VTB20, and VTB25, respectively. Figure 4.2 shows these four models with different pore sizes. Using finite element analysis (FEA), the study precisely investigates the impact of these various pore sizes in the Voronoi lattice structure on the stresses and strains that bones and other dental implant components experience. The objective of this methodology is to better understand the biomechanical effects of pore size variations on implant stability and bone stability.

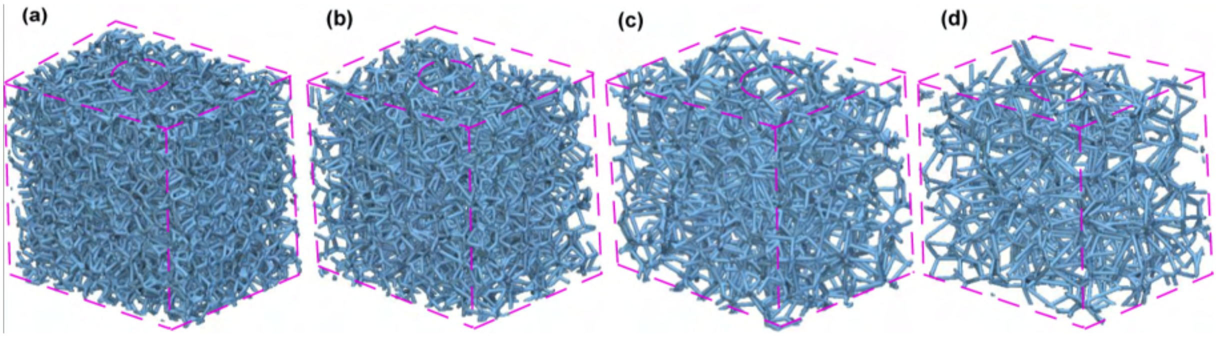

Figure 4.2: Comparative analysis of biomimetic Voronoi latticed spongy bone structures with four distinct pore sizes, a)1.0 mm, b) 1.5 mm, c) 2.0 mm, and d) 2.5 mm, designed using nTopology software.

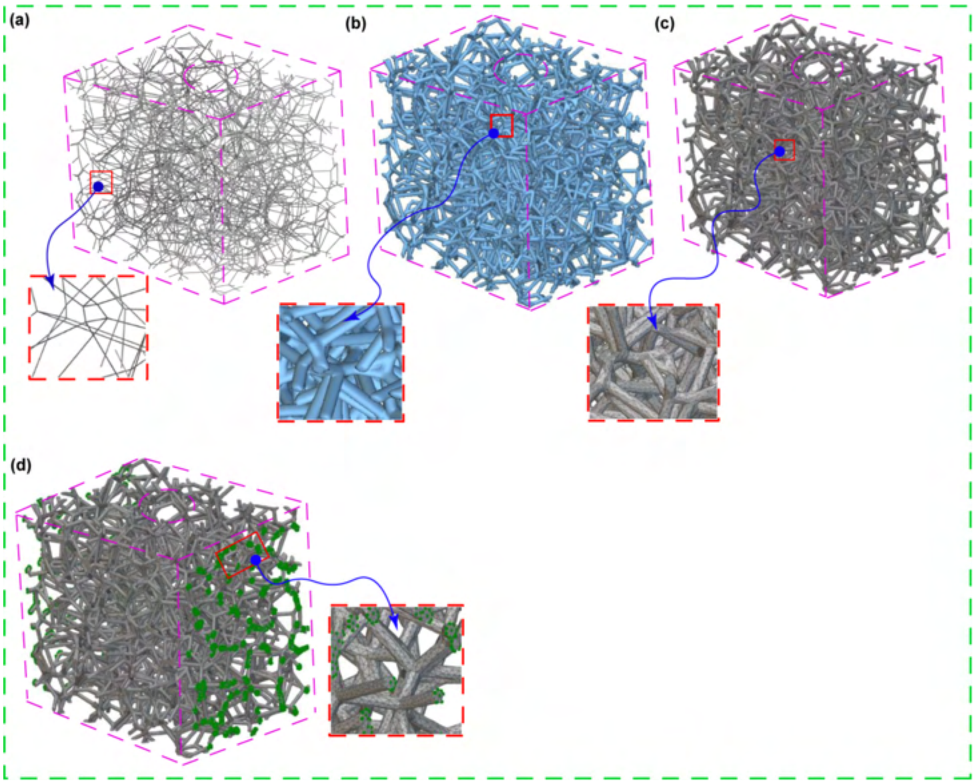

Figure 4.3: Bio-mimetic Voronoi latticed for cancellous bone constructed in nTopology featuring a) open cell randomized lattice graph, b) truncated thicken lattice graph, c) finite element (FE) volume mesh, d) FE boundary configuration utilizing body nodes.

4.2.3 Building, FE Volume Meshing, and Boundary Condition of Voronoi Lattice

Building, FE Volume Meshing, and Boundary Condition of Voronoi Lattice A solid 3D CAD model saved as a Standard ACIS Text (SAT) file is imported and used as the design area to create Voronoi-latticed models that resemble cancellous bone structure. Then, using a randomization seed of 250 and four different pore sizes as shown in Figure 4.2, a randomized lattice structure is produced (as shown in Figure 4.3a). The lattice structure is thickened with a beam diameter of 0.3 mm to strengthen the structure. To reduce structural complexity and remove unnecessary overhangs, a lattice trimming procedure is used with a feature tolerance of 10. Through exercising precision, a biomimetic scaffold that closely mimics the structure of cancellous bone could be designed, allowing for possible exploration of its biomechanical properties.

4.2.4 Oblique Loading and FE Boundary Conditions

As shown in Figure 4.4a, the occlusal crown surface was loaded with three different directions: mesiodistal, buccal-lingual, and apical. This is to show the biomechanical response of the dental implant under multi-axial dynamic oblique loading. There were three different specific force magnitudes applied: 23.4 N, 17.1 N, and 114.6 N. By using a multi-point constraint (MPC) approach, these forces converged at a dummy reference point that was 3 mm from the occlusal surface. This method replicated the complex forces encountered during clinical mastication by generating an equivalent force of 118.2 N, tilted at 75.8 degrees with respect to the occlusal plane **[53, 174, 226, 227]**.To be more specific, the simulation method included explicit dynamic loading at a slower rate to mimic the cyclic mastication stress seen in real life. Notably, to accurately mimic in vivo situations, the load was applied over a 0.5-second period in the dynamic scenario, representing the typical mastication frequency of 2 Hz **[172, 220, 222]**. Specially designed boundary conditions were used to mimic real-life constraints. At the implant-mandible interface, a six-degree-of-freedom (DoF) Encastre boundary condition was used to fix the implant in all three spatial dimensions (X, Y, and Z) (refer to Figure 4.4b). The objective of this configuration was to accurately replicate the distribution of combined stress in the mesiodistal, buccal-lingual, and apical directions.

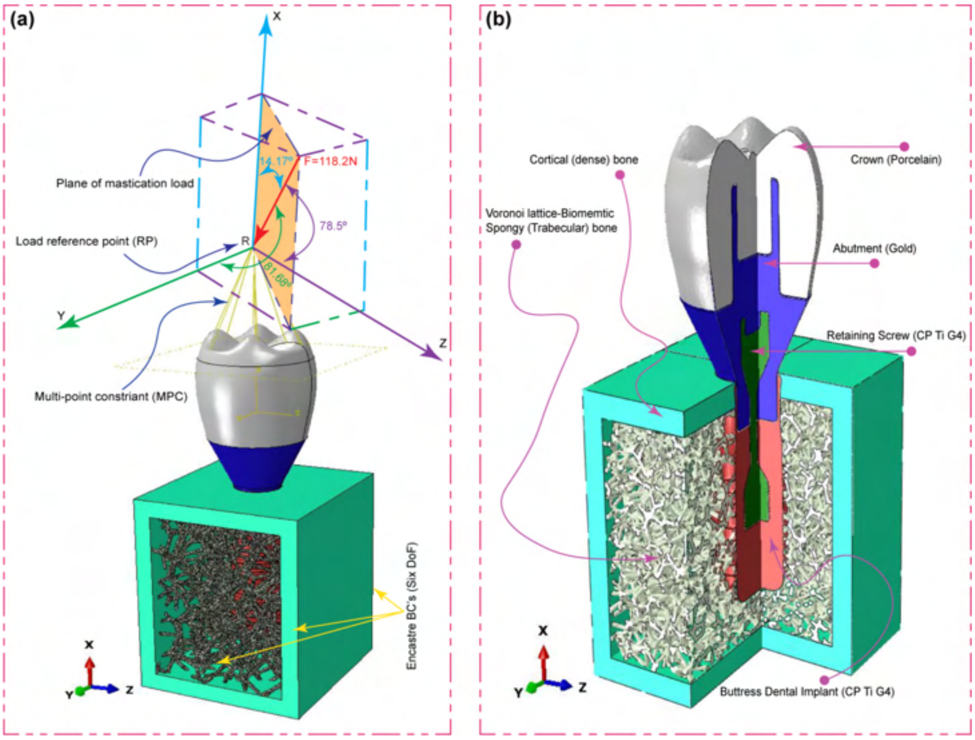

Figure 4.4: Components of the dental implant system, a) application of dynamic explicit oblique loading at load reference point with multi-point constraint, b) 3d model components designed for finite element analysis.

Finite element (FE) boundary by Body Modeling was used to represent the biomimetic Voronoi lattice for cancellous bone structure. As shown in Figure 4.3d, this technique made it easier to accurately export nodes from nTop for boundary condition assignment in the ABAQUS software environment. All dental implant constituents were investigated, including the Voronoi lattice for cancellous bone (Figure 4.3b). The study accurately measured the compressive and tensile stresses in the implant system using finite element analysis with ABAQUS. This makes progress in the study of implant biomechanics under physiologically important loading scenarios.

4.2.5 Physical Properties and FE Mesh

It is very important to mesh the model properly so that there are fewer numerical errors, and the results of finite element analysis (FEA) are more reliable when compared to real-world events. Using nTopology software, the Voronoi cancellous bone meshing was done consecutively in the present study. First, an implicit body was constructed as shown in Figure 4.5. Detailed meshing of dental implant components and Voronoi lattice biomimetic bone, with emphasis on mesh configuration as shown in the zoomed section.

From a traditional 3D solid CAD model of spongy bone that was imported from Creo Parametric software to utilize it as a design space. This implicit design area was then used for building a Voronoi lattice, which was then utilized for lattice meshing. Robust tetrahedral meshing was used after surface re-meshing steps to address the structure's complexity. Figure 4.5 show the choice of an edge length of 1.0 mm and a feature tolerance of 0.25 mm for this purpose. To prepare the model to use finite element analysis, the last step was performing FE volume meshing. To be more precise, several element sizes were used to mesh the dental implant components: 0.2 mm for the implant, 0.15 mm for the screw-retaining components, and 0.35 mm for the remaining components **[53]**. The meshing procedure was carried out using ABAQUS software (see Figure 4.5). The FE mesh statistics for all the implant system components are presented in Table 4.2. The physical properties of the implant and bone materials are presented in Table 4.1. It is assumed that the components of the implant, comprising the screw, abutment, and crown, have homogeneous, elastic properties.

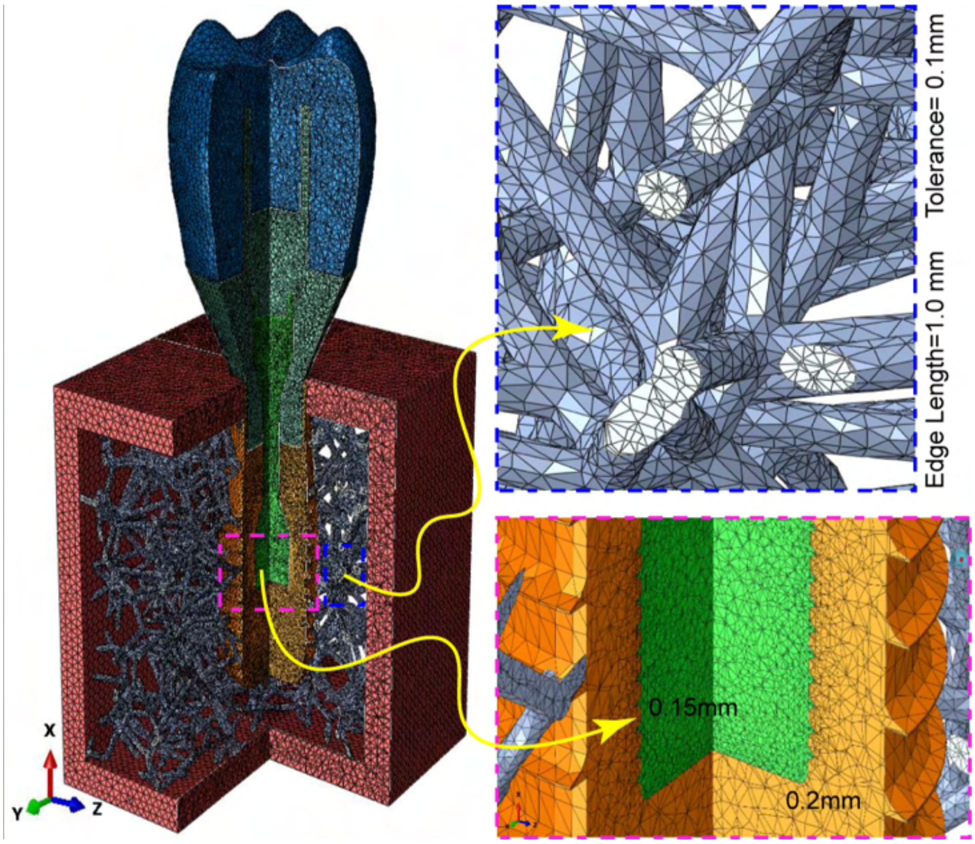

Figure 4.5: Detailed meshing of dental implant components and Voronoi lattice biomimetic bone, with emphasis on mesh configuration as shown in the zoomed section.

Table 4.1: Physical properties of materials for the FEA [**222, 227, 228, 235**].

Material	**Young's Modulus E (MPa)**	**Poisson's Ratio ν**	**Density (g/cm^3)**	**Strength (MPa)**
Cortical bone	$E_x = 12,600$	$\nu_{xy} = 0.3$	1.79	190
	$E_y = 12,600$	$\nu_{yz} = 0.253$		
	$E_z = 19,400$	$\nu_{xz} = 0.253$		
		$\nu_{yx} = 0.3$		
		$\nu_{zy} = 0.39$		
		$\nu_{zx} = 0.39$		
Cancellous bone	$E_x = 1148$	$\nu_{xy} = 0.055$	0.45	10
	$E_y = 210$	$\nu_{yz} = 0.01$		
	$E_z = 1148$	$\nu_{xz} = 0.322$		
		$\nu_{yx} = 0.01$		
		$\nu_{zy} = 0.055$		
		$\nu_{zx} = 0.322$		
Gold abutment *	136,000	0.37	17.5	765
Porcelain	68,900	0.28	2.44	145
Titanium grade 4 *	110,000	0.34	4.5	550

Table 4.2: FE Mesh statistics of different biomimetic lattices for cancellous bone and implant component models.

Component	**VTB10**	**VTB15**	**VTB20**	**VTB25**
Crown: No. Elements	107,954	107,954	107,954	107,954
Crown: No. Nodes	20,670	20,670	20,670	20,670
Abutment: No. Elements	85,243	85,243	85,243	85,243
Abutment: No. Nodes	17,463	17,463	17,463	17,463
Screw: No. Elements	627,098	627,098	627,098	627,098
Screw: No. Nodes	121,624	121,624	121,624	121,624
Implant: No. Elements	160,676	160,676	160,676	160,676
Implant: No. Nodes	31,737	31,737	31,737	31,737
Cortical Bone: No. Elements	146,767	146,767	146,767	146,767
Cortical Bone: No. Nodes	31,180	31,180	31,180	31,180
Cancellous Bone: No. Elements	1,936,663	1,187,637	791,391	591,166
Cancellous Bone: No. Nodes	584,049	363,867	248,917	186,214
Total: No. Elements	3,064,401	2,315,375	1,919,129	1,718,904
Total: No. Nodes	806,723	586,541	471,591	408,888

4.2.6 Relative Density and Porosity of Biomimetic Voronoi Lattice

The nTopology (nTop) program is used to make a Voronoi-latticed biomimetic bone structure, which is different from traditional modeling methods. With this method, the surface area-to-volume ratio, relative density, and porosity of the lattice structure can all be accurately calculated. Understanding the mechanical properties and potential for osteointegration of biomimetic bones requires knowledge of these analyses. The following equations provide a mathematical basis for these key parameters: The **Relative Density** (ρ_{rel}) of a Biomimetic Bone is defined as:

$$\rho_{\text{rel}} = \frac{M_{\text{La}}}{M_{\text{Sol}}} \tag{4.1}$$

The **Surface Area-to-Volume Ratio** (SA/V) of a Voronoi lattice is calculated as:

$$\frac{SA}{V} = \frac{A_{\text{La}}}{V_{\text{La}}} \tag{4.2}$$

The **Porosity** (Φ) relating to relative density is given by:

$$\Phi = 1 - \rho_{\text{rel}} \tag{4.3}$$

Where:

- M_{La}: Mass of the lattice structure,
- M_{Sol}: Mass of the solid (CAD model) volume,
- A_{La}: Total surface area of the lattice,
- V_{La}: Total volume of the lattice.

4.3 Results

4.3.1 Voronoi Lattice Pore Size

Models with four different pore sizes (1 mm, 1.5 mm, 2 mm, and 2.5 mm)were created using nTopology software, all of which had a constant 0.4 mm beam thickness. The influence of these variations in pore size on a variety of essential lattice structure parameters, such as average beam length, number of beams, number of nodes, relative density, and surface area to volume ratio, was well established by our analysis (see Table 4.3). The study found a significant pattern associated with increasing pore size. Notably, the average beam length rose as pore size increased, from 0.4614 mm at 1 mm to 0.9203 mm at 2.5 mm, showing the need for longer beams to cross the increasing distances between nodes. From the smallest to the biggest pore diameters, the lattice beam and node counts significantly decreased simultaneously with increasing pores, falling from 25809 to 3024 and 15186 to 2058, respectively. This reduction allows for bigger spaces of voids by signaling a decline in lattice complexity and density. Additionally, a clear decrease in relative density was seen, decreasing from 22.21% for the 1 mm pore size to 6.27% for the 2.5 mm pore size. This indicates that pore size and lattice density are inversely related.

4.3.2 Pore Size Versus Relative Density and Porosity

The range of pore sizes in biomimetic Voronoi lattice structures, shown in Figure 4.6, from 1.0 mm (VTB10) to 2.5 mm (VTB25), is an important factor for describing the pore scale and has a direct impact on the relative density and porosity of the scaffold. The relative density, which measures the lattice structure's compactness in comparison to its solid equivalent, steadily drops with increasing pore size; it declines from 22.21% at 1.0 mm to 6.27% at 2.5 mm. This trend represents a gradual decline toward a structure that is less dense. On the other hand, porosity measures the volume percentage of empty space within the lattice and has an inverse relationship with relative density. With increasing pore sizes, Figure 6 shows an increasing porosity trend that ranges from 77.79% for VTB10 to 93.73% for VTB25.

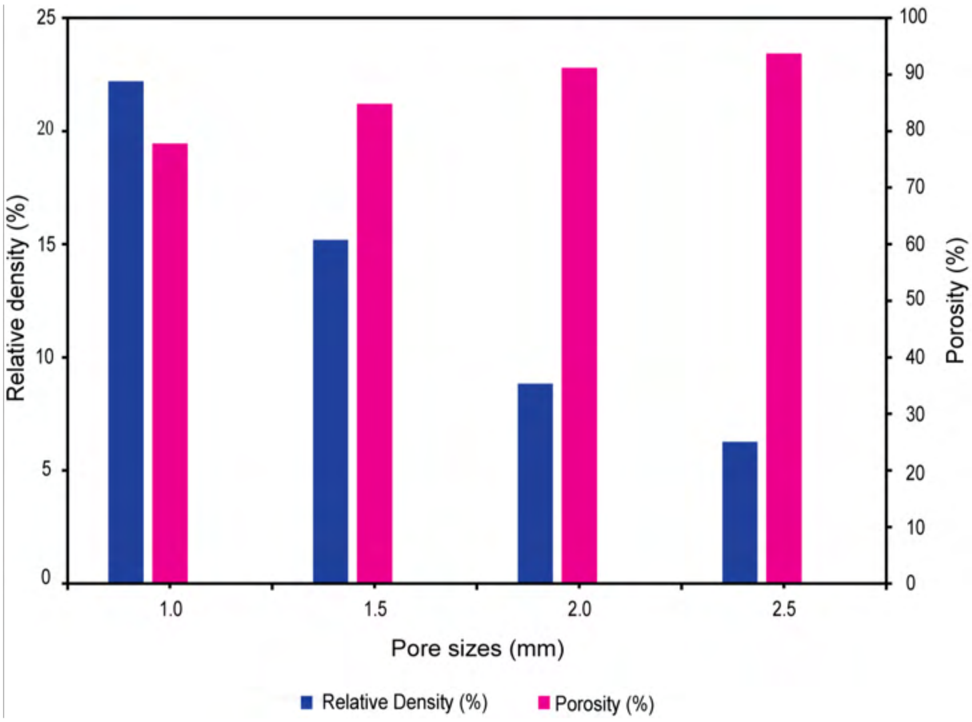

Figure 4.6: Relative density and porosity of biomimetic Voronoi lattice for cancellous bone across various pore sizes.

Table 4.3: Effects of pore size variation on structural parameters of biomimetic Voronoi lattice for cancellous bone.

Component	**VTB10**	**VTB15**	**VTB20**	**VTB25**
Pore Size (mm)	1.0	1.5	2.0	2.5
Beam Thickness (mm)	0.4	0.4	0.4	0.4
Randomization Seed	250	250	250	250
Average Beam Length (mm)	0.4614	0.5681	0.7532	0.9203
Lattice Beam Count	25,809	13,286	5,438	3,024
Lattice Node Count	15,186	8,182	3,535	2,058
Relative Density (%)	22.21	15.19	8.84	6.27
Surface Area-to-Volume Ratio (%)	10.49	11.58	12.21	12.4

4.3.3 Dynamic Oblique Loading

Figure 4.7 displays the application of an oblique dynamic load of 118.2 N to the occlusal surface of the crown. The load is directed in the buccal-lingual, axial, and mesiodistal directions, simulating a 2 Hz mastication cycle with a plane of mastication load. The figure shows the smooth change in load on the crown's occlusal surface across mesiodistal, buccal-lingual, and apical orientations throughout a 0.5-second mastication cycle. The goals of this study were met by using multi-point constraints (MPC) and a reference point as the master control to create a smooth step amplitude on the occlusal surface of the crown. The load distribution was in the three designated directions, which matches the findings of a previous study **[222]**. This proves that the masticatory forces on dental implants that were simulated in this research method are accurate.

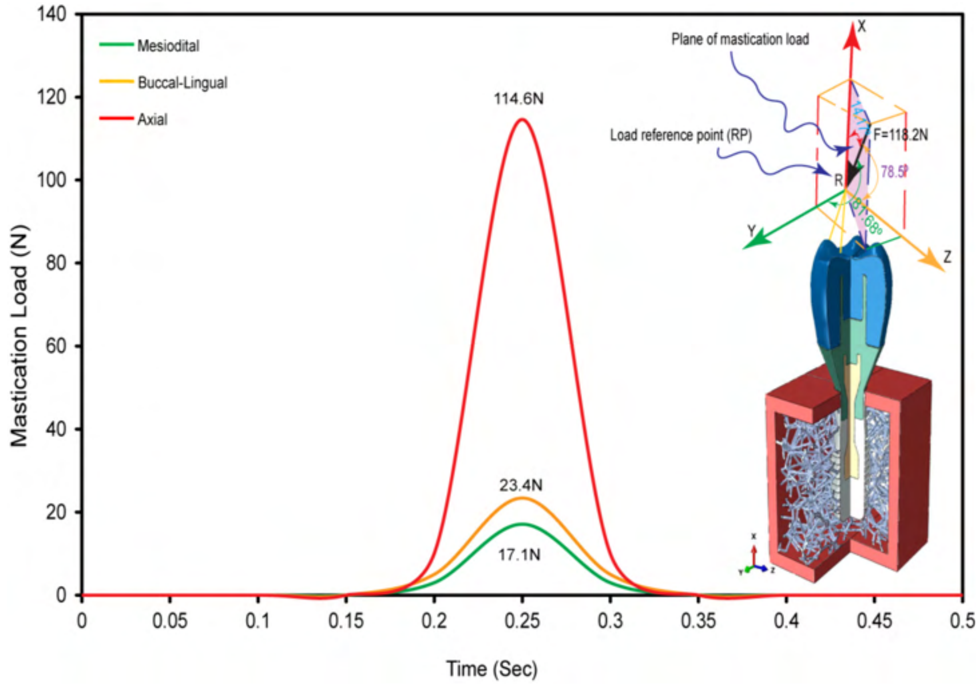

Figure 4.7: An equivalent oblique dynamic load distribution on dental implant crown during mastication, a multidirectional analysis over 0.5s cycle.

4.3.4 Von Mises Stress in Dental Implant Assembly

Figure 4.8 depicts the maximum von Mises stress values for a doubly sliced assembly of dental implant components, exhibiting stress distributions across four different biomimetic Voronoi lattice cancellous bone designs. The findings show a decreasing trend in von Mises stress with increasing pore size. The stress values are reported as 305.93 MPa for a 1 mm pore size (VTB10), subsequently decreasing to 220.96 MPa for 1.5 mm (VTB15), 186.01 MPa for 2 mm (VTB20), and ultimately to 161.16 MPa for 2.5 mm (VTB25).

4.3.5 Von Mises Stress in Dental Implant and Retaining Screw

The Von Mises stress analysis, shown in Figures 4.9a through 4.9h, shows the effect of various pore sizes inside biomimetic Voronoi lattice for cancellous bones on stress distribution in both the dental implant and the retaining screw. The Von Mises stress for the dental implant consistently decreases as the pore size increases, from 1 mm (VTB10) to 2.5 mm (VTB25), falling from 233.84 MPa to 173.48 MPa, respectively. The retaining screw has an identical trend but a less noticeable decline from 220.96 MPa to 184.11 MPa. Interestingly, the 2 mm pore size (VTB20) indicates a key threshold where the implant's Von Mises stress significantly decreases to 179.69 MPa, which is in close alignment with the retaining screw's stress levels (182.09 MPa).

4.3.6 Von Mises Stress in Cortical and Voronoi Lattices for Cancellous Bone

The results from Figures 4.10a through 4.10d, combined with observed stress concentration patterns, provide a comprehensive understanding of maximum von Mises stress behavior in both cortical and biomimetic. Voronoi lattice cancellous bones under a mastication frequency of 2Hz, corresponding to a cycle time of 0.5 sec. Notably, regions of possible mechanical risk are indicated by the concentration of the highest stress around the hole where the cortical bone contacts the implant. Stress distribution inside the Voronoi lattice cancellous bone is consistent throughout different pore sizes, ranging from 12.83 MPa at 1.0 mm (VTB10) to 25.55 MPa at 2.5 mm (VTB25). Likewise, stress in the cortical bone increases from 35.67 MPa (VTB10) to 106.42 MPa (VTB25) ascancellous structure pore size increases, indicating a clear relationship between pore size and stress effect on both types of bone. Stress levels peak at about 0.35 sec. into the mastication cycle, remaining constant even as cycles continue.

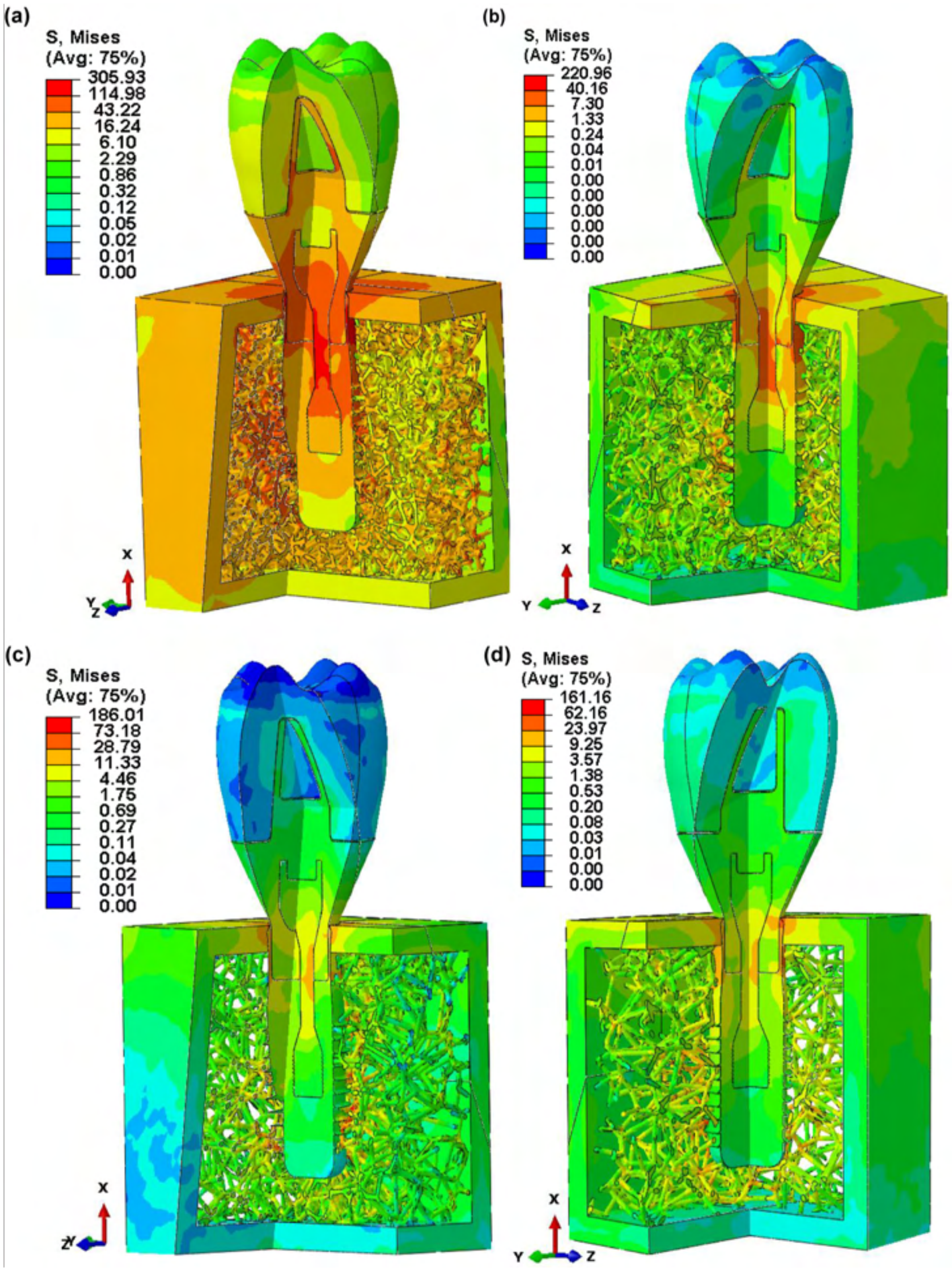

Figure 4.8: Maximum von mises stress distribution in double-sliced assembled implant parts for four biomimetic Voronoi lattices for cancellous bones: a) VTB10, b) VTB15, c) VTB20, and d) VTB25.

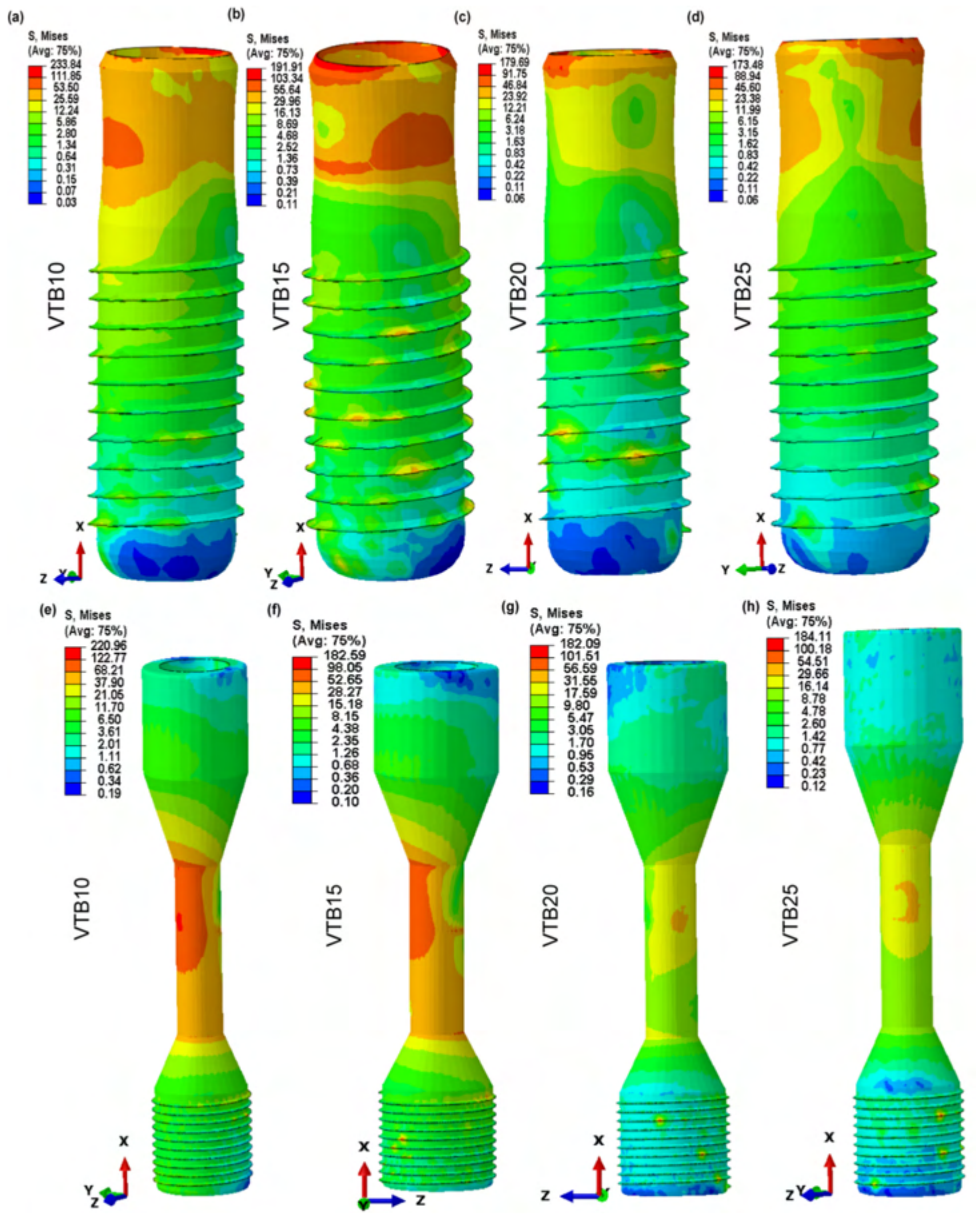

Figure 4.9: Contour von Mises stress distribution in dental implants and retaining screws across biomimetic Voronoi lattices for cancellous bone pore sizes: a) VTB10, b) VTB15, c) VTB20, d) VTB25 for implants, and e) VTB10, f) VTB15, g) VTB20, h) VTB25 for retaining screws.

4.3.7 Deformation in Voronoi Lattices for Cancellous Bone

Figure 4.11, which depicts contour plots of the magnitude of deformation inside the biomimetic Voronoi lattice for cancellous bone subjected to finite element analysis, shows a clear relationship between pore size and deformation magnitude. Specifically, deformation values inside the biomimetic Voronoi for cancellous bone increased gradually as pore diameters increased. For a pore size of 1.0 mm (VTB10), the displacement was 8.00 μm. This deformation increased progressively with pore size; at 1.5 mm (VTB15), it was reported at 10 μm, rising to 13.00 μm at 2.0 mm (VTB20), and reaching 17.00 μm at the maximum pore size of 2.5 mm (VTB25). These results show how important pore size is when studying the biomechanical behavior of the biomimetic Voronoi for cancellous bone, especially deformation when dynamic mastication stresses are present.

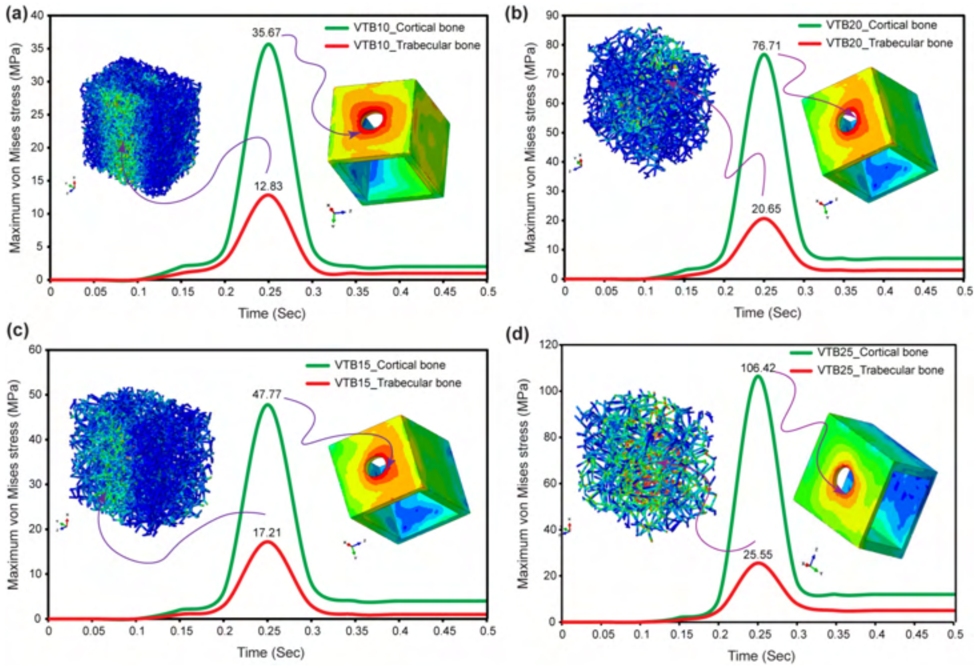

Figure 4.10: Maximum von Mises stresses in biomimetic Voronoi lattice for cancellous and cortical bones for a) VTB10, b) VTB15, c) VTB20, and d) VTB25.

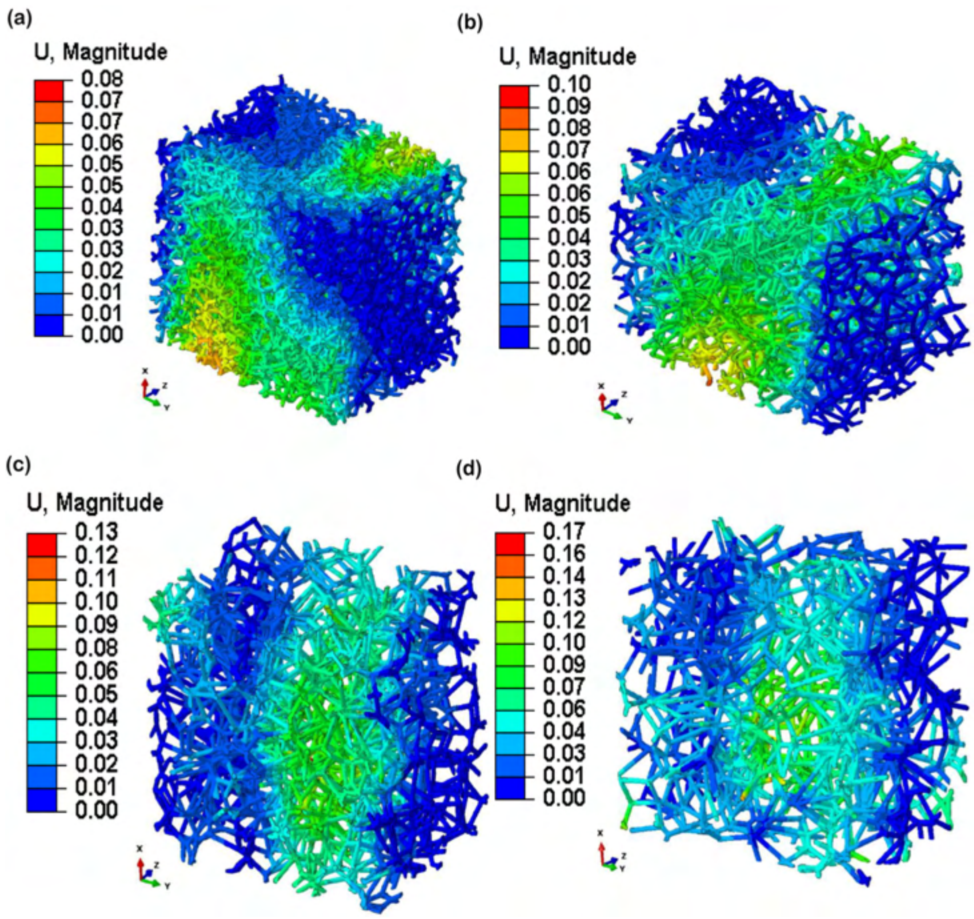

Figure 4.11: Contour plots of magnitude of displacements in biomimetic Voronoi lattice for cancellous bone for pore sizes: a) VTB10, b) VTB15, c) VTB20, d) VTB25.

4.3.8 Displacement in Dental Implant Assembly

Figures 4.12a through 4.12d show the maximum displacement found in the axial, mesiodistal, and buccolingual directions for various pore sizes of biomimetic Voronoi lattice for cancellous bone. The findings show that biomimetic Voronoi lattice for cancellous bones with varied pore sizes (VTB10, VTB15, VTB20, and VTB25) exhibit maximal displacements in the axial, mesiodistal, and buccolingual directions. The displacements in the axial direction range from 111.76 μm for VTB10 to 117.73 μm for VTB25. VTB20 has a mesiodistal displacement peak of 256.55 μm, whereas VTB25 has the largest buccolingual displacement at 310.07 μm.

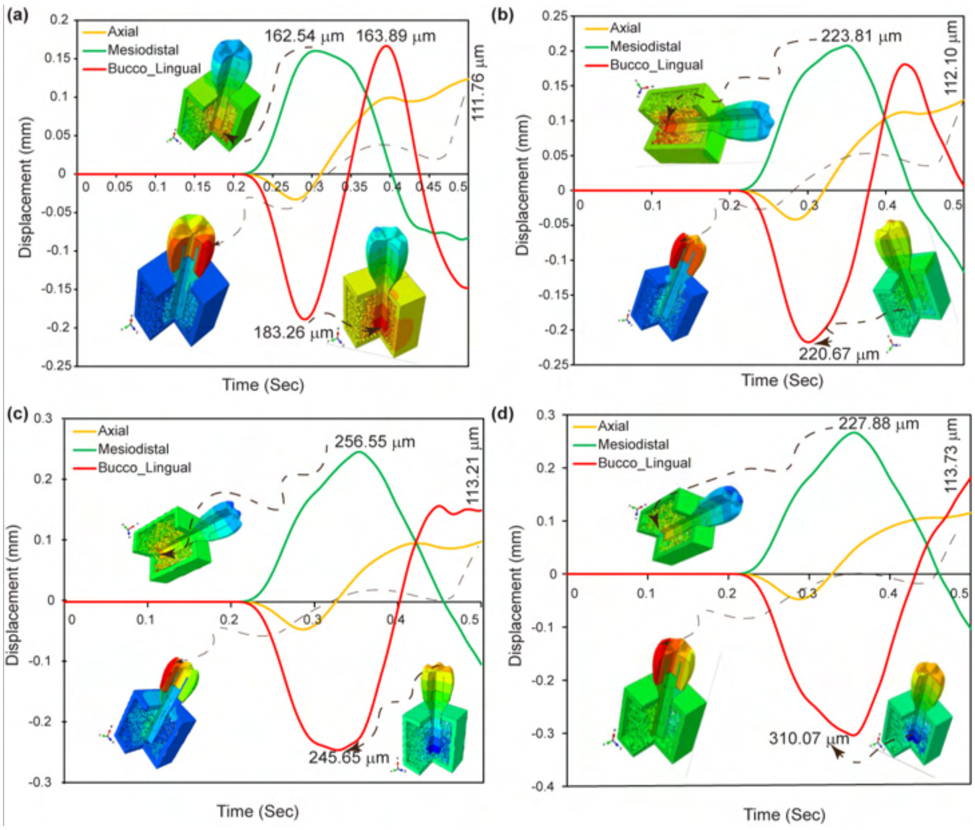

Figure 4.12: Maximum displacement response in axial, mesiodistal, and buccolingual directions for biomimetic Voronoi lattice for cancellous bones: a) VTB10, b) VTB15, c) VTB20, and d) VTB25.

4.3.9 Reaction Forces in Dental Implant Assembly

Figures 4.13a through 4.13d show the dynamic response forces for biomimetic Voronoi lattices for cancellous bones with various pore sizes (VTB10, VTB15, VTB20, and VTB25) in the axial, mesiodistal, and buccolingual directions. Initially, response forces are zero across all models until 0.23 sec., after which they increase in line with the dynamic loading amplitude. After 0.23 sec., the maximum response forces are observed: VTB10 has forces of 529.41 KN axially, 858.6 KN mesiodistally, and 530.86 KN buccolingually; VTB15 has 465.09 KN, 927.27 KN, and 316.98 KN, respectively; VTB20 has 215.25 KN, 717.68 KN, and 259.8 KN; and VTB25 has 224.21 KN, 788.69 KN, and 329.24 KN in the respective directions.

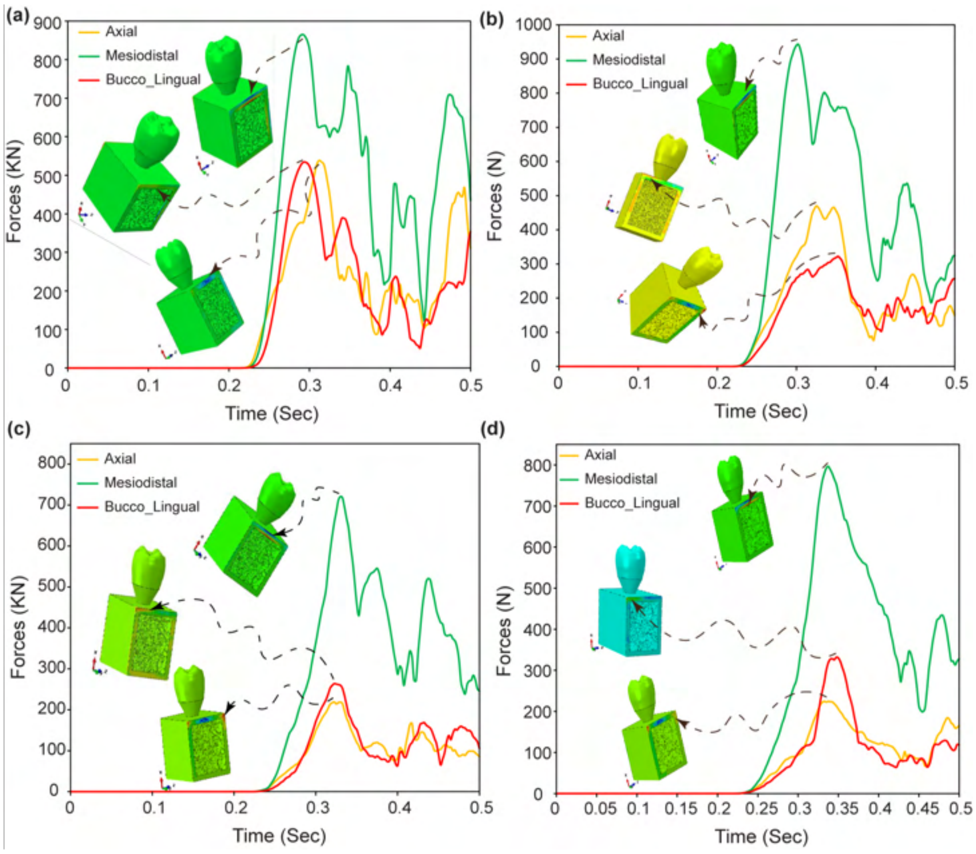

Figure 4.13: Dynamic reaction forces in dental implant assemblies across biomimetic Voronoi lattices for cancellous bone pore sizes: a) VTB10, b) VTB15, c) VTB20, and d) VTB25.

4.4 Discussion

This study investigated the biomechanical design of dental implant systems in detail. It used cutting-edge software like Creo Parametric and nTopology to accurately model both cancellous and cortical bone structures. We used advanced modeling techniques to make biomimetic Voronoi lattice structures with different pore sizes that are very similar to the natural porosity and mechanical properties of human bone. We used Finite Element Analysis (FEA) to assess the impact of these pore sizes on stress and strain distributions within the bone and implant components, aiming to enhance implant stability and osseointegration. The main results showed that holes with an intermediate size, especially those with a diameter of 2.0 mm, made the implants much more biomechanically compatible. This suggests that dental implant designs and clinical uses could be improved in this way. The findings we obtained support the argument that was proposed in the study's introduction. It is suggested that the variation in pore size inside biomimetic Voronoi lattice structures affects the stress distribution and deformation across the dental implant components as well as the surrounding cancellous bone. According to our investigation, a pore size of 1.5 mm provides optimum equilibrium and closely mimics the dynamic loading response observed in human cancellous bone. This pore size makes the stress distribution significantly uniform at the implant-bone contact (BIC) by balancing structural factors like beam length and node count with the biomechanical needs of dental implants. With a relative density of 15.19% and a surface area-to-volume ratio that promotes cell attachment and nutrient transport, this option maintains structural strength while also facilitating osteointegration. The design effectively mimics the porosity structure of real bone, improving both mechanical stability and biological compatibility. Because it distributes stress analogously to naturally occurring cancellous bone, it can sustain physiological loads and lower the likelihood of stress shielding and implant failure. Our present findings show that the lattice structure has a porosity of around 84.81%, which closely matches the porosity range of 75% to 90% seen in real human cancellous bone. This discovery is consistent with previous research, which has repeatedly established that that cancellous bone has porosity greater than 70% [**212, 249–253**], highlighting the biomimetic accuracy of our lattice design. This shows that the chosen pore size worked well. This congruence verifies our study's

biomimetic methodology and supports the integration and vascularization that are essential to dental implants' long-term effectiveness. As such, it highlights the possibility of tailored biomimetic Voronoi lattices to augment the lifetime and efficacy of dental implants. Thus, making them a model option for mimicking the intricate interplay between strength and porosity that characterizes human cancellous bone. Our findings, which show that a 2.0 mm pore size (VTB20) is better for distributing stress and making dental implants last longer, are in line with what other studies have found. Our findings support previous research showing the efficiency of biomimetic implants in distributing stress to neighboring bone structures, ensuring safety and structural integrity under normal loading scenarios **[252]**. This agreement underlines the need for regulating pore size to enhance the biomechanical compatibility and performance of dental implants, establishing the foundations for future advances in implant design and application.
Figure 4.6 depicts the study's findings, which show a significant relationship between pore size and the mechanical integrity of biomimetic Voronoi lattice cancellous bone, particularly in the context of dental implants. Pore diameters increased from 1.0 mm to 2.5 mm, resulting in a decrease in relative density and an increase in porosity. These variations have an immediate influence on the implant's stress distribution properties under dynamic loading conditions. A lower relative density, which means bigger pores, is more like the natural structure of human cancellous bone. This makes it easier for the dental implant system to spread stress evenly. By mimicking the natural load-bearing function, this advancement promotes osseointegration and lowers the possibility of implant failure. The 2.0 mm (VTB20) configuration stands out as the best candidate among the assessed pore sizes as it maintains a compromise between preserving adequate structural strength with a relative density of 8.84% and having sufficient porosity (91.16%) for biological integration. This pore size successfully mimics the mechanical and structural properties of natural cancellous bone, which optimizes stress distribution and ensures the scaffold's endurance under physiological loading conditions **[252]**, thereby extending the lifespan and functionality of dental implants.
Figure 4.8 shows that pore size variations in biomimetic Voronoi lattice cancellous bones have a significant impact on stress distribution across dental implant assemblies. particularly around critical interfaces consisting of implant-bone, implant-abutment, abutment-screw retaining, abutment-crown, and implant-retaining screw contacts. Stress concentrations are significantly reduced when the pore size is increased from 1.0 mm (VTB10) to 2.0 mm (VTB20), which allows for a more uniform stress distribution that is more consistent with the behavior of natural bones. Despite its intended purpose of mimicking human cancellous bone, the stiffness inherent in the smaller pore size (VTB10) assembly hinders stress homogeneity, boosting the possibility of localized failure. The larger pore size (VTB20) assembly makes the implant system more stable and helps it fit together better by improving its mechanical response and closely matching the load bearing and stress-dissipation properties of natural cancellous bone. This optimization shows how important it is to change the size of the pores in Voronoi lattice structures to find the right balance between stiffness and porosity when trying to make a design that can withstand mechanical loads and mimic the biological activity of bone tissue.
Figures 4.9a through 4.9h shows that the maximum von Mises stress inside dental implants and their retaining screws is significantly influenced by pore size in biomimetic Voronoi lattice for cancellous bone designs. As the pore size increases from 1 mm (VTB10) to 2.5 mm (VTB25), the research shows a steady drop in von Mises stress values in both the implant and the retaining screw. Notably, the stress in the retaining screw decreased from 220.96 MPa to 184.11 MPa, and the stress in the dental implant decreased from 233.84 MPa for VTB10 to 173.48 MPa for VTB25. According to this trend, larger pores may help distribute stress uniformly, which could prolong the implant system's lifespan and improve its mechanical stability. Notably, the ideal stress distribution, defined by a compromise between mechanical integrity and biomimetic porosity, was seen for VTB20, demonstrating that a pore size of 2.0 mm is the best for imitating the mechanical properties of human cancellous bone. Stress concentration at the implant's neck and the screw's mid-region—areas that are often prone to failure or fracture under cyclic dynamic loading—is significantly reduced by this improved design. This adaptation mimics human bone's inherent load-bearing properties, with the potential to increase implant lifetime and function in clinical conditions. This work strongly corresponds with previous research aims, highlighting the importance of mechanical strength and biological properties in titanium materials for biomedical applications **[166]**.
Figures 4.10a through 4.10d show the maximum von Mises stress across cortical and biomimetic Voronoi lattice cancellous bones, emphasizing the critical role of pore size in the biomechanical response of different bone types under masticatory stress. As shown, the pore size directly affects the structural integrity and mechanical behavior of the bone-implant system. Even stress distribution inside the Voronoi for cancellous structure and the stress concentration at the cortical bone-implant interface serve as evidence for this. The fact that von Mises stress goes up as pore sizes get bigger and stays the same after 0.35

sec. shows that structural design and dynamic loading response are complicatedly linked. Changing the size of the pores in the Voronoi lattice cancellous bone creates a biomechanical environment that is like how bones naturally behave. This makes the stress distribution better and reduces stress concentrations in certain areas that could cause failure. This optimized distribution pattern not only demonstrates the biomimetic structure's capacity to imitate the physiological stress of human bones, but it also represents a major improvement in finite element analysis (FEA) results. The biomimetic Voronoi lattice is a better way to predict how bone-implant assemblies will act in real life. This is because it changes the size of the pores to find a balance between biological activity and mechanical support. This study uses biomimetic Voronoi latticed cancellous bone for finite element analysis, which is very different from earlier studies that used solid CAD blocks to model bone structures. By adding the Voronoi lattice's detailed, porous design, this study provides a more physiologically realistic description of bone mechanics, improving the predictability of stress distribution patterns under masticatory stresses. This method not only improves biomechanical modeling of bone-implant interfaces, but it also gives a more nuanced knowledge of the effect of pore size on structural integrity and mechanical behavior. In line with what other studies have found [**254**], this discovery opens the door to the creation of bone scaffolds and implants that improve healing by closely imitating the properties of natural bone.

Figure 4.11 shows the sizes of deformation in biomimetic Voronoi lattice for cancellous bones with four different pore sizes. This shows how important deformation is in the biomechanics of dental implants. Larger pore diameters are linked with increased displacement, which increases the risk of bone resorption at the bone-implant interface and fractures in dental implant components, particularly the retaining screw and the implant itself. Additionally, deformation increase the likelihood of corrosion, especially when the implant works in a biofluid environment. Despite these difficulties, the research finds that a pore size of 2.0 mm (VTB20) with a deformation of 13 μm provides an ideal compromise between reducing unfavorable biomechanical consequences and providing a satisfactory degree of mechanical rigidity. This pore size facilitates the structural and functional integration of the implant into the biological system while also reducing the chance of implant system failure. As such, these deformation optimization insights provide an in-depth understanding of the relationship between pore size and implant function, which considerably advances the field of biomechanical dentistry research.

Incorporating the observed displacement patterns from Figures 4.12a to 4.12d, the axial and buccolingual directions show both negative and positive peak displacement amplitudes, indicating that the dental implant can withstand cyclic masticatory stress. The scenario demonstrates the implant's flexibility and mechanical resilience, which are essential for enduring numerous stress cycles while maintaining structural integrity. Such displacement patterns indicate that VTB20, with its nuanced response in all measured directions, not only mimics the normal biomechanical behavior of human bone, but also guarantees the implant's capacity to tolerate dynamic stresses experienced in vivo. This modification emphasizes just how essential it is to choose the right pore size in the Voronoi lattice cancellous bone to maximize the performance of dental implants. VTB20 offers an excellent balance between mechanical rigidity and flexibility, which is crucial for long-term clinical success.

Figures 4.13a through 4.13d show the dynamic reaction forces across different pore sizes of biomimetic Voronoi lattice for cancellous bone (VTB10, VTB15, VTB20, and VTB25), providing significant insight into the biomechanical performance of dental implant assemblies. The consistent lack of response forces for up to 0.23 sec., followed by a rise in alignment with dynamic loading amplitudes, demonstrates the implants' mechanical flexibility to masticatory stresses. Specifically, the research shows that VTB20 outperforms the other models due to its lower axial and buccolingual reaction forces and optimum mesiodistal response. This research implies that a pore size of 2.0 mm promotes a compromise between structural support and flexibility, allowing the implant to efficiently distribute stresses while maintaining its biomechanical integrity. The distinct mechanical responses observed at the 0.5 sec, mark across all models highlight the importance of pore size in tailoring the biomechanical properties of dental implants to mimic natural bone behavior, thereby improving the overall effective-ness and longevity of dental implant systems. This work advances the biomechanical knowledge of bone-implant interactions by using advanced finite element analysis (FEA) that extends beyond typical unrealistic models. Our technique provides a more realistic representation of bone behavior in physiological settings by replicating the nonlinear, and anisotropic features of biological tissues, as well as including dynamic loading conditions that replicate real-world pressures. This technique not only eliminates past shortcomings, but it also gives more in-depth insights into the performance and stability of biomimetic Voronoi lattice implants, making a substantial contribution to biomechanical engineering.

In summary, our results show that larger hole sizes result in a less dense, more open scaffold structure, boosting surface complexity and perhaps improving osteointegration and mechanical bonding with bone tissue. Increased pore size increases the scaffold's structural mimicry of natural bone porosity, which has a major impact on the stress distribution and mechanical endurance of dental implants under dynamic conditions. A 2 mm pore size emerges as the best dimension, achieving a balance in stress distribution while also strengthening the structural integrity of both dental implants and retention screws. This adaptation emphasizes the importance of pore size in optimizing the biomechanical responses of biomimeticcancellous bone and dental implant assemblies to masticatory stresses, hence improving performance and durability.

4.5 Conclusions

This work sought to understand the biomechanical behavior of biomimetic Voronoi lattice for cancellous bone structures. Using finite element analysis (FEA) to evaluate the effect of altering pore sizes on stresses and deformation magnitudes. Hence, the following are significant inferences from the present study:

- A direct relationship was discovered between pore size and deformation magnitude. This highlights the impact of pore size on the biomechanical behavior of biomimetic Voronoi for cancellous bone. This relationship has significance during dental implant designs that optimize biomechanical performance.
- The research shows that the biomimetic Voronoi lattice for cancellous bone used in FEA has properties that are like real human cancellous bone when subjected to applied external dynamic mastication stresses.
- The use of anisotropic properties in these novel biomimetic cancellous bones, as well as the simulation of dynamic mastication stresses, greatly improved the FEA findings. This method gives a more precise description of biomechanical interactions in the oral environment, resulting in more reliable implant designs.
- The study found that a 2.0 mm (VTB20) pore size presents an optimal integration of mechanical rigidity and minimum deformation, making it a better option to further enhance implant lifespan and performance.
- Deformation optimization considerably reduces the chances of implant failure, such as fractures in implant components, bone resorption, and corrosion in a biofluid environment.
- The research gives a significant insight into the biomechanical optimization of dental implant designs by studying biomimetic Voronoi lattices for cancellous bones. This study expands possibilities for the design of dental implants that enhance biomechanical compatibility and performance by using modern FEA methods and considering the anisotropic properties of bone and dynamic loading scenarios.
- These results demonstrate the significance of using biomimetic approaches for developing and evaluating the performance of dental implants, in addition to making advancements in the fields of biomechanical engineering in dentistry.

Chapter 5

CONCLUSION AND RECOMMENDATION

This chapter summarizes the findings and suggestions from a detailed investigation of the mechanical and biomechanical behavior of lattice structures, with a focus on their use in automobile crash boxes and dental implants. It finishes with critical results and suggestions for refining lattice designs to improve energy absorption and biomechanical performance, as well as potential future research topics.

5.1 Conclusions

This study explores the mechanical and biomechanical behavior of different lattice structures, with an emphasis on their use in automobile crash boxes and dental implants. The researchers use a combination of mechanical compression testing and finite element analysis (FEA) to improve the energy absorption and biomechanical performance of composite TPMS gyroid lattices and biomimetic Voronoi lattice structures. The study on composite TPMS gyroid lattices includes creating five distinct types of lattices by mixing walled-TPMS and regular TPMS gyroid lattices using Boolean subtraction. We created the structures by 3D printing PLA using fused deposition modeling (FDM). We tested the mechanical properties and energy absorption capacities under dynamic mechanical compression loading. The findings showed that the 54% relative density crash box had a substantially shorter densification phase and a higher strain energy storage capacity than the 33% and 38% relative density crash boxes, which had optimal energy absorption prior to densification. The research also discovered that composite TPMS gyroid lattices with lower relative densities, especially at 25%, offered the best balance of displacement capacity and mechanical stiffness, indicating increased crashworthiness for vehicle safety applications. Using FEA, this research investigated the biomechanical behavior of dental implants with various lattice designs and cell sizes. The study investigated the distribution of stress in the implants and surrounding bone tissue using complete and hybrid lattice designs in the cancellous and cortical bones. The study found that completely latticed implants with the smallest cell size had the largest concentration of stress, indicating vulnerability to substantial biomechanical stressors. On the other hand, hybrid lattice designs with cell sizes of 2x2x2 mm showed more optimal stress distribution, lowering the risk of mechanical stress-related implant failure. The research also underscored the significance of careful design considerations for retention screws, since smaller cell-sized implants exhibited greater stress levels in these parts. Furthermore, the study on biomimetic Voronoi latticed cancellous bone structures using FEA examined the impact of varying pore sizes on stresses and deformation magnitudes. The research showed a clear correlation between pore size and deformation amplitude, emphasizing the importance of pore size in biomechanical activity. When dynamic mastication loads were applied to biomimetic Voronoi latticed cancellous bones in FEA, they were discovered to have qualities comparable to actual human cancellous bone. The research found that a 2.0 mm pore size provided the best combination of mechanical stiffness and little deformation, making it a better alternative for increasing implant lifetime and performance. These extensive studies provide major contributions to the disciplines of automotive and biomedical engineering by expanding our knowledge of the behavior of lattice structures under stress. The results emphasize the significance of optimizing lattice design for applications, such as increasing energy absorption in automobile crash boxes and improving biomechanical compatibility and performance in dental implants. This study gives important insights for creating more effective and long-lasting engineering solutions, resulting in safer and more robust structures in both automotive and biomedical applications

5.2 Future Work

We propose the following future work to enhance the understanding and application of lattice structures in the automotive and biomedical domains, based on the research findings:

- Investigate Other Lattice Geometries: To improve mechanical and biomechanical performance, investigate lattice geometries other than the TPMS gyroid and Voronoi structures.
- Integrate Multi-Material Printing: By mixing materials with different strengths, multi-material 3D printing can improve the properties of lattice structures.
- Long-Term Biological Testing: In vivo, test biomimetic lattice structures to better understand their interaction with biological tissues over time.
- Dynamic Loading Scenarios: To more closely mimic real-world situations, implement more intricate dynamic loading scenarios in FEA to more closely mimic real-world situations.
- Clinical Trials: Begin clinical trials of dental implants with improved lattice structures to confirm their performance in real-world conditions.
- Promote interdisciplinary research that combines biomechanics, materials science, and computer modeling to provide novel solutions for biomedical and automotive applications.
- Investigate Torque and Twisting Loads: Investigate the effects of torque and twisting loads on dental implants to assure their stability and longevity under varied loading circumstances.
- Determine the effect of pre-loading on the mechanical performance and lifespan of dental implants by replicating situations encountered before and after insertion.

References

[1] S. Rahimi and M. Asghari. “Design and evaluation of two proposed hybrid FCC-BCC lattice structures for enhanced mechanical performance”. Heliyon 11.1 (2025). DOI: 10.1016/j.heliyon.2024.e40911.

[2] X. Wang, Z. Li, J. Deng, T. Gao, K. Zeng, X. Guo, X. Li, W. Zhai, and Z. Wang. “Unprecedented strength enhancement observed in interpenetrating phase composites of aperiodic lattice metamaterials”. Advanced Functional Materials 35.1 (2025), p. 2406890. DOI: 10.1002/adfm.202406890.

[3] N. Kladovasilakis, K. Tsongas, and D. Tzetzis. “Mechanical and FEA-Assisted Characterization of Fused Filament Fabricated Triply Periodic Minimal Surface Structures”. J. Compos. Sci. 5 (2021), p. 58. DOI: 10.3390/jcs5020058.

[4] L.J Gibson and M.F Ashby. “Cellular solids: Structure and properties pergamon press”. New York, USA (1988). Source: Google Scholar.

[5] Y. Liu, L. Wang, J. Zhang, S. Liu, J. Zheng, J. Kang, E. Dong, C. Sun, C. Liu, C. Yang, et al. “A design strategy for long-term stability of porous PEEK implants by regulation of porous structure and in vivo mechanical stimulation”. Bio-Design and Manufacturing (2025), pp. 1–13. DOI: 10.1631/bdm.2400259.

[6] Z.J. Wally, W. Van Grunsven, F. Claeyssens, R. Goodall, and G.C. Reilly. “Porous Titanium for Dental Implant Applications”. Metals 5 (2015), pp. 1902–1920. DOI: 10.3390/met5041902.

[7] M. V. Kiselevskiy, N.Y. Anisimova, A. V. Kapustin, A.A. Ryzhkin, D.N. Kuznetsova, V. V. Polyakova, and N.A. Enikeev. “Development of Bioactive Scaffolds for Orthopedic Applications by Designing Additively Manufactured Titanium Porous Structures: A Critical Review”. Biomimetics 8 (2023), pp. 1–25. DOI: 10.3390/biomimetics8070546.

[8] Matteo Fantini, Michele Curto, and Francesco De Crescenzio. “A numerical approach to design biomimetic bone scaffolds based on Voronoi lattices”. Virtual and Physical Prototyping 11.2 (2016), pp. 77–90. DOI: 10.1080/17452759.2016.1163903. URL: https://doi.org/10.1080/17452759.2016.1163903.

[9] Zaki Alomar, Morteza Aramesh, Andreas Thor, Cecilia Persson, Franco Concli, and Francesco D’Elia. “Towards improved functionality of mandibular reconstruction plates enabled by additively manufactured triply periodic minimal surface structures”. Journal of the Mechanical Behavior of Biomedical Materials 162 (2025), p. 106826. DOI: 10.1016/j.jmbbm.2024.106826. URL: https://doi.org/10.1016/j.jmbbm.2024.106826.

[10] T. Li, Y. Peng, Y. Qiao, W. Zhu, J. Zhang, K. Wang, G. Xie, and H. Zhang. “Experimental Study on Crashworthiness and Lightweight of Cutting-Type Energy-Absorbing Structure of Magnesium Alloy for Trains”. Eng. Struct. 301 (2024), p. 117287. DOI: 10.1016/j.engstruct.2023.117287.

[11] A. Sadat Mirhakimi, D. Dubey, and M.A. Elbestawi. “Laser Powder Bed Fusion of Bio-Inspired Metamaterials for Energy Absorption Applications: A Review”. J. Mater. Res. Technol. 31 (2024), pp. 2126–2155. DOI: 10.1016/j.jmrt.2024.06.234.

[12] J. Deering and K. Grandfield. “Current Interpretations on the in Vivo Response of Bone to Additively Manufactured Metallic Porous Scaffolds: A Review”. Biomater. Biosyst. 2 (2021), p. 100013. DOI: 10.1016/j.bbiosy.2021.100013.

[13] G. Dei Rossi, L.M. Vergani, and F. Buccino. “A Novel Triad of Bio-Inspired Design, Digital Fabrication, and Bio-Derived Materials for Personalised Bone Repair”. Materials (Basel) 17 (2024). DOI: 10.3390/ma17215305.

[14] P. Baghel, S. Kumar Tak, R. Swami, Z. Kagzi, and M. Prajapat. "The Crashworthiness Performance of Thin-Walled Energy Absorbing Devices: An Overview". In: *SCRS Proc. Int. Conf. Undergrad. Students*. 2023, pp. 263–270. DOI: 10.52458/978-81-95502-01-1-29.

[15] R. Yao, T. Pang, B. Zhang, J. Fang, Q. Li, and G. Sun. "On the Crashworthiness of Thin-Walled Multi-Cell Structures and Materials: State of the Art and Prospects". Thin-Walled Struct. 189 (2023), p. 110734. DOI: 10.1016/j.tws.2023.110734.

[16] D. Le, N. Novak, A. Arjunan, A. Baroutaji, Q. Estrada, T. Tran, and H. Le. "Crashworthiness of Bio-Inspired Multi-Stage Nested Multi-Cell Structures with Foam Core". Thin-Walled Struct. 182 (2023), p. 110245. DOI: 10.1016/j.tws.2022.110245.

[17] W. Fan, R. Xie, M. Davidson, H. Yin, K. Lai, and Q. Wu. "Crashworthiness and Energy Absorption of UHPFRC-Steel Composite Sandwich Structures under Impact Loading". Compos. Struct. 311 (2023), p. 116813. DOI: 10.1016/j.compstruct.2023.116813.

[18] C. Zhang, C. Zeng, Z. Wang, T. Zeng, and Y. Wang. "Optimization of Stress Distribution of Bone-Implant Interface (BII)". Biomater. Adv. 147 (2023), p. 213342. DOI: 10.1016/j.bioadv.2023.213342.

[19] A. Elraggal, I.M. Abdelraheem, D.C. Watts, S. Roy, V.K. Dommeti, A. Alshabib, K.A. Althaqafi, and R.R. Afifi. "Biomechanical Reinforcement by CAD-CAM Materials Affects Stress Distributions of Posterior Composite Bridges: 3D Finite Element Analysis". Dent. Mater. 40 (2024), pp. 869–877. DOI: 10.1016/j.dental.2024.04.001.

[20] K. Młynarek-Żak and J. Żmudzki. "The Effect of Porous Compliance Bushings in a Dental Implant on the Distribution of Occlusal Loads". Sci. Rep. 14 (2024), p. 1607. DOI: 10.1038/s41598-024-51429-5.

[21] M. Afazal, S. Afreen, and A. Chanda. "Computational Modelling and Analysis of Hard Tissue Behavior around 0.5 Mm and 0.85 Mm Platform Switched Abutment Using 3D Finite Element Analysis". Forces Mech. 13 (2023), p. 100243. DOI: 10.1016/j.finmec.2023.100243.

[22] M. Ceddia, T. Romasco, N. De Bortoli, B.F. Mello, A. Piattelli, E. Mijiritsky, N. Di Pietro, and B. Trentadue. "Biomechanical Finite Element Analysis of Two Types of Short-Angled Implants Across Various Bone Classifications". Materials (Basel) 17 (2024), p. 5680. DOI: 10.3390/ma17235680.

[23] L.-S. Huang, Y.-C. Huang, C. Yuan, S.-J. Ding, and M. Yan. "Biomechanical Evaluation of Bridge Span with Three Implant Abutment Designs and Two Connectors for Tooth-Implant Supported Prosthesis: A Finite Element Analysis". J. Dent. Sci. 18 (2023), pp. 248–263. DOI: 10.1016/j.jds.2022.05.026.

[24] X. Miao, J. Hu, Y. Xu, J. Su, and Y. Jing. "Review on mechanical properties of metal lattice structures". Composite Structures (2024), p. 118267. DOI: 10.1016/j.compstruct.2024.118267.

[25] N. Xiao, F. Berto, and X. Zhou. "Three-Dimensional Stochastic Reconstruction of Porous Media: A Systematic Review". J. Build. Eng. 91 (2024), p. 109642. DOI: 10.1016/j.jobe.2024.109642.

[26] Jaryong Cho, Eun Suk Lee, Jeong Ho Kim, Chang-Yull Lee, and Jin Yeon Cho. "Design of Lattice-Based Energy-Absorbing Structure for Enhancing the Crashworthiness of Advanced Air Mobility". Aerospace 12.4 (2025), p. 332. DOI: 10.3390/aerospace12040332. URL: https://doi.org/10.3390/aerospace12040332.

[27] Babak Ziaie, Xavier Velay, and Waqas Saleem. "Advanced porous hip implants: A comprehensive review". Heliyon 10 (2024), e37818. DOI: 10.1016/j.heliyon.2024.e37818. URL: https://doi.org/10.1016/j.heliyon.2024.e37818.

[28] Syed Saarim Razi, Salman Pervaiz, Rahmat Agung Susantyoko, and Mozah Alyammahi. "Optimization of Environment-Friendly and Sustainable Polylactic Acid (PLA)-Constructed Triply Periodic Minimal Surface (TPMS)-Based Gyroid Structures". Polymers 16.8 (2024), p. 1175. DOI: 10.3390/polym16081175. URL: https://doi.org/10.3390/polym16081175.

[29] Edoardo Mancini, Mattia Utzeri, Emanuele Farotti, Attilio Lattanzi, and Marco Sasso. "DLP printed 3D gyroid structure: Mechanical response at meso and macro scale". Mechanics of Materials 192 (2024), p. 104970. DOI: 10.1016/j.mechmat.2024.104970. URL: https://doi.org/10.1016/j.mechmat.2024.104970.

[30] Jiaxuan Wang, Chenyi Qian, Xiang Qiu, Binbin Yu, Lixia Yan, Junye Shi, and Jiangping Chen. "Numerical and experimental investigation of additive manufactured heat exchanger using triply periodic minimal surfaces (TPMS)". Thermal Science and Engineering Progress 55 (2024), p. 103007. DOI: 10.1016/j.tsep.2024.103007. URL: https://doi.org/10.1016/j.tsep.2024.103007.

[31] K. Ishikawa. "Bone Substitute Fabrication Based on Dissolution-Precipitation Reactions". Materials (Basel) 3 (2010), pp. 1138–1155. DOI: 10.3390/ma3021138.

[32] G. Chouhan and G. Bala Murali. "Designs, Advancements, and Applications of Three-Dimensional Printed Gyroid Structures: A Review". Proc. Inst. Mech. Eng. Part E J. Process Mech. Eng. 238 (2024), pp. 965–987. DOI: 10.1177/09544089231160030.

[33] J. Feng, J. Fu, X. Yao, and Y. He. "Triply Periodic Minimal Surface (TPMS) Porous Structures: From Multi-Scale Design, Precise Additive Manufacturing to Multidisciplinary Applications". Int. J. Extrem. Manuf. 4 (2022). DOI: 10.1088/2631-7990/ac5be6.

[34] S.A. Tyagi and M. M. "Additive Manufacturing of Titanium-Based Lattice Structures for Medical Applications – A Review". Bioprinting 30 (2023), e00267. DOI: 10.1016/j.bprint.2023.e00267.

[35] I. Maskery, N.T. Aboulkhair, A.O. Aremu, C.J. Tuck, and I.A. Ashcroft. "Compressive Failure Modes and Energy Absorption in Additively Manufactured Double Gyroid Lattices". Addit. Manuf. 16 (2017), pp. 24–29. DOI: 10.1016/j.addma.2017.04.003.

[36] E. Yang, M. Leary, B. Lozanovski, D. Downing, M. Mazur, A. Sarker, A.M. Khorasani, A. Jones, T. Maconachie, S. Bateman, and et al. "Effect of Geometry on the Mechanical Properties of Ti-6Al-4V Gyroid Structures Fabricated via SLM: A Numerical Study". Mater. Des. 184 (2019). DOI: 10.1016/j.matdes.2019.108165.

[37] E. Pei, I. Kabir, T. Breški, D. Godec, and A. Nordin. "A Review of Geometric Dimensioning and Tolerancing (GD""T) of Additive Manufacturing and Powder Bed Fusion Lattices". Prog. Addit. Manuf. 7 (2022), pp. 1297–1305. DOI: 10.1007/s40964-022-00304-8.

[38] D. Myers, A. Abdel-Wahab, F. Hafeez, N. Kovacev, and K. Essa. "Optimisation of the Additive Manufacturing Parameters of Polylactic Acid (PLA) Cellular Structures for Biomedical Applications". J. Mech. Behav. Biomed. Mater. 136 (2022), p. 105447. DOI: 10.1016/j.jmbbm.2022.105447.

[39] R. Winarso, P.W. Anggoro, R. Ismail, J. Jamari, and A.P. Bayuseno. "Application of Fused Deposition Modeling (FDM) on Bone Scaffold Manufacturing Process: A Review". Heliyon 8 (2022), e11701. DOI: 10.1016/j.heliyon.2022.e11701.

[40] H. Zhang, Z. Guo, Z. Zhang, G. Wu, and L. Sang. "Biomimetic Design and Fabrication of PEEK and PEEK/CF Cage with Minimal Surface Structures by Fused Filament Fabrication". J. Mater. Res. Technol. 26 (2023), pp. 5001–5015. DOI: 10.1016/j.jmrt.2023.08.236.

[41] J. Zhang, S. Xie, T. Li, Z. Liu, S. Zheng, and H. Zhou. "A Study of Multi-Stage Energy Absorption Characteristics of Hybrid Sheet TPMS Lattices". Thin-Walled Struct. 190 (2023), p. 110989. DOI: 10.1016/j.tws.2023.110989.

[42] W. Tang, C. Zou, H. Zhou, L. Zhang, Y. Zeng, L. Sun, Y. Zhao, M. Yan, J. Fu, and J. Hu. "A Novel Convective Heat Transfer Enhancement Method Based on Precise Control of Gyroid-Type TPMS Lattice Structure". Appl. Therm. Eng. 230 (2023), p. 120797. DOI: 10.1016/j.applthermaleng.2023.120797.

[43] A. Timercan, P. Terriault, and V. Brailovski. "Axial Tension/Compression and Torsional Loading of Diamond and Gyroid Lattice Structures for Biomedical Implants: Simulation and Experiment". Mater. Des. 225 (2023), p. 111585. DOI: 10.1016/j.matdes.2022.111585.

[44] J. Zhang, X. Chen, Y. Sun, Y. Wang, and L. Bai. "Sound-Absorption and Mechanical Properties of Multisheet Gyroid Lattice Structures by Stereolithography". Compos. Struct. 325 (2023), p. 117589. DOI: 10.1016/j.compstruct.2023.117589.

[45] Enrico Dalpadulo, Mattia Pollon, Alberto Vergnano, and Francesco Leali. "Design for Additive Manufacturing of Lattice Structures for Functional Integration of Thermal Management and Shock Absorption". Journal of Manufacturing and Materials Processing 9.1 (2025), p. 24. DOI: 10.3390/jmmp9010024. URL: https://doi.org/10.3390/jmmp9010024.

[46] B.I. Oladapo, J.F. Kayode, P. Karagiannidis, N. Naveed, H. Mehrabi, and K.O. Ogundipe. "Polymeric Composites of Cubic-Octahedron and Gyroid Lattice for Biomimetic Dental Implants". Mater. Chem. Phys. 289 (2022), p. 126454. DOI: 10.1016/j.matchemphys.2022.126454.

[47] F.N. Depboylu, E. Yasa, Ö. Poyraz, F. Korkusuz, and A.A. Popa. "Choosing between Commercially Pure Titanium and Ti-6Al-4V Gyroid Structures for Orthopedic Applications". Materials Today Communications 39 (2024), p. 109256. DOI: 10.1016/j.mtcomm.2024.109256.

[48] A. Binobaid, A. Guner, J. Camilleri, A. Jiménez, and K. Essa. "A 3D Printed Ultra-Short Dental Implant Based on Lattice Structures and ZIRCONIA/Ca2SiO4 Combination". Journal of the Mechanical Behavior of Biomedical Materials 155 (2024). DOI: 10.1016/j.jmbbm.2024.106559.

[49] F.T. Omigbodun, D.S. Engstrom, and E. Mele. "Improving Mechanical Strength of Bone-Implant with Primitive and Gyroid Lattice of PLA/CHAP and RGO Composites". Colloids and Surfaces A: Physicochemical and Engineering Aspects (2021), p. 127151. DOI: 10.1016/j.colsurfa.2021.127151.

[50] X. Zhang, L. Jiang, X. Yan, Z. Wang, X. Li, and G. Fang. "Revealing the Apparent and Local Mechanical Properties of Heterogeneous Lattice". Virtual and Physical Prototyping 18 (2023), pp. 1–23. DOI: 10.1080/17452759.2022.2120406.

[51] U. Sajjad, T. Rehman, M. Ali, C.W. Park, and W.-M. Yan. "Manufacturing and Potential Applications of Lattice Structures in Thermal Systems". International Journal of Heat and Mass Transfer 198 (2022), p. 123352. DOI: 10.1016/j.ijheatmasstransfer.2022.123352.

[52] B.V.S. Reddy, A.M. Shaik, D. Sundeep, C.S. Chebiyyam, J. Krishnaiah, and U. Chandrasekhar. "Performance Evaluation of Metallic Honeycomb and Gyroid Micro-Lattice Structures for Armoured Fighting Vehicles". Transactions of the Indian Institute of Metals 77 (2024), pp. 615–626. DOI: 10.1007/s12666-023-03146-2.

[53] D.B. Alemayehu and Y.R. Jeng. "Three-Dimensional Finite Element Investigation into Effects of Implant Thread Design and Loading Rate on Stress Distribution in Dental Implants and Anisotropic Bone". Materials (Basel) 14 (2021). DOI: 10.3390/ma14226974.

[54] H. Liang, Y. Zhao, S. Chen, F. Ma, and D. Wang. "Review of Crashworthiness Studies on Cellular Structures". Automotive Innovation 6 (2023), pp. 379–403. DOI: 10.1007/s42154-023-00237-0.

[55] G. Wang, Y. Zhang, Z. Zheng, H. Chen, and J. Yu. "Crashworthiness design and impact tests of aluminum foam-filled crash boxes". Thin-Walled Structures 180 (2022), p. 109937. ISSN: 0263-8231. DOI: 10.1016/j.tws.2022.109937.

[56] A. De Biasio, H. Ghasemnejad, S. Srimanosaowapak, and J. W. Watson. "Development of multi aluminium foam-filled crash box systems to improve crashworthiness performance of road service vehicle". European Journal of Mechanics - A/Solids 109 (2025), p. 105433. DOI: 10.1016/j.euromechsol.2024.105433.

[57] F. Djamaluddin. "Optimization of foam-filled crash-box under axial loading for pure electric vehicle". Results in Materials 21 (2024), p. 100505. ISSN: 2590-048X. DOI: 10.1016/j.rinma.2023.100505.

[58] D. Vališ, K. Hasilová, J. Gajewski, and M. Rogala. "Proper functioning and failure occurrence of energy absorbers modelled for optimization". Engineering Failure Analysis 170 (2025), p. 109238. ISSN: 1350-6307. DOI: 10.1016/j.engfailanal.2024.109238.

[59] T. Abhishek, D. Sundeep, C.C. Sastry, K.V. Eswaramoorthy, G.C. Kesireddy, B.V. Reddy, R.K. Verma, S. Salunkhe, R. Cep, and E.A. Nasr. "Experimental Investigation of Tungsten–Nickel–Iron Alloy, W95Ni3.5Fe1.5, Compared to Copper Monolithic Bullets". Frontiers in Mechanical Engineering 10 (2024). DOI: 10.3389/fmech.2024.1383341.

[60] M. Araya, M. Jaskari, T. Rautio, T. Guillén, and A. Järvenpää. "Assessing the Compressive and Tensile Properties of TPMS-Gyroid and Stochastic Ti64 Lattice Structures: A Study on Laser Powder Bed Fusion Manufacturing for Biomedical Implants". J. Sci. Adv. Mater. Devices 9 (2024), p. 100663. DOI: 10.1016/j.jsamd.2023.100663.

[61] L.-Y. Chen, S.-X. Liang, Y. Liu, and L.-C. Zhang. "Additive Manufacturing of Metallic Lattice Structures". Materials Science and Engineering: R Reports 146 (2021), p. 100648. DOI: 10.1016/j.mser.2021.100648.

[62] E.A.A. Alkebsi, H. Ameddah, T. Outtas, and A. Almutawakel. "Design of Graded Lattice Structures in Turbine Blades Using Topology Optimization". Int. J. Comput. Integr. Manuf. 34 (2021), pp. 370–384. DOI: 10.1080/0951192X.2021.1872106.

[63] F. Vlădulescu and D.M. Constantinescu. "Lattice Topology Homogenization and Crack Propagation through Finite Element Analyses". Procedia Struct. Integr. 28 (2020), pp. 637–647. DOI: 10.1016/j.prostr.2020.10.074.

[64] K. Monkova, P.P. Monka, and A. Vodilka. "Comparison of the Bending Behavior of Cylindrically Shaped Lattice Specimens with Radially and Orthogonally Arranged Cells Made of ABS". Polymers (Basel). 16 (2024), p. 979. DOI: 10.3390/polym16070979.

[65] A. Piros and L. Trautmann. "Creating Interior Support Structures with Lightweight Voronoi Scaffold". Int. J. Interact. Des. Manuf. 17 (2023), pp. 93–101. DOI: 10.1007/s12008-022-01182-8.

[66] S. Chattopadhyay, S.D. Mohapatra, and N.K. Mandal. "Advancements and Challenges in Additive Manufacturing: A Comprehensive Review". Eng. Res. Express 6 (2024). DOI: 10.1088/2631-8695/ad30b1.

[67] G.D. Goh, K.K. Wong, N. Tan, H.L. Seet, and M.L.S. Nai. "Large-Format Additive Manufacturing of Polymers: A Review of Fabrication Processes, Materials, and Design". Virtual Phys. Prototyp. 19 (2024), e2336160. DOI: 10.1080/17452759.2024.2336160.

[68] F. Mehdipour, T. Delrieux, F. Maurer, J.-D. Grunwaldt, C. Klahn, and R. Dittmeyer. "Opportunities and Limitations of Metal Additive Manufacturing of Structured Catalytic Converters". Catal. Commun. (2024), p. 106873. DOI: 10.1016/j.catcom.2024.106873.

[69] P. Tang, X. Zhao, H. Shi, B. Hu, J. Ding, B. Yang, and W. Xu. "A Review of Multi-Axis Additive Manufacturing: Potential, Opportunity and Challenge". Addit. Manuf. (2024), p. 104075. DOI: 10.1016/j.addma.2024.104075.

[70] C. Yan, L. Hao, A. Hussein, P. Young, and D. Raymont. "Advanced Lightweight 316L Stainless Steel Cellular Lattice Structures Fabricated via Selective Laser Melting". Mater. Des. 55 (2014), pp. 533–541. DOI: 10.1016/j.matdes.2013.10.027.

[71] I. Maskery and I.A. Ashcroft. "The Deformation and Elastic Anisotropy of a New Gyroid-Based Honeycomb Made by Laser Sintering". Addit. Manuf. 36 (2020), p. 101548. DOI: 10.1016/j.addma.2020.101548.

[72] F.M. Mwema and E.T. Akinlabi. *Basics of Fused Deposition Modelling (FDM)*. SpringerBriefs Appl. Sci. Technol., 2020, pp. 1–15. DOI: 10.1007/978-3-030-48259-6-1.

[73] R. Kumaresan, M. Samykano, K. Kadirgama, D. Ramasamy, N.W. Keng, and A.K. Pandey. "3D Printing Technology for Thermal Application: A Brief Review". J. Adv. Res. Fluid Mech. Therm. Sci. 83 (2021), pp. 84–97. DOI: 10.37934/ARFMTS.83.2.8497.

[74] P. Gay, D. Blanco, F. Pelayo, A. Noriega, and P. Fernández. "Analysis of Factors Influencing the Mechanical Properties of Flat PolyJet Manufactured Parts". Procedia Eng. 132 (2015), pp. 70–77. DOI: 10.1016/j.proeng.2015.12.481.

[75] M.J. Dantin, W.M. Furr, and M.W. Priddy. "Towards an Open-Source, Preprocessing Framework for Simulating Material Deposition for a Directed Energy Deposition Process". In: *Solid Free. Fabr. Proc. 29th Annu. Int. Solid Free. Fabr. Symp. - An Addit. Manuf. Conf. SFF 2018.* 2020, pp. 1903–1912. DOI: 10.26153/tsw/17192.

[76] O. Pannitz and J.T. Sehrt. "Transferability of Process Parameters in Laser Powder Bed Fusion Processes for an Energy and Cost Efficient Manufacturing". Sustainability 12 (2020). DOI: 10.3390/su12041565.

[77] ASTM International. "1621, Standard Test Method for Compressive Properties of Rigid Cellular Plastics". American Society for Testing and Materials (2010).

[78] M.F. Ashby, T. Evans, N.A. Fleck, J.W. Hutchinson, H.N.G. Wadley, and L.J. Gibson. *Metal Foams: A Design Guide*. Elsevier, 2000. ISBN: 0080511465. DOI: 10.1115/1.1421119.

[79] D. Li, W. Liao, N. Dai, and Y.M. Xie. "Comparison of Mechanical Properties and Energy Absorption of Sheet-Based and Strut-Based Gyroid Cellular Structures with Graded Densities". Mater. (Basel, Switzerland) 12 (2019). DOI: 10.3390/ma12132183.

[80] G. Hu, G. Xu, Q. Gao, Z. Feng, P. Huang, and G. Zu. "Compressive Properties and Energy Absorption Behavior of 316L Steel Foam Prepared by Space Holder Technique". Materials (Basel) 16 (2023). DOI: 10.3390/ma16041419.

[81] A. Bacciaglia, A. Ceruti, and A. Liverani. "Structural Analysis of Voxel-Based Lattices Using 1D Approach". 3D Print. Addit. Manuf. 9 (2022), pp. 365–379. DOI: 10.1089/3dp.2020.0178.

[82] M. McGregor, S. Patel, S. McLachlin, and M. Vlasea. "Data Related to Architectural Bone Parameters and the Relationship to Ti Lattice Design for Powder Bed Fusion Additive Manufacturing". Data Br. 39 (2021), pp. 1–45. DOI: 10.1016/j.dib.2021.107633.

[83] S. Hussain, A. Nazir, S. Waqar, U. Ali, and O. Gokcekaya. "Effect of Additive Manufactured Hybrid and Functionally Graded Novel Designed Cellular Lattice Structures on Mechanical and Failure Properties". Int. J. Adv. Manuf. Technol. (2023), pp. 1–19. DOI: 10.1007/s00170-023-12201-7.

[84] R. Pugliese and S. Graziosi. "Biomimetic Scaffolds Using Triply Periodic Minimal Surface-Based Porous Structures for Biomedical Applications". SLAS Technol. 28 (2023), pp. 165–182. DOI: 10.1016/j.slast.2023.04.004.

[85] K. Shi, W. Yang, H. Mei, Y. Yan, L. Xu, L. Cheng, and L. Zhang. "Characterization and Enhancement of Quasi-Static and Shear Mechanical Properties of 3D Printed Lightweight SiOC Lattices: Effects of Structural Design and Parameters". J. Eur. Ceram. Soc. (2023). DOI: 10.1016/j.jeurceramsoc.2023.06.066.

[86] J. Wu, Y. Zhang, Y. Lyu, and L. Cheng. "On the Various Numerical Techniques for the Optimization of Bone Scaffold". Materials (Basel) 16 (2023), p. 974. DOI: 10.3390/ma16030974.

[87] N. Yang, H. Wei, and Z. Mao. "Tuning Surface Curvatures and Young's Moduli of TPMS-Based Lattices Independent of Volume Fraction". Mater. Des. 216 (2022), p. 110542. DOI: 10.1016/j.matdes.2022.110542.

[88] C. Zhang, H. Zheng, L. Yang, Y. Li, J. Jin, W. Cao, C. Yan, and Y. Shi. "Mechanical Responses of Sheet-Based Gyroid-Type Triply Periodic Minimal Surface Lattice Structures Fabricated Using Selective Laser Melting". Mater. Des. 214 (2022), p. 110407. DOI: 10.1016/j.matdes.2022.110407.

[89] A. Du Plessis, N. Razavi, M. Benedetti, S. Murchio, M. Leary, M. Watson, D. Bhate, and F. Berto. "Properties and Applications of Additively Manufactured Metallic Cellular Materials: A Review". Prog. Mater. Sci. 125 (2022), p. 100918. DOI: 10.1016/j.pmatsci.2021.100918.

[90] A. Du Plessis, C. Broeckhoven, I. Yadroitsava, I. Yadroitsev, C.H. Hands, R. Kunju, and D. Bhate. "Beautiful and Functional: A Review of Biomimetic Design in Additive Manufacturing". Addit. Manuf. 27 (2019), pp. 408–427. DOI: 10.1016/j.addma.2019.03.033.

[91] N. Kladovasilakis, K. Tsongas, and D. Tzetzis. "Finite Element Analysis of Orthopedic Hip Implant with Functionally Graded Bioinspired Lattice Structures". Biomimetics 5.3 (2020), p. 44. DOI: 10.3390/BIOMIMETICS5030044.

[92] M. Pelanconi and A. Ortona. "Nature-Inspired, Ultra-Lightweight Structures with Gyroid Cores Produced by Additive Manufacturing and Reinforced by Unidirectional Carbon Fiber Ribs". Materials (Basel) 12 (2019), pp. 1–14. DOI: 10.3390/ma1224134.

[93] J. Ren, Y. Wang, Y. Yao, Y. Wang, X. Fei, P. Qi, S. Lin, D.L. Kaplan, M.J. Buehler, and S. Ling. "Biological Material Interfaces as Inspiration for Mechanical and Optical Material Designs". Chem. Rev. 119 (2019), pp. 12279–12336. DOI: 10.1021/acs.chemrev.9b00416.

[94] A. Panesar, M. Abdi, D. Hickman, and I. Ashcroft. "Strategies for Functionally Graded Lattice Structures Derived Using Topology Optimisation for Additive Manufacturing". Addit. Manuf. 19 (2018), pp. 81–94. DOI: 10.1016/j.addma.2017.11.008.

[95] M. Pelanconi, S. Zavattoni, L. Cornolti, R. Puragliesi, E. Arrivabeni, L. Ferrari, S. Gianella, M. Barbato, and A. Ortona. "Application of Ceramic Lattice Structures to Design Compact, High Temperature Heat Exchangers: Material and Architecture Selection". Materials (Basel) 14 (2021). DOI: 10.3390/ma14123225.

[96] M. Alizadeh-Osgouei, Y. Li, A. Vahid, A. Ataee, and C. Wen. "High Strength Porous PLA Gyroid Scaffolds Manufactured via Fused Deposition Modeling for Tissue-Engineering Applications". Smart Mater. Med. 2 (2021), pp. 15–25. DOI: 10.1016/j.smaim.2020.10.003.

[97] A. Bouteldja, M.A. Louar, L. Hemmouche, L. Gilson, A. Miranda-Vicario, and L. Rabet. "Experimental Investigation of the Quasi-Static and Dynamic Compressive Behavior of Polymer-Based 3D-Printed Lattice Structures". Int. J. Impact Eng. 180 (2023), p. 104640. DOI: 10.1016/j.ijimpeng.2023.104640.

[98] D. Qin, L. Sang, Z. Zhang, S. Lai, and Y. Zhao. "Compression Performance and Deformation Behavior of 3D-Printed PLA-Based Lattice Structures". Polymers (Basel) 14 (2022). DOI: 10.3390/polym14051062.

[99] R.P. Varma. "Energy Absorption of Multi-Material Cellular Structures". Ph.D. thesis. Arizona State University, 2021.

[100] S. Yu, J. Sun, and J. Bai. "Investigation of Functionally Graded TPMS Structures Fabricated by Additive Manufacturing". Mater. Des. 182 (2019), p. 108021. DOI: 10.1016/j.matdes.2019.108021.

[101] X. Guo, X. Li, E. Wang, J.Y.H. Fuh, W.F. Lu, and W. Zhai. "Bioinspired Hierarchical Diamond Triply Periodic Minimal Surface Lattices with High Energy Absorption and Great Damage Tolerance". Addit. Manuf. (2023), p. 103792. DOI: 10.1016/j.addma.2023.103792.

[102] Y. Ren, W. Ran, Y. Li, B. Xue, and W. Chen. "Enhancing the energy absorption capacity of Ti–6Al–4V lattice structure manufactured by additive manufacturing through β-annealing". Journal of Materials Research and Technology 35 (2025), pp. 2369–2376. ISSN: 2238-7854. DOI: 10.1016/j.jmrt.2025.01.214. URL: https://www.sciencedirect.com/science/article/pii/S2238785425002145.

[103] I. Mahapatra, R. Velmurugan, and R. Jayaganthan. "Enhanced Flexural Performance of Diamond Latticed Triply Periodic Minimal Surface Sandwich Panels". Adv. Eng. Mater. 2300813 (2023). DOI: 10.1002/adem.202300813.

[104] F. Li, J. Gan, L. Zhang, H. Tan, E. Li, and B. Li. "Enhancing Impact Resistance of Hybrid Structures Designed with Triply Periodic Minimal Surfaces". Compos. Sci. Technol. 245 (2024), p. 110365. DOI: 10.1016/j.compscitech.2023.110365.

[105] N. Novak, O. Al-Ketan, M. Borovinšek, L. Krstulović-Opara, R. Rowshan, M. Vesenjak, and Z. Ren. "Development of Novel Hybrid TPMS Cellular Lattices and Their Mechanical Characterisation". J. Mater. Res. Technol. 15 (2021), pp. 1318–1329. DOI: 10.1016/j.jmrt.2021.08.092.

[106] A. Nazir, S. Hussain, H.M. Ali, and S. Waqar. "Design and Mechanical Performance of Nature-Inspired Novel Hybrid Triply Periodic Minimal Surface Lattice Structures Fabricated Using Material Extrusion". Mater. Today Commun. 38 (2024), p. 108349. DOI: 10.1016/j.mtcomm.2024.108349.

[107] A. Ingrole, A. Hao, and R. Liang. "Design and Modeling of Auxetic and Hybrid Honeycomb Structures for In-Plane Property Enhancement". Mater. Des. 117 (2017), pp. 72–83. DOI: 10.1016/j.matdes.2016.12.067.

[108] P.J.L. Lazar, J. Subramanian, E. Natarajan, K. Markandan, and S. Ramesh. "Anisotropic Structure-Property Relations of FDM Printed Short Glass Fiber Reinforced Polyamide TPMS Structures under Quasi-Static Compression". J. Mater. Res. Technol. 24 (2023), pp. 9562–9579. DOI: 10.1016/j.jmrt.2023.05.167.

[109] C. Pasini, S. Pandini, G. Ramorino, and L. Sartore. "Tailoring the Properties of Composite Scaffolds with a 3D-Printed Lattice Core and a Bioactive Hydrogel Shell for Tissue Engineering". J. Mech. Behav. Biomed. Mater. 150 (2024), p. 106305. DOI: 10.1016/j.jmbbm.2023.106305.

[110] X. Li, X. Yu, J.W. Chua, H.P. Lee, J. Ding, and W. Zhai. "Microlattice Metamaterials with Simultaneous Superior Acoustic and Mechanical Energy Absorption". Small 17 (2021), p. 2100336. DOI: 10.1002/smll.202100336.

[111] J. Noronha, M. Qian, M. Leary, E. Kyriakou, and M. Brandt. "Hollow-Walled Lattice Materials by Additive Manufacturing: Design, Manufacture, Properties, Applications and Challenges". Curr. Opin. Solid State Mater. Sci. 25 (2021), p. 100940. DOI: 10.1016/j.cossms.2021.100940.

[112] C.V. Amaechi, E.F. Adefuye, I.M. Kgosiemang, B. Huang, and E.C. Amaechi. "Scientometric Review for Research Patterns on Additive Manufacturing of Lattice Structures". Materials (Basel) 15 (2022), p. 5323. DOI: 10.3390/ma15155323.

[113] Z. Yu, Z. Pan, D. Ding, Z. Rong, H. Li, and B. Wu. "Strut Formation Control and Processing Time Optimization for Wire Arc Additive Manufacturing of Lattice Structures". J. Manuf. Process. 79 (2022), pp. 962–974. DOI: 10.1016/j.jmapro.2022.05.043.

[114] M. Zhao, D.Z. Zhang, Z. Li, T. Zhang, H. Zhou, and Z. Ren. "Design, Mechanical Properties, and Optimization of BCC Lattice Structures with Taper Struts". Compos. Struct. 295 (2022). DOI: 10.1016/j.compstruct.2022.115830.

[115] B. Shen, Y. Chen, C. Li, S. Wang, and X. Chen. "Superconducting Fault Current Limiter (SFCL): Experiment and the Simulation from Finite-Element Method (FEM) to Power/Energy System Software". Energy 234 (2021), p. 121251. DOI: 10.1016/j.energy.2021.121251.

[116] S.D. Müzel, E.P. Bonhin, N.M. Guimarães, and E.S. Guidi. "Application of the Finite Element Method in the Analysis of Composite Materials: A Review". Polymers (Basel) 12 (2020), p. 818. DOI: 10.3390/polym12040818.

[117] D.B. Alemayehu, M. Todoh, and S.-J. Huang. "Advancing 3D Dental Implant Finite Element Analysis: Incorporating Biomimetic Trabecular Bone with Varied Pore Sizes in Voronoi Lattices". J. Funct. Biomater. 15 (2024), p. 94. DOI: 10.3390/jfb15040094.

[118] H. Gharehbaghi and A. Farrokhabadi. "Experimental, Analytical, and Numerical Studies of the Energy Absorption Capacity of Bi-Material Lattice Structures Based on Quadrilateral Bipyramid Unit Cell". Compos. Struct. 337 (2024), p. 118042. DOI: 10.1016/j.compstruct.2024.118042.

[119] Z. Guo, J. Hu, and Z. Kong. "On Impact Loading of Voronoi Functional Graded Porous Structure". Mater. Today Commun. 38 (2024), p. 107765. DOI: 10.1016/j.mtcomm.2023.107765.

[120] M.H. Palmiyanto, E. Surojo, D. Ariawan, and F. Imaduddin. "E-Glass/Kenaf Fibre Reinforced Thermoset Composites Fiiled with MCC and Immersion in a Different Fluid". Sci. Rep. 12 (2022), p. 20332. DOI: 10.1038/s41598-022-24506-w.

[121] O. Al-Ketan, R. Rowshan, and R.K. Abu Al-Rub. "Topology-Mechanical Property Relationship of 3D Printed Strut, Skeletal, and Sheet Based Periodic Metallic Cellular Materials". Addit. Manuf. 19 (2018), pp. 167–183. DOI: 10.1016/j.addma.2017.12.006.

[122] X.Y. Cheng, S.J. Li, L.E. Murr, Z.B. Zhang, Y.L. Hao, R. Yang, F. Medina, and R.B. Wicker. "Compression Deformation Behavior of Ti-6Al-4V Alloy with Cellular Structures Fabricated by Electron Beam Melting". J. Mech. Behav. Biomed. Mater. 16 (2012), pp. 153–162. DOI: 10.1016/j.jmbbm.2012.10.005.

[123] L.J. Gibson. "Cellular Solids". Mrs Bull. 28 (2003), pp. 270–274. DOI: 10.1557/mrs2003.79.

[124] N. Wang, G.K. Meenashisundaram, S. Chang, J.Y.H. Fuh, S.T. Dheen, and A. Senthil Kumar. "A Comparative Investigation on the Mechanical Properties and Cytotoxicity of Cubic, Octet, and TPMS Gyroid Structures Fabricated by Selective Laser Melting of Stainless Steel 316L". J. Mech. Behav. Biomed. Mater. 129 (2022), p. 105151. DOI: 10.1016/j.jmbbm.2022.105151.

[125] C. Iantaffi, E. Bele, D. McArthur, P.D. Lee, and C.L.A. Leung. "Auxetic Response of Additive Manufactured Cubic Chiral Lattices at Large Plastic Strains". Mater. Des. 233 (2023), p. 112207. DOI: 10.1016/j.matdes.2023.112207.

[126] S. Kechagias, R.N. Oosterbeek, M.J. Munford, S. Ghouse, and J.R.T. Jeffers. "Controlling the Mechanical Behaviour of Stochastic Lattice Structures: The Key Role of Nodal Connectivity". Addit. Manuf. 54 (2022), p. 102730. DOI: 10.1016/j.addma.2022.102730.

[127] B.J. Sahariah, A. Namdeo, and P. Khanikar. "Composite-Inspired Multilattice Metamaterial Structure: An Auxetic Lattice Design with Improved Strength and Energy Absorption". Mater. Today Commun. 30 (2022), p. 103159. DOI: 10.1016/j.mtcomm.2022.103159.

[128] F.N. Habib, P. Iovenitti, S.H. Masood, and M. Nikzad. "Fabrication of Polymeric Lattice Structures for Optimum Energy Absorption Using Multi Jet Fusion Technology". Mater. Des. 155 (2018), pp. 86–98. DOI: 10.1016/j.matdes.2018.05.059.

[129] F. Rahimidehgolan and W. Altenhof. "Compressive Behavior and Deformation Mechanisms of Rigid Polymeric Foams: A Review". Compos. Part B Eng. 253 (2023), p. 110513. DOI: 10.1016/j.compositesb.2023.110513.

[130] A. Mahmood, X. Wang, and C. Zhou. "Modeling strategies of 3D woven composites: A review". Composite Structures 93.8 (2011), pp. 1947–1963. ISSN: 0263-8223. DOI: 10.1016/j.compstruct.2011.03.010.

[131] A.K. Toksoy and M. Güden. "Partial Al Foam Filling of Commercial 1050H14 Al Crash Boxes: The Effect of Box Column Thickness and Foam Relative Density on Energy Absorption". Thin-Walled Struct. 48 (2010), pp. 482–494. DOI: 10.1016/j.tws.2010.02.002.

[132] J. Simpson and Z. Kazancı. "Crushing Investigation of Crash Boxes Filled with Honeycomb and Re-Entrant (Auxetic) Lattices". Thin-Walled Struct. 150 (2020), p. 106676. DOI: 10.1016/j.tws.2020.106676.

[133] C. Lu, C. Zhang, P. Wen, and F. Chen. "Mechanical Behavior of Al–Si10–Mg Gyroid Surface with Variable Topological Parameters Fabricated via Laser Powder Bed Fusion". J. Mater. Res. Technol. 15 (2021), pp. 5650–5661. DOI: 10.1016/j.jmrt.2021.11.008.

[134] A.M. Abou-Ali, D.W. Lee, and R.K. Abu Al-Rub. "On the Effect of Lattice Topology on Mechanical Properties of SLS Additively Manufactured Sheet-, Ligament-, and Strut-Based Polymeric Metamaterials". Polymers (Basel) 14 (2022). DOI: 10.3390/polym14214583.

[135] A.M. Abou-Ali, O. Al-Ketan, D.W. Lee, R. Rowshan, and R.K. Abu Al-Rub. "Mechanical Behavior of Polymeric Selective Laser Sintered Ligament and Sheet Based Lattices of Triply Periodic Minimal Surface Architectures". Mater. Des. 196 (2020). DOI: 10.1016/j.matdes.2020.109100.

[136] Xuejin Zhao, Zhenzong Li, Yupeng Zou, and Xiaoyu Zhao. "Compressive Characteristics and Energy Absorption Capacity of Automobile Energy-Absorbing Box with Filled Porous TPMS Structures". Applied Sciences 14.9 (2024), p. 3790. DOI: 10.3390/app14093790.

[137] S. Xie, S. Zheng, J. Zhang, Z. Liu, H. Wang, and H. Zhou. "Study on the crashworthiness of multi-cell thin-walled tubes filled with triply periodic minimal surface lattices". Mechanics of Advanced Materials and Structures 32.3 (2024), pp. 307–323. DOI: 10.1080/15376494.2024.2345206. URL: https://doi.org/10.1080/15376494.2024.2345206.

[138] G. Zheng, L. Zhang, E. Wang, R. Yao, Q. Luo, Q. Li, and G. Sun. "Investigation into Multiaxial Mechanical Behaviors of Kelvin and Octet-B Polymeric Closed-Cell Foams". Thin-Walled Struct. 177 (2022), p. 109405. DOI: 10.1016/j.tws.2022.109405.

[139] G. Yan, M. Sun, Z. Zhang, Y. Liang, N. Jiang, X. Pang, Y. Song, Y. Liu, and J. Zhao. "Experimental Study on Flow and Heat Transfer Performance of Triply Periodic Minimal Surface Structures and Their Hybrid Form as Disturbance Structure". Int. Commun. Heat Mass Transf. 147 (2023), p. 106942. DOI: 10.1016/j.icheatmasstransfer.2023.106942.

[140] H. Fu and S. Kaewunruen. "The Axially-Loaded Behaviours of Schwarz Primitive (SP)-Based Structures: An Experimental and DEM Study". Thin-Walled Struct. 200 (2024), p. 111973. DOI: 10.1016/j.tws.2024.111973.

[141] C. Ma, N.R. de Barros, T. Zheng, A. Gomez, M. Doyle, J. Zhu, H.S. Nanda, X. Li, A. Khademhosseini, and B. Li. "3D Printing and Surface Engineering of Ti6Al4V Scaffolds for Enhanced Osseointegration in an In Vitro Study". Biomimetics 9 (2024), p. 423. DOI: 10.3390/biomimetics9070423.

[142] S. Anju, N. Prajitha, V.S. Sukanya, and P.V. Mohanan. "Complicity of degradable polymers in health-care applications". Mater. Today 16 (2020), p. 100236. DOI: 10.1016/j.mtchem.2019.100236.

[143] C.T. Wanniarachchi, A. Arjunan, A. Baroutaji, M. Singh, J. Robinson, A. Vance, M. Appiah, and A. Arafat. "3D Printed CoCrMo Personalised Load-Bearing Meta-Scaffold for Critical Size Tibial Reconstruction". Ann. 3D Print. Med. 15 (2024), p. 100163. DOI: 10.1016/j.stlm.2024.100163.

[144] Y. Zhu, T. Tang, S. Zhao, D. Joralmon, Z. Poit, B. Ahire, S. Keshav, A.R. Raje, J. Blair, and Z. Zhang. "Recent Advancements and Applications in 3D Printing of Functional Optics". Addit. Manuf. 52 (2022), p. 102682. DOI: 10.1016/j.addma.2022.102682.

[145] Y. Yang, R. Jiang, C. Han, J. Chen, H. Li, Y. Wang, J. Tang, H. Zhou, W. Hu, and B. Zheng. "Frontiers in Laser Additive Manufacturing Technology". Addit. Manuf. Front. (2024), p. 200160. DOI: 10.1016/j.amf.2024.200160.

[146] K.-C. Lai, C. Tsai, S.-Y. Yen, K.-K. Tseng, J.-W. Yeh, and P.-Y. Chen. "Fabrication of Novel 316L Stainless Steel Scaffolds by Combining Freeze-Casting and 3D-Printed Gyroid Templating Techniques". Mater. Sci. Eng. A (2024), p. 147200. DOI: 10.1016/j.msea.2024.147200.

[147] M. Rezapourian, R. Kumar, and I. Hussainova. "Effect of Unit Cell Rotation on Mechanical Performance of Selective Laser Melted Gyroid Structures for Bone Tissue Engineering". Prog. Eng. Sci. 1 (2024), p. 100011. DOI: 10.1016/j.pes.2024.100011.

[148] X. Sheng, H. Liu, Y. Xu, Z. Wang, W. Zhang, C. Li, and J. Wang. “Functionalized Biomimetic Mineralized Collagen Promotes Osseointegration of 3D-Printed Titanium Alloy Microporous Interface”. Mater. Today Bio 24 (2024), p. 100896. DOI: 10.1016/j.mtbio.2023.100896.

[149] X. Sheng, Z. Che, H. Qiao, C. Qiu, J. Wu, C. Li, C. Tan, J. Li, G. Wang, and W. Liu. “A Functional Mineralized Collagen Hydrogel to Promote Angiogenic and Osteogenic for Osseointegration of 3D-Printed Titanium Alloy Microporous Scaffolds”. Int. J. Biol. Macromol. (2024), p. 133806. DOI: 10.1016/j.ijbiomac.2024.133806.

[150] W. Abd-Elaziem, M.M. Mohammed, H.M. Yehia, T.A. Sebaey, and T. Khan. “Porous Titanium for Medical Implants”. Sci. Park Publ 1 (2024), pp. 10–62184. DOI: 10.62184/mmc.jmmc100020241.

[151] A.T. Prakoso, H. Basri, D. Adanta, I. Yani, M.I. Ammarullah, I. Akbar, F.A. Ghazali, A. Syahrom, and T. Kamarul. “The Effect of Tortuosity on Permeability of Porous Scaffold”. Biomedicines 11 (2023), pp. 1–17. DOI: 10.3390/biomedicines11020427.

[152] Z.F.M. Salaha, M.I. Ammarullah, N.N.A.A. Abdullah, A.U.A. Aziz, H.S. Gan, A.H. Abdullah, M.R. Abdul Kadir, and M.H. Ramlee. “Biomechanical Effects of the Porous Structure of Gyroid and Voronoi Hip Implants: A Finite Element Analysis Using an Experimentally Validated Model”. Materials (Basel) 16 (2023). DOI: 10.3390/ma16093298.

[153] S. Davidopoulou, L. Batas, P. Karakostas, D. Tortopidis, P. Barmpalexis, A. Assimopoulou, C. Angelopoulos, and L. Tsalikis. “Multidimensional 3D-Printed Scaffolds for Ridge Preservation and Dental Implant Placement: A Systematic Review”. Appl. Sci. 14 (2024), p. 892. DOI: 10.3390/app14020892.

[154] T. Zhang, W. Zhou, W. Yang, J. Bi, H. Li, X. Gao, B. Zhang, G. Shi, K. Li, and Z. Wei. “Vancomycin-Encapsulated Hydrogel Loaded Microarc-Oxidized 3D-Printed Porous Ti6Al4V Implant for Infected Bone Defects: Reconstruction, Anti-Infection, and Osseointegration”. Bioact. Mater. 42 (2024), pp. 18–31. DOI: 10.1016/j.bioactmat.2024.07.035.

[155] X. Miao, J. Hu, Y. Xu, J. Su, and Y. Jing. “Review on Mechanical Properties of Metal Lattice Structures”. Compos. Struct. (2024), p. 118267. DOI: 10.1016/j.compstruct.2024.118267.

[156] S. He, J. Zhu, Y. Jing, S. Long, L. Tang, L. Cheng, and Z. Shi. “Effect of 3D-Printed Porous Titanium Alloy Pore Structure on Bone Regeneration: A Review”. Coatings 14 (2024), p. 253. DOI: 10.3390/coatings14030253.

[157] M.N. Shahid, M.U. Shahid, S. Rasheed, M. Irfan, and M.A. Obeidi. “Computational Investigation of the Fluidic Properties of Triply Periodic Minimal Surface (TPMS) Structures in Tissue Engineering”. Designs 8 (2024), p. 69. DOI: 10.3390/designs8040069.

[158] E. Maevskaia, C. Ghayor, I. Bhattacharya, J. Guerrero, and F.E. Weber. “TPMS Microarchitectures for Vertical Bone Augmentation and Osteoconduction: An In Vivo Study”. Materials (Basel) 17 (2024), p. 2533. DOI: 10.3390/ma17112533.

[159] X. Peng, S. Li, D. He, J. Li, S. Qu, and Z. Jin. “Expanding the Mechanical and Mass-Transport Combination for Bone Scaffolds: Through Stretched Structure”. Compos. Struct. 329 (2024), p. 117783. DOI: 10.1016/j.compstruct.2023.117783.

[160] A. Taheri, F. Farahmand, and M. Bahraminasab. “Radially and Axially Graded Cellular Tibial Stems for Total Knee Replacement”. Int. J. Mech. Sci. 263 (2024), p. 108772. DOI: 10.1016/j.ijmecsci.2023.108772.

[161] Shangyan Zhao, Yixuan Shi, Chengcong Huang, Xuan Li, Yuchen Lu, Yuzhi Wu, Yageng Li, and Luning Wang. “Integrating Machine Learning into Additive Manufacturing of Metallic Biomaterials: A Comprehensive Review”. Journal of Functional Biomaterials 16.3 (2025), p. 77. DOI: 10.3390/jfb16030077. URL: https://doi.org/10.3390/jfb16030077.

[162] J. Gao, Y. Pan, Y. Gao, H. Pang, H. Sun, L. Cheng, and J. Liu. “Research Progress on the Preparation Process and Material Structure of 3D-Printed Dental Implants and Their Clinical Applications”. Coatings 14 (2024), p. 781. DOI: 10.3390/coatings14070781.

[163] X. Huang, Y. Lou, Y. Duan, H. Liu, J. Tian, Y. Shen, and X. Wei. “Biomaterial Scaffolds in Maxillofacial Bone Tissue Engineering: A Review of Recent Advances”. Bioact. Mater. 33 (2024), pp. 129–156. DOI: 10.1016/j.bioactmat.2023.10.031.

[164] H. Chen, G. Song, T. Xu, C. Meng, Y. Zhang, T. Xin, T. Yu, Y. Lin, and B. Han. “Biomaterial Scaffolds for Periodontal Tissue Engineering”. J. Funct. Biomater. 15 (2024), p. 233. DOI: 10.3390/jfb15080233.

[165] R. Verma, J. Kumar, N.K. Singh, S.K. Rai, K.K. Saxena, and J. Xu. "Design and Analysis of Biomedical Scaffolds Using TPMS-Based Porous Structures Inspired from Additive Manufacturing". Coatings 12 (2022). DOI: 10.3390/coatings12060839.

[166] D.B. Alemayehu, M. Todoh, J.-H. Hsieh, C. Li, and S.-J. Huang. "Improving Pure Titanium's Biological and Mechanical Characteristics through ECAP and Micro-Arc Oxidation Processes". Micromachines 14 (2023), p. 1541. DOI: 10.3390/mi14081541.

[167] P. Xu, W. Guo, L. Yang, C. Yang, D. Ruan, J. Xu, and S. Yao. "Crashworthiness Analysis of the Biomimetic Lotus Root Lattice Structure". Int. J. Mech. Sci. 263 (2024), p. 108774. DOI: 10.1016/j.ijmecsci.2023.108774.

[168] J. Luo, S. Peng, S. Hou, and Y. Kiani. "Vibration Analysis of FGM Anisogrid Lattice Plates with One Width Fold Based on the Continuous Model Using the GDQE Method". Thin-Walled Struct. 195 (2024), p. 111386. DOI: 10.1016/j.tws.2023.111386.

[169] J. Tkac, T. Toth, O. Mizera, V. Molnar, G. Fedorko, and M. Dovica. "Comparison of Quality of Porous Structure Specimens Produced by Different Additive Technologies and from Different Materials". Appl. Sci. 14 (2024), p. 648. DOI: 10.3390/app14020648.

[170] L. Wang, L. He, F. Liu, H. Yuan, J. Li, and M. Chen. "Mechanical Characterization of Multifunctional Metal-Coated Polymer Lattice Structures". Materials (Basel) 17 (2024), p. 741. DOI: 10.3390/ma17030741.

[171] B. Monteiro, F. Rocha, and J. Costa. "Topology Optimization of a Robot Gripper with NTopology". U. Porto J. Eng. 10 (2024), pp. 11–19. DOI: 10.24840/2183-6493_010-001_002051.

[172] P. Munyensanga, M. Bricha, and K. El Mabrouk. "Functional Characterization of Biomechanical Loading and Biocorrosion Resistance Properties of Novel Additively Manufactured Porous CoCrMo Implant: Comparative Analysis with Gyroid and Rhombic Dodecahedron". Mater. Chem. Phys. 316 (2024), p. 129139. DOI: 10.1016/j.matchemphys.2024.129139.

[173] C. Bhat, M.J. Prajapati, A. Kumar, and J.-Y. Jeng. "Additive Manufacturing-Enabled Advanced Design and Process Strategies for Multi-Functional Lattice Structures". Materials (Basel) 17 (2024). DOI: 10.3390/ma17143398.

[174] B.J. Moya, M. Rivas, R. Quiza, and J.P. Davim. "Computer Simulation-Based Multi-Objective Optimisation of Additively Manufactured Cranial Implants". Technologies 12 (2024), p. 125. DOI: 10.3390/technologies12080125.

[175] M.I. Chibinyani, T.C. Dzogbewu, M. Maringa, and A. Muiruri. "Lattice Structures Built with Different Polygon Hollow Shapes: A Review on Their Analytical Modelling and Engineering Applications". Appl. Sci. 14 (2024), p. 1582. DOI: 10.3390/app14041582.

[176] M.T. Rayhan, M.I.H. Rimon, M. Khan, M.A. Hasan, M.H. Mobarak, M.A. Islam, and N. Hossain. "Advances in Additive Manufacturing of Nanocomposite Materials Fabrications and Applications". Eur. Polym. J. (2024), p. 113406. DOI: 10.1016/j.eurpolymj.2024.113406.

[177] S. Alkunte, I. Fidan, V. Naikwadi, S. Gudavasov, M.A. Ali, M. Mahmudov, S. Hasanov, and M. Cheepu. "Advancements and Challenges in Additively Manufactured Functionally Graded Materials: A Comprehensive Review". J. Manuf. Mater. Process. 8 (2024), p. 23. DOI: 10.3390/jmmp8010023.

[178] D. Mrówczyński, T. Gajewski, M. Pośpiech, and T. Garbowski. "Estimation of the Compressive Strength of Cardboard Boxes Including Packaging Overhanging on the Pallet". Appl. Sci. 14 (2024), p. 819. DOI: 10.3390/app14020819.

[179] D.B. Alemayehu, M. Todoh, and S. Huang. "Nonlinear Finite Element Analysis of Bone-Implant Contact in Three Short Dental Implant Models with Varying Osseointegration Percentages". Oral 4 (2024), pp. 505–524. DOI: 10.20944/preprints202408.2180.v1.

[180] D.B. Alemayehu, M. Todoh, and S.J. Huang. "Advancing 3D Dental Implant Finite Element Analysis: Incorporating Biomimetic Trabecular Bone with Varied Pore Sizes in Voronoi Lattices". J. Funct. Biomater. 15 (2024). DOI: 10.3390/jfb15040094.

[181] D.B. Alemayehu and M. Todoh. "Enhanced Energy Absorption with Bioinspired Composite Triply Periodic Minimal Surface Gyroid Lattices Fabricated via Fused Filament Fabrication (FFF)". J. Manuf. Mater. Process. (2024). DOI: 10.3390/jmmp8030086.

[182] S. Thakur and S.R. Chauhan. "Development of a Critical Edge-Based Adaptive Toolpath Strategy to Improve Geometrical Accuracy of Incrementally Formed Titanium Implants". J. Manuf. Process. 110 (2024), pp. 114–125. DOI: 10.1016/j.jmapro.2023.12.053.

[183] T. Meier, R. Li, S. Mavrikos, B. Blankenship, Z. Vangelatos, M.E. Yildizdag, and C.P. Grigoropoulos. "Obtaining Auxetic and Isotropic Metamaterials in Counterintuitive Design Spaces: An Automated Optimization Approach and Experimental Characterization". npj Comput. Mater. 10 (2024), p. 3. DOI: 10.1038/s41524-023-01186-2.

[184] N. YÜKSEL, E. Oğulcan, H.R. BÖRKLÜ, and H.K. SEZER. "Mechanical Properties of Additively Manufactured Lattice Structures Designed by Deep Learning". Thin-Walled Struct. 196 (2024), p. 111475. DOI: 10.1016/j.tws.2023.111475.

[185] F. Liu, M. Chen, S. Liu, Z. Xiang, S. Huang, E.G. Lim, and S. Zhang. "Stress-Driven Generative Design and Numerical Assessment of Customized Additive Manufactured Lattice Structures". Mater. Des. 241 (2024), p. 112956. DOI: 10.1016/j.matdes.2024.112956.

[186] R. Hedayati, M. Alavi, and M. Sadighi. "Effect of Degradation of Polylactic Acid (PLA) on Dynamic Mechanical Response of 3D Printed Lattice Structures". Materials (Basel) 17 (2024), p. 3674. DOI: 10.3390/ma17153674.

[187] Dawit Bogale Alemayehu, Masahiro Todoh, and Song-Jeng Huang. "Hybrid Biomechanical Design of Dental Implants: Integrating Solid and Gyroid Triply Periodic Minimal Surface Lattice Architectures for Optimized Stress Distribution". Journal of Functional Biomaterials 16.2 (2025), p. 54. DOI: 10.3390/jfb16020054. URL: https://doi.org/10.3390/jfb16020054.

[188] P.C. Dechow and G.A. Nail. "Elastic Properties of Human Supraorbital and Mandibular Bone". Am J Phys Anthr 306 (1993), pp. 291–306. DOI: 10.1002/ajpa.1330900304.

[189] A.M. O'Mahony, J.L. Williams, and P. Spencer. "Anisotropic Elasticity of Cortical and Cancellous Bone in the Posterior Mandible Increases Peri-implant Stress and Strain under Oblique Loading". Clin. Oral Implants Res. 12 (2001), pp. 648–657. DOI: 10.1034/j.1600-0501.2001.120614.x.

[190] P. Ausiello, M. Martorelli, I. Papallo, A. Gloria, R. Montanari, M. Richetta, and A. Lanzotti. "Optimal Design of Surface Functionally Graded Dental Implants with Improved Properties". In: *Advances on Mechanics, Design Engineering and Manufacturing IV*. Ed. by S. Gerbino, A. Lanzotti, M. Martorelli, R. Mirálbes Buil, C. Rizzi, and L. Roucoules. Cham, Switzerland: Springer International Publishing, 2023, pp. 294–305.

[191] A.-F. Obaton, J. Fain, M. Djemaï, D. Meinel, F. Léonard, E. Mahé, B. Lécuelle, J.-J. Fouchet, and G. Bruno. "In Vivo XCT Bone Characterization of Lattice Structured Implants Fabricated by Additive Manufacturing". Heliyon 3 (2017), e00374. DOI: 10.1016/j.heliyon.2017.e00374.

[192] M.E. Onder, A. Culhaoglu, O. Ozgul, U. Tekin, F. Atıl, C. Taze, and E. Yasa. "Biomimetic Dental Implant Production Using Selective Laser Powder Bed Fusion Melting: In-Vitro Results". J. Mech. Behav. Biomed. Mater. 151 (2024), p. 106360. DOI: 10.1016/j.jmbbm.2023.106360.

[193] J. Zhang, X. Zhang, Y. Chen, W. Feng, and X. Chen. "Novel Design and Finite Element Analysis of Diamond-like Porous Implants with Low Stiffness". Materials (Basel) 14 (2021). DOI: 10.3390/ma14226918.

[194] M.E. Onder, A. Culhaoglu, O. Ozgul, U. Tekin, F. Atıl, C. Taze, and E. Yasa. "Biomimetic Dental Implant Production Using Selective Laser Powder Bed Fusion Melting: In-Vitro Results". J. Mech. Behav. Biomed. Mater. 151 (2024), p. 106360. DOI: 10.1016/j.jmbbm.2023.106360.

[195] J.M.C. Po, J.A. Kieser, L.M. Gallo, A.J. Tésenyi, P. Herbison, and M. Farella. "Time-Frequency Analysis of Chewing Activity in the Natural Environment". J. Dent. Res. 90 (2011), pp. 1206–1210. DOI: 10.1177/0022034511416669.

[196] J. Lee, L. Li, H.Y. Song, M.J. Son, Y.M. Lee, and K.T. Koo. "Impact of Lattice versus Solid Structure of 3D-Printed Multiroot Dental Implants Using Ti-6Al-4V: A Preclinical Pilot Study". J. Periodontal Implant Sci. 52 (2022), pp. 338–350. DOI: 10.5051/JPIS.2105720286.

[197] F. Yang, C. Chen, Q. Zhou, Y. Gong, R. Li, C. Li, F. Klämpfl, S. Freund, X. Wu, and Y. Sun. "Laser Beam Melting 3D Printing of Ti6Al4V Based Porous Structured Dental Implants: Fabrication, Biocompatibility Analysis and Photoelastic Study". Sci. Rep. 7 (2017), pp. 1–12. DOI: 10.1038/srep45360.

[198] D. Barba, E. Alabort, and R.C. Reed. "Synthetic Bone: Design by Additive Manufacturing". Acta Biomaterialia 97 (2019), pp. 637–656. DOI: 10.1016/j.actbio.2019.07.049.

[199] H.E. Burton, N.M. Eisenstein, B.M. Lawless, P. Jamshidi, M.A. Segarra, O. Addison, D.E.T. Shepherd, M.M. Attallah, L.M. Grover, and S.C. Cox. "The Design of Additively Manufactured Lattices to Increase the Functionality of Medical Implants". Materials Science and Engineering: C 94 (2019), pp. 901–908. DOI: 10.1016/j.msec.2018.10.052.

[200] Y.T. Wang, C.M. Chang, P.H. Liu, and C.L. Lin. "Feasibility Evaluation of a New Lattice for Porous Surface Design in Additive Manufacturing Medical Implants under Interfacial Tensile Bonded Testing". Additive Manufacturing 66 (2023), p. 103455. DOI: 10.1016/j.addma.2023.103455.

[201] E. Anitua, A. Eguia, C. Staudigl, and M.H. Alkhraisat. "Clinical Performance of Additively Manufactured Subperiosteal Implants: A Systematic Review". International Journal of Implant Dentistry (2024). DOI: 10.1186/s40729-024-00521-6.

[202] M. Roy, M. Cerea, W. Hedzelek, L.A. Vaira, and B. Dorocka-Bobkowska. "Additively Manufactured Subperiosteal Implants for the Rehabilitations of Lateral Incisors Agenesis – A Case Series". Journal of Stomatology, Oral and Maxillofacial Surgery (2025), p. 102263. DOI: 10.1016/j.jormas.2025.102263.

[203] R. Alkentar, N. Kladovasilakis, D. Tzetzis, and T. Mankovits. "Effects of Pore Size Parameters of Titanium Additively Manufactured Lattice Structures on the Osseointegration Process in Orthopedic Applications: A Comprehensive Review". Crystals 13 (2023), p. 113. DOI: 10.3390/cryst13010113.

[204] N.K. Sivakumar, S. Palaniyappan, V. Sekar, A. Alodhayb, and M. Braim. "An Optimization Approach for Studying the Effect of Lattice Unit Cell's Design-Based Factors on Additively Manufactured Poly Methyl Methacrylate Cranio-Implant". J. Mech. Behav. Biomed. Mater. 141 (2023), p. 105791. DOI: 10.1016/j.jmbbm.2023.105791.

[205] Y. Du, H. Liang, D. Xie, N. Mao, J. Zhao, Z. Tian, C. Wang, and L. Shen. "Design and Statistical Analysis of Irregular Porous Scaffolds for Orthopedic Reconstruction Based on Voronoi Tessellation and Fabricated via Selective Laser Melting (SLM)". Mater. Chem. Phys. 239 (2020), p. 121968. DOI: 10.1016/j.matchemphys.2019.121968.

[206] Y. Zhou, P. Isaksson, and C. Persson. "An Improved Trabecular Bone Model Based on Voronoi Tessellation". J. Mech. Behav. Biomed. Mater. 148 (2023), p. 106172. DOI: 10.1016/j.jmbbm.2023.106172.

[207] S. Zou, H. Gong, and J. Gao. "Additively Manufactured Multilevel Voronoi-Lattice Scaffolds with Bonelike Mechanical Properties". ACS Biomater. Sci. Eng. 8 (2022), pp. 3022–3037. DOI: 10.1021/acsbiomaterials.1c01482.

[208] S. Kanwar, O. Al-Ketan, and S. Vijayavenkataraman. "A Novel Method to Design Biomimetic, 3D Printable Stochastic Scaffolds with Controlled Porosity for Bone Tissue Engineering". Mater. Des. 220 (2022), p. 110857. DOI: 10.1016/j.matdes.2022.110857.

[209] D. Bahati, M. Bricha, and K. El Mabrouk. "Vat Photopolymerization Additive Manufacturing Technology for Bone Tissue Engineering Applications". Adv. Eng. Mater. 25 (2023), p. 2200859. DOI: 10.1002/adem.202200859.

[210] N. Mamidi, F. Ijadi, and M.H. Norahan. "Leveraging the Recent Advancements in GelMA Scaffolds for Bone Tissue Engineering: An Assessment of Challenges and Opportunities". Biomacromolecules 10 (2023), pp. 1–39. DOI: 10.1021/acs.biomac.3c00279.

[211] M. Rahatuzzaman, M. Mahmud, S. Rahman, and M.E. Hoque. "Design, Fabrication, and Characterization of 3D-Printed ABS and PLA Scaffolds Potentially for Tissue Engineering". Results Eng. 21 (2024), p. 101685. DOI: 10.1016/j.rineng.2023.101685.

[212] P. Zioupos, R.B. Cook, and J.R. Hutchinson. "Some Basic Relationships between Density Values in Cancellous and Cortical Bone". J. Biomech. 41 (2008), pp. 1961–1968. DOI: 10.1016/j.jbiomech.2008.03.025.

[213] N.N.A.A. Abdullah, A.H. Abdullah, and M.H. Ramlee. "Current Trend of Lattice Structures Designed and Analysis for Porous Hip Implants: A Short Review". Mater. Today Proc. (2023). DOI: 10.1016/j.matpr.2023.09.199.

[214] S. Ataollahi. "A Review on Additive Manufacturing of Lattice Structures in Tissue Engineering". Bioprinting (2023), e00304. DOI: 10.1016/j.bprint.2023.e00304.

[215] M. Rezapourian and I. Hussainova. "Optimal Mechanical Properties of Hydroxyapatite Gradient Voronoi Porous Scaffolds for Bone Applications—A Numerical Study". J. Mech. Behav. Biomed. Mater. 148 (2023), p. 106232. DOI: 10.1016/j.jmbbm.2023.106232.

[216] L. Vaiani, A.E. Uva, and A. Boccaccio. "Structural and Topological Design of Conformal Bilayered Scaffolds for Bone Tissue Engineering". Thin-Walled Struct. 192 (2023), p. 111209. DOI: 10.1016/j.tws.2023.111209.

[217] S.R. Atashipour and J. Baqersad. "Noninvasive Identification of Directionally-Dependent Elastic Properties of Soft Tissues Using Full-Field Optical Data". J. Mech. Behav. Biomed. Mater. 151 (2024), p. 106266. DOI: 10.1016/j.jmbbm.2023.106266.

[218] S. Bachmann, D.H. Pahr, and A. Synek. "A Density-Dependent Target Stimulus for Inverse Bone (Re) Modeling with Homogenized Finite Element Models". Ann. Biomed. Eng. 51 (2023), pp. 925–937. DOI: 10.1007/s10439-022-03104-x.

[219] S. Daynes. "Isotropic Cellular Structure Design Strategies Based on Triply Periodic Minimal Surfaces". Addit. Manuf. (2024), p. 104010. DOI: 10.1016/j.addma.2024.104010.

[220] H. Jiang, B.A. Bednarcyk, L. Le Barbenchon, and Y. Chen. "Elastically Anisotropic Architected Metamaterials with Enhanced Energy Absorption". Thin-Walled Struct. 192 (2023), p. 111115. DOI: 10.1016/j.tws.2023.111115.

[221] L. Ritschl, P. Schilling, A. Wittmer, M. Bohner, A. Bernstein, H. Schmal, and M. Seidenstuecker. "Composite Material Consisting of Microporous Beta-TCP Ceramic and Alginate-Dialdehyde-Gelatin for Controlled Dual Release of Clindamycin and Bone Morphogenetic Protein 2". J. Mater. Sci. Mater. Med. 34 (2023), p. 39. DOI: 10.1007/s10856-023-06743-1.

[222] R.G. AboElhassan, D.C. Watts, R.A. Alamoush, and A. Elraggal. "Biomechanical Behavior and Weibull Survival of CAD-CAM Endocrowns with Different Marginal Designs: A 3D Finite Element Analysis". Dent. Mater. 40 (2024), pp. 227–235. DOI: 10.1016/j.dental.2023.11.012.

[223] Ö. Kirmali, G. Icen, H.K. Celik, and A.E.W. Rennie. "Evaluation of Stress Distribution on an Endodontically Treated Maxillary Central Tooth with Lesion Restored with Different Crown Materials: A Finite Element Analysis". Heliyon (2024). DOI: 10.1016/j.heliyon.2024.e25829.

[224] A. Robau-Porrua, J.E. González, J. Rodríguez-Guerra, P. González-Mederos, P. Navarro, J.E. de la Rosa, M. Carbonell-González, E. Araneda-Hernández, and Y. Torres. "Biomechanical Behavior of a New Design of Dental Implant: Influence of the Porosity and Location in the Maxilla". J. Mater. Res. Technol. 29 (2024), pp. 3255–3267. DOI: 10.1016/j.jmrt.2024.02.091.

[225] P. Pandoleon, A. Bakopoulou, L. Papadopoulou, and P. Koidis. "Evaluation of the Biological Behaviour of Various Dental Implant Abutment Materials on Attachment and Viability of Human Gingival Fibroblasts". Dent. Mater. 35 (2019), pp. 1053–1063. DOI: 10.1016/j.dental.2019.04.010.

[226] H.A. Bulaqi, M.M. Mashhadi, H. Safari, M.M. Samandari, and F. Geramipanah. "Effect of Increased Crown Height on Stress Distribution in Short Dental Implant Components and Their Surrounding Bone: A Finite Element Analysis". J. Prosthet. Dent. 113 (2015), pp. 548–557. DOI: 10.1016/j.prosdent.2014.11.007.

[227] O. Kayabaşı, E. Yüzbasıoğlu, and F. Erzincanlı. "Static, Dynamic and Fatigue Behaviors of Dental Implant Using Finite Element Method". Adv. Eng. Softw. 37 (2006), pp. 649–658. DOI: 10.1016/j.advengsoft.2006.02.004.

[228] L. Chen, H.E. Hao, Y.-M. Li, L.I. Ting, X.-P. Guo, and R.-F. Wang. "Finite Element Analysis of Stress at Implant–Bone Interface of Dental Implants with Different Structures". Trans. Nonferrous Met. Soc. China 21 (2011), pp. 1602–1610. DOI: 10.1016/S1003-6326(11)60903-5.

[229] Y.-J. Cheng, T.-H. Wu, Y.-S. Tseng, and W.-F. Chen. "Development of Hybrid 3D Printing Approach for Fabrication of High-Strength Hydroxyapatite Bioscaffold Using FDM and DLP Techniques". Biofabrication 16 (2024), p. 25003. DOI: 10.1088/1758-5090/ad1b20.

[230] F. Distefano, S. Pasta, and G. Epasto. "Titanium Lattice Structures Produced via Additive Manufacturing for a Bone Scaffold: A Review". J. Funct. Biomater. 14 (2023), p. 125. DOI: 10.3390/jfb14030125.

[231] C.M. Suryawanshi, S. Sagar, R. Bhallamudi, and S. Mishra. "Effective Design and Mechanical Response of Gyroid Lattice Scaffold for Orthopedic Implants". Manuf. Lett. 35 (2023), pp. 493–501. DOI: 10.1016/10.1016/j.mfglet.2023.07.015.

[232] Z. Fan, G. Huang, Y. Lu, Y. Chen, F. Zeng, and J. Lin. "Full Compression Response of FG-Based Scaffolds with Varying Porosity via an Effective Numerical Scheme". Int. J. Mech. Sci. 223 (2022), p. 107294. DOI: 10.1016/j.ijmecsci.2022.107294.

[233] M. Rezapourian, N. Kamboj, I. Jasiuk, and I. Hussainova. "Biomimetic Design of Implants for Long Bone Critical-Sized Defects". J. Mech. Behav. Biomed. Mater. 134 (2022), p. 105370. DOI: 10.1016/j.jmbbm.2022.105370.

[234] M. Afshar, A.P. Anaraki, H. Montazerian, and J. Kadkhodapour. "Additive Manufacturing and Mechanical Characterization of Graded Porosity Scaffolds Designed Based on Triply Periodic Minimal Surface Architectures". J. Mech. Behav. Biomed. Mater. 62 (2016), pp. 481–494. DOI: 10.1016/j.jmbbm.2016.05.027.

[235] O. Cantó-Navés, R. Medina-Galvez, X. Marimon, M. Ferrer, Ó. Figueras-Álvarez, and J. Cabratosa-Termes. "A 3D Finite Element Analysis Model of Single Implant-Supported Prosthesis under Dynamic Impact Loading for Evaluation of Stress in the Crown, Abutment and Cortical Bone Using Different Rehabilitation Materials". Materials (Basel) 14 (2021), p. 3519. DOI: 10.3390/ma14133519.

[236] S. Juneja, G. Miranda, A. Eram, N. Shetty, C. KN, and L.G. Keni. "Investigating the Influence of All-Ceramic Prosthetic Materials on Implants and Their Effect on the Surrounding Bone: A Finite Element Analysis". Prosthesis 6 (2024), pp. 74–88. DOI: 10.3390/prosthesis6010006.

[237] P. Kowalczyk. "Elastic Properties of Cancellous Bone Derived from Finite Element Models of Parameterized Microstructure Cells". J. Biomech. 36 (2003), pp. 961–972. DOI: 10.1016/S0021-9290(03)00065-4.

[238] Y.-W. Shen, H.-L. Huang, J.-T. Hsu, and L.-J. Fuh. "Effects of Diameters of Implant and Abutment Screw on Stress Distribution within Dental Implant and Alveolar Bone: A Three-Dimensional Finite Element Analysis". J. Dent. Sci. (2024). DOI: 10.1016/j.jds.2023.12.020.

[239] D. Ulrich, B. van Rietbergen, H. Weinans, and P. Rüegsegger. "Finite Element Analysis of Trabecular Bone Structure: A Comparison of Image-Based Meshing Techniques". J. Biomech. 31 (1998), pp. 1187–1192. DOI: 10.1016/S0021-9290(98)00118-3.

[240] A. Al-Sanea, S. Aktas, T. Celik, and Y. Kisioglu. "Effects of the Internal Contact Surfaces of Dental Implants on Screw Loosening: A 3-Dimensional Finite Element Analysis". J. Prosthet. Dent. 130 (2023), 603–e1. DOI: 10.1016/j.prosdent.2023.07.007.

[241] C. Falcinelli, F. Valente, M. Vasta, and T. Traini. "Finite Element Analysis in Implant Dentistry: State of the Art and Future Directions". Dent. Mater. (2023). DOI: 10.1016/j.dental.2023.04.002.

[242] D. Mishra and B. Basu. "Biomechanical Analysis of Peri-Prosthetic Bone Response to Hybrid Threaded Zirconia Dental Implants: An in Silico Model". J. Mech. Behav. Biomed. Mater. 150 (2024), p. 106310. DOI: 10.1016/j.jmbbm.2023.106310.

[243] P. Qiu, R. Cao, Z. Li, and Z. Fan. "A Comprehensive Biomechanical Evaluation of Length and Diameter of Dental Implants Using Finite Element Analyses: A Systematic Review". Heliyon (2024). DOI: 10.1016/j.heliyon.2024.e26876.

[244] M. Karimi, M. Asadi-Eydivand, N. Abolfathi, Y. Chehrehsaz, and M. Solati-Hashjin. "The Effect of Pore Size and Layout on Mechanical and Biological Properties of 3D-printed Bone Scaffolds with Gradient Porosity". Polym. Compos. 44 (2023), pp. 1343–1359. DOI: 10.1002/pc.27174.

[245] Y. Mao, J. Yuan, Y. Heng, K. Feng, D. Cai, and Q. Wei. "Effect of Hot Isostatic Pressing Treatment on Porosity Reduction and Mechanical Properties Enhancement of 316L Stainless Steel Fabricated by Binder Jetting". Virtual Phys. Prototyp. 18 (2023), e2174703. DOI: 10.1080/17452759.2023.2174703.

[246] G. Zheng, K. Wei, X. Kang, W. Fan, N.L. Ma, M. Verma, H.S. Ng, and S. Ge. "A New Attempt to Control Volatile Organic Compounds (VOCs) Pollution-Modification Technology of Biomass for Adsorption of VOCs Gas". Environ. Pollut. (2023), p. 122451. DOI: 10.1016/j.envpol.2023.122451.

[247] S. Seehanam, S. Khrueaduangkham, C. Sinthuvanich, U. Sae-Ueng, V. Srimaneepong, and P. Promoppatum. "Evaluating the Effect of Pore Size for 3D-Printed Bone Scaffolds". Heliyon (2024). DOI: 10.1016/j.heliyon.2024.e26005.

[248] J. Song, J. Lee, N. Kim, and K. Min. "Artificial Intelligence in the Design of Innovative Metamaterials: A Comprehensive Review". Int. J. Precis. Eng. Manuf. 25.1 (2024), pp. 225–244. DOI: 10.1007/s12541-023-00857-w.

[249] Dennis R. Carter and Wilson C. Hayes. "The Compressive Behavior of Bone as a Two-Phase Porous Structure". J. Bone Joint Surg. Am. 59.7 (1977), pp. 954–962.

[250] Mitchell B. Schaffler and David B. Burr. "Stiffness of Compact Bone: Effects of Porosity and Density". J. Biomech. 21.1 (1988), pp. 13–16. DOI: 10.1016/0021-9290(88)90186-8.

[251] L.J. Gibson. "The Mechanical Behaviour of Cancellous Bone". J. Biomech. 18 (1985), pp. 317–328. DOI: 10.1016/0021-9290(85)90287-8.

[252] L. Chen, X. Guo, Y. Li, and T. Li. "Finite Element Analysis for Interfacial Stress and Fatigue Behaviors of Biomimetic Titanium Implant under Static and Dynamic Loading Conditions". Zhong Nan Da Xue Xue Bao. Yi Xue Ban 35 (2010), pp. 662–672. DOI: 10.3969/j.issn.1672-7347.2010.07.004.

[253] X. Lv, S. Wang, Z. Xu, X. Liu, G. Liu, F. Cao, and Y. Ma. "Structural Mechanical Properties of 3D Printing Biomimetic Bone Replacement Materials". Biomimetics 8 (2023). DOI: 10.3390/biomimetics8020166.

[254] L. Chen, X. Guo, and T. Li Y.and Li. "Finite element analysis for interfacial stress and fatigue behaviors of biomimetic titanium implant under static and dynamic loading conditions". Journal of Central South University. Medical Sciences (Zhong Nan Da Xue Xue Bao. Yi Xue Ban) 35.7 (2010), pp. 662–672. DOI: 10.3969/j.issn.1672-7347.2010.07.004.